POLITECNICO

MILANO 1863

School of Civil, Environmental and Land Management Engineering
Master's degree in civil engineering - Structures

EFFECTS OF INTERNAL PARAMETRIC RESONANCE ON THE AERODYNAMIC BEHAVIOUR OF LONG-SPAN SUSPENSION BRIDGES

Supervisor:
Prof. Ing. Antonio Capsoni

Candidate:
Vincenzo Oliva
ID no. 876556

"If you can meet with triumph and disaster
And treat those two impostors just the same"

Rudyard Kipling

Ai Miei Nonni

RINGRAZIAMENTI

ABSTRACT

Suspended bridges represent the most advantageous solution to afford the necessity for covering very long spans. Due to their flexibility and their high length-to-width ratio, they are highly susceptible to wind induced actions. The latter can produce both static effects, e.g. torsional divergence, and dynamic ones, e.g. vortex induced vibrations, buffeting, torsional and classical flutter.

Recent studies assert that internal parametric resonance phenomena are a possible contributing cause for the occurrence of critical instability conditions in long-span suspension bridges. Such structures are strongly characterized by an intrinsic geometric non-linear behaviour, due to the stiffening cables contribution, which causes a soft coupling between the flexural and the torsional responses. Beyond a certain critical value of vertical amplitude of oscillations, a continuous exchange of energy is established in between the modes in resonance with the parametric action which, in low-damped systems, can lead to the structural failure.

The present work is intended to demonstrate that, in particular conditions, the intrinsic structural non-linear coupling is able to erode the aerodynamic performances of the structure itself, reaching critical conditions of instability for values of wind speeds lower than those for the onset of flutter. To do this, the perturbed bridge equations of motion are condensed into a single Mathieu's equation for the torsional vibration mode, allowing for the evaluation of instability through the well-known Ince-Strutt diagrams.

Keywords:

Long-span Suspension Bridges, Dynamic Instability, Wind-Structure Interaction, Flutter, Torsional Divergence, Vortex Shedding, Parametric Resonance, Structural Non-Linearity

SOMMARIO

I ponti sospesi rappresentano la soluzione più vantaggiosa per sopperire alla necessità di coprire grandi luci. Data la loro flessibilità ed il loro elevato rapporto tra lunghezza e larghezza, essi sono fortemente suscettibili alle azioni provocate dal vento. Queste ultime possono provocare sia effetti di natura statica, e.g. la divergenza torsionale, sia di natura dinamica, quali le azioni indotte da distacco dei vortici, buffeting, flutter torsionale e flutter classico.

Recenti studi affermano che i fenomeni di risonanza parametrica sono una possibile concausa di condizioni critiche di instabilità nei ponti sospesi. Tali strutture sono fortemente caratterizzate da un'intrinseca non-linearità geometrica dovuta al comportamento dei cavi, che provoca un leggero accoppiamento tra la risposta flessionale e torsionale. Oltre un certo valore limite di ampiezza delle oscillazioni flessionali si instaura un continuo scambio di energia tra i modi posti in risonanza dall'azione parametrica che, in sistemi debolmente smorzati, può portare al collasso della struttura.

Con il presente lavoro si intende dimostrare che, in particolari condizioni, l'accoppiamento non-lineare intrinseco della struttura è in grado di erodere le performance aerodinamiche della stessa, raggiungendo condizioni critiche di instabilità per valori di velocità del vento inferiori rispetto a quelli di flutter. Per fare ciò, le equazioni perturbate del moto della sezione del ponte vengono condensate in un'unica equazione di Mathieu per il modo di vibrare torsionale, consentendo di valutare l'instaurarsi di instabilità attraverso ben noti diagrammi di Ince-Strutt.

Parole chiave:
Ponti Sospesi a Grandi Luci, Instabilità Dinamica, Interazione Vento-Struttura, Flutter, Divergenza Statica, Distacco dei Vortici, Risonanza Parametrica, Non-Linearità Strutturale

CONTENTS

INTRODUCTION

The dramatic collapse of the Tacoma Narrows bridge, occurred on November 7, 1940, paved the way for new studies in the field of wind induced effects on long-span suspension bridges. The concepts of vortex shedding, buffeting and Aeroelastic effects on such structures were introduced in structural engineering only after the Tacoma bridge failure, even though they were already known from six years in the aeronautical field.

Up to that time, only static problems were considered in long-span suspension bridges design and several theories were developed during the years, from the Navier's theory of the unstiffened suspension bridge to the well-known deflection theory, passing from the Rankine and the elastic theories of stiffened suspension bridges. It was Steinman in 1929 to take into account for the stiffening effect of the main cables by enforcing the equilibrium in the deformed configuration. The effect of cables stiffness allowed for the design of slender unstiffened bridges, bringing out the wind induced motion as a critical design issue.

The fluid-structure interaction started to assume a considerable importance in bridge's design procedures. Modern analyses include the investigation of various Aeroelastic phenomena, e.g. flutter of the bridge deck and vortex shedding. The modern approach is based on the works of Scanlan [52] who introduced an unified linear formulation to take into account for the self-excited forces due to wind based on the so-called flutter derivatives. Aeroelastic effects make the structural linear system of equations coupled and no more self-adjoint, allowing dynamic instability to occur. Critical conditions can be easily detected by solving the Eigenvalue problem deriving from the Aeroelastic equations of motion.

Recent works by Luco and Turmo [37] showed that linear vertical vibrations of the classic continuum model of a suspension bridge are governed only by two non-dimensional parameters, namely the classical Irvine parameter and the Steinman's stiffness factor. Abdel-Ghaffar [1] extended the classical continuum formulation based on the deflection theory including the effect of the torsional DoF and the coupling between vertical and torsional vibrations.

The structural coupling between two orthogonal modes of vibration highlighted the possibility for long-span suspension bridges to manifest the internal parametric resonance phenomenon. Indeed, it is well known that a non-linear weakly coupled oscillator can exhibit energy transfer from one mode of vibration to another, as far as the energetic level

reaches well-established critical thresholds. Cevik and Pakdemirli [17] demonstrated this possibility solving the system of equations governing the bridge's sectional model by means of an approximate perturbation method, namely the multiple scales. Recent studies by Arioli and Gazzola [7] showed that, also in isolated systems, vertical oscillations may switch to torsional ones for particular torsional-to-flexural frequency ratios.

However, these works do not take into account for the Aeroelastic effects and for the possible interaction between two apparently very different instability phenomena, i.e. flutter and internal parametric resonance. Indeed, the former is characterized by the sudden appearance of exponentially increasing oscillations due to the negative damping of the Aeroelastic system, whilst the latter is characterized by a gradual exchange of energy between the vertical and the torsional vibrating modes.

In reality, in a different field and with different objectives, an interaction between the two aforementioned instability phenomena was already guessed by Herrmann et al. [31] more than 40 years ago. In dealing with the effects of flutter in a 2 DoF$_s$ system subjected to a non-conservative follower force [30], they realized the possibility to capture all the three families of instability already predicted by Bolotin [13], i.e. static divergence, flutter and parametric resonance, introducing a linear spring able to catch the axial extensibility of one beam. This problem seems strictly related to the bridge model, at least to the extent that both are able to exhibit the same instability phenomena.

However, it is demonstrated in this work that the bridge sectional model subjected to wind self-excited forces and the model proposed by Hermann subjected to a follower force are different in some aspects. The bridge's model is capable to exhibit all the instability phenomena also if it is described by 2 DoF$_s$ only, whilst the Herrmann's model needs 3 DoF$_s$ to capture the same phenomena. This is mainly due to the fact that the coupling term is intrinsic in the bridge model system and it directly correlates the two DoF$_s$, whereas in the Herrmann's model the coupling is artificially introduced by means of a 3rd DoF.

Despite the differences between the two models, the approach used by Herrmann to find the instability regions can be used to find out the stability diagrams for the bridge's sectional model. Thus, the linear variational equations governing the bridge behaviour are found considering, as a first step, null torsional oscillations and finite flexural ones. By means of this hypothesis one can define the steady state solution of the flexural equation of motion forced by the vortex shedding action. Then, small perturbations around the equilibrium configuration are introduced, leading to the so-called perturbed system of equations. Neglecting the coupling flutter derivatives, the latter is governed only by the torsional equation of motion subjected to a small but non vanishing flexural perturbation. This is due to the presence of a second order coupling stiffness term dependent simultaneously and linearly on both motions. By means of simple coordinate transformations, the torsional perturbed equation of motion can be re-written in the well-

known Mathieu's format and its stability can be detected by means of the Ince-Strutt diagram.

The boundary lines of instability on the Ince-Strutt diagram are found by solving the Mathieu's equation with the multiple scales technique. The most critical condition for the onset of instability is in correspondence of torsional-to-frequency ratio equal to 0.5, i.e. the so-called subharmonic 2:1 parametric resonance. The analytical approach adopted allows for the determination of an expression in which the A_2^* flutter derivative, responsible for the erosion of the net torsional damping (if positive), is lowered proportionally to the magnitude of the non-linear structural stiffness term and to the modal amplitude of flexural oscillations. The theoretical result obtained indicates that, when the net torsional structural damping is eroded by Aeroelastic effects, the structure becomes more susceptible to parametric resonance and instability can occur for values of wind speed lower than the flutter ones.

The mathematical model is then applied to two different cases, the Tacoma Narrows bridge and a twin box section bridge designed with the non-flutter principle. The former is a bluff deck section very sensitive to vortex shedding and to an erosion of the net torsional damping due to self-excited forces. In this scenario, for torsional-to-frequency ratios around 0.5, the critical instability conditions are reached for wind velocities lower than the once needed for the onset of flutter. On the contrary, the second is a streamlined cross section properly designed to counteract wind-induced effects. Critical conditions for the onset of instability due to parametric resonance are found to be not feasible with the wind induced oscillations due to vortex shedding.

Chapter 1 is intended to provide an historical background of suspension bridges.

Chapter 2 deals with the extended 2 DoF$_s$ deflection theory. The non-linear equations of motion governing the problem are found and the possibility for hangers to slack is detected. Moreover, with regards to a linearized formulation the structural Eigen-properties are identified by means of a modal superposition analysis.

Wind effects on bridges are described in chapter 3. The different kind of instabilities, i.e. torsional divergence, galloping and flutter, are detected with the aid of simplified formulations.

Chapter 4 provides a theoretical background of the parametric resonance phenomenon and of its interaction with the Aeroelastic effects. An expression demonstrating the interaction between torsional flutter and subharmonic resonance is found.

The Tacoma Narrows bridge case is discussed in chapter 5. Firstly all the possible causes of the failure are presented, secondly stability maps are plotted and numerical results are compared with physical observations.

Chapter 6 deals with a numerical application to a twin-box streamlined cross section designed with the non-flutter principle. The results shows that the main issue in the design of this kind of bridges are wind static effects.

1 HISTORICAL OVERVIEW

The first appearances of suspension bridges was due to the ancient civilizations in South East Asia, Equatorial Africa and South America. Incas built a great number of pedestrian suspension bridges to connect all the empire. These bridges were generally constituted by three or more vine cables used as a footway and two additional cables used as handrail. Figure 1.1 shows one of the most famous bridges built during the Inca's empire, the *Q'eswachaka bridge* spanning over the Akpurimac river. It is one of the last bridges survived and maintained for more than 500 years.
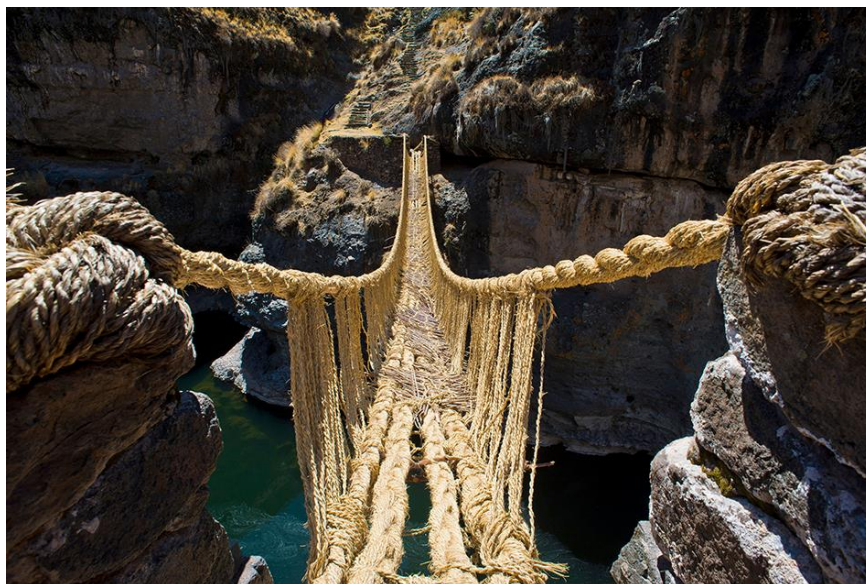
Figure 1.1: Q'eswachaka bridge on the Akpurimac river, Perù

The invention of the modern suspension bridges may be attributed to Fausto Veranzio (1551-1617), who represented two sketches in his most popular work *"Machinae Novae"*.
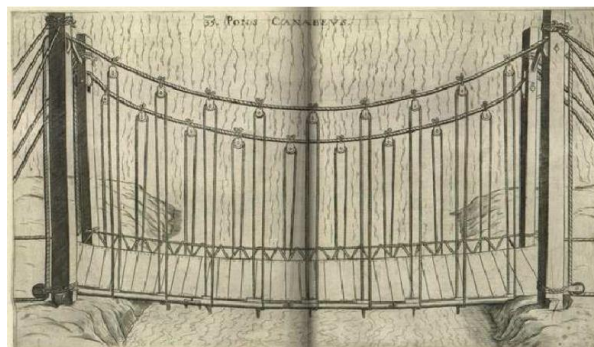
Figure 1.2: The first drawing of a modern suspension bridge by Fausto Veranzio

The first metal suspension bridges are believed to be constructed in China, when the ropes were replaced by iron chains.

However, the first studies on the theory of suspension bridges started in England with Claude Navier, who was sent there to study the early suspension bridges, such as the *Union Bridge* over the Tweed river (completed in 1820, designed by Samuel Brown), the *Chain Pier bridge* at Brighton (1823, Samuel Brown) and the *Menai Strait bridge* (1826, designed by Telford, Figure 1.3). The latter was the longest span bridge at that time, 580 ft, with suspension chains and a slender deck characterized by a little vertical bending stiffness. Due to its slenderness this bridge suffered of wind induced vibrations both in 1826 and in 1836. On January 6, 1839 the Menai bridge was damaged again by vertical and torsional motions, requiring the reconstruction of the deck and the replacement of suspenders.

Figure 1.4: Original section of the Menai Strait Bridge

Figure 1.3: Telford's Menai Straits Bridge, Wales

All the British bridges of that time were designed as unstiffened cables without any stiffening truss (Figure 1.4). Thus, most of this early bridges had undergone to several damages in windstorms. Faced with such induced motions, some structural engineers advocated for the use of a stiffening truss, whereas some others, having doubt on the economy of the stiffened spans, developed other structural systems, e.g. the suspension chains for the *Britannia tubular bridge*, which were abandoned in favour of the stiff tubular girder alone.

In the second half of 19th century, the centre of long span suspension bridges construction moved to United States, with the works of Charles Ellet and John Roebling. The first, in 1847 designed the record-breaking 1010 ft spans of the *Wheeling Bridge* over the Ohio river. Ellet did not provide any vertical stiffening to the deck, which was thought to be provided by a shallow catenary. On May 17, 1854 the Wheeling Bridge failed in a windstorm showing similar oscillations to that happened to the Menai Bridge.

By this time, it was nearing to complete the first railway suspension bridge, namely the Roebling's *Niagara bridge*, depicted in Figure 1.5. It spanned 822 ft and it consisted on an upper deck carrying the railroad track and a lower deck for horse drawn vehicles forming a box stiffening truss. Roebling used also cable stays radiating from the tops of the towers and cable guys attached to the underside of the lower deck and anchored to the ground below, in order to provide additional flexural stiffness to the deck.

Figure 1.5: Niagara Bridge, the 1st railway suspension bridge

Following this successful design, Roebling built the 1057 ft span *Cincinnati Bridge* in 1866 and he designed the 1596 ft span *Brooklyn Bridge*, which was completed in 1883 by his son. Roebling's genius laid in his ability to successfully combine several stiffening systems, so as to ensure that his bridges would remain in the structural static field, which at that time was the most known field both from theoretical and experimental point of view.

Figure 1.6: Brooklyn Bridge main cables and stays

Figure 1.7: Brooklyn Bridge, New York

The adoption of the elastic theory led to a new conception of bridge's design in which the effects of the stiffening truss in the structural behaviour were accounted for. Thanks to this theory the engineers around the turn of the 19th century believed that the wind induced vibrations of long span suspension bridges had been solved with the adoption of a well designed stiffening truss.

The main example of the application of the elastic theory in its simpler form is the *Williamsburg bridge* (Figure 1.8), inaugurated in 1903, spanning over the East river in New York. Its central span has a length of 1600 ft, only 5 ft longer with respect to the Roebling's Brooklyn Bridge. However the Williamsburg stiffening truss is more than twice as deep as that of the Brooklyn, contributing in large part to its bulkier appearance. The design could not be different because the two hinged stiffening truss is the only stiffening element of the girder, which is also characterized by unsuspended side spans.

Figure 1.8: Williamsburg Bridge, New York

Upon the completion of the Williamsburg bridge, only two wind incidents are known, the Niagara-Lewiston bridge failed in 1864 and the Niagara-Clifton failed in 1889. Both of them were light pedestrian bridge.

The elastic theory appeared to allow a reasonable design of the stiffening truss, which alone could sustain both the live loads and the wind effects on the girder. Hence, in absence of any theories of aerodynamic lift, vertical wind forces were no longer a major design issue.

However, this theory did not take into account for the correct interaction between the truss and the supporting cable, leading to oversized stiffening truss girders. The advection of the well-known deflection theory changed the way of designing bridges.

The use of the deflection theory allowed for the design of longer and slender span bridges, e.g. the *Bear Mountain Bridge*, completed in 1924, spanning 1623 ft, the *Delaware river bridge* at Philadelphia, inaugurated in 1926, spanning 1750 ft and the *Ambassador bridge* in Detroit, completed in 1928, spanning 1850 ft.

However, it was not until O. Amman's design of the *George Washington Bridge*, depicted in Figure 1.9, that the importance of weight as a stiffness factor was fully released. In 1931 it was inaugurated with only the upper deck in place, thus at that time it was essentially an unstiffened span having length 3500 ft. No stays are present as additional stiffening element. In this case, for the enormous length of the bridge, the adoption of the elastic theory would have led to an unbuildable stiffening truss because of its dimensions.

Figure 1.9: George Washington Bridge

The introduction of the deflection theory not only led to an economy in the materials, but also to an essential structural diversity, stiffened versus unstiffened girders. Following the example of the George Washington bridge, structural engineers of the first years of 20th century were encouraged to design longer and slender spans.

The most important examples are: the world record-breaking span (4200 ft) *Golden Gate bridge* (Figure 1.10), designed by J.B. Strauss, opened in 1937, the *Bronx-Whitestone bridge* (Figure 1.11), designed by O. Amman, spanning 2300 ft and opened in 1939, the *Deer Isle Bridge* (Figure 1.12), designed by Steinman, completed in 1939 spanning 1080 ft and the *Thousand Islands bridge* (Figure 1.13), designed by Steinman and Robinson, inaugurated in 1938, spanning 800 ft.

Figure 1.10: Golden Gate Bridge, San Francisco

Figure 1.11: Bronx-Whitestone Bridge, New York

Figure 1.12: Deer Isle Bridge

Figure 1.13: Thousand Island Bridge

All these bridges experienced oscillations due to wind effects because of their low value of span-to-depth ratio. The most famous bridge experiencing wind induced vibrations was the *Tacoma Narrows bridge* (Figure 1.16), designed by L. Moiseiff, which collapsed on November 7, 1940. It was designed for low traffic volume, indeed the stiffening girder was only 39 ft wide with two steel plate 8 ft deep (Figure 1.15). The design resulted in a deck characterized by low torsional rigidity. It was this the main difference with respect to the George Washington Bridge, which immense scale makes it an atypical case. In fact, the dead load per foot of the Tacoma Bridge was more than five times less with respect to that of the George Washington bridge. Thus, the resulting dead load tension may have provided effective cable stiffness only against static loads, but not sufficient stiffness against the dynamic wind loads.

Vertical oscillations of the Tacoma Narrows Bridge had been observed since the floor system was completed. Due to these movements the bridge, nicknamed "The Galloping Gertie", became popular and lots of driver used to cross the bridge just to experience these oscillations. Undamped torsional vibrations, never observed before, suddenly appear at 10 am on November 7, 1940 (Figure 1.17), leading to the failure around one hour later (Figure 1.19).
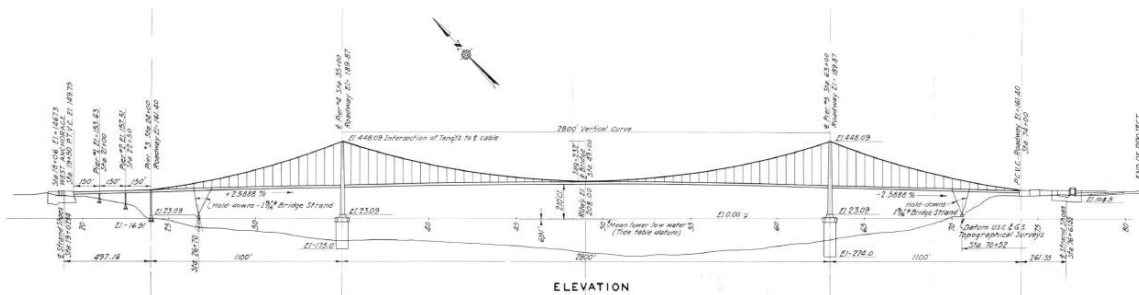
Figure 1.14: Elevation of the Tacoma Narrows Bridge, original drawing
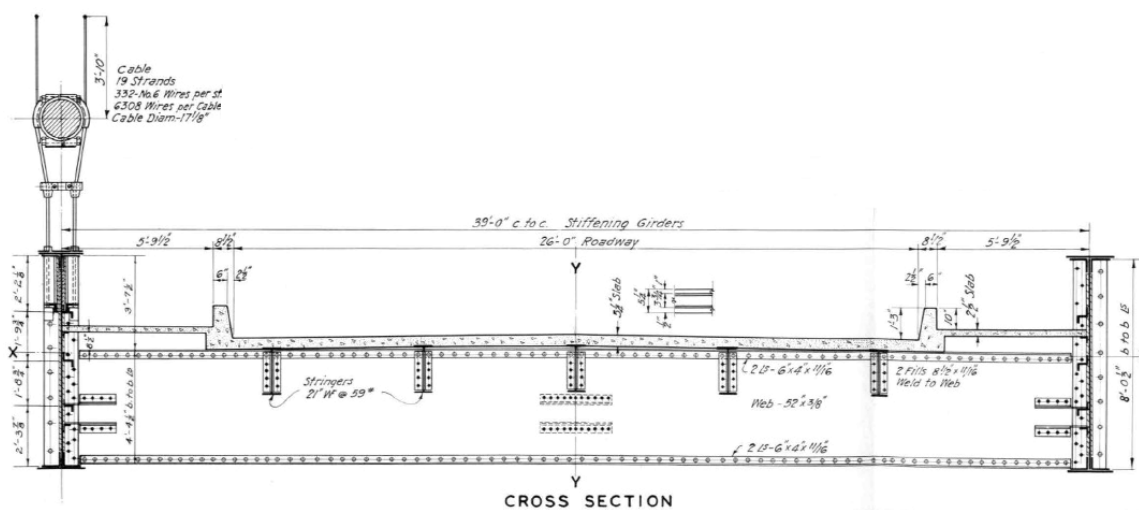
Figure 1.15: Cross section of the Tacoma Narrows Bridge, original drawing

Figure 1.16: Original Tacoma Narrows Bridge
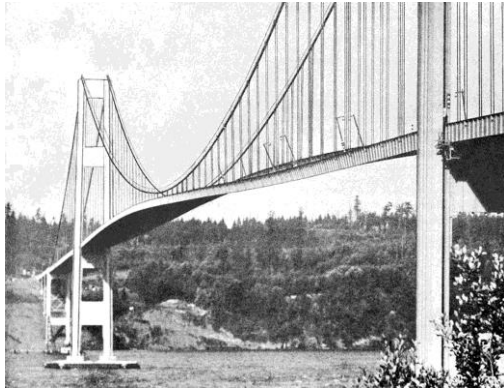
Figure 1.17: Tacoma Narrows Bridge, torsional oscillations

Figure 1.18: Tacoma Narrows bridge, street view of the torsional oscillations
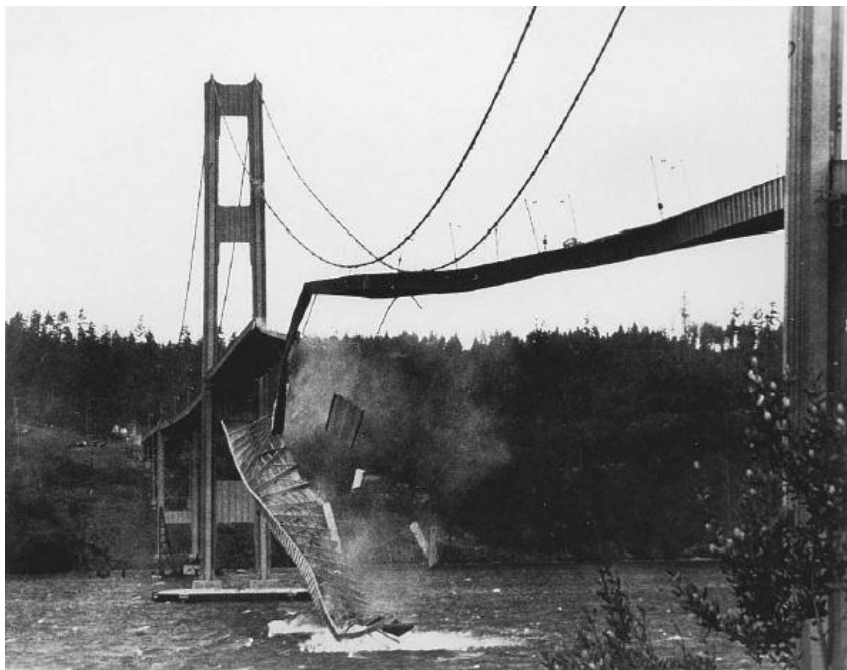
Figure 1.19: Failure of the Tacoma Narrows Bridge

The possibility of eliminating the deck stiffness in both the horizontal and vertical direction allowed for the design of the slender bridges of the 1930s, which ultimately reintroduced wind-induced motion as a critical design issue. The collapse of the Tacoma Narrows bridge has attracted several engineers in studying dynamic vibrations induced by wind. The concept of aerodynamics in the girders design was introduced.

The Tacoma Narrows bridge was rebuilt in 1950. After this, a series of bridges were built, in which aerodynamic stability was again achieved through the use of torsionally rigid stiffness truss, e.g. the *Mackinac bridge*, designed by Steinman with main span of 1158 m, the *Verrazzano Narrows bridge*, designed by O. Amman with a span of 1298 m and the *Tagus river bridge*, designed by Steinman, Boynton, Gronquist and London with a 1013 m main span.

The first European long-span suspension bridge was the Forth road Bridge, opened in 1964. The designer Sir Gilbert Roberts made use of a stiffening truss to build the main span of length 1001 m. However, it was with the advent of wind tunnel testing that it was understood that closed box section could provide aerodynamic stability. Indeed they combine a considerable torsional stiffness to a satisfactory aerodynamic behaviour.

The first suspension bridge built with a concrete closed box section was the *Severn bridge* (Figure 1.20), designed by G. Roberts in 1966.

Figure 1.20: Severn Bridge
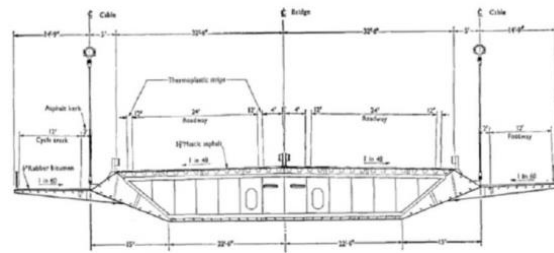
Figure 1.21: Severn Bridge cross section

The closed box girder section becomes the standard solution adopted, because of the lightweight and of the fabrication advantages with respect to the traditional stiffening truss. Thus, a large number of box girder suspension bridges were designed, including the *LilleBaelt bridge* (Denmark), opened in 1970 with a 600 m central span, the *bridge over the Bosphorus*, opened in 1973 with a 1074 m main span, the *Humber bridge*, opened in 1981 with a 1410 central span and the *Great Belt Bridge* (Figure 1.22), completed in 1999 with a central span of 1624 m.

Figure 1.22: The Great Belt Bridge

In this scenario the exception is the *Akashi-Kaikyo bridge* (Figure 1.23), which is actually the longest suspension span in the world, 1991 m. The bridge, connecting the city of Kobe (Japan) with Iwaya, was designed with a two hinged deep stiffening girder system able to provide enough stiffness to counteract wind induced oscillations.

Figure 1.23: Akaishi-Kaikyo bridge

Figure 1.24: Akaishi-Kaikyo stiffening truss

Nowadays, in the design of suspension bridges a comprehensive set of wind related responses are taken into consideration, such as static divergence, vortex-shedding, buffeting and flutter. Hence, the risk of developing Aeroelastic instabilities is always the matter while designing any lightweight long-span structures, characterized by high flexibility due to a low bending/torsional stiffness and a high width-to-depth ratio.

It is the deep knowledge acquired during several years of studies that led to the design of the *Messina Straits Bridge*, having the longest central span in the world (3300 m). The three-box girder aerodynamic cross section (Figure 1.25) allows both to reduce the static wind forces acting on the bridge and the self-induced forces due to Aeroelastic effects, which results in a flutter speed much higher with respect to the design wind speed.

Figure 1.25: Rendering of the Messina Strait Bridge

The efficiency of this cross section is proven by wind tunnel tests in which it is possible to compare the static longitudinal deflection of the Akashi-Kaikyo with the Messina bridge (Figure 1.26). Under the effect of a 60 m/s wind speed, the former shows a maximum horizontal deflection of 30 m, whilst the latter only 10 m.

Figure 1.26: Comparison of Akaishi-Kaikyo (left) and Messina (right) horizontal deflection due to wind in the wind tunnel.

The next challenge of structural and wind engineering is to build the so called "flutter free" bridges, i.e. bridges characterized by airfoil type cross sections and by very low torsional stiffness. In this way the occurrence of torsional flutter is prevented by the streamlined shape of the cross section whilst, since the frequency of the torsional mode of vibration is expressly lower than the correspondent flexural one, classical flutter is prevented.

2 STRUCTURAL SCHEME

The theory of suspension bridges has evolved a lot over the years, starting from the Navier's theory of the unstiffened suspension bridge arriving to the well-known deflection theory, passing from the Rankine and the elastic theories of stiffened suspension bridges.

In 1823, Claude Navier published *"Mémoire sur les ponts suspendus"*, the first book on the history and the theory of suspension bridges. Up to that time the bridges design was based on the experience and the intuition of the designer.

In 1858, William Rankine in his *"Manual of Applied Mechanics"*, presented the first theoretical treatment of the stiffened suspension bridge. He based its theory upon the existing parabolic cable theory by assuming that the total dead load of the bridge was uniformly distributed on the cable. The introduction of the interaction between the cables system and the stiffening girder was such that the latter can be considered as a simple beam subjected to a downward live load and an uniform upward suspender load. Comparing the maximum positive bending moment at the midspan of an unsuspended simple beam, the suspended girder carries only one-fourth of the moment. In reality the benefit on the deck is far higher, so this theory leads to a huge overestimation of the loads acting on the stiffening structure.

In 1888, Melan's second edition of his *"Handbuch der Ingenieurwissenschaften"* included a section on the elastic theory of suspension bridges. In 1913, Steinman published a complete translation of Melan's theory, from which he developed his *"Practical Treatise on Suspension Bridges"* of 1922. Differently from the Rankine theory, the elastic one relates the uniform suspender force to the live load in function of the bending stiffness of the truss and the axial stiffness of the cable. A lower girder bending stiffness with respect to the Rankine's theory is assumed, hence more live load can be transferred to the cable through the hangers, reducing the state of stress of the deck.

In 1888, Melan laid the foundation for the deflection theory in his *"Theorie der eisernen Bogenbrucken und der Hangenbruken"* by accounting for the change in shape of the cable under the live loads. In 1929, Steinman included the deflection theory in the second edition of his *"Practical Treatise"*. The effect of cable stiffness is reintroduced in this theory, showing that it can play a larger role in resisting deformation than the girder stiffness. Due to this beneficial effect, the loads acting on the deck are reduced in a great amount. The deflection theory leads the 20th century bridge's engineers to design slender bridges, reintroducing the wind induced motion as a critical design issue.

2.1 DEFLECTION THEORY

2.1.1 *General Assumptions*

In order to define the equations of motion governing the problem, the following assumptions has to be made:

1. The self-weight of the deck is uniformly distributed along its length and it is much greater than the weight of the cables. Hence, the cables can be considered as subjected to the deck's permanent distributed loads only. The main cables assume therefore a parabolic shape;

2. The stiffening deck is suspended to the cables through closely spaced vertical hangers (curtain behaviour), which are considered to be inextensible;

3. The parabolic shape of the cables is the funicular line of the permanent loads acting on the deck. The deck is therefore supported by a distributed force equal and opposite to its weight, with the consequence that no flexural effects are present in the deck;

4. Cables are inextensible just in the initial condition, when they carry permanent loads only. Moreover their flexural stiffness is negligible;

5. The pylons are stiff enough to guarantee perfect constraints.

The equilibrium equations of the two cables will be written considering just the central span of a suspension bridge (Figure 2.1). Being the pylons very stiff, a perfect clamp constraint is guaranteed at the end of the main cables. But, since they have negligible flexural stiffness, the clamps constraints behave like hinges. Therefore cables are able to resist external vertical loads just thanks to their axial internal tension.
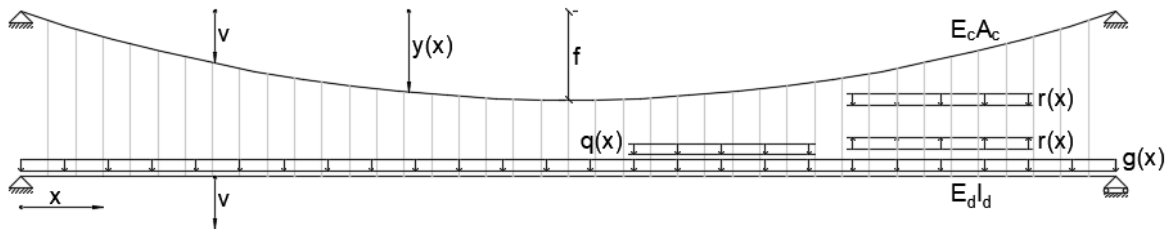
Figure 2.1: Single span suspension bridge model

2.1.2 *Initial Configuration*

As already mentioned, in the initial configuration the main cables assume the shape of a parabola, because subjected to uniformly distributed loads acting along the horizontal projection of their length. Equilibrium conditions in the horizontal and vertical directions are enforced on an infinitesimal piece of cable (Figure 2.2).
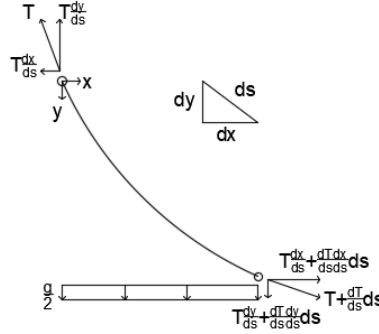
Figure 2.2: Infinitesimal element of the cable

$$\frac{d}{ds}\left(T\frac{dx}{ds}\right)ds = 0 \quad \Rightarrow \quad T\frac{dx}{ds} = H = cost.$$

$$-\frac{d}{ds}\left(T\frac{dy}{ds}\right)ds - \frac{g}{2}dx = 0 \quad \Rightarrow \quad \frac{d}{ds}\left(T\frac{dy}{dx}\frac{dx}{ds}\right)ds = -\frac{g}{2}dx \tag{2.1}$$

Substituting the first equation into the second, one obtain the classical *Parabola equation* (2.2), which holds for taut cables, i.e. for cables in which the tension T is very large.

$$H\frac{d^2y}{dx^2} = -\frac{g}{2} \tag{2.2}$$

This equation is obtained because of the hypothesis of negligible self-weight of the cable, otherwise the catenary equation would be obtained. Due to the shape of the main cables the initial configuration of the deck results to be unstressed. The general solution of the parabola equation (2.2) can be expressed as:

$$y(x) = Ax^2 + Bx + C \tag{2.3}$$

where proper geometrical boundary conditions have to be enforced to find the constants of integration. The perfect hinge at the cable's end, the sag f and the null slope at midspan are used to find *A*, *B* and C coefficients.

$$y(0) = 0 \quad \Rightarrow \quad C = 0$$

$$y\left(\frac{l}{2}\right) = f \quad \Rightarrow \quad f = \frac{Al^2}{4} + \frac{Bl}{2} \quad \Rightarrow \quad B = \frac{4f}{l} \tag{2.4}$$

$$\frac{dy}{dx}\left(\frac{l}{2}\right) = 0 \quad \Rightarrow \quad A = -\frac{B}{l} \quad \Rightarrow \quad A = -\frac{4f}{l^2}$$

Substituting the constants of integration found in (2.4) into (2.3), one obtains the expression for the variation of the height of the cable along the length of the bridge.

$$y(x) = 4\frac{f}{l}x\left(1 - \frac{x}{l}\right) \tag{2.5}$$

2.1.3 *Final Configuration*

The external variable loads are added to the permanent ones. The main cables lose their parabolic shape and the hangers exert an interaction force $r = r(x)$, which increases the force on the cables and contributes in supporting the deck.

The vertical equilibrium configuration of the main cables is the same, but the following quantities have to be substituted in expression (2.1).

$$g \quad \Rightarrow \quad g + r \quad , \quad H \quad \Rightarrow \quad H + h \quad , \quad y \quad \Rightarrow \quad y + v$$

Hence the parabola equation (2.2) becomes:

$$(H+h)\frac{d^2(y+v)}{dx^2} = -\frac{g+r}{2} \quad \Rightarrow \quad H\frac{d^2y}{dx^2} + h\frac{d^2y}{dx^2} + (H+h)\frac{d^2v}{dx^2} = -\frac{g}{2} + \frac{r}{2} \tag{2.6}$$

Deleting the terms related to the initial equilibrium condition:

$$r = -2(H+h)\frac{d^2v}{dx^2} - 2h\frac{d^2y}{dx^2} \tag{2.7}$$

The deck sustains a partial amount of the total external load equal to q(x)-r(x), so it is subjected to a deflection that involves its flexural stiffness. The vertical equilibrium equation of the infinitesimal piece of bridge's deck comes from the classical format of the Euler-Bernoulli beam theory. Moreover due to the hypothesis of inextensible hangers the deflection of the deck must be the same of the deflection of the main cables v.

$$EI\frac{d^4v}{dx^4} = q - r \quad \Rightarrow \quad EI\frac{d^4v}{dx^4} - 2(H+h)\frac{d^2v}{dx^2} - 2h\frac{d^2y}{dx^2} = q \tag{2.8}$$

This equilibrium equation links the cable and the deck response coupling the horizontal component of the cable's tension with the vertical displacement of the deck. Since both these quantities are unknowns, a compatibility equation is necessary to solve the problem in closed form. The *compatibility condition* is such that the total change in the projected horizontal length of the cable must be null, due to the very high stiffness of the pylons which cannot get closer. The mathematical format of this statement is:

$$\Delta u = \int_0^l \frac{du}{dx}dx = 0 \tag{2.9}$$

The initial and the final configuration of the cable are respectively:

$$ds^2 = dx^2 + dy^2$$

$$(ds + dL)^2 = (dx + du)^2 + (dy + dv)^2$$

Developing the squares and deleting the terms related to the initial length:

$$\cancel{ds^2} + dL^2 + 2dsdL = \cancel{dx^2} + du^2 + 2dxdu + \cancel{dy^2} + dv^2 + 2dydv \tag{2.10}$$

Deriving two times with respect to x and collecting the horizontal strain component:

$$\frac{d^2L}{dx^2} + 2\frac{dsdL}{dx^2} = \frac{d^2u}{dx^2} + 2\frac{du}{dx} + \frac{d^2v}{dx^2} + 2\frac{dydv}{dx^2}$$

$$\frac{du}{dx} = \frac{ds}{dx}\frac{dL}{dx} - \frac{dy}{dx}\frac{dv}{dx} + \frac{1}{2}\frac{d^2L}{dx^2} - \frac{1}{2}\frac{d^2u}{dx^2} - \frac{1}{2}\frac{d^2v}{dx^2}$$

where

$$\frac{dL}{dx} = \frac{dL}{ds}\frac{ds}{dx} = \frac{t(x)}{EA(x)}\frac{1}{\cos(\vartheta)} = \frac{h}{EA(x)}\frac{1}{\cos^2(\vartheta)}$$

The infinitesimal change in the projected horizontal length of the cable can be expressed as:

$$\frac{du}{dx} = \frac{h}{EA(x)}\frac{1}{\cos^3(\vartheta)} - \frac{dy}{dx}\frac{dv}{dx} - \frac{1}{2}\frac{d^2v}{dx^2} + \frac{1}{2}\frac{d^2L}{dx^2} - \frac{1}{2}\frac{d^2u}{dx^2} \tag{2.11}$$

where the last two contributions are in general negligible in the hypothesis of small displacements. Integrating the equation (2.11) along the horizontal length of the cable, the compatibility condition (2.9) becomes:

$$\Delta u = \int_0^l \frac{du}{dx}dx = h\int_0^l \frac{dx}{E_cA(x)\cos^3(\vartheta)} - \int_0^l y'v'dx - \frac{1}{2}\int_0^l v'^2dx = \frac{h}{E_cA_c}L_c + \int_0^l y''vdx + $$
$$ + \frac{1}{2}\int_0^l v'^2dx = 0 \tag{2.12}$$

being $\frac{L_c}{A_c} = \int_0^l \frac{dx}{A(x)\cos^3(\vartheta)}$ the ratio between the *equivalent cable's length* and its area.

Equation (2.12) allows to find an approximate value for the increment of tension in the cable and to solve the problem in closed form.

$$h = \left(\frac{1}{2}\int_0^l v'^2dx - \int_0^l y''v\,dx\right)\frac{E_cA_c}{L_c} = \frac{E_cA_c}{L_c} \cdot \Delta L \tag{2.13}$$

It is worth nothing that the previous expression for the cable's elongation is an approximation, because the complete expression would lead to a contribution of the slope of the cable at the denominator, which is neglected as usual in small perturbations approaches. Anyway it can be demonstrated that this handy expression is on the safe side.

2.2 EXTENSION TO A 2 DOF$_S$ MODEL

The classical deflection theory does not take into account the possibility of a torsional rotation of the deck, which instead can happen in the real bridge's behaviour. The *Total Potential Energy (TPE)* formulation is an useful tool to extend the classical deflection theory to a 2 DoF$_s$ format.

It is worth noting that a more accurate model can be built considering 4 DoF$_s$, where the axial extensibility of the hangers is included. Anyway Luco and Turmo [38] found that the effects of hanger flexibility on the response of a suspension bridge to localized impulsive loads are very small. This justifies the traditional assumption of inextensible hangers and the choice of a model with 2 DoF$_s$.

2.2.1 *TPE Formulation for the SDoF flexural model*

With reference to equation (2.10), it is possible to introduce some useful fundamental quantities, such as the cable's axial strain, its associated tension and the horizontal component of the cable's tension.

$$\varepsilon(s) = \frac{dL}{ds} = \frac{dx\,du}{ds^2} + \frac{dy\,dv}{ds^2} + \frac{dv^2}{2ds^2} = \frac{u' + y'v' + \frac{1}{2}v'^2}{s'^2} = \frac{\tilde{\varepsilon}}{s'^2}$$

$$\tau(s) = E_c A_c \varepsilon(s) = \frac{E_c A_c \tilde{\varepsilon}}{s'^2} \tag{2.14}$$

$$h(x) = \tau(s) \cdot \cos(\vartheta) = \frac{\tau(s)}{s'} = \frac{E_c A_c \tilde{\varepsilon}}{s'^3}$$

The Total Potential Energy variation of the bridge's model starting from the initial equilibrium configuration up to the final perturbed configuration, can be written as:

$$\Delta V(u, v, q) = V(u, y + v, g + q) - V(0, y, g) = E_{deck} + 2E_{cable} - L_{ext} \tag{2.15}$$

where:

1. E_{deck} is the elastic flexural energy stored by the deck;

2. E_{cable} is the elastic energy stored by the cable. It is the sum of two different contributions, one associated to the initial constant tension needed to sustain the self-weight of the deck and one associated to the nonlinear stiffening response of the cable when subjected also to the variable loads;

3. L_{ext} is the external work done by both permanent and variable loads.

The mathematical definition of these three terms is:

$$E_{deck} = \frac{1}{2}\int_0^l M(x)\chi(x)dx = \frac{1}{2}\int_0^l E_d I_d \left(\frac{d^2 v}{dx^2}\right)^2 dx$$

$$E_{cable} = \int_0^{l_c} T(x)\varepsilon(x)ds + \frac{1}{2}\int_0^{l_c} \tau(x)\varepsilon(x)ds = H\int_0^l \tilde{\varepsilon}(x)dx + \frac{1}{2}\int_0^l \frac{E_c A_c \tilde{\varepsilon}^2(x)}{s'^3}dx \qquad (2.16)$$

$$L_{ext} = \int_0^l (g+q)\cdot w dx$$

The Total Potential Energy (2.15) is:

$$\Delta V(u,w,g,q) = \frac{1}{2}\int_0^l E_d I_d w''^2 dx + 2H\int_0^l \left(u' + y'w' + \frac{1}{2}w'^2\right)dx + \int_0^l \frac{E_c A_c}{s'^3}\left(u' + y'w' + \right.$$
$$\left. + \frac{1}{2}w'^2\right)^2 dx - \int_0^l (g+q)\cdot v dx$$

Integrating by parts and enforcing boundary conditions it is possible to extract from the TPE the initial equilibrium configuration of equation (2.2) and to eliminate some terms.

$$H\int_0^l y'w'dx - \int_0^l g\cdot w dx = H[y'v]_0^l - H\int_0^l y''w dx - \int_0^l g\cdot w dx = -\int_0^l (Hy'' + g)w dx = 0$$

Hence the TPE (2.15) can be simplified as follows:

$$\Delta V(u,w,q) = \frac{1}{2}\int_0^l E_d I_d w''^2 dx + 2H\int_0^l \left(u' + \frac{1}{2}w'^2\right)dx + \int_0^l \frac{E_c A_c}{s'^3}\left(u' + y'w' + \right.$$
$$\left. + \frac{1}{2}w'^2\right)^2 dx - \int_0^l q\cdot w dx \qquad (2.17)$$

In order to find the equilibrium position, the stationarity of the variation of the TPE must be enforced with suitable boundary conditions.

Concerning the longitudinal equilibrium equation, the fixed rigid pylons guarantee null horizontal displacements at the top of the tower.

$$u(0) = u(l) = 0 \quad \Rightarrow \quad du(0) = du(l) = 0$$

$$H = const. \quad \Rightarrow \quad H' = 0$$

$$\delta_u V = 2H \int_0^l du' dx + \int_0^l 2 \frac{E_c A_c}{s'^3} \left(u' + y' w' + \frac{1}{2} w'^2 \right) du' dx = 2 \int_0^l (H + h) du' dx =$$

$$2[(H + h)du]_0^l - 2 \int_0^l (H + h)' du dx = -2 \int_0^l h' du dx = 0$$

(2.18)

Hence:

$$h'(x) = 0 \quad \Rightarrow \quad h(x) = const. \tag{2.19}$$

According to this result, being the horizontal increment of tension in the cable constant, the *global (or non local) increment of the cable's tension* can be defined. It is the integral along the length of the cable of $h(x)$ and it is not dependent on the coordinate of the position along the cable.

$$h(w) = \int_0^l h(x) dx = \int_0^l \frac{E_c A_c}{s'^3} \left(u' + y' w' + \frac{1}{2} w'^2 \right) dx = \frac{\overline{E_c A_c}}{L_c} \int_0^l \left(y' w' + \frac{1}{2} w'^2 \right) dx \tag{2.20}$$

being L_c the equivalent cable's length defined in treating with the equation (2.12).

The non local increment of the cable's tension is characteristic of the 2 DoFs model because the hangers are considered perfectly rigid both in tension and in compression, so the cable's stiffening effect has a global distributed effect on all the structure. In a 4 DoFs model, where the axial extensibility of the hangers is considered, the increment of tension in the cable is local and it is dependent on the x coordinate.

With regards to vertical equilibrium equations, boundary conditions associated to a simply supported beam are enough to solve the problem.

$$w(0) = w(l) = 0 \quad \Rightarrow \quad dw(0) = dw(l) = 0$$

$$w''(0) = w''(l) = 0$$

$$H, h(w) = const.$$

$$\delta_w V = \int_0^l E_d I_d w'' dw'' dx + 2H \int_0^l w' dw' dx + \int_0^l \frac{E_c A_c}{s'^3} 2 \left(u' + y' w' + \frac{1}{2} w'^2 \right) (y' +$$

$$+ w') dw' dx - \int_0^l q \cdot dw dx$$

(2.21)

The integration by parts of equation (2.21) and the substitution of the boundary conditions, leads to:

$$\delta_w V = \int_0^l E_d I_d w'' dw'' dx + 2H \int_0^l w' dw' dx + 2h(w) \int_0^l (y' + w') dw' dx - \int_0^l q dw dx =$$
$$[E_d I_d w'' dw']_0^l - \int_0^l (E_d I_d w'')' dw' dx + 2H[w' dw]_0^l - 2H \int_0^l w'' dw dx + 2h(w)[(y' + w') dw]_0^l - 2h(w) \int_0^l (y' + w')' dw dx - \int_0^l q \cdot dw dx = [(E_d I_d w'')' dw]_0^l + \int_0^l (E_d I_d w'')'' dw dx +$$
$$-2H \int_0^l w'' dw dx - 2h(w) \int_0^l (y'' + w'') dw dx - \int_0^l q \cdot dw dx = \int_0^l [(E_d I_d w'')'' - 2(H + h) w'' + -2hy'' - q] dw dx = 0$$

Enforcing the stationarity of the TPE, the equilibrium equation in the perturbed configuration is:

$$(E_d I_d w'')'' - 2(H + h) w'' - 2hy'' = q \qquad (2.22)$$

For the following treatment it is useful to take just the perturbed vertical displacements in the TPE formulation (2.17) and then to extend it to a 2 DoFs model.

$$\Delta V(w, q) = \frac{1}{2} \int_0^l E_d I_d w''^2 dx + 2H \int_0^l \frac{1}{2} w'^2 dx + 2 \left[\frac{1}{2} \int_0^l \frac{E_c A_c}{s'^3} \left(y' w' + \frac{1}{2} w'^2 \right)^2 dx \right] +$$
$$- \int_0^l q \cdot w dx = \int_0^l \left[\frac{1}{2} E_d I_d w''^2 + \frac{1}{2} 2H w'^2 + \int_0^{w'} 2h(w)(y' + w') dw' - q w \right] dx \qquad (2.23)$$

In this SDoF model it is evident that each of the two main cables introduces the same elastic energy in the system. Instead in the 2 DoFs model each cable introduces a different amount of elastic energy because of the difference in the kinematics of the two elements.

2.2.2 *Generalization to 2 DoFs*

A new coordinate taking into account for the rotation of the section of the bridge around its axis is introduced (Figure 2.3) with the aim of extending the classical deflection theory.
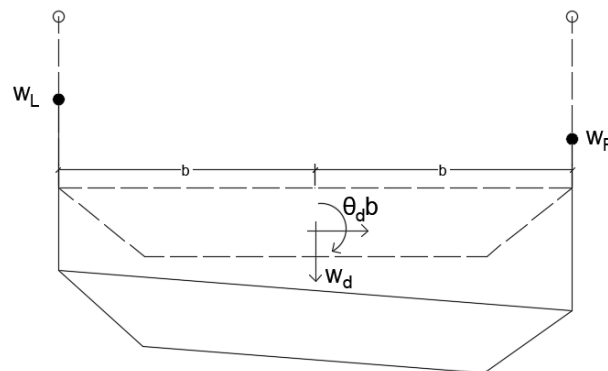
Figure 2.3: 2 dofs kinematic of the deck

Assuming the positive flexural motion when directed downward and the positive torsional rotation when clockwise, the displacements at the two extreme sides can be expressed as:

$$w_R = w_d + \theta_d \cdot b$$
$$w_L = w_d - \theta_d \cdot b$$

(2.24)

The introduction of a new Degree of Freedom introduces additional elastic energy in the system, since this model is more deformable than the previous one. Hence, The TPE (2.15) has one more term related to the torsion of the deck:

$$E_{deck,\theta_d} = \frac{1}{2}\int_0^l G_d J_d \theta_d'^2 dx + \frac{1}{2}\int_0^l E_d \Gamma_d \theta_d''^2 dx$$

(2.25)

where the first term is related to the primary torsion typical of the De Saint Venant theory and the second is related to the warping deformation typical of the Wagner-Vlasov theory. Modern bridges usually have closed box sections which allows to have high torsional rigidity and to neglect the secondary torsional effects. Hence, the warping deformation can be very important in those bridge characterized by very thin decks with I shaped longitudinal beams.

Moreover, the presence of the additional Degree of Freedom allows for the introduction of the associated external action in the external work.

The TPE variation assumes the following mathematical format:

$$\Delta V(w_d, \theta_d, q, m) = \int_0^l \left[\frac{1}{2} E_d I_d w''^2 + \frac{1}{2} E_d \Gamma_d \theta_d''^2 + \frac{1}{2} G_d J_d \theta_d'^2 + \frac{1}{2} H(w_r'^2 + w_L'^2) + \right.$$
$$\left. + \int_0^{w_R'} h(w_R)(y' + w_R') dw_R' + \int_0^{w_L'} h(w_L)(y' + w_L') dw_L' - q w_d - m \theta_d \right] dx$$

(2.26)

where the product between the cable's tension and the square derivative of the displacement can be simplified as:

$$H(w_r'^2 + w_L'^2) = H[(w_d' + \theta_d' b)^2 + (w_d' - \theta_d' b)^2] = H[w_d'^2 + \theta_d'^2 b^2 + 2 w_d' \theta_d' b + w_d'^2 +$$
$$+ \theta_d'^2 b^2 - 2 w_d' \theta_d' b] = 2H(w_d'^2 + \theta_d'^2 b^2)$$

The substitution of this last equation into (2.26) and the zeroing of the first differential of the TPE, leads to:

$$\delta V = \int_0^l [E_d I_d w_d'' dw_d'' + E_d \Gamma_d \theta_d'' d\theta_d'' + G_d J_d \theta_d' d\theta_d' + 2H(w_d' dw_d' + b^2 \theta_d' d\theta_d') + h(w_R)(y' +$$
$$+ w_d' + \theta_d' b) d(w_d' + \theta_d' b) + h(w_L)(y' + w_d' - \theta_d' \cdot b) d(w_d' - \theta_d' b) - q dw_d - m d\theta_d] dx = 0$$

Integrating by parts and substituting the proper boundary conditions, some terms can be deleted and the first differential of the TPE reads:

$$
\delta V = \int_0^l [(E_d I_d w_d'')'' \, dw_d + (E_d \Gamma_d \theta_d'')'' \, d\theta_d'' - (G_d J_d \theta_d')' \, d\theta_d - 2H(w_d'' \, dw_d + b^2 \theta_d'' \, d\theta_d) +
$$
$$
-h(w_R)(y'' + w_d'' + \theta_d'' b) d(w_d + \theta_d b) - h(w_L)(y'' + w_d'' - \theta_d'' b) d(w_d - \theta_d b) - q \, dw_d +
$$
$$
-m \, d\theta_d] \, dx = 0
$$

where according to equation (2.20), the global increment of cable's tension can be written as:

$$
h(w_d \pm \theta_d b) = \frac{\overline{E_c A_c}}{L_c} \int_0^l \left(y'(w_d' \pm \theta_d' b) + \frac{1}{2}(w_d' \pm \theta_d' b)^2 \right) dx = \frac{\overline{E_c A_c}}{L_c} \int_0^l \left[\left(y' w_d' + \frac{w_d'^2}{2} \right) +
$$
$$
-(y' \theta_d' b + w_d' \theta_d' b) + \left(\frac{\theta_d'^2}{2} b^2 \right) \right] dx
$$

so:

$$
h(w_d \pm \theta_d b) = h_w \pm h_{w\theta} + h_\theta \tag{2.27}
$$

having defined the following parameters:

$$
h_w = \frac{\overline{E_c A_c}}{L_c} \int_0^l \left(-y'' w_d + \frac{w_d'^2}{2} \right) dx
$$

$$
h_{w\theta} = \frac{\overline{E_c A_c}}{L_c} \int_0^l (-y'' \theta_d b + w_d' \theta_d' b) \, dx \tag{2.28}
$$

$$
h_\theta = \frac{\overline{E_c A_c}}{L_c} \int_0^l \left(\frac{\theta_d'^2}{2} b^2 \right) dx
$$

Some terms inside the equation for the variation of the TPE can be rewritten in a more compact form as:

$$
h(w_d + \theta_d b)(y'' + w_d'' + \theta_d'' b) d(w_d + \theta_d b) + h(w_d - \theta_d b)(y'' + w_d'' - \theta_d'' b) d(w_d - \theta_d b) =
$$
$$
2\{[(h_w + h_\theta)(y'' + w_d'') + h_{w\theta} b \theta_d''] dw_d + [(h_w + h_\theta) b^2 \theta_d'' + h_{w\theta} b(y'' + w_d'')] d\theta_d\}
$$

The substitution of this last expression into the first differential of the TPE leads to:

$$
\delta V = \int_0^l \{[(E_d I_d w_d'')'' - 2H w_d'' - 2(h_w + h_\theta)(y'' + w_d'') - 2h_{w\theta} b \theta_d'' - q] dw_d +
$$
$$
+[(E_d \Gamma_d \theta_d'')'' - (G_d J_d \theta_d')' - 2H b^2 \theta_d'' - 2(h_w + h_\theta) b^2 \theta_d'' - 2h_{w\theta} b(y'' + w_d'') + \tag{2.29}
$$
$$
-m]\} dx = 0
$$

To satisfy the condition of null TPE variation (2.29) each of the two terms inside the brackets must be equal to zero. This leads to a self-adjoint system representing the static equilibrium of the structural system.

$$(E_d I_d w_d'')'' - 2H w_d'' - 2(h_w + h_\theta)(y'' + w_d'') - 2h_{w\theta} b \theta_d'' = q \tag{2.30}$$

$$(E_d \Gamma_d \theta_d'')'' - (G_d J_d \theta_d')' - 2H b^2 \theta_d'' - 2(h_w + h_\theta) b^2 \theta_d'' - 2h_{w\theta} b (y'' + w_d'') = m \tag{2.31}$$

In order to extend the equations of motion to the dynamic field it is simply necessary to add the inertial terms. Moreover, for the sake of simplicity it is assumed to consider constant values for the section properties of both the cables and the deck.

$$(m_d + 2m_c)\ddot{w}_d(x,t) + E_d I_d w_d'^v(x,t) - 2H w_d''(x,t) - 2(h_w + h_\theta)(y'' + w_d''(x,t)) + \\ -2h_{w\theta} b \theta_d''(x,t) = q(x,t) \tag{2.32}$$

$$(J_t + 2m_c b^2)\ddot{\theta}_d(x,t) + E_d \Gamma_d \theta_d'^v(x,t) - G_d J_d \theta_d''(x,t) - 2H b^2 \theta_d''(x,t) - 2(h_w + \\ +h_\theta)b^2\theta_d''(x,t) - 2h_{w\theta} b(y'' + w_d''(x,t)) = m(x,t) \tag{2.33}$$

The two equations of motion obtained are nonlinear due to the presence of the global increment of the cable's tension (2.27).

Furthermore, the two equations are coupled, always due to the presence of the non local cable's stiffening term. It is usual in nonlinear mechanics to have coupled system of equations.

It is important to separate the terms with different order of magnitude in order to find the degree of nonlinearity and to have an estimate of the degree of coupling of the system. To do this and to estimate the parameters affecting the problem, the equations of motion can be written in non-dimensional format.

2.3 NON-DIMENSIONAL FORMAT

The first passage to do is to introduce some fundamental non-dimensional quantities.

$$\xi = \frac{x}{l} \qquad\qquad \text{Non-dimensional space parameter}$$

$$\widetilde{w}_d(\xi, \tau) = \frac{w_d(x,t)}{f} \qquad \text{Non-dimensional flexural DoF} \tag{2.34}$$

$$\tilde{\theta}_d(\xi, \tau) = \frac{\theta_d(x,t) \cdot b}{f} \qquad \text{Non-dimensional torsional DoF}$$

where the non-dimensional time parameter τ will be defined in the following. Let us expand some terms before considering the complete equations of motion.

$$(h_w + h_\theta)(y'' + w_d'') = h_w y'' + h_w w_d'' + h_\theta y'' + h_\theta w_d'' = \frac{E_c A_c}{L_c}\left[y'' \int_0^l \left(-y'' w_d + \frac{w_d'^2}{2}\right) dx + \right.$$

$$w_d'' \int_0^l \left(-y'' w_d + \frac{w_d'^2}{2}\right) dx + y'' \int_0^l \left(\frac{\theta_d'^2}{2} b^2\right) dx + w_d'' \int_0^l \left(\frac{\theta_d'^2}{2} b^2\right) dx\right] = \frac{E_c A_c}{L_c}\left[-y''^2 fl \int_0^1 \widetilde{w}_d \, d\xi + \right.$$

$$\frac{1}{2} y'' \frac{f^2}{l} \int_0^1 \widetilde{w}_d'^2 \, d\xi - y'' \widetilde{w}_d'' \frac{f^2}{l} \int_0^1 \widetilde{w}_d \, d\xi + \frac{1}{2} \widetilde{w}_d'' \frac{f^3}{l^3} \int_0^1 \widetilde{w}_d'^2 \, d\xi + \frac{1}{2} y'' \frac{f^2}{l} \int_0^1 \widetilde{\theta}_d'^2 \, d\xi + $$

$$\left. \frac{1}{2} \widetilde{w}_d'' \frac{f^3}{l^3} \int_0^1 \widetilde{\theta}_d'^2 \, d\xi\right]$$

$$h_{w\theta} b\theta_d'' = \frac{E_c A_c}{L_c} b\theta_d'' \int_0^l (-y'' \theta_d b + w_d' \theta_d' b) \, dx = \frac{E_c A_c}{L_c}\left[-\widetilde{\theta}_d'' y'' \frac{f^2}{l} \int_0^1 \widetilde{\theta}_d \, d\xi + \widetilde{\theta}_d'' \frac{f^3}{l^3} \int_0^1 \widetilde{w}_d' \, \widetilde{\theta}_d' d\xi\right]$$

$$(h_w + h_\theta) b^2 \theta_d'' = \frac{E_c A_c}{L_c}\left[b^2 \theta_d'' \int_0^l \left(-y'' w_d + \frac{w_d'^2}{2}\right) dx + b^2 \theta_d'' \int_0^l \left(\frac{\theta_d'^2}{2} b^2\right) dx\right] = $$

$$\frac{E_c A_c}{L_c}\left[-\widetilde{\theta}_d'' y'' \frac{f}{l} b \int_0^1 \widetilde{w}_d \, d\xi + \frac{1}{2} \widetilde{\theta}_d'' \frac{f^3}{l^3} b \int_0^1 \widetilde{w}_d'^2 \, d\xi + \frac{1}{2} \widetilde{\theta}_d'' \frac{f^3}{l^3} b \int_0^1 \widetilde{\theta}_d'^2 \, d\xi\right]$$

$$h_{w\theta} b(y'' + w_d'') = \frac{E_c A_c}{L_c}\left[y'' b \int_0^l(-y'' \theta_d b + w_d' \theta_d' b) \, dx + b w_d'' \int_0^l(-y'' \theta_d b + w_d' \theta_d' b) \, dx\right] = $$

$$\frac{E_c A_c}{L_c}\left[-y''^2 fbl \int_0^1 \widetilde{\theta}_d \, d\xi + y'' \frac{f^2}{l} b \int_0^1 \widetilde{w}_d' \, \widetilde{\theta}_d' d\xi - y'' \widetilde{w}_d'' \frac{f}{l} b \int_0^1 \widetilde{\theta}_d \, d\xi + \widetilde{w}_d'' \frac{f^3}{l^3} b \int_0^1 \widetilde{w}_d' \, \widetilde{\theta}_d' d\xi\right]$$

2.3.1 *Flexural equation of motion*

Substituting the previous expressions into the flexural equation of motion (2.32):

$$(m_d + 2m_c)f \frac{d^2 \widetilde{w}_d}{dt^2} + E_d I_d \widetilde{w}_d'^v \frac{f}{l^4} - 2H \frac{f}{l^2} \widetilde{w}_d'' - 2\frac{E_c A_c}{L_c}\left(-y''^2 fl \int_0^1 \widetilde{w}_d \, d\xi + \frac{1}{2} y'' \frac{f^2}{l} \int_0^1 \widetilde{w}_d'^2 \, d\xi + \right.$$

$$-y'' \widetilde{w}_d'' \frac{f^2}{l} \int_0^1 \widetilde{w}_d \, d\xi + \frac{1}{2} \widetilde{w}_d'' \frac{f^3}{l^3} \int_0^1 \widetilde{w}_d'^2 \, d\xi + \frac{1}{2} y'' \frac{f^2}{l} \int_0^1 \widetilde{\theta}_d'^2 \, d\xi + \frac{1}{2} \widetilde{w}_d'' \frac{f^3}{l^3} \int_0^1 \widetilde{\theta}_d'^2 \, d\xi + $$

$$\left. -\widetilde{\theta}_d'' y'' \frac{f^2}{l} \int_0^1 \widetilde{\theta}_d \, d\xi + \widetilde{\theta}_d'' \frac{f^3}{l^3} \int_0^1 \widetilde{w}_d' \, \widetilde{\theta}_d' d\xi\right) = q$$

where the prime indicates the derivative with respect to ξ.

Collecting the terms associated to the initial tension in the cable $2H\frac{f}{l^2}$:

$$(m_d + 2m_c)\frac{l^2}{2H} \frac{d^2 \widetilde{w}_d}{dt^2} + \frac{E_d I_d}{2Hl^2} \widetilde{w}_d'^v - \widetilde{w}_d'' + \frac{E_c A_c}{H} \frac{l}{L_c}(y'' l)^2 \int_0^1 \widetilde{w}_d \, d\xi - \frac{1}{2}\frac{E_c A_c}{H} \frac{l}{L_c} y'' f \int_0^1 \widetilde{w}_d'^2 \, d\xi + $$

$$+\frac{E_c A_c}{H} \frac{l}{L_c} y'' f \widetilde{w}_d'' \int_0^1 \widetilde{w}_d \, d\xi - \frac{1}{2}\frac{E_c A_c}{H} \frac{l}{L_c}\left(\frac{f}{l}\right)^2 \widetilde{w}_d'' \int_0^1 \widetilde{w}_d'^2 \, d\xi - \frac{1}{2}\frac{E_c A_c}{H} \frac{l}{L_c} y'' f \int_0^1 \widetilde{\theta}_d'^2 \, d\xi + $$

$$-\frac{1}{2}\frac{E_c A_c}{H} \frac{l}{L_c}\left(\frac{f}{l}\right)^2 \widetilde{w}_d'' \int_0^1 \widetilde{\theta}_d'^2 \, d\xi + \frac{E_c A_c}{H} \frac{l}{L_c} y'' f \widetilde{\theta}_d'' \int_0^1 \widetilde{\theta}_d \, d\xi - \frac{E_c A_c}{H} \frac{l}{L_c}\left(\frac{f}{l}\right)^2 \widetilde{\theta}_d'' \int_0^1 \widetilde{w}_d' \, \widetilde{\theta}_d' d\xi = \frac{l^2}{2Hf} q$$

Others non-dimensional parameters can be introduced in this last expression.

$$\tau = \frac{t}{l}\sqrt{\frac{2H}{m_d + 2m_c}} \qquad \text{Non-dimensional time parameter}$$

$$\tilde{q}(\xi,\tau) = \frac{l^2}{2Hf}q(x,t) \qquad \text{Non-dimensional equivalent flexural external forcing}$$

$$\mu^2 = \frac{E_d I_d}{2H l^2} \qquad \text{Steinman's stiffness factor}$$

$$\lambda_1{}^2 = \frac{E_c A_c}{H}\frac{l}{L_c}(y''l)^2 \qquad \text{First order Irvine's parameter}$$

$$\lambda_2{}^2 = -\frac{E_c A_c}{H}\frac{l}{L_c}y''f \qquad \text{Second order Irvine's parameter}$$

$$\lambda_3{}^2 = \frac{E_c A_c}{H}\frac{l}{L_c}\left(\frac{f}{l}\right)^2 \qquad \text{Third order Irvine's parameter}$$

(2.35)

The Steinman's stiffness factor is the ratio between the deck and the cables flexural stiffness. It reflects the weight of each contribution in the whole flexural stiffness of the bridge.

The Irvine's parameters measure the extensibility of the cables compared to the initial tension needed to sustain the self-weight of the suspended deck. Each one of them multiply respectively the linear, the quadratic and the cubic terms of the deck configuration.

Thanks to the hypothesis of initial parabolic shape of the cable, it is possible to estimate the influence of the nonlinear terms, indeed being $y'' = -\frac{8f}{l^2}$, then:

$$\lambda_1{}^2 = 64\frac{E_c A_c}{H}\frac{l}{L_c}\left(\frac{f}{l}\right)^2$$

$$\lambda_2{}^2 = 8\frac{E_c A_c}{H}\frac{l}{L_c}\left(\frac{f}{l}\right)^2$$

$$\lambda_3{}^2 = \frac{E_c A_c}{H}\frac{l}{L_c}\left(\frac{f}{l}\right)^2$$

From the previous statement it is evident that $\lambda_1{}^2 = 8\lambda_2{}^2 = 64\lambda_3{}^2$. Hence higher order terms are order of magnitude less than the linear ones. It is possible to state that the model assumed for the suspension bridge is characterised by *soft nonlinearities*. The reason of this is hidden in the assumption of inextensible hangers. In fact, considering a 4 DoFs model, with the axial extensibility of the hangers and taking into account the possibility for them to slack, stronger nonlinearities would arise because of the different behaviour in tension and in compression of the hangers themselves.

Introducing also:

$$\tilde{h}_w = \int_0^1 \widetilde{w}_d \, d\xi$$

$$\tilde{h}_\theta = \int_0^1 \tilde{\theta}_d \, d\xi$$

$$\tilde{h}_{w'w'} = \int_0^1 \widetilde{w}_d'^2 \, d\xi \tag{2.36}$$

$$\tilde{h}_{\theta'\theta'} = \int_0^1 \tilde{\theta}_d'^2 \, d\xi$$

$$\tilde{h}_{w'\theta'} = \int_0^1 \widetilde{w}_d' \, \tilde{\theta}_d' \, d\xi$$

The flexural equation of motion (2.32) can be rewritten in non-dimensional format as:

$$\frac{d^2\widetilde{w}_d}{d\tau^2} + \mu^2 \cdot \widetilde{w}_d'^v - \widetilde{w}_d'' + \lambda_1^2 \cdot \tilde{h}_w - \lambda_2^2 \cdot \left[\tilde{h}_w \cdot \widetilde{w}_d'' + \tilde{h}_\theta \cdot \tilde{\theta}_d'' - \frac{1}{2}\left(\tilde{h}_{w'w'} + \tilde{h}_{\theta'\theta'}\right)\right] +$$
$$-\lambda_3^2 \left[\frac{1}{2}\left(\tilde{h}_{w'w'} + \tilde{h}_{\theta'\theta'}\right) \cdot \widetilde{w}_d'' + \tilde{h}_{w'\theta'} \cdot \tilde{\theta}_d''\right] = \tilde{q} \tag{2.37}$$

2.3.2 *Torsional equation of motion*

The same passages can be done also for the torsional equation of motion (2.33) in which, firstly the non-dimensional quantities introduced in (2.34) are substituted into it and secondly the terms related to the initial tension in the cable $2H\frac{fb}{l^2}$ are collected.

$$(J_t + 2m_c b^2)\frac{f}{b}\frac{d^2\tilde{\theta}_d}{dt^2} + \frac{E_d\Gamma_d}{2Hb^2l^2}\tilde{\theta}_d'^v - \frac{G_d J_d}{2Hb^2}\tilde{\theta}_d'' - \tilde{\theta}_d'' + \frac{E_c A_c}{H}\frac{l}{L_c}y''f\tilde{\theta}_d''\int_0^1 \widetilde{w}_d \, d\xi +$$
$$-\frac{1}{2}\frac{E_c A_c}{H}\frac{l}{L_c}\left(\frac{f}{l}\right)^2\tilde{\theta}_d''\int_0^1 \widetilde{w}_d'^2 \, d\xi - \frac{1}{2}\frac{E_c A_c}{H}\frac{l}{L_c}\left(\frac{f}{l}\right)^2\tilde{\theta}_d''\int_0^1 \tilde{\theta}_d'^2 \, d\xi + \frac{E_c A_c}{H}\frac{l}{L_c}(y''l)^2\int_0^1 \tilde{\theta}_d \, d\xi +$$
$$-\frac{E_c A_c}{H}\frac{l}{L_c}y''f\int_0^1 \widetilde{w}_d' \, \tilde{\theta}_d' \, d\xi + \frac{E_c A_c}{H}\frac{l}{L_c}y''f\widetilde{w}_d''\int_0^1 \tilde{\theta}_d \, d\xi - \frac{E_c A_c}{H}\frac{l}{L_c}\left(\frac{f}{l}\right)^2\widetilde{w}_d''\int_0^1 \widetilde{w}_d' \, \tilde{\theta}_d' \, d\xi = \frac{l^2}{2Hfb}m$$

Other few non-dimensional terms must be defined:

$$\tilde{J}_t = \frac{(J_t + 2m_c b^2)}{(m_d + 2m_c)b^2} = \left(\frac{\rho_d}{b}\right)^2 \qquad \text{Non-dimensional torsional inertia}$$

$$\tilde{m} = \frac{l^2}{2Hfb}m \qquad \text{Non-dimensional external torsional moment}$$

$$\beta^2 = \frac{G_d J_d}{2Hb^2} \qquad \text{Ratio between the primary torsional stiffness and the torsional stiffness given by the two cables} \tag{2.38}$$

$$\gamma^2 = \frac{E_d\Gamma_d}{2Hb^2l^2} = \frac{\beta^2}{\chi^2} \qquad \text{Ratio between the warping torsional stiffness and the torsional stiffness given by the two cables}$$

$$\chi^2 = \frac{G_d J_d l^2}{E_d\Gamma_d} \qquad \text{Warping coefficient}$$

The torsional equation of motion (2.33) can be rewritten in non-dimensional format as:

$$\tilde{J}_t \cdot \frac{d^2\tilde{\theta}_d}{d\tau^2} + \frac{\beta^2}{\chi^2} \cdot \tilde{\theta}_d''^v - (1+\beta^2) \cdot \tilde{\theta}_d'' + \lambda_1^2 \cdot \tilde{h}_\theta - \lambda_2^2 \cdot \left[\tilde{h}_\theta \cdot \tilde{w}_d'' + \tilde{h}_w \cdot \tilde{\theta}_d'' - \tilde{h}_{w'\theta'}\right] +$$
$$- \lambda_3^2 \left[\tilde{h}_{w'\theta'} \cdot \tilde{w}_d'' + \frac{1}{2}\left(\tilde{h}_{w'w'} + \tilde{h}_{\theta'\theta'}\right) \cdot \tilde{\theta}_d''\right] = \tilde{m} \tag{2.39}$$

It is evident from (2.37) and (2.39) that the equations of motion are nonlinear up to the third order. Moreover only the higher order terms couple the flexural with the torsional equation and vice-versa. This is an important feature of the structural system which becomes completely uncoupled when linearized. Being the linearized structural system uncoupled, the principle of superposition of the effects is valid and a modal analysis can be performed separately on the two equations, so as to find the structural frequencies and modes of vibration.

2.3.3 *Structural Damping*

The previous flexural and torsional equations of motion (2.37) and (2.39) have been written without taking into account for the effect of the structural damping which in reality is present in every structure. A linear viscous damping component can be introduced in the equations of motion:

$$\frac{d^2\tilde{w}_d}{d\tau^2} + \tilde{c}_w \frac{d\tilde{w}_d}{d\tau} + \mu^2 \tilde{w}_d''^v - \tilde{w}_d'' + \lambda_1^2 \tilde{h}_w - \lambda_2^2\left[\tilde{h}_w \tilde{w}_d'' + \tilde{h}_\theta \tilde{\theta}_d'' - \frac{1}{2}\left(\tilde{h}_{w'w'} + \tilde{h}_{\theta'\theta'}\right)\right] +$$
$$- \lambda_3^2 \left[\frac{1}{2}\left(\tilde{h}_{w'w'} + \tilde{h}_{\theta'\theta'}\right)\tilde{w}_d'' + \tilde{h}_{w'\theta'}\tilde{\theta}_d''\right] = \tilde{q} \tag{2.40}$$

$$\tilde{J}_t \frac{d^2\tilde{\theta}_d}{d\tau^2} + \tilde{c}_\theta \frac{d\tilde{\theta}_d}{d\tau} + \frac{\beta^2}{\chi^2}\tilde{\theta}_d''^v - (1+\beta^2)\tilde{\theta}_d'' + \lambda_1^2\tilde{h}_\theta - \lambda_2^2\left[\tilde{h}_\theta\tilde{w}_d'' + \tilde{h}_w\tilde{\theta}_d'' - \tilde{h}_{w'\theta'}\right] +$$
$$- \lambda_3^2 \left[\tilde{h}_{w'\theta'}\tilde{w}_d'' + \frac{1}{2}\left(\tilde{h}_{w'w'} + \tilde{h}_{\theta'\theta'}\right)\tilde{\theta}_d''\right] = \tilde{m} \tag{2.41}$$

where the new parameters introduced $\tilde{c}_w$ and $\tilde{c}_\theta$ are the non-dimensional damping parameters which can be defined, starting from the dimensional linear damping, as:

$$c_w \frac{dw_d}{dt} = c_w \frac{f}{l}\sqrt{\frac{2H}{m_d + 2m_c}}\frac{l^2}{2Hf}\frac{d\tilde{w}_d}{d\tau} = c_w \frac{l}{\sqrt{2H(m_d + 2m_c)}}\frac{d\tilde{w}_d}{d\tau} = \tilde{c}_w \frac{d\tilde{w}_d}{d\tau}$$

$$c_\theta \frac{d\theta_d}{dt} = c_\theta \frac{f}{bl}\sqrt{\frac{2H}{m_d + 2m_c}}\frac{l^2}{2Hfb}\frac{d\tilde{\theta}_d}{d\tau} = c_\theta \frac{l}{b^2\sqrt{2H(m_d + 2m_c)}}\frac{d\tilde{\theta}_d}{d\tau} = \tilde{c}_\theta \frac{d\tilde{\theta}_d}{d\tau} \tag{2.42}$$

2.4 MODAL SUPERPOSITION ANALYSIS

Modal analysis is a simple separation of variable process which allows to study the problem in two different spaces, permitting to pass from partial differential equations to ordinary ones. Being based on the superposition principle, the modal analysis can be applied only to linear equations of motion. Hence, only the linear components are held in the equations of motion, leading to an uncoupled system. The flexural and torsional structural behaviour of the structure can be therefore studied separately. Moreover since the objective of this study is to define the structural properties, the external forcing terms do not affect the modal response of the structure and they have not to be considered.

2.4.1 Flexural Modes of Vibration

For the flexural modes the decomposition can be written as:

$$\widetilde{w}_d(\xi,\tau) = \sum_{n=1}^{+\infty} W_n(\xi) \cdot z_n(\tau) \tag{2.43}$$

where $W_n(\xi)$ is the flexural modal shape and the time function varies exponentially according to the Euler formula:

$$z_n(\tau) = Z_n \exp\left(i \cdot \tilde{\Omega}_{w,n} \cdot \tau\right) + Z_n^* \exp\left(-i \cdot \tilde{\Omega}_{w,n} \cdot \tau\right) \tag{2.44}$$

The complex conjugate Z_n^* is a necessary quantity in order to obtain a real value of the time varying function, which otherwise would be a complex quantity, in fact:

$$z_n(\tau) = (Z_n^R + iZ_n^I)\left[\cos(\tilde{\Omega}_{w,n} \cdot \tau) + i \cdot \sin(\tilde{\Omega}_{w,n} \cdot \tau)\right] + (Z_n^R - iZ_n^I)\left[\cos(\tilde{\Omega}_{w,n} \cdot \tau) - i \cdot \sin(\tilde{\Omega}_{w,n} \cdot \tau)\right] = 2\left[Z_n^R \cos(\tilde{\Omega}_{w,n} \cdot \tau) - Z_n^I \sin(\tilde{\Omega}_{w,n} \cdot \tau)\right] = \bar{Z}_n \cos(\tilde{\Omega}_{w,n} \cdot \tau + \varphi_{w,n})$$

being:

$$\bar{Z}_n = 2\sqrt{(Z_n^R)^2 + (Z_n^I)^2}$$

$$\tan(\varphi_{w,n}) = \frac{Z_n^I}{Z_n^R} \tag{2.45}$$

$$\tilde{\Omega}_{w,n} = \Omega_{w,n} l \sqrt{\frac{m_d + 2m_c}{2H}}$$

The amplitude of oscillations becomes a real quantity when the imaginary terms are considered, that is the same to introduce a phase lag. Considering this the response of the structure can change when superimposing the different flexural and torsional motions. Moreover the time function contains a non-dimensional term related to the circular Eigen-frequency of each specific mode.

The introduction of the modal decomposition of equation (2.43) in the linearized undamped flexural equation of motion of the free vibrating system leads to:

$$\sum_{n=1}^{+\infty} \left(-\tilde{\Omega}_{w,n}^2 W_n(\xi) + \mu^2 W_n'^v(\xi) - W_n''(\xi) + \lambda_1^2 \tilde{h}_{W,n} \right) \cdot z_n(\tau) = 0 \qquad (2.46)$$

In order to satisfy the dynamic equilibrium at each instant of time, the spatial-dependent term inside the bracket must be null. The resulting equation is a fourth order differential equation which can be solved in order to find the two unknowns of the problem, namely the modal shapes and the associated circular Eigen-frequencies. Of course, the solvability of the spatial 4th order ODE is grant only if four proper boundary conditions are applied at the extremes of the interval. The model considered is the one of a simply supported beam and therefore, null vertical displacements and null moments are imposed at the extremes of the bridge.

The analytical procedure allows to find particular conditions that a numerical approach can neglect. First of all a distinction between symmetric and skew-symmetric modes has to be made.

Skew-Symmetric modes

In correspondence of even wave numbers the linear contribution to cable's elongation vanishes, therefore the stiffening term $\tilde{h}_{W,n}$ is null and the 4th order spatial ODE to be solved is:

$$-\tilde{\Omega}_{w,n}^2 W_n(\xi) + \mu^2 W_n'^v(\xi) - W_n''(\xi) = 0 \qquad (2.47)$$

This is the classical equation of motion of a simply supported Euler-Bernoulli beam, which solution is represented by a sinusoidal motion with even number of half waves.

$$W_n(\xi) = sin(n \cdot \pi \cdot \xi) \quad (n = 2,4,6,\dots) \qquad (2.48)$$

A posteriori it is easy to demonstrate that the stiffening term is effectively null for each choice of half wave number, in fact:

$$\tilde{h}_{W,n} = \int_0^1 W_n(\xi)d\xi = -\frac{1}{2\pi}(cos(\pi \cdot n) - 1) = 0 \quad (\forall n = 2,4,6,\dots) \qquad (2.49)$$

Once that the modal shapes have been determined, the remaining unknowns are the circular Eigen-frequencies, which can be found substituting the modal shapes (2.48) inside the ODE to be solved (2.47).

$$\left(-\tilde{\Omega}_{w,n}^2 + \mu^2 \cdot (n\pi)^4 + (n\pi)^2\right) \cdot \sin(n \cdot \pi \cdot \xi) = 0 \tag{2.50}$$

Hence, the modal Eigen-frequencies are:

$$\tilde{\Omega}_{w,n} = n\pi\sqrt{1 + \mu^2(n\pi)^2} \quad (n = 2,4,6,\dots) \tag{2.51}$$

Symmetric Modes

In the case of symmetric modes, the cable's stiffening term does not vanish and it affects the bridge's flexural response. The equation to be solved is a complete ode in the spatial variable, which solution can be expressed as a combination of an homogeneous and a particular integral.

$$-\tilde{\Omega}_{w,n}^2 W_n(\xi) + \mu^2 W_n^{\prime v}(\xi) - W_n^{\prime\prime}(\xi) + \lambda_1^2 \tilde{h}_{W,n} = 0 \tag{2.52}$$

Being the stiffening term constant, also the particular solution must be a constant because it has to solve by itself the complete ODE without any need for boundary conditions.

$$W_{n,p}(\xi) = C_n = \frac{\lambda_1^2 \tilde{h}_{W,n}}{\tilde{\Omega}_{w,n}^2} \tag{2.53}$$

This is an implicit solution, because the stiffening term is dependent on the complete solution for the modal shape.

To find the homogeneous solution of an ODE with constant coefficients, the Euler method is used. It consists in writing the solution as a superposition of four exponential terms, multiplied by constant coefficients which have to be found enforcing the boundary conditions.

$$W_{n,0}(\xi) = \sum_{n=1}^{4} C_{n,i} \cdot \exp(\alpha_{n,i} \cdot \xi) \tag{2.54}$$

The substitution of the assumed solution (2.54) in the homogeneous ODE with constant coefficient (2.52) leads to:

$$\sum_{n=1}^{4} C_{n,i} \cdot \left(\mu^2 \cdot \alpha_{n,i}^4 - \alpha_{n,i}^2 - \tilde{\Omega}_{w,n}^2\right) \cdot \exp(\alpha_{n,i} \cdot \xi) = 0 \tag{2.55}$$

The solution of equation (2.55), independent on i and n, is:

$$\alpha_{n,i}^2 = \frac{1}{2\mu^2}\left(1 \pm \sqrt{1 + 4\mu^2\tilde{\Omega}_{w,n}^2}\right) \tag{2.56}$$

For the sake of simplicity it is useful to express the solution by means of the two coefficients defined below.

$$\eta_{w,n}^2 = \frac{1}{2\mu^2}\left(\sqrt{1 + 4\mu^2\tilde{\Omega}_{w,n}^2} - 1\right)$$

$$\Psi_{w,n}^2 = \frac{1}{2\mu^2}\left(\sqrt{1 + 4\mu^2\tilde{\Omega}_{w,n}^2} + 1\right) = \eta_{w,n}^2 + \frac{1}{\mu^2} \tag{2.57}$$

The modal shape is the superposition of the homogeneous and the particular solution.

$$W_n(\xi) = W_{n,0}(\xi) + W_{n,p}(\xi) = \left(\frac{\lambda_1^2\tilde{h}_{W,n}}{\tilde{\Omega}_{w,n}^2} + C_{n,1} \cdot \exp\left(\Psi_{w,n}\xi\right) + C_{n,2} \cdot \right.$$

$$\left. \exp\left(-\Psi_{w,n}\xi\right) + C_{n,3} \cdot \exp\left(i \cdot \eta_{w,n}\xi\right) + C_{n,4} \cdot \exp\left(-i \cdot \eta_{w,n}\xi\right)\right) \tag{2.58}$$

It is clear that the modal shapes are real, being formed by a complex combination of sine and cosine spatial functions which together are a complex conjugate number.

Enforcing the boundary conditions to find the coefficients appearing in equation (2.58) and exploiting some trigonometric relationships, the solution for the modal shapes is:

$$W_n(\xi) = \frac{\lambda_1^2\tilde{h}_{W,n}}{\tilde{\Omega}_{w,n}^2}\left[1 - \frac{1}{\Psi_{w,n}^2 + \eta_{w,n}^2}\left(\eta_{w,n}^2 \cdot \frac{\cosh\left(\Psi_{w,n}\left(\xi - \frac{1}{2}\right)\right)}{\cosh\left(\frac{\Psi_{w,n}}{2}\right)} + \Psi_{w,n}^2 \cdot \frac{\cos\left(\eta_{w,n}\left(\xi - \frac{1}{2}\right)\right)}{\cos\left(\frac{\eta_{w,n}}{2}\right)}\right)\right] \tag{2.59}$$

All the passages to arrive to this solution are described in Appendix A.

The actual expression is again implicit because of the presence of the cable's stiffening term that depends itself on the modal shape. But since the Eigen-modes have to be normalised with respect to the maximum value of the deflection, it is not important to consider the cable's stiffening contribution. However, the problem is that the modal shape remains unknown because the parameters inside the bracket are function of the unknown circular Eigen-frequency. In order to solve this problem it is important to recall the definition of the stiffening term due to cable's elongation, from which it is possible to compute the circular Eigen-frequencies associated to the symmetrical flexural modal shapes.

$$\tilde{h}_{W,n} = \int_0^1 W_n(\xi)d\xi = \frac{\lambda_1^2 \tilde{h}_{W,n}}{\tilde{\Omega}_{w,n}^2} \cdot \int_0^1 \left[1 - \frac{1}{\Psi_{w,n}^2 + \eta_{w,n}^2} \cdot \left(\eta_{w,n}^2 \cdot \frac{\cosh\left(\Psi_{w,n}\left(\xi - \frac{1}{2}\right)\right)}{\cosh\left(\frac{\Psi_{w,n}}{2}\right)} + \Psi_{w,n}^2 \cdot \right. \right.$$
$$\left. \left. \frac{\cos\left(\eta_{w,n}\left(\xi - \frac{1}{2}\right)\right)}{\cos\left(\frac{\eta_{w,n}}{2}\right)} \right) \right] d\xi \tag{2.60}$$

The stiffening term can be cancelled out from the equation to find the general Eigen-function of the problem

$$\frac{\tilde{\Omega}_{w,n}^2}{\lambda_1^2} - 1 + \frac{1}{\Psi_{w,n}^2 + \eta_{w,n}^2} \left(\eta_{w,n}^2 \cdot \frac{\tanh\left(\frac{\Psi_{w,n}}{2}\right)}{\frac{\Psi_{w,n}}{2}} + \Psi_{w,n}^2 \cdot \frac{\tan\left(\frac{\eta_{w,n}}{2}\right)}{\frac{\eta_{w,n}}{2}} \right) = 0 \tag{2.61}$$

This expression is again implicit, but it can be solved numerically by means of simple methods to find the zeros of a non-linear function, e.g. the bisection method. It's important to underline the fact that this Eigen-function is able to capture all the symmetrical flexural modes since it has an infinite number of zeros. However, the complexity of the root finding grows with the order of the mode because the continuous branch of the solution tends to move the zero nearer and nearer to the discontinuity points. Since each Eigen-frequency is in between two asymptotes, it is not difficult to find the correct solution. As an example, the Eigen-function for the first five symmetric modes of the Tacoma Narrows Bridge is depicted in Figure 2.4.
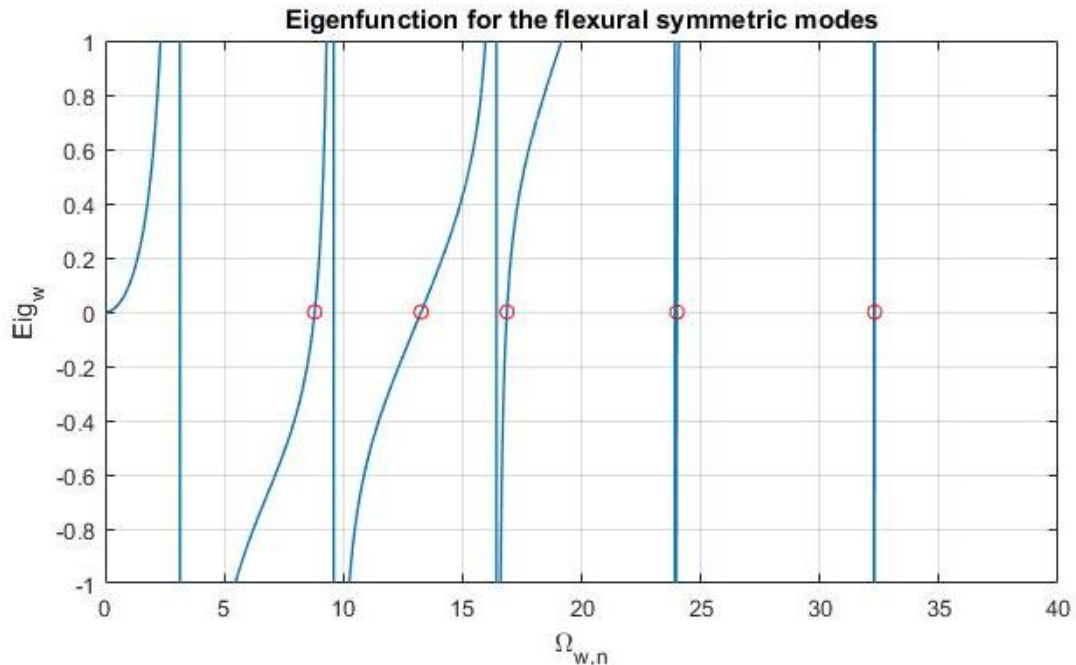

Figure 2.4: Eigen-function for the first five symmetric modes of the Tacoma Narrows Bridge

2.4.2 *Torsional Modes of Vibration*

The treatment for determining the torsional oscillations modes is completely analogous to the passages already done for the flexural counterpart. So the first passage to do is to introduce the modal decomposition for the torsional non-dimensional rotation:

$$\tilde{\theta}_d(\xi,\tau) = \sum_{m=1}^{+\infty} \Theta_m(\xi) \cdot \gamma_m(\tau) \tag{2.62}$$

with the time varying function defined as:

$$\gamma_m(\tau) = \Gamma_m \exp\left(i \cdot \tilde{\Omega}_{\theta.m} \cdot \tau\right) + \Gamma_m^* \exp\left(-i \cdot \tilde{\Omega}_{\theta,m} \cdot \tau\right) = \bar{\Gamma}_m \cos\left(\tilde{\Omega}_{\theta,m} \cdot \tau + \varphi_{\theta,m}\right) \tag{2.63}$$

where:

$$\bar{\Gamma}_m = 2\sqrt{(\Gamma_m^R)^2 + (\Gamma_m^I)^2}$$

$$\tan(\varphi_{\theta,m}) = \frac{\Gamma_m^I}{\Gamma_m^r} \tag{2.64}$$

$$\tilde{\Omega}_{\theta,m} = \Omega_{\theta,m} l \sqrt{\frac{m_d + 2m_c}{2H}}$$

The substitution of the modal decomposition (2.62) in the linearized undamped torsional equation of motion of the free vibrating system leads to its modal format. Enforcing the dynamic equilibrium at each instant of time the following 4th order spatial ODE with Eigen-modes and circular Eigen-frequencies unknowns is obtained.

$$-\tilde{J}_t \tilde{\Omega}_{\theta,m}^2 \Theta_m(\xi) + \frac{\beta^2}{\chi^2} \Theta_m'^v(\xi) - (1 + \beta^2)\Theta_m''(\xi) + \lambda_1^2 \tilde{h}_{\theta,m} = 0 \tag{2.65}$$

Skew-Symmetric modes

Also in this case, the vanishing of the cable's stiffening term allows the definition of the modal shapes and the corresponding circular Eigen-frequencies without any difficulties.

$$\Theta_m(\xi) = sin(m \cdot \pi \cdot \xi) \quad (m = 2,4,6,\dots) \tag{2.66}$$

$$\tilde{\Omega}_{\theta,m} = \frac{1}{\sqrt{\tilde{J}_t}} m\pi \sqrt{1 + \beta^2 + \frac{\beta^2}{\chi^2}(m\pi)^2} \quad (m = 2,4,6,\dots) \tag{2.67}$$

Symmetric Modes

In complete accordance to the flexural case, the solution of the complete ODE with constant coefficients is a superposition of the homogeneous and the particular solution, which can be expressed as:

$$\Theta_m(\xi) = \Theta_{m,0}(\xi) + \Theta_{m,p}(\xi) = \left(\frac{\lambda_1^2 \tilde{h}_{\Theta,m}}{\tilde{J}_t \tilde{\Omega}_{\theta,m}^2} + C_{m,1} \cdot \exp(\Psi_{\theta,m}\xi) + C_{m,2} \cdot \right.$$
$$\left. \exp(-\Psi_{\theta,m}\xi) + C_{m,3} \cdot \exp(i \cdot \eta_{\theta,m}\xi) + C_{m,4} \cdot \exp(-i \cdot \eta_{\theta,m}\xi)\right) \tag{2.68}$$

where

$$\eta_{\theta,m}^2 = \frac{\chi^2}{2\beta^2}\left(\sqrt{1 + \beta^2 + 4\frac{\beta^2}{\chi^2}\tilde{J}_t\tilde{\Omega}_{\theta,m}^2} - (1 + \beta^2)\right)$$

$$\Psi_{\theta,m}^2 = \frac{\chi^2}{2\beta^2}\left(\sqrt{1 + \beta^2 + 4\frac{\beta^2}{\chi^2}\tilde{J}_t\tilde{\Omega}_{\theta,m}^2} + (1 + \beta^2)\right) = \eta_{\theta,m}^2 + \frac{\chi^2}{\beta^2}(1 + \beta^2) \tag{2.69}$$

Hence enforcing proper boundary conditions for the fork support and exploiting some trigonometric relationships, the solution for the modal shape is:

$$\Theta_m(\xi) = \frac{\lambda_1^2 \tilde{h}_{\Theta,m}}{\tilde{J}_t \tilde{\Omega}_{\theta,m}^2}\left[1 - \frac{1}{\Psi_{\theta,m}^2 + \eta_{\theta,m}^2}\left(\eta_{\theta,m}^2 \cdot \frac{\cosh\left(\Psi_{\theta,m}\left(\xi - \frac{1}{2}\right)\right)}{\cosh\left(\frac{\Psi_{\theta,m}}{2}\right)} + \Psi_{\theta,m}^2 \cdot \frac{\cos\left(\eta_{\theta,m}\left(\xi - \frac{1}{2}\right)\right)}{\cos\left(\frac{\eta_{\theta,m}}{2}\right)}\right)\right] \tag{2.70}$$

Moreover, exploiting the definition of the stiffening term due to elongation of the cables, the Eigen-function for the circular non-dimensional torsional frequencies can be found.

$$\tilde{h}_{\Theta,m} = \int_0^1 \Theta_m(\xi)d\xi = \frac{\lambda_1^2 \tilde{h}_{\Theta,m}}{\tilde{J}_t \tilde{\Omega}_{\theta,m}^2}\int_0^1\left[1 - \frac{1}{\Psi_{\theta,m}^2 + \eta_{\theta,m}^2}\left(\eta_{\theta,m}^2 \cdot \frac{\cosh\left(\Psi_{\theta,m}\left(\xi - \frac{1}{2}\right)\right)}{\cosh\left(\frac{\Psi_{\theta,m}}{2}\right)} + \Psi_{\theta,m}^2 \cdot \right.\right.$$
$$\left.\left. \frac{\cos\left(\eta_{\theta,m}\left(\xi - \frac{1}{2}\right)\right)}{\cos\left(\frac{\eta_{\theta,m}}{2}\right)}\right)\right]d\xi \tag{2.71}$$

$$\frac{\tilde{J}_t\tilde{\Omega}_{\theta,m}^2}{\lambda_1^2} - 1 + \frac{1}{\Psi_{\theta,m}^2 + \eta_{\theta,m}^2}\left(\eta_{\theta,m}^2 \cdot \frac{\tanh\left(\frac{\Psi_{\theta,m}}{2}\right)}{\frac{\Psi_{\theta,m}}{2}} + \Psi_{\theta,m}^2 \cdot \frac{\tan\left(\frac{\eta_{\theta,m}}{2}\right)}{\frac{\eta_{\theta,m}}{2}}\right) = 0 \tag{2.72}$$

This expression again can be solved numerically with the well-known bisection method.

2.5 PROJECTION IN THE MODAL SPACE

In order to obtain spatial independent equations of motion their modal projection in the Galerkin plane is performed, so as to discretize the problem. Thanks to the modal decomposition already defined in equations (2.43) and (2.62) it is possible to split the spatial and the time dependence of variables and to perform a modal superposition analysis to find the structural Eigen-modes and associated circular Eigen-frequencies. Then the projection in the modal plane is performed multiplying each equation of motion, i.e. eq. (2.40) and (2.41), by the respective modals shape and then integrating over the spatial domain.

The flexural projected equations of motion is:

$$
\int_0^1 W_n^2(\xi)d\xi \frac{d^2 z_n}{d\tau^2} + \int_0^1 W_n^2(\xi)d\xi \, \tilde{c}_w \frac{dz_n}{d\tau} + \left[\int_0^1 W_n(\xi)\left(\mu^2 W_n^{iv}(\xi) - W_n''(\xi) \right)d\xi + \lambda_1^2 \tilde{h}_{W_n}^2 \right] z_n(\tau) +
$$
$$
-\lambda_2^2 \tilde{h}_{W_n} \left[\int_0^1 W_n(\xi) W_n''(\xi)d\xi - \frac{1}{2} \tilde{h}_{W_n'^2} \right] z_n^2(\tau) + -\lambda_2^2 \left[\tilde{h}_{\Theta_m} \int_0^1 W_n(\xi) \Theta_m''(\xi)d\xi -
$$
$$
\frac{1}{2} \tilde{h}_{W_n} \tilde{h}_{\Theta_m'^2} \right] \gamma_m^2(\tau) - \frac{1}{2}\lambda_3^2 \left[\tilde{h}_{W_n'^2} \int_0^1 W_n(\xi) W_n''(\xi)d\xi \right] z_n^3(\tau) + -\lambda_3^2 \left[\frac{1}{2} \tilde{h}_{\Theta_m'^2} \int_0^1 W_n(\xi) W_n''(\xi)d\xi +
$$
$$
\tilde{h}_{W_n'\Theta_m'} \int_0^1 W_n(\xi) \Theta_m''(\xi)d\xi \right] z_n(\tau)\gamma_m^2(\tau) = \int_0^1 W_n(\xi)\,\tilde{q}(\xi,t)d\xi
$$

The torsional projected equation of motion is:

$$
\tilde{J}_t \int_0^1 \Theta_m^2(\xi)d\xi \frac{d^2 \gamma_m}{d\tau^2} + \int_0^1 \Theta_m^2(\xi)d\xi \, \tilde{c}_\theta \frac{d\gamma_m}{d\tau} + \left[\int_0^1 \Theta_m(\xi)\left(\frac{\beta^2}{\chi^2} \Theta_m^{iv}(\xi) - (1+\beta^2)\Theta_m''(\xi) \right)d\xi +
$$
$$
+\lambda_1^2 \tilde{h}_{\Theta_m}^2 \right] \gamma_m(\tau) + -\lambda_2^2 \left[\tilde{h}_{\Theta_m} \int_0^1 \Theta_m(\xi) W_n''(\xi)d\xi + \tilde{h}_{W_n} \int_0^1 \Theta_m(\xi)\Theta_m''(\xi)d\xi -
$$
$$
\tilde{h}_{W_n'\Theta_m'} \tilde{h}_{\Theta_m} \right] z_n(\tau)\gamma_m(\tau) + -\lambda_3^2 \left[\tilde{h}_{W_n'\Theta_m'} \int_0^1 \Theta_m(\xi) W_n''(\xi)d\xi +
$$
$$
\frac{1}{2} \tilde{h}_{W_n'^2} \int_0^1 \Theta_m(\xi)\Theta_m''(\xi)d\xi \right] z_n^2(\tau)\gamma_m(\tau) + -\frac{1}{2}\lambda_3^2 \left[\tilde{h}_{\Theta_m'^2} \int_0^1 \Theta_m(\xi)\Theta_m''(\xi)d\xi \right] \gamma_m^3(\tau) =
$$
$$
\int_0^1 \Theta_m(\xi)\,\tilde{m}(\xi,t)d\xi
$$

Defining masses, damping and stiffness parameters of different orders, the abovementioned equations can be written in the classical format as:

$$
M_{w,n}\ddot{z}_n + D_{w,n}\dot{z}_n + K_{w,n}^{(L)}z_n + K_{w,n}^{(Q)}z_n^2 + K_{w\theta,nm}^{(Q)}\gamma_m^2 + K_{w,n}^{(C)}z_n^3 + K_{w\theta,nm}^{(C)}z_n\gamma_m^2 = \Gamma_{w,n} \qquad (2.73)
$$

$$
J_{\theta,m}\ddot{\gamma}_m + D_{\theta,m}\dot{\gamma}_m + K_{\theta,m}^{(L)}\gamma_m + K_{\theta w,mn}^{(Q)}\gamma_m z_n + K_{\theta,m}^{(C)}\gamma_m^3 + K_{\theta w,mn}^{(C)}\gamma_m z_n^2 = \Gamma_{\theta,m} \qquad (2.74)
$$

where the definitions of all the parameters are listed in the following page.

$$M_{w,n} = \int_0^1 W_n^2(\xi)d\xi$$

$$J_{\theta,m} = \tilde{J}_t M_{\theta,m} = \tilde{J}_t \int_0^1 \Theta_m^2(\xi)d\xi$$

$$D_{w,n} = \tilde{c}_w M_{w,n} = 2\Delta_{w,n}\tilde{\Omega}_{w,n}M_{w,n}$$

$$D_{\theta,m} = \tilde{c}_\theta M_{\theta,m} = 2\Delta_{\theta,m}\tilde{\Omega}_{\theta,m}\tilde{J}_t M_{\theta,m}$$

$$K_{w,n}^{(L)} = \int_0^1 W_n(\xi)\left(\mu^2 W_n^{iv}(\xi) - W_n''(\xi)\right)d\xi + \lambda_1^2 \tilde{h}_{W_n}^2 = \tilde{\Omega}_{w,n}^2 M_{w,n}$$

$$K_{\theta,m}^{(L)} = \int_0^1 \Theta_m(\xi)\left(\frac{\beta^2}{\chi^2}\Theta_m^{iv}(\xi) - (1+\beta^2)\Theta_m''(\xi)\right)d\xi + \lambda_1^2 \tilde{h}_{\Theta_m}^2 = \tilde{\Omega}_{\theta,m}^2 J_{\theta,m}$$

$$K_{w,n}^{(Q)} = -\lambda_2^2 \tilde{h}_{W_n}\left[\int_0^1 W_n(\xi)W_n''(\xi)d\xi - \frac{1}{2}\tilde{h}_{W_n'}^2\right] = \frac{3}{2}\lambda_2^2 \tilde{h}_{W_n}\tilde{h}_{W_n'}^2$$

$$K_{w\theta,nm}^{(Q)} = -\lambda_2^2\left[\tilde{h}_{\Theta_m}\int_0^1 W_n(\xi)\Theta_m''(\xi)d\xi - \frac{1}{2}\tilde{h}_{W_n}\tilde{h}_{\Theta_m'}^2\right] = \lambda_2^2\left[\tilde{h}_{\Theta_m}\tilde{h}_{W_n'\Theta_m'} + \frac{1}{2}\tilde{h}_{W_n}\tilde{h}_{\Theta_m'}^2\right] \qquad (2.75)$$

$$K_{\theta w,mn}^{(Q)} = \lambda_2^2\left[2\tilde{h}_{\Theta_m}\tilde{h}_{W_n'\Theta_m'} + \tilde{h}_{W_n}\tilde{h}_{\Theta_m'}^2\right]$$

$$K_{w,n}^{(C)} = -\frac{1}{2}\lambda_3^2\left[\tilde{h}_{W_n'}^2\int_0^1 W_n(\xi)W_n''(\xi)d\xi\right] = \frac{1}{2}\lambda_3^2\left(\tilde{h}_{W_n'}^2\right)^2$$

$$K_{w\theta,nm}^{(C)} = \lambda_3^2\left[\frac{1}{2}\tilde{h}_{\Theta_m'}^2\tilde{h}_{W_n'}^2 + \left(\tilde{h}_{W_n'\Theta_m'}\right)^2\right]$$

$$K_{\theta,m}^{(C)} = -\frac{1}{2}\lambda_3^2\left[\tilde{h}_{\Theta_m'}^2\int_0^1 \Theta_m(\xi)\Theta_m''(\xi)d\xi\right] = \frac{1}{2}\lambda_3^2\left(\tilde{h}_{\Theta_m'}^2\right)^2$$

$$K_{\theta w,mn}^{(C)} = \lambda_3^2\left[\left(\tilde{h}_{W_n'\Theta_m'}\right)^2 + \frac{1}{2}\tilde{h}_{W_n'}^2\tilde{h}_{\Theta_m'}^2\right]$$

$$\Gamma_{w,n} = \int_0^1 W_n(\xi)\tilde{q}(\xi,t)d\xi$$

$$\Gamma_{\theta,m} = \int_0^1 \Theta_m(\xi)\tilde{m}(\xi,t)d\xi$$

The equations (2.73) and (2.74) just obtained represent a 2 DoF$_s$ non-linear system and the linear terms do not couple the equations, which instead are coupled with the quadratic and cubic terms.

Moreover it is very important to notice that the modal torsional equation of motion does not have a torsional second order term independent from the flexural component. This feature is due to the fact that a rotation of the deck induces an asymmetric response in the two main cables, which is strongly dependent on the flexural amplitude of vibration that affect the stiffness of the cables system. The stability of the system will be conditioned by the coupling quadratic term $K_{\theta w,mn}^{(Q)}$, which in particular conditions can provoke the passage of energy from flexural to torsional oscillations and vice versa. This well-known phenomenon is recognized as internal parametric resonance.

2.6   SLACKENING OF HANGERS

The proposed model is a continuous 2 DoF$_s$ representation of a generic suspension bridge where many restrictive hypothesis have been assumed, e.g. the possibility of hangers not to undergo slackening. In reality this contribution has an important effect on the structural response during large oscillations, because of the variation of the actual stiffness of the structural system. In order to model accurately the real behaviour of hangers it would be necessary to increase the number of DoF$_s$ from two to four. In fact in doing this it is possible to introduce an appropriate constitutive model able to capture the linear elastic response of hangers in tension and their slackening in compression. Anyhow, introducing further simplification in the hangers behaviour it can be possible to remain to a 2 DoF$_s$ formulation.

Up to now the hangers have been considered perfectly rigid both in tension and in compression so as to avoid all problems related to their slackening. The further improvement of the model is to consider the hangers as perfectly rigid in tension and perfectly flexible in compression. This is a good representation of both the tension response of real bridges during serviceability conditions, where the hangers remain in the linear branch also for large displacements, and of the compression response, once that the displacements are enough large to provoke slackening. The curtain assumption allows us to consider hangers as uniformly smeared along the bridge's span losing the local effect due to their effective location. Hence the local contribution given by slackening of hangers is approximate also in term of the actual position in which hangers could effectively undergo to slackening.

The aim of this paragraph is to find a proper limit condition for the initiation of slackening. As long as hangers remain taut they are able to transfer the loads acting on the stiffening girder to the main cable, while on those regions where the vertical displacement is so high that slackening occurs, the load acting on the deck cannot be transferred to the main cable. Hence a flow of forces occurs from the more flexible towards the stiffer elements.

2.6.1 *Modified Equations of Motion*

In order to find a proper threshold for slackening initiation it is necessary to reformulate the equations of motion starting from the definition of the Total Potential Energy variation.

$$\Delta V(w_d, \theta_d, q, m) = \int_0^l \left(\frac{1}{2}E_dI_dw_d''^2 + \frac{1}{2}E_d\Gamma_d\theta_d''^2 + \frac{1}{2}G_dJ_d\theta_d'^2\right)dx + \int_0^{l_R^+}\left(\frac{1}{2}Hw_R'^2 + \right.$$
$$+ \int_0^{w_R'} h^+(w_R)(y'+w_R')dw_R'\right)dx + \int_0^{l_L^+}\left(\frac{1}{2}Hw_L'^2 + \int_0^{w_L'} h^+(w_L)(y'+w_L')dw_L'\right)dx + \quad (2.76)$$
$$+ \int_0^l(-qw_d - m\theta_d)dx$$

where it is not possible to collect the terms under the same sign of integration since each of them has a different domain in which it is able to make work. In order to integrate the contribution of the stiffening effect of the cable along a piecewise continuous domain the integral along the length of the cable can be defined as the sum of an infinite number of integral in which the work is positive. The stiffening effect on the different cables are defined as in (2.27).

Integrating by parts the variation of the TPE and equating it to zero:

$$\delta V = \int_0^l\left[(E_dI_dw_d^{iv}-q)dw_d + (E_d\Gamma_d\theta_d^{iv}-G_dJ_d\theta_d''-m)d\theta_d\right]dx - \int_0^{l_R^+}\left[H(w_d''+b\theta_d'')dw_d + \right.$$
$$+H(w_d''+b\theta_d'')bd\theta_d + (h_{w_R}^+ + h_{(w\theta)_R}^+ + h_{\theta_R}^+)(y''+w_d''+b\theta_d'')dw_d + (h_{w_R}^+ + h_{(w\theta)_R}^+ +$$
$$h_{\theta_R}^+)(y''+w_d''+b\theta_d'')bd\theta_d\right]dx - \int_0^{l_L^+}\left[H(w_d''-b\theta_d'')dw_d + H(b\theta_d''-w_d'')bd\theta_d + (h_{w_L}^+ + \right.$$
$$-h_{(w\theta)_L}^+ + h_{\theta_L}^+)(y''+w_d''-b\theta_d'')dw_d - (h_{w_L}^+ - h_{(w\theta)_L}^+ + h_{\theta_L}^+)(y''+w_d''-b\theta_d'')bd\theta_d\right]dx = 0$$

So the flexural and the torsional equilibrium equations are:

$$\int_0^l(E_dI_dw_d^{iv}-q)dx - \int_0^{l_R^+}\left[H(w_d''+b\theta_d'') + (h_{w_R}^+ + h_{(w\theta)_R}^+ + h_{\theta_R}^+)(y''+w_d'' + \right.$$
$$+b\theta_d'')\right]dx - \int_0^{l_L^+}\left[H(w_d''-b\theta_d'') + (h_{w_L}^+ - h_{(w\theta)_L}^+ + h_{\theta_L}^+)(y''+w_d''-b\theta_d'')\right]dx = 0 \quad (2.77)$$

$$\int_0^l(E_d\Gamma_d\theta_d^{iv}-G_dJ_d\theta_d''-m)dx - \int_0^{l_R^+}\left[H(w_d''+b\theta_d'') + (h_{w_R}^+ + h_{(w\theta)_R}^+ + +h_{\theta_R}^+)(y'' + \right.$$
$$+w_d''+b\theta_d'')\right]bdx - \int_0^{l_L^+}\left[H(b\theta_d''-w_d'') - (h_{w_L}^+ - h_{(w\theta)_L}^+ + h_{\theta_L}^+)(y''+w_d'' + \right.$$
$$-b\theta_d'')\right]bdx = 0 \quad (2.78)$$

For the sake of simplicity, just the linear components of the equations are considered. Moreover, the inertial terms are added, but the structural damping terms not.

$$\int_0^l(m_d\ddot{w}_d + E_dI_dw_d^{iv}-q)dx - \int_0^{l_R^+}\left[-m_c(\ddot{w}_d+b\ddot{\theta}_d) + H(w_d''+b\theta_d'') - \int_0^{l_R^+}\frac{E_cA_c}{L_c}y''^2(w_d + \right.$$
$$+b\theta_d)dx\right]dx - \int_0^{l_L^+}\left[-m_c(\ddot{w}_d-b\ddot{\theta}_d) + H(w_d''-b\theta_d'') - \int_0^{l_L^+}\frac{E_cA_c}{L_c}y''^2(w_d-b\theta_d)dx\right]dx = 0$$

$$\int_0^l \left(J_t\ddot{\theta}_d + E_d\Gamma_d\theta_d^{iv} - G_dJ_d\theta_d'' - m\right)dx - b\int_0^{l_R^\ddagger}\left[-m_c\left(\ddot{w}_d + b\ddot{\theta}_d\right) + H\left(w_d'' + b\theta_d''\right) - \right.$$
$$\left. \int_0^{l_R^\ddagger}\frac{E_cA_c}{L_c}y''^2(w_d + b\theta_d)dx\right]dx - b\int_0^{l_L^\ddagger}\left[-m_c\left(b\ddot{\theta}_d - \ddot{w}_d\right) + H\left(b\theta_d'' - w_d''\right) - \int_0^{l_L^\ddagger}\frac{E_cA_c}{L_c}y''^2(b\theta_d + \right.$$
$$\left. -w_d)dx\right]dx = 0$$

Let us write the forces and couples transmitted by the deck to the main cables from the initial to the perturbed configuration. Having considered a symmetric section of the deck, in the initial condition, it is able to transfer to the cable's system its weight only.

$$\overline{F}_d(t) = \int_0^l F_d(x,t)dx = \int_0^l \left(m_a g + q - m_a\ddot{w}_d - E_dI_dw_d^{iv}\right)dx \tag{2.79}$$

$$\overline{C}_d(t) = \int_0^l C_d(x,t)dx = \int_0^l \left(m - J_t\ddot{\theta}_d - E_d\Gamma_d\theta_d^{iv} + G_dJ_d\theta_d''\right)dx \tag{2.80}$$

The substitution into these last two equations of the previous linearized equilibrium equations leads to:

$$\overline{F}_d(t) = \int_0^l m_a g\,dx - \int_0^{l_R^\ddagger}\left[-m_c\left(\ddot{w}_d + b\ddot{\theta}_d\right) + H\left(w_d'' + b\theta_d''\right) - \int_0^{l_R^\ddagger}\frac{E_cA_c}{L_c}y''^2(w_d + \right.$$
$$\left. +b\theta_d)dx\right]dx - \int_0^{l_L^\ddagger}\left[-m_c\left(\ddot{w}_d - b\ddot{\theta}_d\right) + H\left(w_d'' - b\theta_d''\right) - \int_0^{l_L^\ddagger}\frac{E_cA_c}{L_c}y''^2(w_d + \right. \tag{2.81}$$
$$\left. -b\theta_d)dx\right]dx$$

$$\overline{C}_d(t) = -b\int_0^{l_R^\ddagger}\left[-m_c\left(\ddot{w}_d + b\ddot{\theta}_d\right) + H\left(w_d'' + b\theta_d''\right) - \int_0^{l_R^\ddagger}\frac{E_cA_c}{L_c}y''^2(w_d + b\theta_d)dx\right]dx +$$
$$-b\int_0^{l_L^\ddagger}\left[-m_c\left(b\ddot{\theta}_d - \ddot{w}_d\right) + H\left(b\theta_d'' - w_d''\right) - \int_0^{l_L^\ddagger}\frac{E_cA_c}{L_c}y''^2(b\theta_d - w_d)dx\right]dx \tag{2.82}$$

Notice that, even if only the linear terms have been considered, the equations of motion are coupled due to the asymmetric response of the two main cables.

Introducing the non-dimensional quantities already seen in (2.34), the terms under the integral are all similar and they become:

$$\overline{F}_c^i(x,t) = -m_c f\left(\frac{d^2\widetilde{w}_d}{dt^2} \pm \frac{d^2\widetilde{\theta}_d}{dt^2}\right) + \frac{Hf}{l^2}\left(\widetilde{w}_d'' \pm \widetilde{\theta}_d''\right) - \frac{E_cA_c}{L_c}y''^2 fl\alpha_h^i\int_0^1\left(\widetilde{w}_d \pm \widetilde{\theta}_d\right)d\xi$$

where α_h^i represents the ratio between the contributions of the part of the span in which the deck can transfer forces to the main cables and the ideal condition without slackening in which all the deck transfer forces and couples to the cable's system. In general these parameter would be different for each side of the deck section.

$$\alpha_h^R = \frac{\int_0^{l_R^{\pm}}(w_d \pm \theta_d)\,dx}{\int_0^{l}(w_d \pm \theta_d)\,dx}$$

$$\alpha_h^L = \frac{\int_0^{l_L^{\pm}}(w_d \pm \theta_d)\,dx}{\int_0^{l}(w_d \pm \theta_d)\,dx}$$

(2.83)

In order to obtain simpler expressions, other similar parameters can be defined so as to collect all terms under the same integral sign.

$$\alpha_c^R = \frac{\int_0^{l_R^{\pm}} F_c^R(x,t)\,dx}{\int_0^{l} F_c^R(x,t)\,dx}$$

$$\alpha_c^L = \frac{\int_0^{l_L^{\pm}} F_c^L(x,t)\,dx}{\int_0^{l} F_c^L(x,t)\,dx}$$

(2.84)

(2.83) and (2.84) are called *General Slackening Parameters*.

To arrive to the local format of the previous equations of motion it is necessary to introduce the non-dimensional time parameter, the first order Irvine parameter (2.35) and the non-dimensional mass, which can be obtained from the initial equilibrium condition of the cables under the self-weight of the deck.

$$-2Hy'' = (m_d + 2m_c)g \quad \Rightarrow \quad \frac{Hf}{l^2 g} = \frac{(m_d + 2m_c)}{16}$$

$$\tilde{m}_d = \frac{m_d}{m_d + 2m_c} = 1 - \frac{2m_c}{m_d + 2m_c} = 1 - 2\tilde{m}_c$$

(2.85)

So the non-dimensional equations for the forces and couples transmitted to the cables, become:

$$\tilde{F}_d(\xi,t) = \frac{F_d(x,t)l^2}{Hf} = 16\tilde{m}_d - \alpha_c^R\left[(\tilde{m}_d - 1)\left(\frac{d^2\tilde{w}_d}{d\tau^2} + \frac{d^2\tilde{\theta}_d}{d\tau^2}\right) + \left(\tilde{w}_d^{''} + \tilde{\theta}_d^{''}\right) - \alpha_h^R\lambda_1^2\int_0^1\left(\tilde{w}_d + \right.\right.$$
$$\left.\left. + \tilde{\theta}_d\right)d\xi\right] - \alpha_c^L\left[(\tilde{m}_d - 1)\left(\frac{d^2\tilde{w}_d}{d\tau^2} - \frac{d^2\tilde{\theta}_d}{d\tau^2}\right) + \left(\tilde{w}_d^{''} - \tilde{\theta}_d^{''}\right) - \alpha_h^L\lambda_1^2\int_0^1(\tilde{w}_d - \tilde{\theta}_d)d\xi\right]$$

(2.86)

$$\tilde{C}_d(\xi,t) = \frac{C_d(x,t)l^2}{Hfb} = -\alpha_c^R\left[(\tilde{m}_d - 1)\left(\frac{d^2\tilde{w}_d}{d\tau^2} + \frac{d^2\tilde{\theta}_d}{d\tau^2}\right) + \left(\tilde{w}_d^{''} + \tilde{\theta}_d^{''}\right) - \alpha_h^R\lambda_1^2\int_0^1(\tilde{w}_d + \right.$$
$$\left. + \tilde{\theta}_d)d\xi\right] - \alpha_c^L\left[(1 - \tilde{m}_d)\left(\frac{d^2\tilde{w}_d}{d\tau^2} - \frac{d^2\tilde{\theta}_d}{d\tau^2}\right) - \left(\tilde{w}_d^{''} - \tilde{\theta}_d^{''}\right) + \alpha_h^L\lambda_1^2\int_0^1(\tilde{w}_d - \tilde{\theta}_d)d\xi\right]$$

(2.87)

Notice that this formulation is slightly different with respect to the one found by Guerrieri [29]. In fact there is a different sign in the terms of the couple transmitted to the left cable

$\tilde{C}_d(\xi, t)$. Due to this fact, it is impossible to arrive to the same format proposed in [29] because the force $\tilde{F}_d(\xi, t)$ cannot be written in function of the couple transmitted to the cables system $\tilde{C}_d(\xi, t)$.

The hangers are subjected to slackening when they are no more able to transfer the external actions from the deck to the main cables. Therefore the critical condition for slackening corresponds to those amplitude which induces negative forces and null couple in the cable system.

$$\tilde{F}_d(\xi, t) \leq 0$$

$$\tilde{C}_d(\xi, t) = 0$$

The two conditions cannot be satisfied at the same time which means that, even if locally the hangers do not transmit any force, they can transfer couples and vice versa.

2.6.2 *Slackening initiation*

Up to the slackening initiation all the hangers are still taut, so the General Slackening Parameters are contemporary equal to unity, since the cable system contribution is integrated along the whole length of the bridge's span.

$$\begin{aligned} \alpha_h^R = \alpha_h^L = 1 \\ \alpha_c^R = \alpha_c^L = 1 \end{aligned} \tag{2.88}$$

The critical conditions for the initiation of slackening correspond to that amplitude that induces null actions in the cables system. In fact, when an hanger slacks there is no transmission of forces or couples from the deck to the main cables. The critical conditions for slackening can be found without the definition of any slackening parameter since the definitions (2.88) are substituted into equations (2.86) and (2.87). The threshold conditions read as:

$$\tilde{F}_d(\xi, t) = 8\tilde{m}_d + (1 - \tilde{m}_d)\frac{d^2\tilde{w}_d(\xi,t)}{d\tau^2} - \tilde{w}_d''(\xi, t) + \lambda_1^2\tilde{h}_w = 0 \tag{2.89}$$

$$\tilde{C}_d(\xi, t) = (1 - \tilde{m}_d)\frac{d^2\tilde{\theta}_d(\xi,t)}{d\tau^2} - \tilde{\theta}_d''(\xi, t) + \lambda_1^2\tilde{h}_\theta = 0 \tag{2.90}$$

It is noticeable that this definition is in complete agreement with the one proposed by Guerrieri [29] because there is no dependence on the General Slackening Parameters. These critical conditions are completely uncoupled because they take trace only of the motion of the deck axis and not of the actual position of the cables. Then there are two

different critical conditions for slackening initiation, one associated to pure vertical oscillations and one associated to pure torsional oscillations.

The modal expansion of the structural response already introduced in (2.43) and (2.62) is exploited and substituted into the threshold condition for slackening:

$$\tilde{F}_{d,n} = 8\tilde{m}_d - \left[(1 - \tilde{m}_d)W_n(\xi)\tilde{\Omega}_{w,n}^2 + W_n''(\xi) - \lambda_1^2\tilde{h}_{W,n}\right]\left[Z_n\exp\left(i\tilde{\Omega}_{w,n}\tau\right) + Z_n^*\exp\left(-i\tilde{\Omega}_{w,n}\tau\right)\right] = 0$$

$$\tilde{C}_{d,m} = -\left[(1 - \tilde{m}_d)\Theta_m(\xi)\tilde{\Omega}_{\theta,m}^2 + \Theta_m''(\xi) - \lambda_1^2\tilde{h}_{\theta,m}\right]\left[\Gamma_m\exp\left(i\tilde{\Omega}_{\theta,m}\tau\right) + \Gamma_m^*\exp\left(-i\tilde{\Omega}_{\theta,m}\tau\right)\right] = 0$$

Remembering that the summation between a complex number multiplied by the exponential time variation and its complex conjugate gives rise to a cosine variation of time, shifted of a phase lag, then:

$$\tilde{F}_{d,n} = 8\tilde{m}_d - \left[(1 - \tilde{m}_d)W_n(\xi)\tilde{\Omega}_{w,n}^2 + W_n''(\xi) - \lambda_1^2\tilde{h}_{W,n}\right]\left[\bar{Z}_n\cos\left(\tilde{\Omega}_{w,n}\tau + \varphi_{w,n}\right)\right] = 0 \qquad (2.91)$$

$$\tilde{C}_{d,m} = -\left[(1 - \tilde{m}_d)\Theta_m(\xi)\tilde{\Omega}_{\theta,m}^2 + \Theta_m''(\xi) - \lambda_1^2\tilde{h}_{\theta,m}\right]\left[\bar{\Gamma}_m\cos\left(\tilde{\Omega}_{\theta,m}\tau + \varphi_{\theta,m}\right)\right] = 0 \qquad (2.92)$$

Now it is possible to find out the critical flexural and torsional amplitude able to induce the slackening of the hangers. The trigonometric time dependent terms can be neglected, since the objective is to find a critical condition valid for any time. The critical amplitude condition can be found from the previous equations (2.91) and (2.92) and it is:

$$Z_{n,slack} = 8\tilde{m}_d \cdot min\left|(1 - \tilde{m}_d)W_n(\xi)\tilde{\Omega}_{w,n}^2 + W_n''(\xi) - \lambda_1^2\tilde{h}_{W,n}\right|^{-1} \qquad (2.93)$$

$$\Theta_m''(\xi) = \lambda_1^2\tilde{h}_{\theta,m} - (1 - \tilde{m}_d)\Theta_m(\xi)\tilde{\Omega}_{\theta,m}^2 \qquad (2.94)$$

The expressions found are in complete agreement with the ones found by Luco and Turmo [37]. It is noticeable that only for the flexural oscillation component a critical amplitude can be defined, indeed the hangers are pre-tensioned by a symmetric force given by the deck self-weight which does not introduce an asymmetry in the initial configuration. For what concern the torsional limit it is possible to state that the cable system cannot sustain any torque in all the points where the deck reaches a critical warping independently on the actual maximum rotation.

3 WIND EFFECTS

For short bridges wind actions generally do not produce any particular problem. Increasing the span length and according to the typology, the bridge becomes very flexible, with decreasing values of the natural frequencies. The bridge motion due to wind action becomes more and more important and it affects the variation of the aerodynamic forces that may lead to instability conditions.

In the following chapter, a brief description of the wind characteristic is presented and the properties of the flow over immersed bodies are discussed, including vortex shedding and buffeting. Then Aeroelastic effects are introduced into the bridge model and simplified formulations for capturing the phenomenon of torsional divergence and flutter are obtained.

Particular attention is given to flutter, which for long-span suspension bridges can be of different kinds, depending on the aerodynamic properties of the deck section. Inter alia there is the possibility to have galloping, Single Degree of Freedom torsional flutter and classical 2 Degrees of Freedom flutter.

It seems that, due to his nature, flutter involves nonlinear aerodynamics, but the problem can be successfully treated by linear approaches. The main reason for this is that the starting condition that separates the stable from the unstable regimes, i.e. the onset of flutter, may be treated as having small amplitude. The flutter analysis can be therefore based on the standard stability considerations of linear elastic systems.

3.1 THE ATMOSPHERIC BOUNDARY LAYER

As the wind approaches the Earth's surface, frictional forces caused by the terrain exert on the moving air an horizontal drag force, whose effect is to retard the flow. Wind becomes a turbulent flow varying randomly both in space and in time. The height where the surface friction effects are zero is called Gradient Height and it is dependent upon the wind intensity, the roughness of the terrain and the angle of latitude. The part of the atmosphere below the gradient height is called *Atmospheric Boundary Layer* (ABL), depicted in Figure 3.1, where the wind speed increases with elevation reaching the so called *Gradient Speed* at the top of the boundary layer. In the free atmosphere, outside the boundary layer, the wind flows with the gradient speed along the isobars. The study of all the aspects of the boundary layer is an interesting topic, since it affects the structural design.
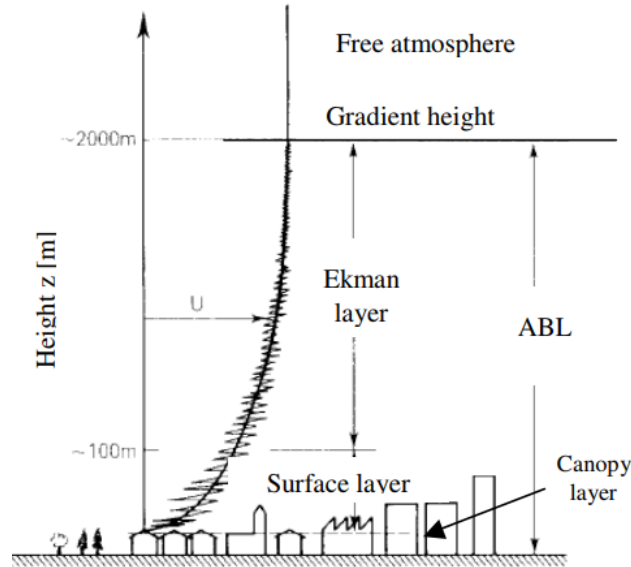
Figure 3.1: Atmospheric Boundary Layer (ABL)

It is possible to define the wind mean velocity as the sum of the average wind velocity, which is not time dependent, and the turbulence velocity.

$$U(z,t) = U(z) + u(z,t) \tag{3.1}$$

The mean wind velocity profile depends on the aerodynamic roughness length parameter $z_0(m)$, which characterize the surface roughness, and it can be expressed trough a logarithmic profile. Up to 200 m in fact this is a good approximation, based on the Buckingham Pi Theory.

$$U(z) = \frac{u^*}{k} \ln\left(\frac{z}{z_0}\right) \tag{3.2}$$

where:

1. k is the Von Karman constant, which is not a function of the flow nor of the surface. It assumes a value around $k = 0.4$;

2. $u^* = \sqrt{\frac{\tau_0}{\rho_a}}$ is the friction velocity, which is an abstraction to express the shear stress of the terrain.

The wind in the atmospheric boundary layer is characterized by turbulence, a random process which cannot be described in a deterministic way, but with a stochastic approach. Therefore basing on the eddy model of turbulence it is possible to introduce the power spectrum that describes the distribution of the turbulence with frequency (Figure 3.2).
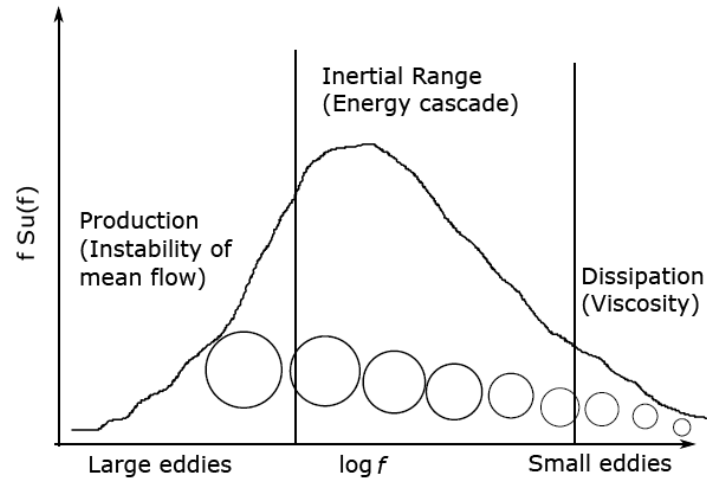
Figure 3.2: Turbulence power spectrum

Obviously the variance of the turbulence is represented by the area under the curve depicted in Figure 3.2, which can be divided in three different ranges:

1. A production range in which the turbulence is generated as large eddies;

2. An inertial range characterized by the energy cascade phenomenon, that is the large eddies break up transferring their energy to smaller scales;

3. A dissipation range where eddies become very small and the energy is dissipated by heat. In this range viscosity assumes an important role.

It is useful to introduce a non-dimensional parameter called Turbulence Intensity, defined as the ratio between the standard deviation, which can be considered almost constant up to 200 m, and the mean wind velocity. For the along wind turbulence component u, it is:

$$I_u(z) = \frac{\sigma_u(z)}{U(z)} \cong \frac{1}{\ln\left(\frac{z}{z_0}\right)} \tag{3.3}$$

Notice that the turbulence intensity is proportional to the roughness and it is inversely proportional to the height above the ground.

Another important parameter to be defined is the *Integral Length Scale*, which is a measure of the sizes of the vortices in the wind. The integral length scale for the turbulence component u measured in the longitudinal direction x is formally defined trough the cross-correlation function between two different points separated longitudinally.

$$L_u^x(z) = \int_0^{+\infty} R_u(r_x) dr_x \tag{3.4}$$

The integral length scale can be measured in a simpler way, assuming valid the Taylor's hypothesis. Taylor suggested to consider the turbulence as "frozen" and translated by the mean wind speed, i.e. the spatial variations of the wind velocity field can be based on temporal variations and vice versa. According to this it is possible to calculate the longitudinal scale of turbulence basing on the measurement performed in one point, so:

$$L_u^x(z) = T_u(z)U(z) \tag{3.5}$$

where $T_u(z) = \int_0^{+\infty} R_u(z,\tau)d\tau$ is the time scale.

Also the integral length scale is a function of the height from the ground and the terrain roughness.

Thanks to the definition of these quantities it is possible to define the wind power spectrum, which in the literature assumes different formulations. One of the most reliable spectrum is provided by the works of Von Karman:

$$\frac{fS_u(f)}{\sigma_u^2} = \frac{4\left(\frac{fL_u^x}{U}\right)}{\left(1 + 70.8\left(\frac{fL_u^x}{U}\right)^2\right)^{5/6}} \tag{3.6}$$

Although wind effects are usually treated with a stochastic approach, due to the nature of the wind turbulence, a fully deterministic approach will be used in the following treatment. This assumption is justified by the fact that the wind turbulence effects mainly affect the buffeting phenomenon, which can be considered not relevant in a 2 DoF$_s$ sectional model.

3.2 FLOW OVER IMMERSED BODIES

The presence of a body in the fluid flow alters the flow according to its geometrical shape and to the flow characteristics. The modification of the fluid flow induced by the body determines a distribution of velocities and pressure in the fluid around the body that produce a global force on the body, called *Aerodynamic Force*. In the case of motion of the body, the motion itself influences the aerodynamic forces, which in turn influence the body motion. This phenomenon is called *Fluid-Structure Interaction* (*FSI*). The possible tools for the investigations of the wind forces on the structures are:

1. Full scale measurements, which usually are not available during the design process. Moreover they are very difficult because it is impossible to have the control on the environmental conditions;

2. Wind tunnel experiments, which are a very useful tool, despite the fact that a possible limitation is the scaled reproduction;

3. Computational Fluid Dynamics (CFD), which consists in the numerical solution of the Navier-Stokes equations. This tool is very demanding by the computational point of view;

4. Analytical formulations, which are defined only for some specific and simple problems.

Aerodynamic forces are generated when there is a relative velocity between the air and the structure, the higher is the relative velocity and the higher are the aerodynamic forces. Moreover they are also influenced by the geometry of the body, in fact it is possible to make a distinction between *streamlined bodies*, which produce low perturbations in the flow, and *bluff bodies*, which produce high perturbations in the flow, increasing the value of aerodynamic forces they are subjected to.

Two regions with different characteristics may be defined in the flow around a body:

1. The Boundary Layer, the region very close to the body , in which the fluid particles are influenced by the presence of the body with a variation both in the path and in the speed;

2. The Potential Flow Region, where the fluid particles are not influenced by the presence of the body.

The region close to the body surface is characterized by large gradients of velocity, since the no-slip condition guarantees that the particles close to the wall have the same velocity of the body surface. In this region viscous effects become more important than inertial ones, due to the relative speed slowing down. The ratio between inertial and viscous forces acting on the fluid is called *Reynolds number*:

$$Re = \frac{UL\rho}{\mu} = \frac{UL}{\nu} \tag{3.7}$$

where U is the fluid speed, L a reference length, ρ the fluid density, μ the fluid dynamic viscosity and ν the fluid kinematic viscosity equal to $1.5 \cdot 10^{-5} m^2/s$ for air at 20°C.

It is common practice to assume that the threshold of separation between the Boundary Layer region, dominated by viscosity, and the Potential Flow region, where the fluid can be considered inviscid, is located at a distance from the body surface where the flow velocity has reached the 99% of the undisturbed flow speed.

In the Potential Flow region, for inviscid and incompressible fluids the *Bernoulli equation* holds for a fluid particle:

$$\frac{P}{\rho} + \frac{U^2}{2} + gy = \text{Const.} \tag{3.8}$$

where the three terms at the LHS are the static pressure, the kinetic energy and the gravitational force per unit mass, respectively. The latter, in common structural engineering problems can usually be neglected. According to this equation, when a particle is moving towards a lower pressure zone, it increases its velocity.

Instead, in the Boundary layer region the Bernoulli equation is no more valid and Navier-Stokes equations have to be solved if one is interested to the velocity field.
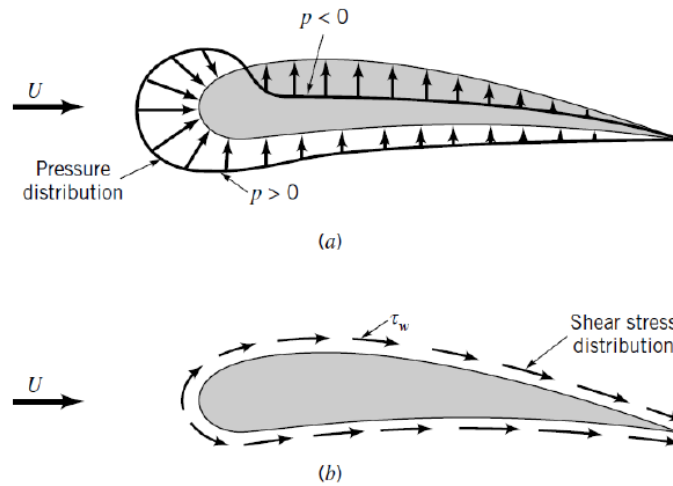

Figure 3.3: Pressure and shear stresses distribution on a thin airfoil

3.2.1 *Aerodynamic Coefficients*

Aerodynamic forces can be computed integrating the pressures and shear stresses (Figure 3.3) over the whole body surface.
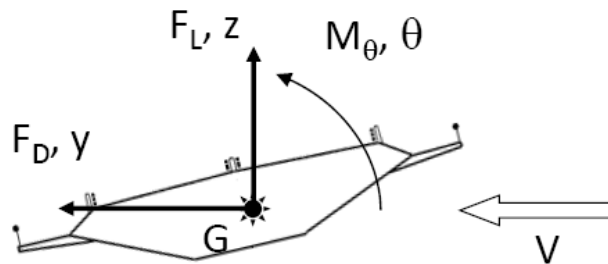

Figure 3.4: Aerodynamic forces acting on a bridge deck section

However, in wind engineering, it is common practice to define aerodynamic forces by means of the so called *Aerodynamic Coefficients*. In Figure 3.4 the three different components of aerodynamic forces, are depicted for a generic bridge's deck section. Thus, three Aerodynamic coefficients can be defined, namely the drag, lift and moment coefficient.

$$
C_D = \frac{D}{\frac{1}{2}\rho U^2 B}
$$
$$
C_L = \frac{L}{\frac{1}{2}\rho U^2 B} \tag{3.9}
$$
$$
C_M = \frac{M}{\frac{1}{2}\rho U^2 B^2}
$$

where ρ is the air density, U is the mean wind speed and B is a reference dimension of the body, which in the case of a bridge's deck is its width. Aerodynamic forces and coefficients are dependent on the following quantities:

1. The shape of the body, bluff or streamlined;

2. The wind angle of attack;

3. The Reynolds number Re, which determines if the flow is in laminar or turbulent conditions. It affects the thickness of the boundary layer zone indeed, for a circular cylinder, in the range of $2 \cdot 10^5 \leq Re \leq 5 \cdot 10^5$ there is a transition from laminar to turbulent flow inside the boundary layer region. Separation of the boundary layer occurs much farther back in the surface of the cylinder and the wake narrows, reducing the value of the aerodynamic drag coefficient;

4. The Mach number M_∞, which indicates how much compressible effects are important. In typical structural engineering problems the wind velocity is always such that $Ma < 0.3$, i.e. incompressible flow regime;

5. The free stream turbulence intensity I_u, which determines the point of detachment or reattachment of the flow, if it happens;

6. The surface roughness ratio $\frac{\varepsilon}{l}$, which is able to influence the transition from laminar to turbulent flow in the boundary layer region. For large surface roughness ratio the transition is anticipated, thus making the value of the aerodynamic drag coefficient increases.

3.2.2 *Separation of the Boundary Layer*

Boundary layer separation is a phenomenon that can happen if fluid particles are sufficiently decelerated by inertial forces that the flow near the surfaces becomes reversed. These deceleration effects occur as a result of the presence in the flow of adverse pressure gradients, which can be produced for example by the flow over a sharp corner of a body.

Let us consider the case of a circular shape immersed in a fluid. Solving the Navier-Stokes equations with simplified assumptions the results depicted in Figure 3.5is obtained.
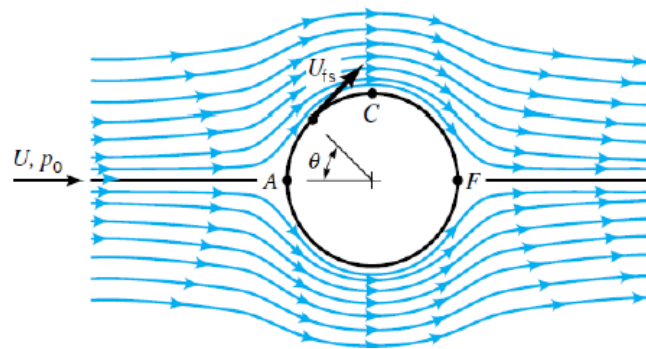

Figure 3.5: Potential flow prediction around a circular cylinder

This solution leads to a symmetric pressure distribution around the cylinder which coincides with a null drag force. It is the so called *"D'alembert paradox"*, because it is impossible to obtain a null drag force. In fact, the real flow forms the boundary layer only in the front part of the cylinder, while in the rear part of the body it is detached forming a wake region. The pressure distribution is therefore asymmetric producing a global drag force (Figure 3.6).
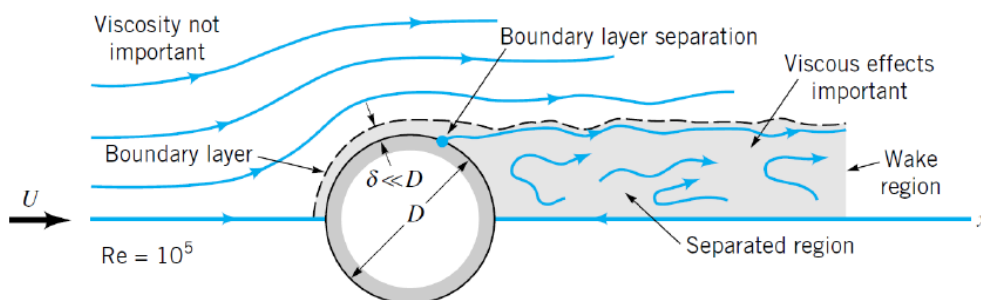

Figure 3.6: Boundary layer around a circular cylinder at Re=10^5

The boundary layer separation occurs on any curved surface characterized by low curvature radius because the centrifugal inertial component along the streamline is no more withstandable. On bodies with sharp corners or discontinuities in the surface slope the separation occurs at the corner.

The width of the wake region and the detachment point of the boundary layer are strictly dependent on the Reynolds number, the surface roughness ratio and the turbulence intensity. The wake is also affected by the streamwise length and the general form of the body, as well as by its bluff face.

In the wake region there is the possibility to have the formation of vortices, which induces in the body a periodic variation of the aerodynamic forces.

3.2.3 *Vortex Shedding*

Vortex shedding is due to an alternate separation of the boundary layer from opposite parts of the body that generate a fluctuating force due to the subsequently alternation of regions of positive and negative pressure distribution. The frequency at which the vortex are shed is proportional to the wind speed and to the Strouhal number and inversely proportional to a reference dimension of the body.

$$f_s = St \cdot \frac{U}{D} \tag{3.10}$$

The Strouhal number *St* depends upon the Reynolds number and the body geometry. For a circular cylinder the Strouhal number is equal to 0.18 whilst for bluff deck sections it assumes different values depending on the shape of the deck (Figure 3.7).

Steady state load coefficients and flow field at time $tU/B = 10$	C_D	C_L^{rms}	St
G1	0.08	0.07	0.17
G2	0.08	0.08	0.17
G3	0.10	0.08	0.10
G4	0.08	0.12	0.17
G5	0.27	0.33	0.11

Figure 3.7: Strouhal number for different deck sections

Let us consider a cylindrical body subjected to vortex shedding. The response of the body is different if it is able to vibrate or not.

In the case of a fixed circular cylinder three quarter of the cylinder surface is subjected to a negative pressure with the peak moving from one side to the other as the vortices are formed. Due to the alternating vortex wake, named *"Karman street"*, the oscillations of the lift force occur at the vortex shedding frequency and the oscillations of the drag force occur at twice the vortex shedding frequency. Anyway the process is not fully periodic, but it is of random nature and it does not occur simultaneously along the cylinder axis. The lift force value therefore is very small.

In the case of a vibrating circular cylinder, when the vortex shedding frequency is equal to one frequency of the body, this starts to oscillate. The vibration amplitude increases and reaches a steady state value. It is experimentally observed that the body mechanical frequency controls the vortex shedding phenomenon even when variations in flow velocity displace the nominal Strouhal frequency away from the natural mechanical frequency by a few percent. This control of the phenomenon is commonly known as *lock-in*. Figure 3.8 shows how this phenomenon works: when the vortex shedding frequency is in the lock-in region, it remains constant rather than being a linear function of wind velocity.
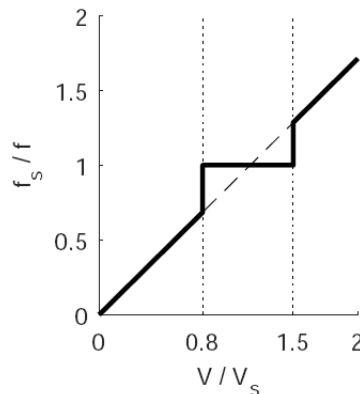
Figure 3.8: Lock-in phenomenon on a vibrating cylinder

Another important feature of this phenomenon is that the lift force, that was observed to have a random nature in case of fixed cylinder, in all the synchronization range becomes fully periodic and can be expressed in an approximate way by a sine function.

$$L = \frac{1}{2}\rho U^2 2bC_L \cdot sin(\omega_{VS}t) \tag{3.11}$$

Vortex induced vibrations have not to be considered a forced motion, but a self-excited mechanism. Moreover it is also a self-contained phenomenon, which guarantees that the

amplitude of oscillations are limited because there is a drag damping effect that drives the phase of the lift force close to zero when the amplitudes are increasing.

The maximum amplitude of vibrations due to vortex shedding depends upon the Scruton number, a non-dimensional parameter function of the damping.

$$Sc = \frac{2\pi\xi m}{\rho D^2} \tag{3.12}$$

being ξ the non-dimensional damping coefficient, m the body mass per unit length, D the body reference dimension and ρ the fluid density.
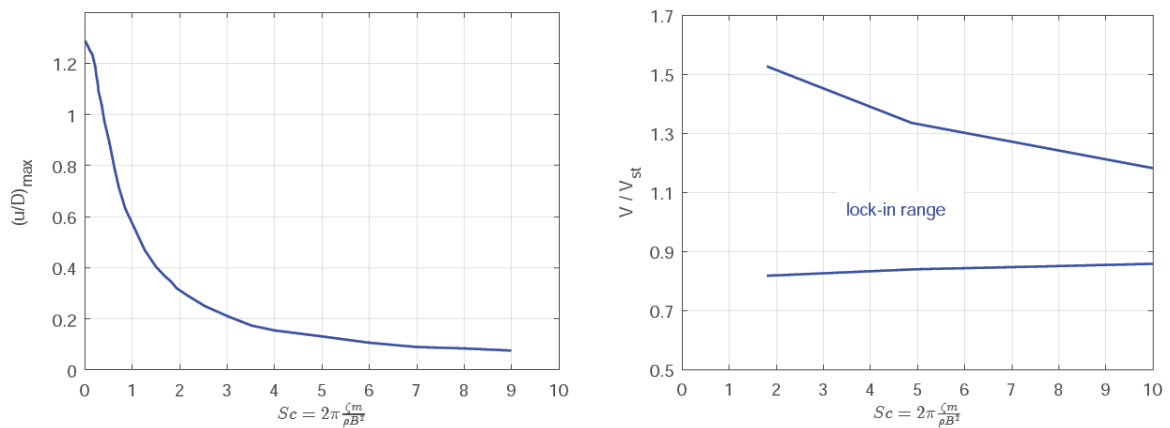
Figure 3.9: Maximum vibration amplitude and synchronization range as a function of Sc

Figure 3.9 represents the maximum vibration amplitude and the width of the synchronization range for increasing values of the Scruton number. The higher is the damping of the system, the higher is the Scruton number and the lower is the amplitude of vibrations. As well as the oscillations amplitude, also the synchronization range decreases its width for increasing values of the Scruton number. For very low values of damping the synchronization range is comprised between $0.8 \leq U/U_s \leq 1.5$.

Another important parameter affecting the vortex shedding phenomenon is the Reynolds number. In fact both the boundary layer separation and the boundary layer transition from laminar to turbulent depend on Re. The effect of Reynolds number is much more important for a body characterized by a curved shape because it directly affects the detachment point of the flow from the body, while for body with sharp edges the boundary layer detaches at the corners.

The circular section is fully affected by Re and a lot of wind tunnel tests have been done on it. The drag coefficient as a function of Re and the transition from many different fluid regimes, in laminar flow conditions and for smooth surface of the body, are reported in Figure 3.10 and Figure 3.11.
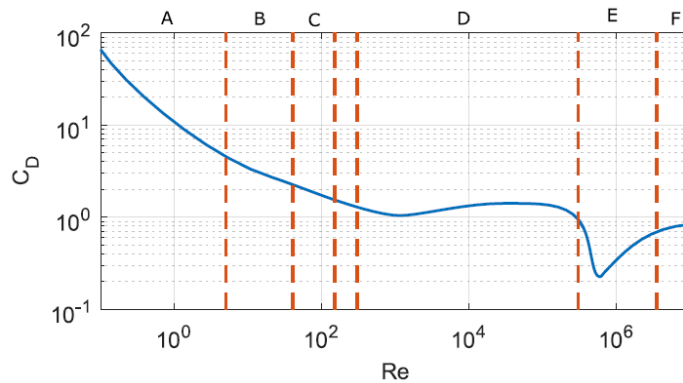
Figure 3.10: Drag coefficient as a function of Re
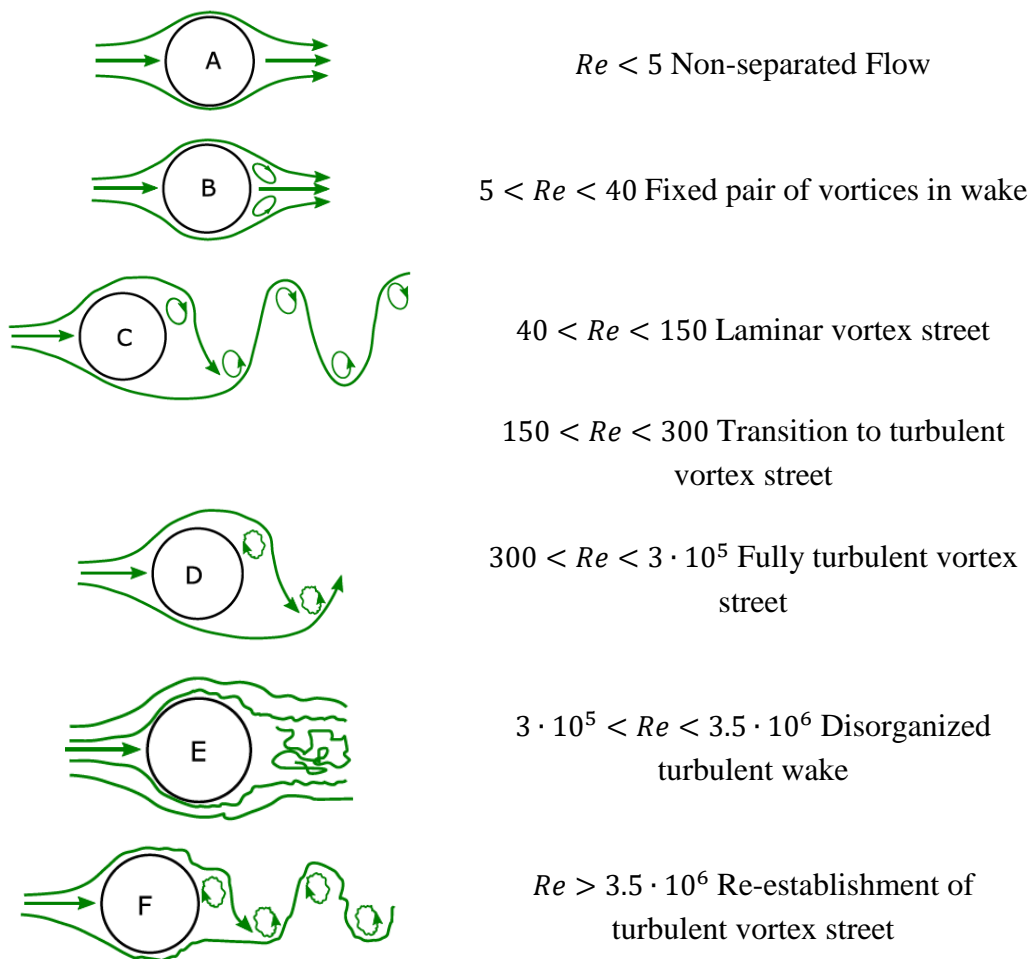
Figure 3.11: Vortex shedding from a circular cylinder

Vortex shedding occurs for very low Re, up to $Re = 3 \cdot 10^5$, where the drag force is more or less constant. Increasing Re the drag force starts to decrease because the boundary layer becomes turbulent and the separation point moves downstream. In this critical region vortex shedding disappears. For $Re > 10^6$ (post-critical range), even in presence of a

turbulent boundary layer, the Karman vortex street reappears and vortex induced vibrations excitation occurs with features that are similar to those of the sub-critical range.

In addition, the *Re* value for which each transition occurs is also function of the cylinder roughness and of the incoming flow turbulence. In particular the increase of roughness as well as the increase of turbulence shift the transition from sub-critical to critical regime towards lower Reynolds number.

3.2.4 *Buffeting*

Buffeting is, with vortex shedding, the other fluctuating part of the aerodynamic coefficients. It is induced by the presence of turbulent fluctuations in the incoming flow. The buffeting aerodynamic force depends on the body shape and on the turbulence characteristics. For many structures in which the wind induced resonant vibrations are negligible, the fluctuating wind responses can be computed using procedures applicable for static loads, such as the quasi-steady approach. Fluctuations of wind due to turbulence usually excite the low frequency turbulence, therefore a very long-span bridge can be very excited. The vibration amplitudes can be controlled by increasing the aerodynamic damping or equivalently by increasing the stability of the bridge.

The usual practice to measure buffeting forces in long-span suspension bridges is to measure the coefficients of the admittance matrix trough well defined wind tunnel tests.

3.3   AEROELASTIC MODEL OF A LONG-SPAN SUSPENSION BRIDGE

Suspended-span bridges must be designed to withstand both static and dynamic problems due to wind effects.

Static problems are related to the effect of the mean wind speed on the response of the structure. The static loads are functions both of the aerodynamic coefficients and of the angle of attack. In order to reduce the load transferred at the top of the supporting towers, the drag coefficient of the deck must be as small as possible. Static instability can occur for torsionally weak cross sections when a certain wind velocity is reached.

Dynamic problems are due to Aeroelastic effects, which include vortex induced vibrations, flutter, galloping and buffeting in the presence of self-excited forces.

Among the different approaches the *Quasi Steady Theory (QST)* is the most suitable to better understand the physics of the dynamic problems.

3.3.1 Quasi Steady Theory

The quasi steady theory well reproduces the aerodynamic forces on a deck if the reduced velocity $U^* = \frac{U}{fB}$ is greater than 10-15.

The reduced velocity represent the ratio between the period associated to the deck oscillation $T = \frac{1}{f}$ and the time $\frac{B}{U}$ needed by the fluid particle to move through the deck width. Thus, high reduced velocity means that the aerodynamic forces are not influenced by the motion frequency because the time needed by a fluid particle to cross the deck is very small compared to the period of oscillation of the deck itself. Instead, looking at f as the frequency of fluctuation of the turbulence spectrum, high reduced velocity means that the turbulence frequency must be small compared to the frequency associated to the fluid particle velocity $\frac{U}{B}$.

Let us consider a generic section of the bridge free to move in horizontal and vertical direction and to rotate in plane subjected to the mean wind speed, buffeting and self-excited motion of the deck, like the one depicted in Figure 3.12.
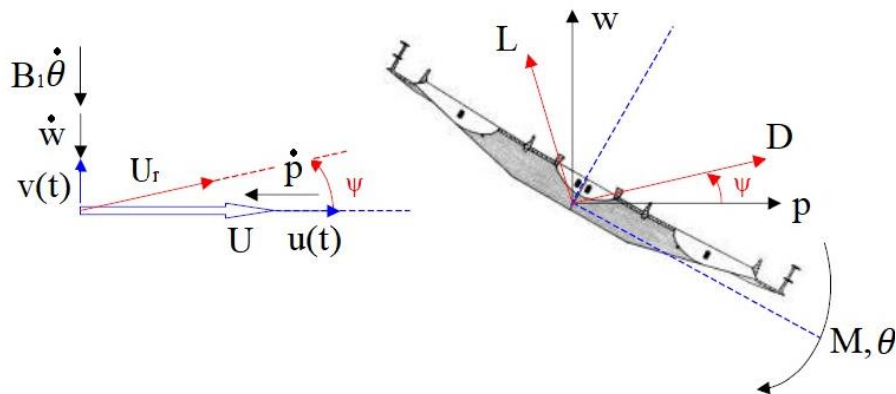
Figure 3.12: Deck aerodynamic forces and wind components

Aerodynamic forces are expressed in function of the aerodynamic coefficients, which are computed in the wind tunnel for different angles of attack, as a function of the relative velocity of the fluid with respect to the body U_r.

$$D = \frac{1}{2}\rho U_r^2 BLC_D(\alpha)$$

$$L = \frac{1}{2}\rho U_r^2 BLC_L(\alpha) \qquad (3.13)$$

$$M = \frac{1}{2}\rho U_r^2 B^2 LC_M(\alpha)$$

where $\alpha = \Psi + \theta$ is the angle of attack between the relative velocity and the bridge deck section.

The relative velocity U_r and the relative angle of attack Ψ are defined as:

$$U_r^2 = (U + u(t) - \dot{p})^2 + \left(v(t) - \dot{w} - B_1\dot{\theta}\right)^2$$

$$\Psi = arctg\left(\frac{v(t) - \dot{w} - B_1\dot{\theta}}{U + u(t) - \dot{p}}\right)$$

(3.14)

where B_1 indicates the position of a specific point upwind the deck centre G, essential to define the effect of a rotation in the vertical direction. This coefficient is different for each component of the aerodynamic forces and it can be computed trough wind tunnel tests.

With this simplified model the linear equation of motion of the deck reads as:

$$m_p\ddot{p} + c_p\dot{p} + k_p p = \tfrac{1}{2}\rho BL\left[(U + u(t) - \dot{p})^2 + \left(v(t) - \dot{w} - B_1\dot{\theta}\right)^2\right][C_D(\alpha)\cos(\Psi) + \\ -C_L\sin(\Psi)] = F_p$$

(3.15)

$$m_w\ddot{w} + c_w\dot{w} + k_w w = \tfrac{1}{2}\rho BL\left[(U + u(t) - \dot{p})^2 + \left(v(t) - \dot{w} - B_1\dot{\theta}\right)^2\right][C_D(\alpha)\sin(\Psi) + \\ +C_L\cos(\Psi)] = F_w$$

(3.16)

$$J_\theta\ddot{\theta} + c_\theta\dot{\theta} + k_\theta\theta = \tfrac{1}{2}\rho B^2 L\left[(U + u(t) - \dot{p})^2 + \left(v(t) - \dot{w} - B_1\dot{\theta}\right)^2\right]C_M(\alpha) = F_\theta$$

(3.17)

where it is clear that aerodynamic forces are dependent upon the motion of the deck, the wind turbulence component and the mean wind velocity.

A linear formulation of the aerodynamic forces may be considered in the hypothesis of small oscillations and small variations of the buffeting components. Thus, the linearized Aeroelastic forces, without considering the static wind components, can be written as:

$$F_p = \frac{1}{2}\rho BLU^2\left[K_D\left(\bar{\theta} + \frac{v - \dot{w} - B_{1y}\dot{\theta}}{U}\right) - C_{L0}\left(\frac{v - \dot{w} - B_{1y}\dot{\theta}}{U}\right)\right] + \rho BLUC_{D0}(u - \dot{p})$$

$$F_w = \frac{1}{2}\rho BLU^2\left[K_L\left(\bar{\theta} + \frac{v - \dot{w} - B_{1z}\dot{\theta}}{U}\right) - C_{L0}\left(\frac{v - \dot{w} - B_{1z}\dot{\theta}}{U}\right)\right] + \rho BLUC_{L0}(u - \dot{p})$$

(3.18)

$$F_\theta = \frac{1}{2}\rho B^2 LU^2\left[K_M\left(\bar{\theta} + \frac{v - \dot{w} - b_{1\theta}\dot{\theta}}{U}\right)\right] + \rho B^2 LUC_{M0}(u - \dot{p})$$

having linearized the aerodynamic coefficients around the equilibrium configuration as:

$$C_D(\alpha) = C_{D0} + \left(\frac{\partial C_D}{\partial \alpha}\right)_0 \alpha = C_{D0} + K_D \cdot \alpha$$

$$C_L(\alpha) = C_{L0} + \left(\frac{\partial C_L}{\partial \alpha}\right)_0 \alpha = C_{L0} + K_L \cdot \alpha \qquad (3.19)$$

$$C_M(\alpha) = C_{M0} + \left(\frac{\partial C_M}{\partial \alpha}\right)_0 \alpha = C_{M0} + K_M \cdot \alpha$$

The entire system can be written in matrix form.

$$\underline{\underline{M}}_s \underline{\ddot{X}} + \left(\underline{\underline{R}}_s - \underline{\underline{R}}_a\right)\underline{\dot{X}} + \left(\underline{\underline{K}}_s - \underline{\underline{K}}_a\right)\underline{X} = \underline{\underline{A}}_m \underline{b} \qquad (3.20)$$

where:

$\underline{X} = [p \ \ w \ \ \theta]^t$	Vector of displacements and rotation

$\underline{\underline{M}}_s, \underline{\underline{R}}_s, \underline{\underline{K}}_s$	Structural mass, damping and stiffness matrices

$$\underline{\underline{K}}_a = \frac{1}{2}\rho B L U^2 \begin{bmatrix} 0 & 0 & K_D \\ 0 & 0 & K_L \\ 0 & 0 & BK_M \end{bmatrix} \qquad \text{Aerodynamic stiffness matrix} \qquad (3.21)$$

$$\underline{\underline{R}}_a = -\frac{1}{2}\rho B L U \begin{bmatrix} 2C_{D0} & K_D - C_{L0} & B_{1y}(K_D - C_{L0}) \\ 2C_{L0} & K_L + C_{D0} & B_{1z}(K_L + C_{D0}) \\ 2C_{M0}B & BK_M & B_{1\theta}BK_M \end{bmatrix} \qquad \text{Aerodynamic damping matrix}$$

$$\underline{\underline{A}}_m = \frac{1}{2}\rho B L U \begin{bmatrix} 2C_{D0} & K_D - C_{L0} \\ 2C_{L0} & K_L + C_{D0} \\ 2C_{M0}B & BK_M \end{bmatrix} \qquad \text{Aerodynamic admittance matrix}$$

The Aeroelastic effects change the structural damping and stiffness matrices in function of the wind velocity. The higher is the wind velocity, the higher the self-excited terms become important. Moreover the system is no more symmetric and self-adjoint, thus it can be subjected to different kind of dynamic instabilities.

3.3.2 *Flutter Derivatives*

The Quasi Steady Theory uses aerodynamic coefficients computed thanks to static wind tunnel tests and it is valid only for high reduced velocity, which is a too restrictive hypothesis.

In order to define the aerodynamic forces as a function of the deck motion and the incoming turbulence, dynamic wind tunnel tests have to be done. In particular two different methods are available, the "Free motion method" and the "Forced motion method". The latter is more expensive, but it is much more reliable. It consists in forcing a deck sectional model to vibrate harmonically in the horizontal, vertical or torsional direction and to measure the drag, lift and moment forces in function of the reduced velocity. Obviously, for high reduced velocity, the aerodynamic coefficients must be the same of the ones computed with the Quasi Steady Theory. The problem is non linear, because the input is an harmonic motion and the output is not harmonic, so with the aim of simplifying it, aerodynamic coefficients are linearized by considering a fixed angle of attack. Several tests at different angles of attack are generally done. To find the stiffness and the damping Aeroelastic matrices, it is necessary to compute the transfer functions between the input and the output at the given reduced velocity. The real part of the transfer function indentifies the terms of the stiffness matrix, being in phase with the displacements, while the imaginary part identifies the damping matrix, since it is out of phase with the displacements and in phase with the velocities.

Aerodynamic transfer functions are usually presented trough *Flutter Derivatives*. The most used formulation is the one proposed by Simiu and Scanlan [52].

$$D = \frac{1}{2}\rho U^2 B \left[KP_1^* \frac{\dot{p}}{U} + KP_2^* \frac{B\dot{\theta}}{U} + K^2 P_3^* \theta + K^2 P_4^* \frac{p}{B} \right]$$

$$L = \frac{1}{2}\rho U^2 B \left[KH_1^* \frac{\dot{w}}{U} + KH_2^* \frac{B\dot{\theta}}{U} + K^2 H_3^* \theta + K^2 H_4^* \frac{w}{B} \right] \tag{3.22}$$

$$M = \frac{1}{2}\rho U^2 B^2 \left[KA_1^* \frac{\dot{w}}{U} + KA_2^* \frac{B\dot{\theta}}{U} + K^2 A_3^* \theta + K^2 A_4^* \frac{w}{B} \right]$$

where:

1. $K = \frac{B\omega}{U}$ is the reduced frequency, defined as the inverse of the reduced velocity;

2. P_i^*, H_i^* and A_i^* are the flutter derivatives, function of the reduced frequency, correspondent to the drag, lift and moment forces, respectively.

Theoretically, equations (3.22) must contain also some terms related to the acceleration $\ddot{y}$, $\ddot{z}$ and $\ddot{\theta}$. These terms are omitted as being of negligible importance in common structural engineering problems. In fact they give rise to an aerodynamic mass matrix, which is much lower with respect to the structural mass matrix.

Moreover it is important to notice that the terms inside the brackets are non-dimensional and can be viewed as following the classical pattern of the expressions for aerodynamic coefficients.

Chen and Kareem [20] studied the influence of the drag aerodynamic coefficients on the bridge's flutter stability. The contribution of the drag force is not significant in the case of hard type flutter, where the aerodynamic damping generated by lift and pitching moment rapidly develops as wind velocity increases. The drag aerodynamic coefficients become important for truss deck sections, e.g. the Akashi Kaikyo Bridge. For this kind of sections, the drag force induced by torsional motion has a large contribution and its negative damping effect affects the flutter performances of the bridge. However, for bridges characterized by low static drag force and large self-excited lift and pitching moment, the contribution of self-excited drag force is negligible. In this context it is possible to consider a 2 DoF$_s$ model, without taking into considerations for the drag self-excited forces.

The modal expansion already exploited in (2.43) and (2.62) is now recalled with the aim of projecting the Aeroelastic forces in the modal space.

$$w(x,t) = \sum_{n=1}^{+\infty} W_n(x) \cdot z_n(t)$$

$$\theta(x,t) = \sum_{m=1}^{+\infty} \Theta_m(x) \cdot \gamma_m(t)$$

(3.23)

Substituting the modal expansion (3.23) into the expressions of the aerodynamic lift and moment forces (3.22) and projecting them into the Galerkin plane:

$$L = \frac{1}{2}\rho U^2 2b \left[\frac{KH_1^*}{U} \int_0^l W_n^2(x)\,dx \cdot \dot{z}_n(t) + \frac{KH_2^* 2b}{U} \int_0^l W_n(x)\,\Theta_m(x)dx \cdot \dot{\gamma}_m(t) + \right.$$
$$\left. + K^2 H_3^* \int_0^l W_n(x)\,\Theta_m(x)dx \cdot \gamma_m(t) + \frac{K^2 H_4^*}{2b} \int_0^l W_n^2(x)\,dx \cdot z_n(t) \right]$$

(3.24)

$$M = \frac{1}{2}\rho U^2 (2b)^2 \left[\frac{KA_1^*}{U} \int_0^l W_n(x)\,\Theta_m(x)dx \cdot \dot{z}_n(t) + \frac{KA_2^* 2b}{U} \int_0^l \Theta_m^2(x)dx \cdot \dot{\gamma}_m(t) + \right.$$
$$\left. + K^2 A_3^* \int_0^l \Theta_m^2(x)dx \cdot \gamma_m(t) + \frac{K^2 A_4^*}{2b} \int_0^l W_n(x)\,\Theta_m(x)dx \cdot z_n(t) \right]$$

It is possible to introduce some coefficients indicating the integration of the shape functions over the whole span:

$$G_{W_n W_n} = \int_0^l W_n^2(x)\, dx$$

$$G_{W_n \Theta_m} = \int_0^l W_n(x)\, \Theta_m(x) \tag{3.25}$$

$$G_{\Theta_m \Theta_m} = \int_0^l \Theta_m^2(x)\, dx$$

Thus, the aerodynamic stiffness and damping matrix $\underline{\underline{K}}_a$ and $\underline{\underline{R}}_a$ can be written as:

$$\underline{\underline{K}}_a = \frac{1}{2}\rho U^2 K^2 \begin{bmatrix} G_{W_n W_n} \cdot H_4^* & 2b G_{W_n \Theta_m} \cdot H_3^* \\ 2b G_{W_n \Theta_m} \cdot A_4^* & (2b)^2 G_{\Theta_m \Theta_m} \cdot A_3^* \end{bmatrix} \tag{3.26}$$

$$\underline{\underline{R}}_a = \rho U^2 \frac{bK}{U} \begin{bmatrix} G_{W_n W_n} \cdot H_1^* & 2b G_{W_n \Theta_m} \cdot H_2^* \\ 2b G_{W_n \Theta_m} \cdot A_1^* & (2b)^2 G_{\Theta_m \Theta_m} \cdot A_2^* \end{bmatrix} \tag{3.27}$$

Without considering the buffeting forces the system corresponds to:

$$\underline{\underline{M}}_s \ddot{\underline{q}} + \left(\underline{\underline{R}}_s - \underline{\underline{R}}_a \right) \dot{\underline{q}} + \left(\underline{\underline{K}}_s - \underline{\underline{K}}_a \right) \underline{q} = 0 \tag{3.28}$$

where $\underline{q} = [z_n \ \gamma_m]^t$ is the vector of modal displacements and rotations. The structural mass, damping and stiffness matrices are diagonal.

$$\underline{\underline{M}}_s = \begin{bmatrix} m_w \int_0^l W_n^2(x)\, dx & 0 \\ 0 & J_\theta \int_0^l \Theta_m^2(x)\, dx \end{bmatrix} = \begin{bmatrix} m_{w,n} & 0 \\ 0 & J_{\theta,m} \end{bmatrix} \tag{3.29}$$

$$\underline{\underline{R}}_s = \begin{bmatrix} 2 m_{w,n} \Delta_{w,n} \Omega_{w,n} & 0 \\ 0 & 2 J_{\theta,m} \Delta_{\theta,m} \Omega_{\theta,m} \end{bmatrix} \tag{3.30}$$

$$\underline{\underline{K}}_s = \begin{bmatrix} m_{w,n} \Omega_{w,n}^2 & 0 \\ 0 & J_{\theta,m} \Omega_{\theta,m}^2 \end{bmatrix} \tag{3.31}$$

The modal frequencies and damping ratios affected by the self-excited forces can be computed by seeking a solution in the form of:

$$\underline{q} = \underline{q}_0 e^{\lambda t} \tag{3.32}$$

leading to the following Eigenvalue problem:

$$\left[\lambda^2 \underline{\underline{M}}_s + \lambda \left(\underline{\underline{R}}_s - \underline{\underline{R}}_a \right) + \left(\underline{\underline{K}}_s - \underline{\underline{K}}_a \right) \right] \underline{q}_0 e^{\lambda t} = 0 \tag{3.33}$$

where $\lambda = -\xi\omega + i\omega\sqrt{1 - \xi^2}$ is the Eigenvalue, being ξ and ω the circular frequency and damping ratio of the complex modal branch of interest, respectively.

Notice the difference between the groups $[\Omega, \Delta]$ and $[\omega, \xi]$ which indicate the circular frequency and the modal damping ratio coming from the structural model and the complete Aeroelastic one, respectively.

The term inside the brackets is a matrix called impedance matrix, or state matrix $\underline{\underline{H}}(\lambda)$.

$$\underline{\underline{H}}(\lambda) \underline{q}_0 e^{\lambda t} = 0 \tag{3.34}$$

The stability limits of the problem are determined by the condition:

$$\det \left[\underline{\underline{H}}(\lambda) \right] = \left| \underline{\underline{H}}(\lambda) \right| = 0 \tag{3.35}$$

Different kinds of instability can occur:

1. Static torsional divergence;

2. Galloping (or 1 DoF flexural instability);

3. 1 DoF torsional flutter;

4. Classical 2 DoFs flutter.

3.3.3 *Torsional Divergence*

The phenomenon of torsional divergence is of static nature and it is due to a loss of torsional stiffness. More specifically, the structure under the effect of wind is subjected to a drag, a lift and a twisting moment force. In particular, as the wind velocity increases, the twisting moment and the torsional rotation of the structure increases too. The relative angle of attack of the wind changes leading to an increase in the twisting moment, which then

demands additional reactive moment from the structure. At a given wind velocity, namely the divergence speed, the magnitude of the wind-induced moment cannot be counteracted by the torsional deck stiffness, leading the structure to an unstable condition. This problem is similar to the structural stability of a column subjected to a buckling load, with the difference that torsional divergence occurs at some critical divergence velocity of the wind and it is not associated to a critical load.

To analyze the torsional divergence phenomenon, let us consider the section of the deck free to rotate around its centroid. Considering a linearization of the moment coefficient around the equilibrium position correspondent to $\theta = 0$, the static equation of motion of this system is:

$$k_\theta \theta = \frac{1}{2} \rho U^2 (2b)^2 (C_{M0} + K_M \cdot \theta) \tag{3.36}$$

The two-dimensional description of the divergence problem is well represented by equation (3.36), which has the following solution.

$$\theta = \frac{2\rho U^2 b^2 C_{M0}}{k_\theta - 2\rho U^2 b^2 K_M} \tag{3.37}$$

The solution (3.37) diverges for:

$$k_\theta - 2\rho U^2 b^2 K_M = 0 \tag{3.38}$$

From equation (3.38) it is possible to find the critical divergence velocity:

$$U_D = \sqrt{\frac{k_\theta}{2\rho b^2 K_M}} \tag{3.39}$$

The phenomenon depends upon the structural torsional stiffness of the deck and upon the slope of the moment coefficient K_M. Some kind of structures can be immune to torsional divergence, depending on their relation between aerodynamic moment and angle of attack. Anyhow in most case of practical interest in civil engineering the critical divergence velocity is extremely high, well beyond the range of velocities normally considered in design. Only torsionally weak bridges deck incur the actual danger of torsional divergence at wind speed attainable in practice.

It should be noted that if the slope of the moment coefficient is negative, the deck creates a negative angle of attack with the incoming wind. Such decks are not highly susceptible to

torsional divergence at wind speeds in the usual range, whereas if the slope of the moment coefficient is positive a theoretical torsional divergence is still possible.

In the case studied the torsional stiffness can be expressed in non-dimensional form as:

$$k_\theta = \Omega_{\theta,m}^2 J_{\theta,m} = \tilde{\Omega}_{\theta,m}^2 \frac{2H}{l^2(m_d + 2m_c)} \tilde{J}_t(m_d + 2m_c)b^2 \qquad (3.40)$$

Thus, the critical divergence velocity (3.39) becomes:

$$U_D = \sqrt{\tilde{J}_t}\,\tilde{\Omega}_{\theta,m}\sqrt{\frac{2H}{2\rho l^2 K_M}} \qquad (3.41)$$

The slope of the moment coefficient can be determined from wind tunnel tests on rigid models for different angles of attack. For simple sectional shapes of the wing, it is possible to get analytical expressions for the aerodynamic coefficients. In particular, for the case of thin plate in steady motion, Bisplinghoff et al. [12] found that:

$$C_M = \pi\alpha\left(a + \frac{1}{2}\right) \qquad (3.42)$$

being a the distance between the elastic centre of the section and the Aeroelastic one. Considering the Aeroelastic centre perfectly coincident with the elastic one ($a = 0$), the derivative of the moment coefficient with respect to the angle of attack is $K_M = \frac{\pi}{2}$.

The divergence velocity can be expressed in a very simple way as:

$$U_D = \sqrt{\tilde{J}_t}\,\tilde{\Omega}_{\theta,m}\sqrt{\frac{2H}{\rho\pi l^2}} \qquad (3.43)$$

The value of the critical divergence velocity is important to provide an upper limit to the admissible wind speed which must be taken into account for a flutter analysis. In fact, as it usually happens, the static unstable limit requires higher extreme conditions with respect to its dynamic counterpart. Hence, the divergence critical speed is the threshold beyond which is no more interesting to investigate further the dynamic instability problem since the system undergoes to a static unstable condition.

3.3.4 1 DoF Flexural Instability

Galloping, or 1 DoF flexural instability, is a single mode instability phenomenon characterized by an oscillating motion perpendicular to the wind direction. It is worth mentioning that the term galloping in this case is not related to vortex shedding, as usual in cable aerodynamics. The occurrence of this phenomenon is due to the negative aerodynamic net flexural damping, which can bring the system to have null damping in the flexural motion.

The total net flexural damping is given by the difference between the first diagonal terms of equations (3.30) and (3.27). The condition for galloping initiation is when this damping is null:

$$2m_{w,n}\Delta_{w,n}\Omega_{w,n} - \frac{1}{2}\rho U^2 \frac{2bK}{U} H_1^* G_{W_n W_n} = 0 \qquad (3.44)$$

Therefore, the onset for the initiation of 1 DoF flexural instability is when:

$$H_1^* G_{W_n W_n} \geq \frac{m_{w,n}\Delta_{w,n}}{\rho b^2} \qquad (3.45)$$

with $H_1^* > 0$.

It is worth nothing that H_1^* is strictly related with the slope of the lift coefficient, indeed comparing the damping matrices in (3.21) and (3.27), it results that H_1^* coincides with $-K_L$. Hence, galloping can happen only for negative slope of the lift coefficient, which is unusual in airfoil deck types.

The expression (3.45) can be extended to our model simply substituting the proper expression for the mass $m_{w,n} = (m_d + 2m_c)G_{W_n W_n}$:

$$H_1^* \geq \frac{(m_d + 2m_c)\Delta_{w,n}}{\rho b^2} \qquad (3.46)$$

Thanks to the definition given by Theodorsen [53] of non-dimensional Aerodynamic mass:

$$\widetilde{m}_a = \frac{\rho \pi b^2}{m_d + 2m_c} \qquad (3.47)$$

the condition on the flutter derivative H_1^* for galloping initiation becomes:

$$H_1^* \geq \frac{\pi}{\widetilde{m}_a}\Delta_{w,n} \qquad (3.48)$$

3.3.5 *1 DoF Torsional Flutter*

Mono-dimensional flutter, or 1 DoF torsional instability, is a single mode instability phenomenon caused by negative aerodynamic net torsional damping. Usually it happens for the lowest torsional degree of freedom, which in modern contemporary bridges is expected to be the first symmetric torsional mode.

The condition for the zeroing of the net torsional damping reads as:

$$2J_{\theta,m}\Delta_{\theta,m}\Omega_{\theta,m} - \frac{1}{2}\rho U^2 \frac{2bK}{U}A_2^*(2b)^2 G_{\Theta_m\Theta_m} = 0 \tag{3.49}$$

Simplyfing equation (3.49), the following formula for the onset of 1 DoF torsional flutter is found.

$$A_2^* G_{\Theta_m\Theta_m} \geq \frac{J_{\theta,m}\Delta_{\theta,m}}{4\rho b^4} \tag{3.50}$$

with $A_2^* > 0$.

It has to be noted that A_2^* represents the slope of the moment coefficient, because it is strictly related to $-K_M$. Therefore 1 DoF torsional instability can happen only in the case of negative slope of the moment coefficient.

In general for flat plates and for streamlined bridge deck sections A_2^* is negative, which means that they cannot suffer of this kind of instability phenomenon. Instead this flutter derivative can be positive for bluff deck section. The most important example in bridge engineering of positive value of A_2^* is the Tacoma Narrows bridge.

The closed formula given by equation (3.50) is the same of the one found by Simiu and Scanlan [52], with the simplified assumption of negligible aerodynamic stiffness effect due to A_3^*.

The straightforward extension of the expression (3.50) to our model, considering the deck inertia $J_{\theta,m} = \tilde{J}_t(m_d + 2m_c)b^2 G_{\Theta_m\Theta_m}$ and the definition of Aerodynamic mass $\tilde{m}_a$ provided by equation (3.47), is:

$$A_2^* \geq \frac{\pi}{4}\frac{\tilde{J}_t}{\tilde{m}_a}\Delta_{\theta,m} \tag{3.51}$$

This simple formulation allows us to find the critical flutter velocity simply knowing the main structural parameters and the variation of A_2^* with the reduced velocity, easily found by wind tunnel tests.

It is important to stress the fact that the formulas provided for the occurrence of 1 DoF flexural or torsional instability (eq. (3.48) and (3.51)) have been found considering a single mode approximation to the total response. This kind of assumption is justifiable from observation of the fact that typically just one prominent mode becomes unstable and dominate the structural response. However, the complex Eigenvalue analysis approach postulated in (3.33) is computationally effective and it gives the exact wind velocity causing instability, whatever the kind of unstable motion is.

3.3.6 *Classical Flutter*

Classical flutter, or 2 DoFs flutter, implies an Aeroelastic phenomenon in which two Degrees of Freedom of the structure, namely the rotation and the vertical translation, couple together in a flow-driven unstable oscillation. Coupling of the two DoFs has come to be the identifying sign for classical flutter.

The method to find the flutter critical conditions is to solve the Eigenvalue problem (3.33) by setting the determinant of the state matrix equal to zero. This complex Eigenvalue analysis approach is very effective from the computational point of view and it provides the exact critical flutter speed, both in the case of 1 DoF flutter and classical flutter. The solution of the equations of motion of Aeroelastic bridge systems provides information on how the self-excited forces influence modal frequencies, damping ratios and intermodal coupling as the wind velocity increases.

However, in order to better understand the main paramethers affecting flutter and to understand the significance of structural and aerodynamic characteristics, a bimodal coupled flutter analysis is an accurate and useful tool. In fact experimental evidence have shown that bridge flutter is often dominated by the fundamental vertical bending and torsional modes with only secondary contributions from other modes. In particular, Chen and Kareem [19] presented a framework with closed-form solutions to estimate the modal frequencies, damping ratios and coupled motions of both vertical and torsional modal branches at varying wind velocities.

With the aim of doing a bimodal coupled flutter analysis, only two vibrating modes are considered in the system of equation (3.33), $z_1(t)$ and $\gamma_2(t)$.

$$\left[\lambda^2 \underline{\underline{M}}_s + \lambda \underline{\underline{R}}_s + \underline{\underline{K}}_s\right] \underline{q}_0 e^{\lambda t} = \left[\underline{\underline{R}}_a \lambda + \underline{\underline{K}}_a\right] \underline{q}_0 e^{\lambda t} \tag{3.52}$$

where the different structural and aerodynamic matrices are defined as:

$$\underline{\underline{M}}_s = \begin{bmatrix} m_{w,1} & 0 \\ 0 & J_{\theta,2} \end{bmatrix}$$

$$\underline{\underline{R}}_s = \begin{bmatrix} 2m_{w,1}\Delta_{w,1}\Omega_{w,1} & 0 \\ 0 & 2J_{\theta,2}\Delta_{\theta,2}\Omega_{\theta,2} \end{bmatrix}$$

$$\underline{\underline{K}}_s = \begin{bmatrix} m_{w,1}\Omega_{w,1}^2 & 0 \\ 0 & J_{\theta,2}\Omega_{\theta,2}^2 \end{bmatrix} \tag{3.53}$$

$$\underline{\underline{K}}_a = \frac{1}{2}\rho U^2 K^2 \begin{bmatrix} H_4^* G_{W_1 W_1} & H_3^* B G_{W_1 \Theta_2} \\ A_4^* B G_{W_1 \Theta_2} & A_3^* B^2 G_{\Theta_2 \Theta_2} \end{bmatrix}$$

$$\underline{\underline{R}}_a = \frac{1}{2}\rho U^2 \frac{BK}{U} \begin{bmatrix} H_1^* G_{W_1 W_1} & H_2^* B G_{W_1 \Theta_2} \\ A_1^* B G_{W_1 \Theta_2} & A_2^* B^2 G_{\Theta_2 \Theta_2} \end{bmatrix}$$

The critical flutter velocity is determined when one of the modal damping ratios becomes zero. The problem can be solved in closed form only assuming a low level of damping, which means:

$$\lambda^2 \cong -\omega^2 - 2i\omega^2\xi$$

$$\lambda \cong i\omega \tag{3.54}$$

Due to this hypothesis, the flutter derivatives are function of the reduced frequency only and not of the damping. This approximation is by no means restrictive.

Bringing the uncoupled terms on the left-hand side and leaving the coupled ones on the right-hand side, the equations of motion become:

$$\left[-\omega^2 - 2i\omega^2\xi + 2i\Delta_{w,1}\Omega_{w,1}\,\omega - \frac{1}{2}\frac{\rho(2b)^2}{m_{w,1}}\,G_{W_1 W_1} i\omega^2 H_1^* + \Omega_{w,1}^2 - \frac{1}{2}\frac{\rho(2b)^2}{m_{w,1}}\,G_{W_1 W_1}\omega^2 H_4^* \right] \cdot$$

$$z_{10}e^{\lambda t} = 2b \cdot \left[\frac{1}{2}\frac{\rho(2b)^2}{m_{w,1}}\,G_{W_1 W_1}\omega^2 (H_3^* + iH_2^*) \frac{G_{W_1 \Theta_2}}{\sqrt{G_{W_1 W_1} G_{\Theta_2 \Theta_2}}} \sqrt{\frac{G_{\Theta_2 \Theta_2}}{G_{W_1 W_1}}} \right] \cdot \gamma_{20}e^{\lambda t} \tag{3.55}$$

$$\left[-\omega^2 - 2i\omega^2\xi + 2i\Delta_{\theta,2}\Omega_{\theta,2}\,\omega - \frac{1}{2}\frac{\rho(2b)^4}{J_{\theta,2}}\,G_{\Theta_2 \Theta_2} i\omega^2 A_2^* + \Omega_{\theta,2}^2 - \frac{1}{2}\frac{\rho(2b)^4}{J_{\theta,2}}\,G_{\Theta_2 \Theta_2}\omega^2 A_3^* \right] \cdot$$

$$\gamma_{20}e^{\lambda t} = \frac{1}{2b} \cdot \left[\frac{1}{2}\frac{\rho(2b)^4}{J_{\theta,2}}\,G_{\Theta_2 \Theta_2}\omega^2 (A_4^* + iA_1^*) \frac{G_{W_1 \Theta_2}}{\sqrt{G_{W_1 W_1} G_{\Theta_2 \Theta_2}}} \sqrt{\frac{G_{W_1 W_1}}{G_{\Theta_2 \Theta_2}}} \right] \cdot z_{10}e^{\lambda t} \tag{3.56}$$

Some non-dimensional quantities can be defined in order to write the equations in a simpler form:

$$\mu = \frac{1}{2}\frac{\rho B^2}{m_{w,1}}\,G_{W_1 W_1} = 2\frac{\rho b^2}{m_{w,1}}\,G_{W_1 W_1}$$

$$\nu = \frac{1}{2}\frac{\rho B^4}{J_{\theta,2}}\,G_{\Theta_2 \Theta_2} = 8\frac{\rho b^4}{J_{\theta,2}}\,G_{\Theta_2 \Theta_2}$$

$$\bar{\omega}_1 = \Omega_{w,1}\left[1 - \mu\left(\frac{\omega}{\Omega_{w,1}}\right)^2 H_4^*\right]^{\frac{1}{2}}$$

$$\bar{\xi}_1 = \Delta_{w,1}\frac{\Omega_{w,1}}{\bar{\omega}_1} - \xi\frac{\omega}{\bar{\omega}_1} - \frac{1}{2}\mu\frac{\omega}{\bar{\omega}_1}H_1^*$$

$$\bar{\omega}_2 = \Omega_{\theta,2}\left[1 - \nu\left(\frac{\omega}{\Omega_{\theta,2}}\right)^2 A_3^*\right]^{\frac{1}{2}}$$

$$\bar{\xi}_2 = \Delta_{\theta,2}\frac{\Omega_{\theta,2}}{\bar{\omega}_2} - \xi\frac{\omega}{\bar{\omega}_2} - \frac{1}{2}\nu\frac{\omega}{\bar{\omega}_2}A_2^*$$

$$D = \frac{G_{W_1 \Theta_2}}{\sqrt{G_{W_1 W_1} G_{\Theta_2 \Theta_2}}}$$

(3.57)

where:

1. $\bar{\omega}_j$ and $\bar{\xi}_j$ ($j = 1,2$) are the frequencies and damping ratios influenced only by the uncoupled self-excitation forces associated with H_1^*, H_4^*, A_2^* and A_3^*;

2. D is the similarity factor in modal shapes of the fundamental vertical and torsional modes, i.e., $D = 0$ and $D = 1$ indicate that two mode shapes are orthogonal and identical, respectively.

Thus:

$$\left[-\omega^2 + 2i\omega\bar{\omega}_1\bar{\xi}_1 + \bar{\omega}_1^2\right]z_{10}e^{\lambda t} = \mu D\omega^2(H_3^* + iH_2^*)\sqrt{\frac{G_{\Theta_2 \Theta_2}}{G_{W_1 W_1}}}\,2b\gamma_{20}e^{\lambda t} \tag{3.58}$$

$$\left[-\omega^2 + 2i\omega\bar{\omega}_2\bar{\xi}_2 + \bar{\omega}_2^2\right]2b\gamma_{20}e^{\lambda t} = \nu D\omega^2(A_4^* + iA_1^*)\sqrt{\frac{G_{W_1 W_1}}{G_{\Theta_2 \Theta_2}}}\,z_{10}e^{\lambda t} \tag{3.59}$$

Chen and Kareem [19] solved equations (3.58) and (3.59) in closed form.

In the case of uncoupled system, i.e. when H_2^*, H_3^*, A_1^* and A_4^* are contemporary null for a given reduced frequency, the modal frequencies and damping ratios are provided by Scanlan [50]:

$$\omega_{10} = \Omega_{w,1}(1 + \mu H_4^*)^{-\frac{1}{2}}$$

$$\xi_{10} = \Delta_{w,1}\frac{\Omega_{w,1}}{\bar{\omega}_1} - \frac{1}{2}\mu H_1^*$$

$$\omega_{20} = \Omega_{\theta,2}(1 + \nu A_3^*)^{-\frac{1}{2}} \tag{3.60}$$

$$\xi_{20} = \Delta_{\theta,2}\frac{\Omega_{\theta,2}}{\bar{\omega}_2} - \frac{1}{2}\nu A_2^*$$

In this particular case $\omega_{10} = \bar{\omega}_1$, $\omega_{20} = \bar{\omega}_2$, $\bar{\bar{\xi}}_1 = 0$ and $\bar{\bar{\xi}}_2 = 0$.

However, being the flutter derivatives function of the reduced frequency, for the bimodal coupled system in general $\omega_{10} \neq \bar{\omega}_1$ and $\omega_{20} \neq \bar{\omega}_2$. But Chen [18] states that: "The modal frequencies of the coupled system are generally very close to those of the corresponding uncoupled system at the same wind velocity. In addition, the influence of the uncoupled self-excited forces on modal frequencies is not sensitive to the change in reduced frequency."

Hence:

$$\bar{\omega}_1 = \Omega_{w,1}\left[1 - \mu\left(\frac{\omega}{\Omega_{w,1}}\right)^2 H_4^*\right]^{\frac{1}{2}} \approx \omega_{10}$$

$$\tag{3.61}$$

$$\bar{\omega}_2 = \Omega_{\theta,2}\left[1 - \nu\left(\frac{\omega}{\Omega_{\theta,2}}\right)^2 A_3^*\right]^{\frac{1}{2}} \approx \omega_{20}$$

The solution of the coupled system of equations (3.58) and (3.59) is found considering the solution of the vertical mode branch $\omega = \omega_1$ closer to $\bar{\omega}_1$ than $\bar{\omega}_2$ and the damping ratio $\xi = \xi_1$. The associated amplitude ratio Φ and phase difference between the vertical motion and torsion ϕ, as defined by $B\gamma_{20}/z_{10} = \Phi e^{i\phi}$ are:

$$\omega_1 = \Omega_{w,1}(1 + \mu H_4^* + \mu\nu D^2\Phi'\cos\phi')^{-\frac{1}{2}} \tag{3.62}$$

$$\xi_1 = \Delta_{w,1}\frac{\Omega_{w,1}}{\bar{\omega}_1} - \frac{1}{2}\mu H_1^* - \frac{1}{2}\mu\nu D^2\Phi'\sin\phi' \tag{3.63}$$

$$\Phi = \nu D R_{d1}\left\{[(A_4^*)^2 + (A_1^*)^2]\frac{G_{W_1 W_1}}{G_{\Theta_2\Theta_2}}\right\}^{\frac{1}{2}} \tag{3.64}$$

$$\phi = \tan^{-1}\frac{A_1^*}{A_4^*} - \tan^{-1}\frac{2\bar{\xi}_2\frac{\omega_1}{\bar{\omega}_2}}{1 - \left(\frac{\omega_1}{\bar{\omega}_2}\right)^2} \tag{3.65}$$

where:

$$R_{d1} = \left(\frac{\omega_1}{\overline{\omega}_2}\right)^2 \left\{ \left[1 - \left(\frac{\omega_1}{\overline{\omega}_2}\right)^2 \right]^2 + \left[2\overline{\xi}_2 \frac{\omega_1}{\overline{\omega}_2} \right]^2 \right\}^{-\frac{1}{2}}$$

$$\Phi' = R_{d1}\{[(H_3^*)^2 + (H_2^*)^2][(A_4^*)^2 + (A_1^*)^2]\}^{\frac{1}{2}}$$

$$\phi' = \tan^{-1}\frac{H_2^*}{H_3^*} + \phi$$

(3.66)

Notice that a positive value of the phase difference indicates that the vertical motion lags the torsional one.

In a complete similar way, for the torsional modal branch, considering $\omega = \omega_2$ closer to $\overline{\omega}_2$ than $\overline{\omega}_1$ and the damping ratio $\xi = \xi_2$, the solution, expressed trough the amplitude ratio Ψ and phase difference between the vertical motion and torsion ψ, as defined by $z_{10}/B\gamma_{20} = \Psi e^{i\psi}$ are expressed as:

$$\omega_2 = \Omega_{\theta,2}(1 + \nu A_3^* + \mu\nu D^2\Psi' \cos\psi')^{-\frac{1}{2}}$$

(3.67)

$$\xi_2 = \Delta_{\theta,2}\frac{\Omega_{\theta,2}}{\overline{\omega}_2} - \frac{1}{2}\nu A_2^* - \frac{1}{2}\mu\nu D^2\Psi' \sin\psi'$$

(3.68)

$$\Psi = \nu D R_{d2}\left\{[(H_3^*)^2 + (H_2^*)^2]\frac{G_{\Theta_2\Theta_2}}{G_{W_1W_1}}\right\}^{\frac{1}{2}}$$

(3.69)

$$\psi = \tan^{-1}\frac{H_2^*}{H_3^*} - \tan^{-1}\frac{2\overline{\xi}_1\frac{\omega_2}{\overline{\omega}_1}}{1 - \left(\frac{\omega_2}{\overline{\omega}_1}\right)^2}$$

(3.70)

where:

$$R_{d2} = \left(\frac{\omega_2}{\overline{\omega}_1}\right)^2 \left\{ \left[1 - \left(\frac{\omega_2}{\overline{\omega}_1}\right)^2 \right]^2 + \left[2\overline{\xi}_1 \frac{\omega_2}{\overline{\omega}_1} \right]^2 \right\}^{-\frac{1}{2}}$$

$$\Psi' = R_{d2}\{[(H_3^*)^2 + (H_2^*)^2][(A_4^*)^2 + (A_1^*)^2]\}^{\frac{1}{2}}$$

$$\psi' = \tan^{-1}\frac{A_1^*}{A_4^*} + \phi$$

(3.71)

Now a positive value of the phase difference indicates that the torsional motion lags the vertical one.

It is clear from the previous solutions that uncoupled aerodynamic stiffness and damping forces enter directly in the equation for the frequency and damping, while the coupled terms are represented by the amplitude ratio and the phase difference. The influence of the coupled aerodynamic contribution on the variation of frequencies is relatively small, but they change in a significant way the torsional and flexural damping.

Also with this closed form solution, the quantification of the modal frequencies and damping ratios of the coupled system requires an iterative process, since the right-hand side terms involve unknown frequencies and damping. This iterative process converge rapidly and, if one uses the values of frequencies and damping ratios computed at the previous wind velocity, it is possible to eliminate the iterative calculations.

Equations (3.63) and (3.68) highlights the fact that galloping or single torsional mode flutter may arise only when $H_1^* > 0$ or $A_2^* > 0$, respectively, in complete agreement with §3.3.4 and §3.3.5.

For bridges with slender deck sections, usually $H_1^* < 0$ and $A_2^* < 0$, which means that the uncoupled self-excited forces introduce positive aerodynamic damping in the system. In this case, instability is produced by the coupled self-excited terms which introduce a phase lag between the modes of vibration. In particular the coupled motion allows the coupled self-excited forces to produce a positive damping to the vertical modal branch, being $\sin \phi' < 0$ in equation (3.63), and a negative damping to the torsional modal branch, being $\sin \psi' > 0$ in equation (3.68). Therefore the bimodal coupled flutter is likely to be initiated from the zeroing of the damping in the torsional branch.

The proposed framework offers intuitive insight into the significance of both structural and aerodynamic characteristics to classical flutter instability. In particular Chen and Kareem [19] state that: "The uncoupled self-excited forces due to displacements, i.e., terms related to H_4^* and A_3^*, reduce the modal frequencies and thus have unfavourable influences on flutter. The uncoupled self-excited forces due to bridge deck velocities, i.e., terms related to H_1^* and A_2^*, increase the modal damping and thus these are beneficial to flutter. The negative damping generated by the coupled forces, i.e., terms related to H_2^*, A_4^*, H_3^* and A_1^*, is the main contributing source that drives the bridge to coupled flutter instability."

The flutter derivatives H_3^*, A_1^*, A_2^* and A_3^* are the most influential to coupled flutter.

3.3.7 *Simplified closed-Form solutions and Critical Flutter Velocity*

Having said that the modal frequencies of the coupled system are generally very close to those of the corresponding uncoupled one, it is possible to simplify equations (3.62) and (3.67) without taking into account for the coupling terms:

$$\omega_1 \approx \bar{\omega}_1 = \Omega_{w,1}\left[1 - \mu\left(\frac{\omega}{\Omega_{w,1}}\right)^2 H_4^*\right]^{\frac{1}{2}} = \omega_{10} = \Omega_{w,1}(1 + \mu H_4^*)^{-\frac{1}{2}} \tag{3.72}$$

$$\omega_2 \approx \bar{\omega}_2 = \Omega_{\theta,2}\left[1 - \nu\left(\frac{\omega}{\Omega_{\theta,2}}\right)^2 A_3^*\right]^{\frac{1}{2}} = \omega_{20} = \Omega_{\theta,2}(1 + \nu A_3^*)^{-\frac{1}{2}} \tag{3.73}$$

When the modal frequencies of the uncoupled system are well separated one from each other, R_{d1} and R_{d2} are not influenced by the values of $\bar{\bar{\xi}}_2$ and $\bar{\bar{\xi}}_1$ respectively, thus they may be approximated as:

$$R_{d1} \approx \left|1 - \left(\frac{\omega_{20}}{\omega_{10}}\right)^2\right|$$

$$R_{d2} \approx \left|1 - \left(\frac{\omega_{10}}{\omega_{20}}\right)^2\right| \tag{3.74}$$

Moreover, since the most influential flutter derivatives to coupled flutter are H_3^*, A_1^*, A_2^* and A_3^* it is possible to accept that $H_3^* A_1^* + H_2^* A_4^* \approx H_3^* A_1^*$. Due to this approximation, the solutions for the modal damping ratios given by equations (3.63) and (3.68) can be simplified as:

$$\xi_1 = \Delta_{w,1}\frac{\Omega_{w,1}}{\omega_{10}} - \frac{1}{2}\mu H_1^* + \frac{1}{2}\mu\nu D^2 \frac{H_3^* A_1^*}{1 - \left(\frac{\omega_{20}}{\omega_{10}}\right)^2} \tag{3.75}$$

$$\xi_2 = \Delta_{\theta,2}\frac{\Omega_{\theta,2}}{\omega_{20}} - \frac{1}{2}\nu A_2^* - \frac{1}{2}\mu\nu D^2 \frac{H_3^* A_1^*}{1 - \left(\frac{\omega_{10}}{\omega_{20}}\right)^2} \tag{3.76}$$

Neglecting the flutter derivative H_4^* in equation (3.72) and considering the flutter derivative A_3^* still important in the equation of torsional circular frequency (3.73), the critical flutter velocity is determined at the condition of zero modal damping.

When $\xi_2 = 0$, equation (3.76) becomes:

$$K_{cr}^2 - \eta^2 K_{cr}^2 (1 + \nu A_3^*) - \frac{\mu \nu D^2 (-K_{cr}^2 H_3^*)(K_{cr} A_1^*)}{\left[(-K_{cr} A_2^* + 2K_{cr} \xi_{\theta,2}(1 + \nu A_3^*)^{\frac{1}{2}}\right]} = 0 \qquad (3.77)$$

where:

1. $K_{cr} = \frac{\omega_2 2b}{U_{cr}}$ is the critical reduced frequency associated to the torsional modal branch;

2. $\eta = \frac{\Omega_{w,1}}{\Omega_{\theta,2}}$ is the frequency ratio.

Realizing that $K_{0,cr}^2 = K_{cr}^2 (1 + \nu A_3^*)$, with $K_{0,cr} = \frac{\Omega_{\theta,2} b}{U_{cr}}$, equation (3.77) can be simplified:

$$K_{0,cr}^2 (1 - \eta^2) = \nu K_{cr}^2 A_3^* + \frac{\mu \nu D^2 (-k_{cr}^2 H_3^*)(k_{cr} A_1^*)}{\left[(-k_{cr} A_2^* + 2k_{cr} \Delta_{\theta,2}(1 + \nu A_3^*)^{\frac{1}{2}}\right]} \qquad (3.78)$$

According to Chen and Kareem [20], equation (3.78) leads to the critical flutter velocity, which can be expressed trough the following closed-form formula:

$$U_{cr} = \gamma \Omega_{\theta,2} 2b \sqrt{(1 - \eta^2)\left(\frac{mr}{8\rho b^3}\right)} \qquad (3.79)$$

with:

$$\gamma = \frac{1}{\sqrt{F_1 + F_2}}$$

$$F_1 = \frac{r}{2b} \frac{D^2 (-K_{cr}^2 H_3^*)(K_{cr} A_1^*)}{\left[(-K_{cr} A_2^* + 2K_{cr} \xi_{\theta,2}(1 + \nu A_3^*)^{\frac{1}{2}}\right]} \qquad (3.80)$$

$$F_2 = \frac{2b}{r} K_{cr}^2 A_3^*$$

$$r = \sqrt{\frac{J}{m}} = \sqrt{\frac{J_{\theta,2}}{m_{w,1}} \frac{G_{W_1 W_1}}{G_{\Theta_2 \Theta_2}}} = 2b \sqrt{\frac{\mu}{\nu}}$$

The parameter γ depends only on the most important flutter derivatives H_3^*, A_1^*, A_2^* and A_3^*. Obviously the importance of additional flutter derivatives on bridge flutter depends on their values and associated mode shape integrals.

The equation for the evaluation of the flutter critical velocity (3.79) is very similar to the well-known empirical Selberg's formula, proposed in his work published in 1961 [51]. Nevertheless there is a slight difference between the two formulas, indeed in the one found by Chen and Kareem [20] the parameter γ depends on the reduced flutter velocity, while in the Selberg's formula, it is taken as a constant assuming the value of 0.416. Moreover since Selberg found its empirical formulation based on the numerical prediction of critical flutter velocities of flat plate section bridges, the simplified formulation written in (3.79) can be considered as its extension for bridges with generic cross section.

Another important aspect is that the parameter γ is insensitive to the value of the reduced velocity when it becomes very high, $U^* = \frac{U}{fB} > 10 \div 15$, in accordance with the Quasi steady theory (§3.3.1). Hence, it allows for an expeditious assessment of flutter performance of a given deck section, without implementing a flutter analysis.

3.4 NON-DIMENSIONAL AEROELASTIC EQ. OF MOTION

Up to now all the considerations about Aeroelastic effects have been done considering generic dimensional deck equations of motion. It is necessary to write the Aeroelastic components in non-dimensional format, so as to adapt this theory to the structural model considered. It is possible to do that starting from equations (2.32) and (2.33) considering only the linear components and the Aeroelastic effects.

$$(m_d + 2m_c) \cdot \ddot{w}_d + E_d I_d \cdot w_d''^v - 2H \cdot w_d'' - 2y'' \cdot h_w = L = \frac{1}{2}\rho U^2 2b \cdot \left[K_w H_1^* \frac{\dot{w}_d}{U} + \right.$$
$$\left. + K_\theta H_2^* \frac{2b\dot{\theta}_d}{U} + K_\theta^2 H_3^* \theta_d + K_w^2 H_4^* \frac{w_d}{2b} \right] \tag{3.81}$$

$$(J_t + 2m_c b^2) \cdot \ddot{\theta}_d + E_d \Gamma_d \cdot \theta_d''^v - G_d J_d \cdot \theta_d'' - 2Hb^2 \cdot \theta_d'' - 2h_\theta b^2 \cdot \theta_d'' = M =$$
$$\frac{1}{2}\rho U^2 (2b)^2 \cdot \left[K_w A_1^* \frac{\dot{w}_d}{U} + K_\theta A_2^* \frac{2b\dot{\theta}_d}{U} + K_\theta^2 A_3^* \theta_d + K_w^2 A_4^* \frac{w_d}{2b} \right] \tag{3.82}$$

Repeating the same passages of §2.3 and introducing the same non-dimensional quantities the equations of motion become:

$$\ddot{\widetilde{w}}_d + \tilde{c}_w \cdot \dot{\widetilde{w}}_d + \mu^2 \cdot \widetilde{w}_d''^v - \widetilde{w}_d'' + \lambda_1^2 \cdot \tilde{h}_w = \rho U b K_w H_1^* \frac{l}{\sqrt{2H(m_d + 2m_c)}} \cdot \dot{\widetilde{w}}_d +$$
$$+ \rho U 2b K_\theta H_2^* \frac{l}{\sqrt{2H(m_d + 2m_c)}} \cdot \dot{\tilde{\theta}}_d + \rho U^2 K_\theta^2 H_3^* \frac{l^2}{2H} \cdot \tilde{\theta}_d + + \frac{1}{2}\rho U^2 K_w^2 H_4^* \cdot \widetilde{w}_d \tag{3.83}$$

$$\check{J}_t \cdot \ddot{\tilde{\theta}}_d + \tilde{c}_\theta \dot{\tilde{\theta}}_d + \frac{\beta^2}{\chi^2} \cdot \tilde{\theta}_d^{IV} - (1 + \beta^2) \cdot \tilde{\theta}_d'' + \lambda_1^2 \tilde{h}_\theta = \frac{1}{2} \rho U 4 b K_w A_1^* \frac{l}{\sqrt{2H(m_d + 2m_c)}} \cdot \dot{\tilde{w}}_d +$$

$$\rho U 4 b K_\theta A_2^* \frac{l}{\sqrt{2H(m_d + 2m_c)}} \cdot \dot{\tilde{\theta}}_d + 2\rho U^2 K_\theta^2 A_3^* \frac{l^2}{2H} \cdot \tilde{\theta}_d + \rho U^2 K_w^2 A_4^* \cdot \tilde{w}_d \tag{3.84}$$

Introducing the definition of the torsional divergence (eq. (3.43)) and recalling the definition of aerodynamic mass (eq. (3.47)), the two equations of motion can be rewritten in non-dimensional form:

$$\ddot{\tilde{w}}_d + \tilde{c}_w \cdot \dot{\tilde{w}}_d + \mu^2 \cdot \tilde{w}_d^{IV} - \tilde{w}_d'' + \lambda_1^2 \cdot \tilde{h}_w = \frac{1}{\pi} \tilde{u} \sqrt{\check{J}_t} \sqrt{\widetilde{m}_a} K_w H_1^* \tilde{\Omega}_{\theta,m} \cdot \dot{\tilde{w}}_d +$$

$$\frac{2}{\pi} \tilde{u} \sqrt{\check{J}_t} \sqrt{\widetilde{m}_a} K_\theta H_2^* \tilde{\Omega}_{\theta,m} \cdot \dot{\tilde{\theta}}_d + \frac{1}{\pi} \tilde{u}^2 \check{J}_t K_\theta^2 H_3^* \tilde{\Omega}_{\theta,m}^2 \cdot \tilde{\theta}_d + + \frac{1}{2\pi} \tilde{u}^2 \check{J}_t K_w^2 \tilde{\Omega}_{\theta,m}^2 H_4^* \cdot \tilde{w}_d \tag{3.85}$$

$$\check{J}_t \cdot \ddot{\tilde{\theta}}_d + \tilde{c}_\theta \cdot \dot{\tilde{\theta}}_d + \frac{\beta^2}{\chi^2} \cdot \tilde{\theta}_d^{IV} - (1 + \beta^2) \cdot \tilde{\theta}_d'' + \lambda_1^2 \cdot \tilde{h}_\theta = \frac{2}{\pi} \tilde{u} \sqrt{\check{J}_t} \sqrt{\widetilde{m}_a} K_w A_1^* \tilde{\Omega}_{\theta,m} \cdot \dot{\tilde{w}}_d +$$

$$+ \frac{4}{\pi} \tilde{u} \sqrt{\check{J}_t} \sqrt{\widetilde{m}_a} K_\theta A_2^* \tilde{\Omega}_{\theta,m} \cdot \dot{\tilde{\theta}}_d + \frac{2}{\pi} \tilde{u}^2 \check{J}_t K_\theta^2 A_3^* \tilde{\Omega}_{\theta,m}^2 \cdot \tilde{\theta}_d + + \frac{1}{\pi} \tilde{u}^2 \check{J}_t K_w^2 \tilde{\Omega}_{\theta,m}^2 A_4^* \cdot \tilde{w}_d \tag{3.86}$$

where $\tilde{u} = \frac{U}{U_D}$ represents the mean wind speed normalized with respect to the critical torsional divergence velocity.

The reduced frequency must be converted in non-dimensional form by changing the dimensional circular frequency with the non-dimensional one:

$$K_{(\cdot)} = \frac{2b}{U} \left(\omega_{D,(\cdot)} + i\xi_{(\cdot)} \omega_{(\cdot)} \right) = \frac{2b}{U} \sqrt{\frac{2H}{l^2}} \frac{1}{\sqrt{(m_d + 2m_c)}} \left(\widetilde{\omega}_{D,(\cdot)} + i\xi_{(\cdot)} \widetilde{\omega}_{(\cdot)} \right)$$

$$= \frac{2\sqrt{\widetilde{m}_a}}{\sqrt{\check{J}_t} \tilde{\Omega}_{\theta,m} \tilde{u}} \left(\widetilde{\omega}_{D,(\cdot)} + i\xi_{(\cdot)} \widetilde{\omega}_{(\cdot)} \right) \tag{3.87}$$

The imaginary part of the frequency comes out from the generalization of the time varying terms in the modal projection (2.43) and (2.62). In fact, in order to take into account for the damping effect, they have to be slightly modified as:

$$z_n(\tau) = Z_n \exp(\tilde{\lambda}_{w,n} \cdot \tau) + Z_n^* \exp(-\tilde{\lambda}_{w,n} \cdot \tau) \tag{3.88}$$

$$\gamma_m(\tau) = \Gamma_m \exp(\tilde{\lambda}_{\theta,m} \cdot \tau) + \Gamma_m^* \exp(-\tilde{\lambda}_{\theta,m} \cdot \tau) \tag{3.89}$$

being $\tilde{\lambda}_{(\cdot)} = -\xi_{(\cdot)} \widetilde{\omega}_{(\cdot)} + i\widetilde{\omega}_{(\cdot)} \sqrt{1 - \xi_{(\cdot)}^2} = -\xi \widetilde{\omega}_{(\cdot)} + i\widetilde{\omega}_{D,(\cdot)}$.

The non-dimensional equations of motion can be then projected in the modal space following the same procedure adopted in §2.4.

$$M_{w,n} \cdot \ddot{z}_n + \left(D_{w,n} - D_{w,n}^{Aero}\right) \cdot \dot{z}_n + D_{w\theta,nm}^{Aero} \cdot \dot{\gamma}_m + \left(K_{w,n}^{(L)} - K_{w,n}^{(L),Aero}\right) \cdot z_n +$$
$$+ K_{w\theta,nm}^{(L),Aero} \gamma_m = \Gamma_{w,n}$$

(3.90)

$$J_{\theta,m} \cdot \ddot{\gamma}_m + \left(D_{\theta,m} - D_{\theta,m}^{Aero}\right) \cdot \dot{\gamma}_m + D_{\theta w,mn}^{Aero} \cdot \dot{z}_n + \left(K_{\theta,m}^{(L)} - K_{\theta,m}^{(L),Aero}\right) \cdot \gamma_m +$$
$$+ K_{\theta w,mn}^{(L),Aero} z_n + K_{\theta w,mn}^{(Q)} \cdot \gamma_m z_n = \Gamma_{\theta,m}$$

(3.91)

The quadratic stiffness coupling term in the second equation is retained in view of its importance on the stability analysis and the forcing terms $\Gamma_{w,n}$ and $\Gamma_{\theta,m}$ can be associated to buffeting, vortex shedding or other external actions acting on the bridge deck section.

All the structural and aerodynamic terms governing the Aeroelastic system of equations of motion are listed below.

$$M_{w,n} = \int_0^1 W_n^2(\xi) d\xi$$

$$J_{\theta,m} = \tilde{J}_t M_{\theta,m} = \tilde{J}_t \int_0^1 \Theta_m^2(\xi) d\xi$$

$$D_{w,n} = 2\Delta_{w,n} \tilde{\Omega}_{w,n} M_{w,n}$$

$$D_{\theta,m} = 2\Delta_{\theta,m} \tilde{\Omega}_{\theta,m} \tilde{J}_t M_{\theta,m}$$

$$D_{w,n}^{Aero} = \frac{1}{\pi} \tilde{u} \sqrt{\tilde{J}_t} \sqrt{\widetilde{m}_a} K_w H_1^* \tilde{\Omega}_{\theta,m} M_{w,n}$$

$$D_{w\theta,nm}^{Aero} = \frac{2}{\pi} \tilde{u} \sqrt{\tilde{J}_t} \sqrt{\widetilde{m}_a} K_\theta H_2^* \tilde{\Omega}_{\theta,m} \tilde{h}_{W_n \Theta_m}$$

(3.92)

$$D_{\theta,m}^{Aero} = \frac{4}{\pi} \tilde{u} \sqrt{\tilde{J}_t} \sqrt{\widetilde{m}_a} K_\theta A_2^* \tilde{\Omega}_{\theta,m} M_{\theta,m}$$

$$D_{\theta w,mn}^{Aero} = \frac{2}{\pi} \tilde{u} \sqrt{\tilde{J}_t} \sqrt{\widetilde{m}_a} K_w A_1^* \tilde{\Omega}_{\theta,m} \tilde{h}_{W_n \Theta_m}$$

$$K_{w,n}^{(L)} = \tilde{\Omega}_{w,n}^2 M_{w,n}$$

$$K_{\theta,m}^{(L)} = \tilde{\Omega}_{\theta,m}^2 \tilde{J}_t M_{\theta,m}$$

$$K_{\theta w,mn}^{(Q)} = \lambda_2^2 \left[2\tilde{h}_{\Theta_m} \tilde{h}_{W_n'\Theta_m'} + \tilde{h}_{W_n} \tilde{h}_{\Theta_m'^2} \right]$$

$$K_{w,n}^{(L),Aero} = \frac{1}{2\pi} \tilde{u}^2 \tilde{J}_t K_w^2 \tilde{\Omega}_{\theta,m}^2 H_4^* M_{w,n}$$

$$K_{w\theta,nm}^{(L),Aero} = \frac{1}{\pi} \tilde{u}^2 \tilde{J}_t K_\theta^2 H_3^* \tilde{\Omega}_{\theta,m}^2 \tilde{h}_{W_n\Theta_m}$$

$$K_{\theta,m}^{(L),Aero} = \frac{2}{\pi} \tilde{u}^2 \tilde{J}_t K_\theta^2 A_3^* \tilde{\Omega}_{\theta,m}^2 M_{\theta,m}$$

$$K_{\theta w,mn}^{(L),Aero} = \frac{1}{\pi} \tilde{u}^2 \tilde{J}_t K_w^2 \tilde{\Omega}_{\theta,m}^2 A_4^* \tilde{h}_{W_n\Theta_m}$$

In the present case, the unsteady forcing terms appearing in the right hand-side of the modal equations of motion of the complete Aeroelastic model (3.90) and (3.91) are related to vortex shedding only. Assuming that the periodic resultant force due to vortex shedding is applied in the centre of stiffness of the deck section, no external forcing moments are generated by the vortex shedding effect ($\Gamma_{\theta,m} = 0$). The lift force acting on the deck sectional model is periodic and in the lock-in range it can be expressed trough a sinusoidal function, as in equation (3.11).

In order to model the self-limiting behaviour of vortex induced vibrations, the simple formula proposed in equation (3.11) has to be slightly modified. To do this, a damping term dependent on the vibration itself can be introduced, e.g. a Van der Pol oscillator. Scanlan [49] proposed a linearized form for the vortex induced oscillations modelling that brings it into conformity with the flutter derivative expressions. The principal difficulties of doing this was that, while flutter derivatives methods remain linear, at least for small amplitudes, vortex excitation is recognized as a distinctly nonlinear phenomenon. Anyway, in the lock-in range the author proposed the following formula for the lift force due to vortex shedding:

$$L = \frac{1}{2}\rho U^2 2b \cdot \left(K H_1^* \frac{\dot{w}}{U} + C_L \cdot sin(\omega_{VS}t) \right) \tag{3.93}$$

Since the proposed Aeroelastic model already takes into account for the complete set of flutter derivatives, in order not to consider the contribution due to H_1^* twice, only the sinusoidal term is retained in the lift force expression (3.93). Thus expression (3.11) for the lift force is still valid.

In order to introduce this external sinusoidal forcing term due to vortex shedding in the presented model, it is necessary to make it non-dimensional and to project it in the modal

space. Therefore, starting from equation (3.11) it is possible to write the non-dimensional projected external forcing term $\Gamma_{w,n}$ as:

$$
\Gamma_{w,n} = \frac{1}{2}\rho U^2 2bC_L \cdot \frac{l^2}{2Hf} \cdot sin\left(\omega_{VS} \cdot l\sqrt{\frac{m_d+2m_c}{2H}} \cdot \tau\right) \cdot \int_0^1 W_n(\xi)d\xi = 2 \cdot \frac{b}{f} \cdot \frac{U^2}{U_D^2} \cdot \frac{C_L}{2\pi} \cdot
$$
$$
\tilde{\Omega}_{\theta,m}^2 \tilde{J}_t \cdot sin(\widetilde{\omega}_{VS} \cdot \tau) \cdot \tilde{h}_{W_n} = 2\tilde{b}\tilde{c}_L\tilde{\Omega}_{\theta,m}^2\tilde{J}_t \cdot \tilde{u}^2 \cdot \tilde{h}_{W_n} \cdot sin(\widetilde{\omega}_{VS} \cdot \tau)
$$

(3.94)

where:

1. $\tilde{b} = \frac{b}{f}$ is the half deck-width adimensionalized with respect to the sag of the cables;

2. $\tilde{c}_L = \frac{C_L}{2\pi}$ is the lift coefficient adimensionalized with respect to the flat plate condition;

3. $\tilde{u} = \frac{U}{U_D}$ is the mean wind speed normalized with respect to the critical torsional divergence velocity.

In a more compact form:

$$
\Gamma_{w,n} = \Gamma_0 \cdot \tilde{h}_{W_n} \cdot sin(\widetilde{\omega}_{VS} \cdot \tau)
$$

(3.95)

being

$$
\Gamma_0 = 2\tilde{b}\tilde{c}_L\tilde{\Omega}_{\theta,m}^2\tilde{J}_t \cdot \tilde{u}^2
$$

(3.96)

The vortex shedding frequency in non-dimensional format is:

$$
\widetilde{\omega}_{VS} = \omega_{VS} \cdot l\sqrt{\frac{m_d+2m_c}{2H}} = 2\pi St \cdot \frac{U}{D}\sqrt{\frac{l^2(m_d+2m_c)}{2H}} = \frac{2b}{D}\pi St \frac{U}{U_D}\sqrt{\frac{\tilde{J}_t}{\tilde{m}_a}}\tilde{\Omega}_{\theta,m}
$$

(3.97)

The introduction of a new non-dimensional parameter, namely the *deck sectional aspect ratio* $\tilde{\alpha} = \frac{2b}{D}$, leads to the following expression for the shedding frequency:

$$
\widetilde{\omega}_{VS} = \pi St\tilde{\alpha}\sqrt{\frac{\tilde{J}_t}{\tilde{m}_a}}\tilde{\Omega}_{\theta,m} \cdot \tilde{u}
$$

(3.98)

From literature the deck sectional aspect ratio ranges from a value of $\tilde{\alpha} = 3$ to a value of $\tilde{\alpha} = 12$. The smaller is $\tilde{\alpha}$, the bluffer is the body.

The vortex shedding phenomenon is characterized by a lock-in range in which the frequency of vibration of the structure drives the frequency of shedding of the vortices. It happens in a range of velocity that, for systems characterized by low structural damping, is in between $0.8 \leq \tilde{u}_{lock-in} \leq 1.5$. It is possible to find the lock-in velocity by setting $\tilde{\omega}_{VS} = \tilde{\Omega}_{w,n}$ in equation (3.98):

$$\tilde{u}_{lock-in} = \frac{\tilde{\Omega}_{w,n}}{\tilde{\Omega}_{\theta,m}} \cdot \sqrt{\frac{\widetilde{m}_a}{\tilde{J}_t}} \cdot \frac{1}{\pi St \tilde{\alpha}} \tag{3.99}$$

4 INTERRELATION BETWEEN DIVERGENCE, FLUTTER AND PARAMETRIC RESONANCE

A recent work by Arioli and Gazzola [7] showed that suspension bridges can suffer of instability due to internal parametric resonance. They suggested a mathematical model for the study of the bridge's dynamical behaviour, able to explain that the appearance of torsional oscillation is due to internal parametric resonance. This phenomenon is characterized by a continuous exchange of energy between the flexural and the torsional mode of vibrations and it can happen for particular torsional to flexural frequency ratio.

The simplest model able to exhibit the parametric resonance instability phenomenon is the elastic pendulum, a simple pendulum with a spring incorporated in its string. Several studies were carried out by different authors about the elastic pendulum. Anicin et al. [5] studied the linear theory of the elastic pendulum, while Arinstein and Davidovic [6] developed a non-linear analysis on the inverted spring pendulum highlighting the principal differences with the linear analysis. Cross [23] made different experimental tests for two different pendulums, explaining the conditions for the appearance of parametric resonance instability and the continuous transfer of energy between two vibrating modes.

A long-span suspension bridge is prone to suffer of static divergence and flutter. The simplest structural model able to represent these two phenomena is the inverted 2 DoFs pendulum subjected to a non-conservative follower force. Herrmann and Bungay [30] found different regions of instability due to static divergence and flutter, in function of only one parameter describing the inclination of the force with respect to the beam.

Few years later this work, Herrmann and Hauger [31] extended the previous model with the addition of a 3rd Degree of Freedom, a linear spring able to catch the axial extensibility of one beam. By doing this, the inverted pendulum subjected to a follower force is capable to exhibit all the three instability phenomena possible also on a suspension bridge, i.e. static divergence, flutter and internal parametric resonance. Different regions of instability can be determined as a function of the parameter describing the inclination of the force with respect to the beam, demonstrating that these three different kind of instability are strictly related.

Inspired by the work of Hermann and Hauger [31] the equations of motion of the deck sectional model can be extended in order to find a possible interrelation between the aforementioned instability phenomena.

4.1 THE ELASTIC PENDULUM

The extensible, or elastic, pendulum is a simple pendulum with a spring incorporated in its string (Figure 4.1).
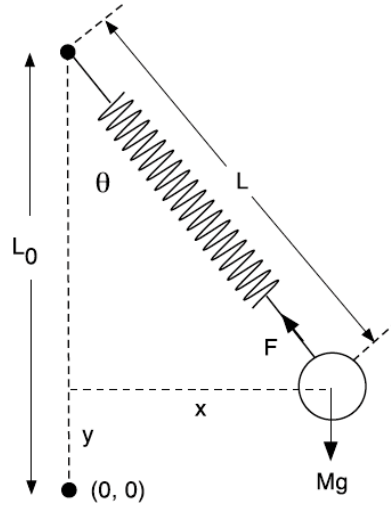

Figure 4.1: The elastic pendulum

The linear equations of motion can be written by means of the Lagrange equations:

$$\frac{d}{dt}\left(\frac{\partial L}{\partial \dot{y}}\right) - \frac{\partial L}{\partial y} = 0$$

$$\frac{d}{dt}\left(\frac{\partial L}{\partial \dot{\theta}}\right) - \frac{\partial L}{\partial \theta} = 0$$

(4.1)

being $L = T - V = \frac{1}{2}M(\dot{y}^2 + L^2\dot{\theta}^2) - \frac{1}{2}ky^2 - Mg(L_0 - L \cdot cos\theta)$ the Lagrange function, defined as the difference between the kinetic and the potential energy.

The substitution of this expression into (4.1) leads to the two governing equations of the elastic pendulum:

$$\ddot{y} + \omega_2^2 y - g \cdot cos\theta - L\dot{\theta}^2 = 0$$

$$\ddot{\theta} + \frac{2 \cdot \dot{y} \cdot \dot{\theta} + g \cdot sin\theta}{L} = 0$$

(4.2)

having defined $\omega_2^2 = \frac{k}{M}$ and $\omega_1^2 = \frac{g}{L_0}$ the circular frequencies of the spring motion and of the pendulum motion respectively.

The mass attached at the end of the spring can oscillate vertically, horizontally or both at the same time. Experimental investigations show a particular behaviour when the combination of pendulum length, spring stiffness and mass are such that the frequency of the vertical harmonic oscillations is exactly or nearly twice the pendulum frequency. In fact under those circumstances the vertical oscillations become parametrically unstable and any small perturbation of the mass from the vertical equilibrium configuration results in an exponentially increasing horizontal (or pendulum) oscillation. The growth of the latter stops when most of the energy of the original vertical oscillation is converted into energy of pendulum motion. The process is now reversed as the centrifugal force, with two cycles of oscillation in the pendulum period, acts as an excitation term to the vertical harmonic oscillations, which build up until the initial state is restored, only to start a new cycle of the recurrence process.

Thus, energy is constantly flowing from the vertical motion into the horizontal and vice versa. This result is easily observed in Figure 4.2, taken by [23], where the time history of oscillations of an elastic pendulum having double vertical frequency with respect to the pendulum frequency is plotted.
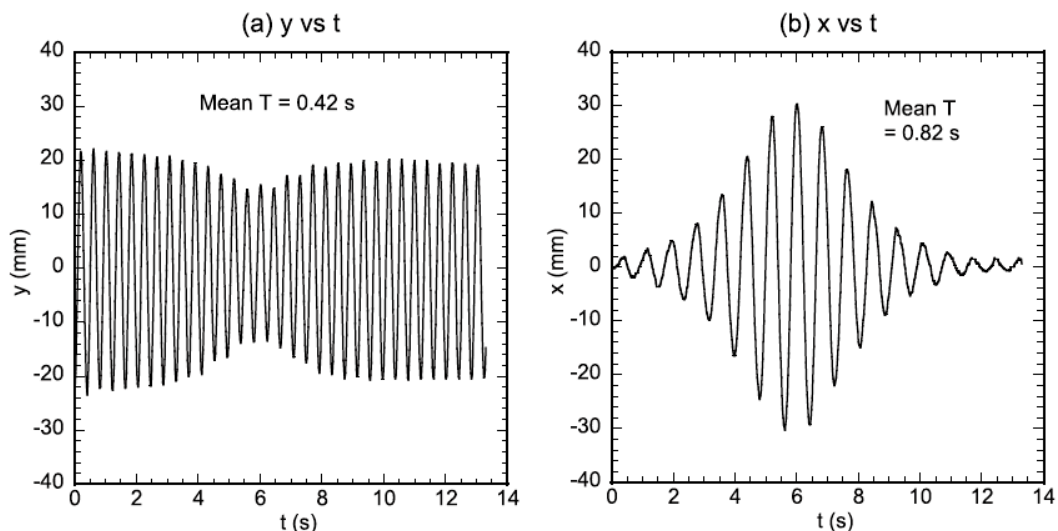

Figure 4.2: x and y coordinates versus time for a mass released from the vertical equilibrium position

The vertical equilibrium position of the mass attached to the spring is perturbed at the beginning of the experiment. After few seconds an horizontal oscillation develops and grows in amplitude with time because of the horizontal restoring force on the mass, which is a nonlinear function of the horizontal displacement. As a result, the oscillation frequency in the vertical direction decreases, the vertical and horizontal oscillations drift into phase and the horizontal amplitude stops increasing. The phase between x and y continues to drift, causing the horizontal amplitude to decrease until the oscillation is almost purely vertical. This process then repeats several times if the pendulum is lightly damped.

4.2 THE INVERTED 2 DOFs PENDULUM SUBJECTED TO A FOLLOWER FORCE

Free motions of a linear elastic non-dissipative two Degree of Freedom system, subjected to a static non-conservative force (Figure 4.3), are analyzed by Hermann and Bungay [30] with the aim of studying the connection between two different instability mechanisms, namely the static divergence and flutter.
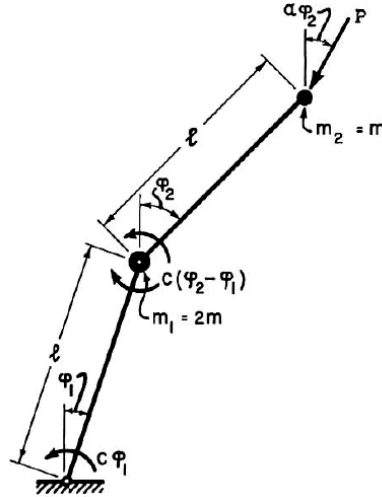

Figure 4.3: Inverted 2 DoFs pendulum subjected to a static non-conservative force

By means of simple equilibrium considerations it is possible to write the non-linear equations governing the system:

$$(m_1 + m_2)l^2\ddot{\varphi}_1 + m_2l^2\ddot{\varphi}_2 \cos(\varphi_2 - \varphi_1) - m_2l^2\dot{\varphi}_2^2 \sin(\varphi_2 - \varphi_1) + c(2\varphi_1 - \varphi_2) + \\ + Ql\sin(\alpha\varphi_2 - \varphi_1) = 0$$

$$m_2l^2\ddot{\varphi}_1 \cos(\varphi_2 - \varphi_1) + m_2l^2\ddot{\varphi}_2 + m_2l^2\dot{\varphi}_1^2 \sin(\varphi_2 - \varphi_1) - c\varphi_1 + c\varphi_2 + \\ + Ql\sin((\alpha - 1)\varphi_2) = 0$$

(4.3)

The stability analysis can be restricted to a linearized formulation:

$$(m_1 + m_2)l^2\ddot{\varphi}_1 + m_2l^2\ddot{\varphi}_2 + c(2\varphi_1 - \varphi_2) = Ql\varphi_1 - Ql\alpha\varphi_2$$

(4.4)

$$m_2l^2\ddot{\varphi}_1 + m_2l^2\ddot{\varphi}_2 - c\varphi_1 + c\varphi_2 = -(\alpha - 1)\varphi_2 Ql$$

This is a system of Ordinary Differential Equations which can be solved by seeking a solution in the form $\varphi_k = A_k e^{i\omega t}$.

The analysis consists in the determination of the two natural frequencies of free vibration as a function of the loading. They can be determined by substituting the solution into the system of equations (4.4) and by setting the determinant of the resulting system equal to zero. From the latter condition the following equation is obtained:

$$(m_1 m_2)l^4 \omega^4 + (cm_1 + 5cm_2 - 2m_2 Ql - (1-\alpha)Qlm_1)l^2 \omega^2 + \big(c^2 + (1-\alpha)Q^2 l^2 + \\ -3cQl(1-\alpha)\big) = 0 \tag{4.5}$$

This results in four characteristic roots occurring in pairs, the positive and negative roots of ω^2. Depending on the values of the natural frequencies, different possibilities can occur:

1. For a negative value of ω^2, one root describes an exponential divergent motion, indicating the condition for static buckling;

2. $\omega^2 = 0$ corresponds to the neutral equilibrium in the adjacent configuration;

3. For a complex value of ω^2, having passed a common real value at the critical loading, the roots describe an oscillatory motion with a definite period but with an exponentially increasing amplitude. This is the condition for flutter.

Therefore the system is stable if and only if both ω^2 are real and positive. With the aid of the parameter α the authors have been able to show a connection between instability phenomena of divergence and flutter, as shown in Figure 4.4.
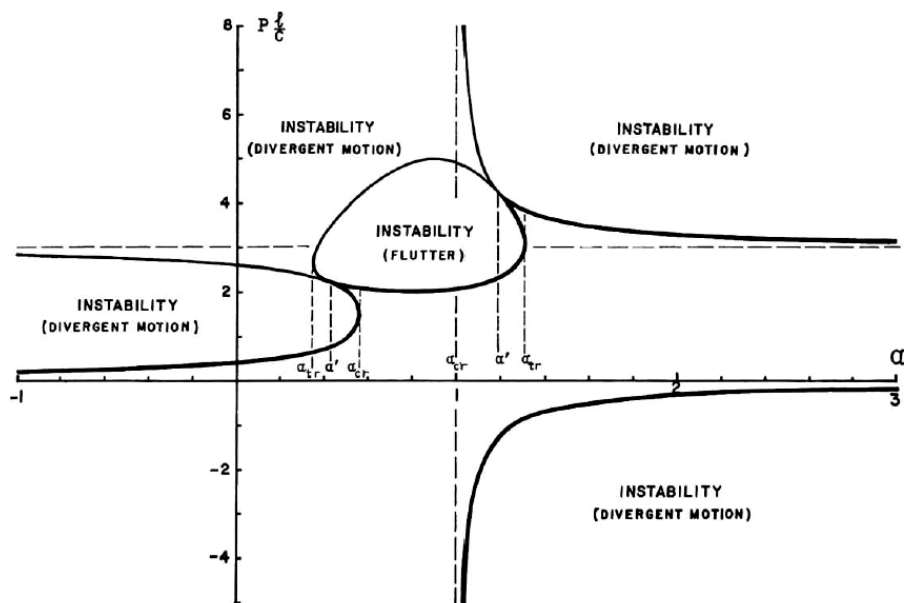

Figure 4.4: Critical loads vs. α

Obviously $\alpha = 0$ represents a conservative system, whereas $\alpha = 1$ represents the case of a follower force. The phenomenon of flutter is limited only to a range of positive values of α, which means that the corresponding critical load are compressive.

4.3 THE INVERTED 2 DOFₛ ELASTIC PENDULUM SUBJECTED TO A FOLLOWER FORCE

The idea had from Herrmann and Hauger was to modify the 2 DoFₛ pendulum model, taking into account also for the effect of compressibility. To do this, one of the rigid bars was replaced by a linear elastic spring, assumed to be always straight regardless of its length. The model obtained is the 3 DoFₛ model depicted in Figure 4.5.
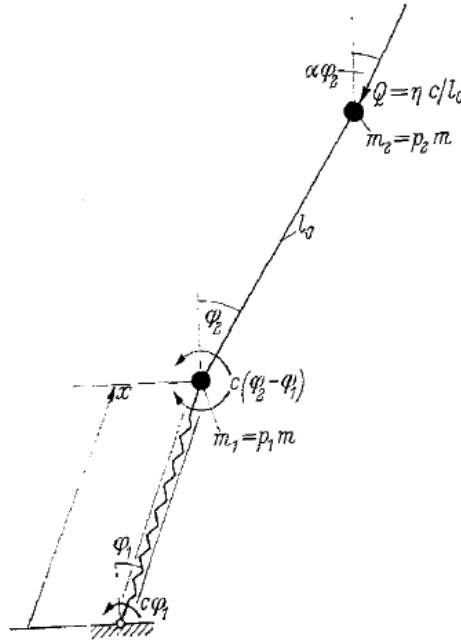

Figure 4.5: Inverted 2 DoFₛ elastic pendulum subjected to a follower force

It is important to highlight the fact that this model is able to capture all the instability phenomena of interest, namely static divergence, flutter and parametric resonance. In fact:

1. The suppression of the DoF associated to the linear spring leads to the same model already analyzed in §4.2, able to exhibit both flutter and static divergence;

2. The suppression of one of the two rotational DoFₛ leads to the inverted elastic pendulum described in §4.1, able to exhibit the parametric resonance phenomenon.

Therefore, through this model, it is possible to study the interaction between divergence and flutter on one hand and auto-parametric excitation on the other.

The equations of motion of the system depicted in Figure 4.5 are written considering the dimensionless generalized coordinates $q_1 = \varphi_1, q_2 = \varphi_2$ and $q_3 = \frac{x}{l_0}$.

From simple equilibrium considerations:

$$(m_1 + m_2)l_0^2 \ddot{q}_1 q_3^2 + m_2 l_0^2 \ddot{q}_2 q_3 \cos(q_2 - q_1) + 2(m_1 + m_2)l_0^2 \dot{q}_1 \dot{q}_3 q_3 +$$
$$-m_2 l_0^2 \dot{q}_2^2 q_3 \sin(q_2 - q_1) + 2cq_1 - cq_2 = -q_3 Q l_0 \sin(\alpha q_2 - q_1)$$

$$m_2 l_0^2 [\ddot{q}_1 q_3 \cos(q_2 - q_1) + \ddot{q}_2 - \ddot{q}_3 \sin(q_2 - q_1) + 2\dot{q}_1 \dot{q}_3 \cos(q_2 - q_1) + \dot{q}_1^2 q_3 \sin(q_2 + $$
$$-q_1)] - cq_1 + cq_2 = -Q l_0 \sin((\alpha - 1)q_2) \tag{4.6}$$

$$(m_1 + m_2)l_0^2 \ddot{q}_3 - m_2 l_0^2 \ddot{q}_2 \sin(q_2 - q_1) - (m_1 + m_2)l_0^2 \dot{q}_1^2 q_3 - m_2 l_0^2 \dot{q}_2^2 \cos(q_2 - q_1) +$$
$$Kl_0^2 q_3 - Kl_0^2 = -Q l_0 \cos(\alpha q_2 - q_1)$$

where:

1. l_0 is the unloaded length of the two bars;

2. K is the stiffness of the spring;

3. Q is the intensity of the load applied at an angle $\alpha \varphi_2$ with respect to the vertical.

The abovementioned system is a non-linear system of Differential Equations for which it is not possible to give a general solution. However, a particular solution can be expressed as:

$$q_1^f \equiv 0$$
$$q_2^f \equiv 0 \tag{4.7}$$

which, substituted in the equations of motions, yields to:

$$(m_1 + m_2)\ddot{q}_3^f + Kq_3^f = K - \frac{Q}{l_0} \tag{4.8}$$

This is the classical equation of a 1 DoF oscillator, which has general solution:

$$q_3^f = 1 - \frac{Q}{Kl_0} + \xi \cos(\omega t + \epsilon) \tag{4.9}$$

where:

1. $\omega^2 = \frac{K}{m_1 + m_2}$ is the circular frequency of oscillation;

2. ξ and ϵ are the amplitude and the phase lag of the response, respectively.

The aim of the analysis is to obtain information regarding the stability of the particular solution (4.9).

The approach used is the one proposed by Bolotin [13], which consists in the introduction of a small, but non vanishing perturbation of the motion in order to find the so called *linear Variational equations*.

$$q_j = q_j^f + q_j^p \tag{4.10}$$

The substitution of the perturbed motion (4.10) into equations (4.6) leads to a set of non-linear equations:

$$
\begin{aligned}
&(m_1 + m_2)l_0^2 \ddot{q}_1 q_3^2 + (m_1 + m_2)l_0^2 \ddot{q}_1 q_3^{f\,2} + m_2 l_0^2 \ddot{q}_2 q_3 \cos(q_2 - q_1) + \\
&+ m_2 l_0^2 \ddot{q}_2 q_3^f \cos(q_2 - q_1) + 2(m_1 + m_2)l_0^2 \dot{q}_1 \dot{q}_3 q_3 + 2(m_1 + m_2)l_0^2 \dot{q}_1 \dot{q}_3^f q_3^f + \\
&- m_2 l_0^2 \dot{q}_2^2 q_3 \sin(q_2 - q_1) - m_2 l_0^2 \dot{q}_2^2 q_3^f \sin(q_2 - q_1) + 2cq_1 - cq_2 + q_3 Q l_0 \sin(\alpha q_2 + \\
&- q_1) + q_3^f Q l_0 \sin(\alpha q_2 - q_1) = 0
\end{aligned}
$$

$$
\begin{aligned}
&m_2 l_0^2 \big[\ddot{q}_1 q_3 \cos(q_2 - q_1) + \ddot{q}_1 q_3^f \cos(q_2 - q_1) + \ddot{q}_2 - \ddot{q}_3 \sin(q_2 - q_1) - \ddot{q}_3^f \sin(q_2 + \\
&- q_1) + 2\dot{q}_1 \dot{q}_3 \cos(q_2 - q_1) + 2\dot{q}_1 \dot{q}_3^f \cos(q_2 - q_1) + \dot{q}_1^2 q_3 \sin(q_2 - q_1) + \\
&+ \dot{q}_1^2 q_3^f \sin(q_2 - q_1) \big] - cq_1 + cq_2 + Q l_0 \sin\big((\alpha - 1)q_2\big) = 0
\end{aligned}
\tag{4.11}
$$

$$
\begin{aligned}
&(m_1 + m_2)l_0^2\big(\ddot{q}_3 + \ddot{q}_3^f\big) - m_2 l_0^2 \ddot{q}_2 \sin(q_2 - q_1) - (m_1 + m_2)l_0^2 \dot{q}_1^2\big(q_3 + q_3^f\big) + \\
&- m_2 l_0^2 \dot{q}_2^2 \cos(q_2 - q_1) + K l_0^2\big(q_3 + q_3^f\big) - K l_0^2 + Q l_0 \cos(\alpha q_2 - q_1) = 0
\end{aligned}
$$

Notice that the superscript p is omitted from here on. Considering only small perturbations, the system of non-linear equation (4.11) can be linearized. Moreover the substitution of the particular solution (4.9) inside (4.11) leads to the so called system of variational equation.

$$
\begin{aligned}
&(m_1 + m_2)l_0^2 \ddot{q}_1 \left[1 - \tfrac{Q}{Kl_0} + \xi \cos(\omega t + \epsilon)\right]^2 + m_2 l_0^2 \ddot{q}_2 \left[1 - \tfrac{Q}{Kl_0} + \xi \cos(\omega t + \epsilon)\right] + \\
&+ 2(m_1 + m_2)l_0^2 \dot{q}_1 \left[1 - \tfrac{Q}{Kl_0} + \xi \cos(\omega t + \epsilon)\right] \left[-\xi\omega \sin(\omega t + \epsilon)\right] + 2cq_1 - cq_2 + \\
&+ \left[1 - \tfrac{Q}{Kl_0} + \xi \cos(\omega t + \epsilon)\right] Q l_0 \,(\alpha q_2 - q_1) = 0
\end{aligned}
$$

$$
\begin{aligned}
&m_2 l_0^2 \left\{\ddot{q}_1 \left[1 - \tfrac{Q}{Kl_0} + \xi \cos(\omega t + \epsilon)\right] + \ddot{q}_2 + [\xi\omega^2 \cos(\omega t + \epsilon)](q_2 - q_1) + \\
&- 2\dot{q}_1 [\xi\omega \sin(\omega t + \epsilon)]\right\} - cq_1 + cq_2 + Q l_0 q_2(\alpha - 1) = 0
\end{aligned}
\tag{4.12}
$$

$$
\begin{aligned}
&(m_1 + m_2)l_0^2[-\xi\omega^2 \cos(\omega t + \epsilon)] + (m_1 + m_2)l_0^2 \ddot{q}_3 + K l_0^2 \left[1 - \tfrac{Q}{Kl_0} + \xi \cos(\omega t + \epsilon)\right] + \\
&+ K l_0^2 q_3 - K l_0^2 + Q l_0 = 0
\end{aligned}
$$

The system of differential equations (4.12) for the perturbations q_j^p has the periodic coefficients q_3^f. In judging the stability around the configuration of unperturbed motion q_3^f, the variational equations have decisive importance. In fact according to Lyapunov: "If all of the roots of the characteristic equation are smaller in absolute value than unity, then the unperturbed motion is asymptotically stable, regardless of the terms of higher order in the equations of perturbed motion. But if the characteristic equation has roots larger in absolute value than unity, then the unperturbed motion is unstable. If the characteristic equation has no roots larger in absolute value than unity, but it has roots equal in absolute value to unity, then the stability remains uncertain. In this critical case the first approximation does not solve the problem of the stability of motion. For the solution of this problem, it is necessary to consider higher order terms in the differential equations of perturbed motion; the stability of motion will depend on the magnitudes of these terms."

Some terms can be deleted from the 3rd equation of system (4.12) due to the introduction of the general solution q_3^f. The general solution for this last equation is:

$$q_3 = \xi^* \cos(\omega t + \epsilon^*) \tag{4.13}$$

being ξ^* and ϵ^* the amplitude and the phase lag of the perturbation of the Degree of Freedom correspondent to the elongation of the spring.

The solution (4.13) corresponds to a root of the characteristic equation which has modulus equal to 1 in the Liapunov's line of reasoning. Therefore, according to Liapunov's theorem, it is not possible to assure the stability of the particular solution by means of a linear analysis, regardless of the behaviour of the first two variational equations. However, it is possible to obtain conditions for the critical situation from the behaviour of the first two equation of (4.12). To this end, it is useful to introduce some non-dimensional terms in order to write the system of equations (4.12) in a more convenient way.

$$\tau = \omega \cdot t + \epsilon$$

$$\lambda = 1 - \frac{Q}{K l_0}$$

$$m_i = p_i \cdot m \tag{4.14}$$

$$r = \frac{c}{m \cdot l_0^2 \cdot \omega^2}$$

$$s = \frac{Q \cdot l_0}{m \cdot l_0^2 \cdot \omega^2}$$

Considering only small amplitude of longitudinal vibrations ($\xi << 1$), the variational system of equation (4.12) reads as:

$$(p_1 + p_2)(\lambda^2 + 2\lambda\xi\cos(\tau)) \cdot \ddot{q}_1 + p_2(\lambda + \xi\cos(\tau)) \cdot \ddot{q}_2 - 2(p_1 + p_2)(\lambda\xi\sin(\tau)) \cdot \dot{q}_1 +$$
$$+(2r - \lambda s - s\xi\cos(\tau)) \cdot q_1 - (r - \lambda\alpha s - \alpha s\xi\cos(\tau)) \cdot q_2 = 0$$

$$p_2(\lambda + \xi\cos(\tau)) \cdot \ddot{q}_1 + p_2 \cdot \ddot{q}_2 - 2p_2\xi\sin(\tau) \cdot \dot{q}_1 - (r + p_2\xi\cos(\tau)) \cdot q_1 +$$
$$+[r - (1 - \alpha)s + p_2\xi\cos(\tau)] \cdot q_2 = 0$$

$$(4.15)$$

This is a system of linear homogeneous differential equations with periodic coefficients.

Two different kind of instabilities are possible, namely the subharmonic and combinational resonance.

4.3.1 *Subharmonic Resonances*

According to Bolotin [13], the boundaries of instability of first kind can be found by constructing periodic solutions with period T and 2T, being T the period of the exciting longitudinal oscillation. In this particular case, the periods used to build the periodic solutions are $T_1 = 4\pi$ and $T_2 = 2\pi$.

Solutions with period $T_1 = 4\pi$ can be represented by the following Fourier series:

$$q_j(\tau) = \sum_{k=1,3,5,\dots}^{+\infty} \left(a_{jk}\sin\left(\frac{k\tau}{2}\right) + b_{jk}\cos\left(\frac{k\tau}{2}\right) \right), \quad (j = 1,2) \tag{4.16}$$

The substitution of this solution into the system of equations (4.15) and the zeroing of the coefficients of $\sin\left(\frac{k\tau}{2}\right)$ and $\cos\left(\frac{k\tau}{2}\right)$ yields to two infinite systems of linear homogeneous equations for the Fourier coefficients a_{jk} and b_{jk} (4.17) and (4.18).

$$\left[-(p_1 + p_2)\frac{\lambda^2 k^2}{4} + 2r - \lambda s\right] \cdot a_{1k} + \left[-(p_1 + p_2)\xi\frac{\lambda(k-2)^2}{4} + (p_1 + p_2)\xi\frac{\lambda(k-2)}{2} - \frac{s\xi}{2}\right] \cdot$$
$$a_{1(k-2)} - \left[(p_1 + p_2)\xi\frac{\lambda(k+2)^2}{4} + (p_1 + p_2)\xi\frac{\lambda(k+2)}{2} + \frac{s\xi}{2}\right] \cdot a_{1(k+2)} - \left[p_2\frac{\lambda k^2}{4} + r + \right.$$
$$\left. -\lambda\alpha s\right] \cdot a_{2k} + \left[-p_2\xi\frac{(k-2)^2}{8} + \frac{\alpha s\xi}{2}\right] \cdot a_{2(k-2)} + \left[-p_2\xi\frac{(k+2)^2}{8} + \frac{\alpha s\xi}{2}\right] \cdot a_{2(k+2)} = 0$$

$$(4.17)$$

$$\left[-p_2\frac{\lambda k^2}{4} - r\right] \cdot a_{1k} + \left[-p_2\xi\frac{(k-2)^2}{8} + p_2\xi\frac{(k-2)}{2} - \frac{p_2\xi}{2}\right] \cdot a_{1(k-2)} - \left[-p_2\xi\frac{(k+2)^2}{8} + \right.$$
$$\left. +p_2\xi\frac{(k+2)}{2} + \frac{p_2\xi}{2}\right] \cdot a_{1(k+2)} + \left[-p_2\frac{k^2}{4} + r - (1-\alpha)s\right] \cdot a_{2k} + \left[\frac{p_2\xi}{2}\right] \cdot a_{2(k-2)} + \left[\frac{p_2\xi}{2}\right] \cdot$$
$$a_{2(k+2)} = 0$$

$$\left[-(p_1 + p_2)\frac{\lambda^2 k^2}{4} + 2r - \lambda s \right] \cdot b_{1k} - \left[(p_1 + p_2)\xi \frac{\lambda(k-2)^2}{4} + (p_1 + p_2)\xi \frac{\lambda(k-2)}{2} + \frac{s\xi}{2} \right] \cdot$$

$$b_{1(k-2)} - \left[(p_1 + p_2)\xi \frac{\lambda(k+2)^2}{4} - (p_1 + p_2)\xi \frac{\lambda(k+2)}{2} + \frac{s\xi}{2} \right] \cdot b_{1(k+2)} - \left[p_2 \frac{\lambda k^2}{4} + r + \right.$$

$$\left. -\lambda \alpha s \right] \cdot b_{2k} + \left[-p_2 \xi \frac{(k-2)^2}{8} + \frac{\alpha s \xi}{2} \right] \cdot b_{2(k-2)} + \left[-p_2 \xi \frac{(k+2)^2}{8} + \frac{\alpha s \xi}{2} \right] \cdot b_{2(k+2)} = 0$$

$$(4.18)$$

$$\left[-p_2 \frac{\lambda k^2}{4} - r \right] \cdot b_{1k} - \left[p_2 \xi \frac{(k-2)^2}{8} + p_2 \xi \frac{(k-2)}{2} + \frac{p_2 \xi}{2} \right] \cdot b_{1(k-2)} - \left[p_2 \xi \frac{(k+2)^2}{8} + \right.$$

$$\left. -p_2 \xi \frac{(k+2)}{2} + \frac{p_2 \xi}{2} \right] \cdot b_{1(k+2)} + \left[-p_2 \frac{k^2}{4} + r - (1-\alpha)s \right] \cdot b_{2k} + \left[\frac{p_2 \xi}{2} \right] \cdot b_{2(k-2)} + \left[\frac{p_2 \xi}{2} \right] \cdot$$

$$b_{2(k+2)} = 0$$

All the passages to derive these two systems of infinite equations are described in Appendix B.

For the special case of vanishing amplitude ξ there is only one system equal for both the a_{jk} and b_{jk} coefficients. The latter has nontrivial solutions if the following determinant is null.

$$\begin{vmatrix} -(p_1 + p_2)\lambda^2 \dfrac{k^2}{4} + 2r - \lambda s & -p_2 \lambda \dfrac{k^2}{4} - r + \lambda \alpha s \\ -p_2 \lambda \dfrac{k^2}{4} - r & -p_2 \dfrac{k^2}{4} + r - (1-\alpha)s \end{vmatrix} = 0 \qquad (4.19)$$

Equation (4.19) represents a family of curves, i.e. the boundaries of the regions of instability, in the $\alpha - \eta$ plane. Notice that, the coefficient η is defined as $\eta = \frac{s}{r} = \frac{Q l_0}{c}$, which is a sort of equivalent critical load.

Solutions with period $T_2 = 2\pi$ can be represented by the Fourier series:

$$q_j(\tau) = \sum_{k=0,2,4,\dots}^{+\infty} \left(a_{jk} \sin\left(\frac{k\tau}{2}\right) + b_{jk} \cos\left(\frac{k\tau}{2}\right) \right), \quad (j = 1,2) \qquad (4.20)$$

Again, the substitution of this solution into the system of equations (4.15) yields to two infinite systems of linear homogeneous equations for the Fourier coefficients a_{jk} and b_{jk}. As before, instability curves in the $\alpha - \eta$ plane can be obtained for vanishing amplitude ξ.

It can be shown [13] that, for $\xi = 0$, the subharmonic resonances are characterized by

$$\frac{\Omega_v}{\omega} = \frac{k}{2}, \quad (k = 0,1,2,3,\dots) \qquad (4.21)$$

Therefore each value of k indicates the frequency ratio which assure the occurrence of subharmonic resonance. In particular, it is possible to distinguish different regions of instability, i.e. the first (characterized by $k = 1$), the second ($k = 2$), the third etc. The principal region of instability is the widest one and it corresponds to *subharmonic resonance 2:1*. It occurs when the exciting frequency is the double of the free vibration frequency. Thus parametric resonance can excite vibrations with frequencies smaller than the frequency of the principal resonance.

The condition $k = 0$ corresponds to divergent motion, which emerges to be a special case of subharmonic resonances.

Furthermore, a small value of amplitude ξ can lead the system to be unstable. For non vanishing amplitude of vibration, only a finite number of term is taken into account in the infinite system of equations (4.15) to determine the regions of instability. The more are the term retained, the more are the unstable regions obtained.

4.3.2 *Combination Resonances*

The boundaries for the combination resonances, also called instability of the second kind, are not so easy to be found, indeed there exists no comparably simple procedure as the case of subharmonic resonances, in which boundaries can be obtained by constructing periodic solutions. Thus, for the special case of vanishing amplitudes one can find the solution of the system of equations (4.15) as:

$$q_j(\tau) = a_j e^{i\Omega t}, \quad (j = 1,2) \tag{4.22}$$

Similarly to the solution for the subharmonic resonances (4.21), for the combination resonances:

$$\frac{\Omega_\mu}{\omega} \pm \frac{\Omega_v}{\omega} = \frac{k^*}{2}, \quad (k^* = 0,1,2,3,\dots) \tag{4.23}$$

being Ω_μ and Ω_v the natural frequencies of the transverse and longitudinal motion.

The condition for the flutter onset is when $\Omega_\mu = \Omega_v$, which corresponds to the case $k^* = 0$. Hence flutter emerges to be a special case of the instability of the second kind, namely the combinational resonances. Equation (4.23) yields a family of curves in the $\alpha - \eta$ plane, analogous to the curves obtained for the subharmonic resonances. All the curves are plotted by Herrmann both in the $\alpha - \eta$ plane , for the case of vanishing longitudinal amplitude (Figure 4.7), and in the $\eta - \xi$ plane, for a defined value of α (Figure 4.6).
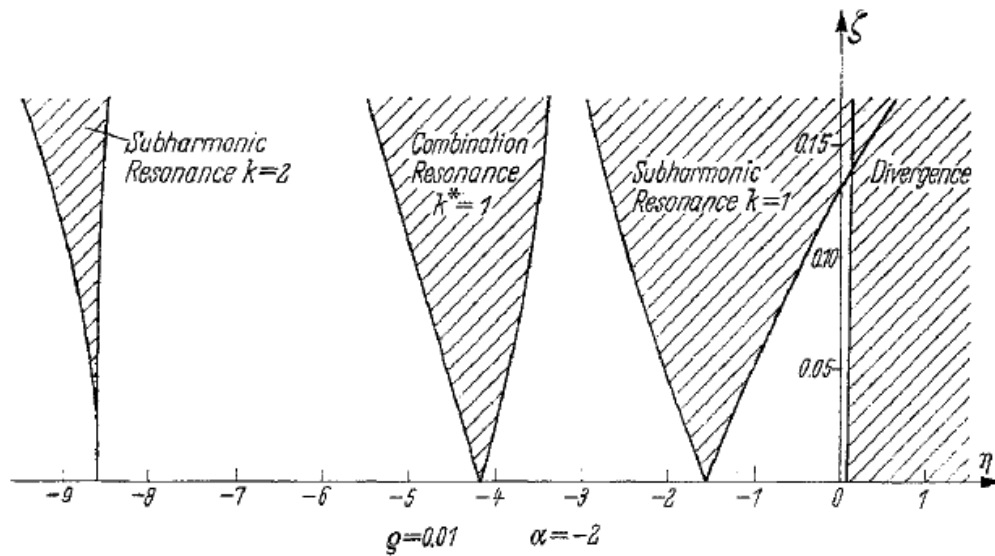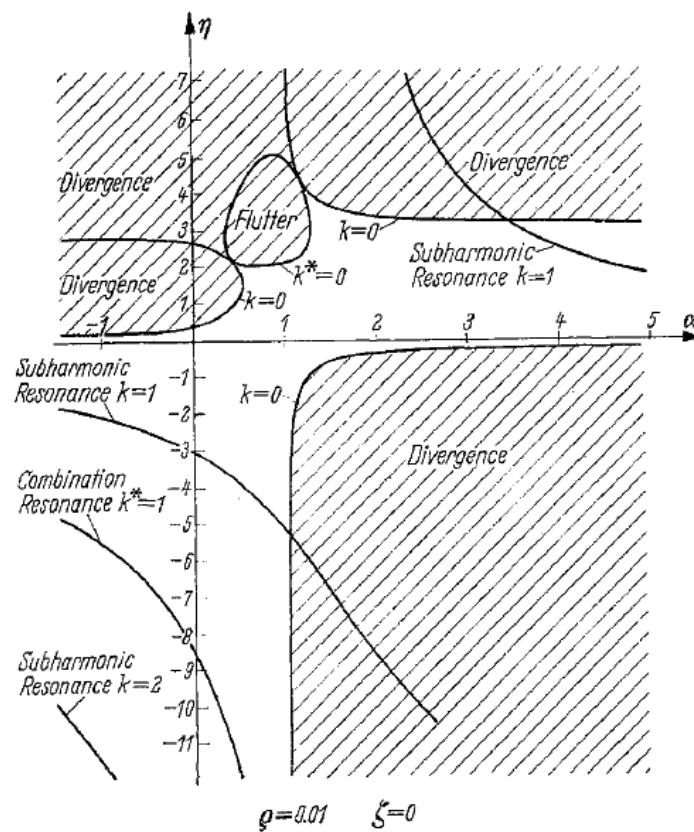
Figure 4.6: Instability region in the η – ξ plane

Figure 4.7: Instability region in the α − η plane

Notice that the value chosen by Herrmann to evaluate the stability in the $\eta - \xi$ plane is $\alpha = -2$. From Figure 4.7 it is clear that this value chosen can make the system unstable only for the cases of subharmonic resonances, combination resonances and divergence. In fact, the region of flutter is limited to some specific values of the coefficient α only.

4.4 COMPARISONS BETWEEN THE HERRMANN'S MODELS AND THE BRIDGE DECK SECTIONAL MODEL

It is evident that the bridge deck sectional model characterized by 2 DoFs subjected to aerodynamic forces is comparable to the 3 DoFs elastic inverted pendulum subjected to a follower force. At least these two problems are combined to the extent which these different schemes are able to capture the same instability phenomena, i.e. static divergence, flutter and internal parametric resonance. The aim of this paragraph is to find a strict link between the two different models and to explain the main common features and the main differences.

The model proposed by Herrmann and Hauger [31] seems to be the model with less DoFs able to capture all the instability phenomena. In fact, on one hand, the elastic pendulum is able to describe only the internal parametric resonance phenomenon, because the linear spring couples the two different modes of vibrations, i.e. the spring and the pendulum motion. On the other hand this model is not able to manifest flutter instability because it does not have enough rotational DoFs to sustain a follower force. Nevertheless the 2 DoFs inverted pendulum is able to sustain a follower force and it can become unstable either for static divergence or flutter, but two modes of vibrations are not coupled and internal parametric resonance cannot happen.

The question arising from this discussion is: "How is it possible that the bridge deck sectional model, characterized by only 2 DoFs, is able to exhibit all the aforementioned instability phenomena?"

The first thing to notice is the different nature of the forces characterizing the two problems. Both of them are non-conservative forces, but the Aeroelastic wind action is dependent on the bridge displacements and velocities. On the other hand the follower force introduced in the elastic pendulum model is dependent only on the displacements of the structure. Therefore, the latter is "poorer" with respect to the former.

However the main difference lies in the way the equations are coupled one to each other. For the sake of clarity, let us consider the 2 DoFs pendulum proposed by Herrmann and Bungay [30], which behaviour is described by equations (4.4), and the bridge model subjected to wind Aeroelastic effects, which behaviour is described by equations (3.90) and (3.91). In absence of damping these two models are completely equivalent, except for the quadratic stiffness coupling term present in the bridge's behaviour $K_{\theta w,mn}^{(Q)}$. This term is due to the cable's stiffness increment, which in principle is a Degree of Freedom of the system that in the present model has been parameterized and connected to the flexural and torsional DoFs thanks to the sectional compatibility. Indeed, the cables can be schematized by two non-linear springs which have different behaviour in tension and in compression. Their constitutive law is of hardening kind when subjected to tensile forces and of

softening king when subjected to compressive forces [8]. Therefore, when the deck cross section is subjected to a rigid rotation, the cables produce two different reactions, which provoke an asymmetric behaviour and a medium vertical displacement. On the other hand, in order to obtain coupled equations of motion for the 2 DoF$_s$ elastic pendulum, a linear elastic spring is introduced by Herrmann in this model. In conclusion, the 3rd Degree of Freedom must be added in the inverted pendulum model, just to take into account for a coupling between the other two DoF$_s$. This is not necessary in the bridge deck sectional model, for which the coupling term is intrinsic in the system and it is given by the cable's increment of stiffness.

Moreover, it is noticeable that the Degree of Freedom q_3 associated to the spring's elongation in the elastic pendulum is an artificial tool to couple indirectly the other two DoF$_s$. In fact there is not a direct coupling between q_1 and q_2, but the coupling is always between $q_1 - q_3$ and $q_2 - q_3$. Instead in the bridge's sectional model the quadratic coupling stiffness term $K_{\theta w,mn}^{(Q)}$ directly correlates the flexural and the torsional modes of vibrations. Because of these differences, it is impossible to find a static scheme able to simulate the nonlinear coupling present in the bridge.

The model proposed by Herrmann was studied by means of a parametric analysis governed by the parameter α. In a certain sense, this parameter is strictly related to the complete set of flutter derivatives, because it quantifies the effect of the applied force in terms of the projection in the direction of the system. Anyhow, the problem of the bridge's sectional model, comsidering the complete set of flutter derivatives is not mono-parametric. Thus it is not simple to handle with a parametric analysis.

The interesting thing is that the way of dynamic bifurcation of the bridge's model, or its loss of stability in general sense, depends upon the type of the flutter derivatives coefficients. In other words, without considering the quadratic coupling stiffness term, these terms would affect only the static divergence and the flutter velocity. Nonetheless, in the case that the quadratic coupling stiffness term becomes significant, other scenarios can be possible. In fact, the values of the flutter derivative coefficients are able to guarantee other instability limits in which the internal parametric resonance can be predominant.

4.5 VARIATIONAL EQUATIONS FOR THE BRIDGE'S DECK SECTIONAL MODEL

The perturbation approach used by Herrmann and Hauger [31] can be adopted for studying the stability of the suspension bridge vibrations as long as dominant flexural motion occurs.

4.5.1 *Perturbed System of Equations*

Firstly, a reference solution for equations (3.90) and (3.91) has to be assumed. The hypothesis consists in seeking a solution with small flexural vibrations and negligible torsional ones, so as to neglect non-linear flexural contributions and to assume a lift coefficient in correspondence of a null torsional angle. Hence:

$$z_n(\tau) < \epsilon \quad \Rightarrow \quad z_n^2(\tau) \cong 0, z_n^3(\tau) \cong 0$$

$$\gamma_m(\tau) \cong 0 \quad \Rightarrow \quad \tilde{c}_L = \frac{C_L(\theta_d = 0)}{2\pi} \tag{4.24}$$

Due to this assumption, the flexural equation of motion (3.90) becomes completely analogous to the linear equation of motion of a SDoF damped and periodically forced oscillator:

$$M_{w,n} \cdot \ddot{z}_n + \left(D_{w,n} - D_{w,n}^{Aero}\right) \cdot \dot{z}_n + \left(K_{w,n}^{(L)} - K_{w,n}^{(L),Aero}\right) \cdot z_n = \Gamma_{w,n} \tag{4.25}$$

The solution of this equation is characterized by the superposition of an homogeneous-transient and a particular steady-state integral.

The transient conditions are not of interest with regards to a stability analysis, because they are always damped in time. This is not true for a negative value of damping, which grant self-sustained oscillations. This case is possible only if the wind velocity is enough high to reach the flutter onset, but this condition is a priori an unstable solution. Thus, we are allowed to neglect the homogeneous solutions in the stability analysis.

In order to find the particular integral for equation (4.25) it is necessary to introduce the equation that rules the displacement $s_n(\tau)$ of the same system subjected to an out of phase periodic force with respect to the one appearing in (4.25), i.e. $\Gamma_{w,n} = \Gamma_0 \cdot \tilde{h}_{W_n} \cdot cos(\widetilde{\omega}_{VS} \cdot \tau)$.

$$M_{w,n} \cdot \ddot{s}_n + \left(D_{w,n} - D_{w,n}^{Aero}\right) \cdot \dot{s}_n + \left(K_{w,n}^{(L)} - K_{w,n}^{(L),Aero}\right) \cdot s_n = \Gamma_0 \cdot \tilde{h}_{W_n} \cdot cos(\widetilde{\omega}_{VS} \cdot \tau) \tag{4.26}$$

Now let us introduce the complex variable:

$$y_n(\tau) = s_n(\tau) + i \cdot z_n(\tau) \tag{4.27}$$

The sum of equation (4.26) with equation (4.25) multiplied by the imaginary part, leads to:

$$\ddot{y}_n + \frac{D_{w,n}^{TOT}}{M_{w,n}} \cdot \dot{y}_n + \frac{K_{w,n}^{TOT}}{M_{w,n}} \cdot y_n = \frac{\Gamma_0 \cdot \tilde{h}_{W_n}}{M_{w,n}} \cdot exp(i \cdot \widetilde{\omega}_{VS} \cdot \tau) \tag{4.28}$$

where:

$$\frac{D_{w,n}^{TOT}}{M_{w,n}} = \frac{D_{w,n} - D_{w,n}^{Aero}}{M_{w,n}} = 2\Delta_{w,n}\tilde{\Omega}_{w,n} - \frac{1}{\pi}\sqrt{\tilde{J}_t}\sqrt{\tilde{m}_a}\tilde{\Omega}_{\theta,m} \cdot \tilde{u}K_w H_1^*$$

$$\frac{K_{w,n}^{TOT}}{M_{w,n}} = \frac{K_{w,n}^{(L)} - K_{w,n}^{(L),Aero}}{M_{w,n}} = \tilde{\Omega}_{w,n}^2 - \frac{1}{2\pi}\tilde{J}_t\tilde{\Omega}_{\theta,m}^2 \cdot \tilde{u}^2 K_w^2 H_4^*$$

(4.29)

The solution for the equation (4.28) can be found more easily with respect to the equation (4.25). Then the particular integral for equation (4.25) can be found extracting the imaginary part of the solution $y_n(\tau)$.

To this purpose let us seek for a particular integral of the type:

$$y_n(\tau) = \Gamma_0 \cdot \tilde{h}_{W_n} \cdot \tilde{H}(\omega_{VS}) \cdot exp(i \cdot \tilde{\omega}_{VS} \cdot \tau)$$

(4.30)

The substitution of the assumed solution (4.30) in the governing equation (4.28), allows to get the amplification factor $\tilde{H}(\omega_{VS})$. Thanks to the introduction of a coefficient $\beta = \frac{\tilde{\omega}_{VS}}{\tilde{\Omega}_{w,n}}$ representing the ratio between the vortex shedding circular frequency and the structural flexural one, $\tilde{H}$ can be expressed, in function of β itself, as:

$$\tilde{H}(\beta) = \frac{1}{K_{w,n}^{(L)}} \cdot \frac{1}{-\beta^2 + \frac{D_{w,n}^{TOT}}{M_{w,n}\tilde{\Omega}_{w,n}} \cdot i \cdot \beta + \frac{K_{w,n}^{TOT}}{M_{w,n}\tilde{\Omega}_{w,n}^2}}$$

(4.31)

The solution can also be expressed by splitting $\tilde{H}(\beta)$ with its modulus and a phase lag:

$$\tilde{H}(\beta) = \frac{1}{K_{w,n}^{(L)}} \cdot N(\beta) \cdot exp(-i \cdot \varphi(\beta))$$

(4.32)

being

$$N(\beta) = \left[\sqrt{\left(\frac{K_{w,n}^{TOT}}{M_{w,n}\tilde{\Omega}_{w,n}^2} - \beta^2 - Im\left(\frac{D_{w,n}^{TOT}}{M_{w,n}\tilde{\Omega}_{w,n}}\right) \cdot \beta\right)^2 + \left(Re\left(\frac{D_{w,n}^{TOT}}{M_{w,n}\tilde{\Omega}_{w,n}}\right) \cdot \beta\right)^2} \right]^{-1}$$

$$\varphi(\beta) = arctg\left(\frac{Re\left(\frac{D_{w,n}^{TOT}}{M_{w,n}\tilde{\Omega}_{w,n}}\right) \cdot \beta}{\frac{K_{w,n}^{TOT}}{M_{w,n}\tilde{\Omega}_{w,n}^2} - \beta^2 - Im\left(\frac{D_{w,n}^{TOT}}{M_{w,n}\tilde{\Omega}_{w,n}}\right) \cdot \beta} \right)$$

(4.33)

Notice that the damping term must be divided in its real and imaginary part because, with regards to the Aeroelastic problem, the reduced frequency K_w is a complex function.

The solution for equation (4.28) can be therefore expressed as:

$$y_n(\tau) = \frac{\Gamma_0 \cdot \tilde{h}_{W_n}}{K_{w,n}^{(L)}} \cdot N(\beta) \cdot exp\left(i \cdot \widetilde{\omega}_{VS} \cdot \tau - i \cdot \varphi(\beta)\right) \qquad (4.34)$$

where both Γ_0 and β are function of the wind non-dimensional velocity $\tilde{u}$.

In order to find the solution for equation (4.25) only the imaginary part of $y_n(\tau)$ must be retained. Hence, by exploiting the well-known Euler formula:

$$z_{n,SS}(\tau) = \frac{\Gamma_0 \cdot \tilde{h}_{W_n}}{K_{w,n}^{(L)}} \cdot N(\beta) \cdot sin\left(\widetilde{\omega}_{VS} \cdot \tau - \varphi(\beta)\right) = z_{n,0} \cdot sin\left(\widetilde{\omega}_{VS} \cdot \tau - \varphi(\beta)\right) \qquad (4.35)$$

where $z_{n,0}$ is the modal flexural amplitude normalized with respect to the initial cable sag.

With the aim of defining the so called *variational equations*, a small but non vanishing perturbation of both the flexural and the torsional modes of vibrations must be introduced.

$$z_n(\tau) = z_{n,SS}(\tau) + z_n^P(\tau) \quad with\ z_n^P(\tau) < \epsilon$$

$$\gamma_m(\tau) = \gamma_m^P(\tau) \quad with\ \gamma_m^P(\tau) < \epsilon$$

$$(4.36)$$

By substituting the above definitions in the complete modal Aeroelastic system of equations (3.90) and (3.91) and by a suitable linearization, one gets the so called *Perturbed System*.

$$M_{w,n} \cdot \ddot{z}_n^P + \left(D_{w,n} - D_{w,n}^{Aero}\right) \cdot \dot{z}_n^P + D_{w\theta,nm}^{Aero} \cdot \dot{\gamma}_m^P + \left(K_{w,n}^{(L)} - K_{w,n}^{(L),Aero}\right) \cdot z_n^P +$$
$$+ K_{w\theta,nm}^{(L),Aero} \gamma_m^P = 0 \qquad (4.37)$$

$$J_{\theta,m} \cdot \ddot{\gamma}_m^P + \left(D_{\theta,m} - D_{\theta,m}^{Aero}\right) \cdot \dot{\gamma}_m^P + D_{\theta w,mn}^{Aero} \cdot \dot{z}_n^P + K_{\theta w,mn}^{(L),Aero} \cdot z_n^P + \left(K_{\theta,m}^{(L)} - K_{\theta,m}^{(L),Aero} + \right.$$
$$\left. + K_{\theta w,mn}^{(Q)} z_{n,0} \cdot sin(\widetilde{\omega}_{VS} \cdot \tau - \varphi)\right) \cdot \gamma_m^P = 0 \qquad (4.38)$$

The second order coupling stiffness term $K_{\theta w,mn}^{(Q)}$ is dependent simultaneously and linearly on both motions, thus it survives in the linearization of the perturbed equations of motion. This makes possible that a small but non vanishing vertical perturbation influences the torsional response due to a periodically varying structural parameter, even in a linearized

formulation. This kind of phenomenon can be classified as a parametric excitation problem.

The fact that the vertical perturbation depends on the vortex shedding excitation is hidden inside the terms $z_{n,0}$ and φ, that are implicitly dependent on the non-dimensional wind speed and on the lift coefficient since they are obtained as the solution of equation (4.25). Moreover it is important to remark that vortex shedding is a self-limiting phenomenon, which can induce just small flexural perturbations. However, because the effects due to these flexural perturbations on torsional vibrations is amplified by the quadratic coupled modal stiffness $K_{\theta w,mn}^{(Q)}$, it is of basic importance to understand its influence on the system response.

4.5.2 *Mathieu's Equation for the Torsional Perturbed Motion*

Let us consider the system of perturbed equations (4.37) and (4.38) decoupled because of the assumption that the coupling flutter derivatives A_1^* and A_4^* are of less importance in mono-dimensional flutter with respect to A_2^* and A_3^*. The decoupled system of perturbed equations reads as:

$$M_{w,n} \cdot \ddot{z}_n^P + \left(D_{w,n} - D_{w,n}^{Aero} \right) \cdot \dot{z}_n^P + \left(K_{w,n}^{(L)} - K_{w,n}^{(L),Aero} \right) \cdot z_n^P = 0 \tag{4.39}$$

$$J_{\theta,m} \cdot \ddot{\gamma}_m^P + \left(D_{\theta,m} - D_{\theta,m}^{Aero} \right) \cdot \dot{\gamma}_m^P + \left(K_{\theta,m}^{(L)} - K_{\theta,m}^{(L),Aero} + K_{\theta w,mn}^{(Q)} z_{n,0} \cdot sin(\widetilde{\omega}_{VS} \cdot \tau - \varphi) \right) \cdot \\ \gamma_m^P = 0 \tag{4.40}$$

As usual for commons bridge's deck sections it can be assumed that $H_1^* < 0$ for each wind speed. In this way the damping term in equation (4.39) is always positive, avoiding the possibility to have 1 DoF flexural instability. Thus z_n^P will not diverge in time for any wind velocity considered.

This result allows us to study only the behaviour of the torsional equation (4.40). The objective is to reduce the damped torsional equation to the well-known Mathieu's format, so as to focus the attention on the internal parametric resonance phenomenon.

First of all, a proper choice of the reference initial time allows us to shift the flexural perturbation acting on the torsional motion from a periodic sine function to a cosine one.

$$J_{\theta,m} \cdot \ddot{\gamma}_m^P + \left(D_{\theta,m} - D_{\theta,m}^{Aero} \right) \cdot \dot{\gamma}_m^P + \left(K_{\theta,m}^{(L)} - K_{\theta,m}^{(L),Aero} + K_{\theta w,mn}^{(Q)} z_{n,0} \cdot cos(\widetilde{\omega}_{VS} \cdot \tau) \right) \cdot \\ \gamma_m^P = 0 \tag{4.41}$$

Then some non-dimensional parameters, defined as the ratio between the Aeroelastic components and the structural ones, are introduced.

$$
\alpha = \frac{D_{\theta,m}^{Aero}}{D_{\theta,m}} = \frac{2\tilde{u}\sqrt{\tilde{m}_a}K_\theta A_2^*}{\pi \Delta_{\theta,m}\sqrt{\tilde{J}_t}}
$$

$$
\beta = \frac{K_{\theta,m}^{(L),Aero}}{K_{\theta,m}^{(L)}} = \frac{2\tilde{u}^2 K_\theta^2 A_3^*}{\pi}
$$

(4.42)

Hence the torsional equation (4.41) is transformed into:

$$
\ddot{\gamma}_m^P + 2\Delta_{\theta,m}\tilde{\Omega}_{\theta,m}(1-\alpha)\cdot\dot{\gamma}_m^P + \tilde{\Omega}_{\theta,m}^2\left((1-\beta) + \frac{K_{\theta w,mn}^{(Q)}}{K_{\theta,m}^{(L)}}z_{n,0}\cdot cos(\widetilde{\omega}_{VS}\cdot\tau)\right)\cdot\gamma_m^P = 0 \quad (4.43)
$$

In order to pass to the Mathieu's format, it is necessary to define a new time variable.

$$
\bar{\tau} = \widetilde{\omega}_{VS}\cdot\tau \quad\Rightarrow\quad d\tau = \frac{d\bar{\tau}}{\widetilde{\omega}_{VS}}, d\tau^2 = \frac{d\bar{\tau}^2}{\widetilde{\omega}_{VS}^2}
$$

(4.44)

Notice that this time variable transformation does not lead to the classical Mathieu's format of the equation, but to a more convenient one. The substitution of the new time variable and its derivatives (4.44) into the torsional equation (4.43) is such that:

$$
\frac{d^2\gamma_m^P}{d\bar{\tau}^2} + 2\Delta_{\theta,m}\frac{\tilde{\Omega}_{\theta,m}}{\widetilde{\omega}_{VS}}(1-\alpha)\cdot\frac{d\gamma_m^P}{d\bar{\tau}} + \frac{\tilde{\Omega}_{\theta,m}^2}{\widetilde{\omega}_{VS}^2}\left((1-\beta) + \frac{K_{\theta w,mn}^{(Q)}}{K_{\theta,m}^{(L)}}z_{n,0}\cdot cos(\bar{\tau})\right)\cdot\gamma_m^P = 0 \quad (4.45)
$$

The last step is to define the following quantities:

$$
\delta' = \frac{\tilde{\Omega}_{\theta,m}^2}{\widetilde{\omega}_{VS}^2}
$$

$$
c' = 2\Delta_{\theta,m}\frac{\tilde{\Omega}_{\theta,m}}{\widetilde{\omega}_{VS}} = 2\Delta_{\theta,m}\sqrt{\delta'}
$$

$$
\delta = \delta'(1-\beta) = \frac{\tilde{\Omega}_{\theta,m}^2}{\widetilde{\omega}_{VS}^2}\left(1 - \frac{K_{\theta,m}^{(L),Aero}}{K_{\theta,m}^{(L)}}\right)
$$

(4.46)

$$
c = c'(1-\alpha) = 2\Delta_{\theta,m}\frac{\tilde{\Omega}_{\theta,m}}{\widetilde{\omega}_{VS}}\left(1 - \frac{D_{\theta,m}^{Aero}}{D_{\theta,m}}\right)
$$

$$
\varepsilon = \frac{\tilde{\Omega}_{\theta,m}^2}{\widetilde{\omega}_{VS}^2}\frac{K_{\theta w,mn}^{(Q)}}{K_{\theta,m}^{(L)}}z_{n,0} = \delta'\frac{K_{\theta w,mn}^{(Q)}}{K_{\theta,m}^{(L)}}z_{n,0}
$$

Finally:

$$\frac{d^2\gamma_m^P}{d\bar{\tau}^2} + c \cdot \frac{d\gamma_m^P}{d\bar{\tau}} + \left(\delta + \varepsilon \cdot cos(\bar{\tau})\right) \cdot \gamma_m^P = 0 \tag{4.47}$$

Equation (4.47) represents the Mathieu's format of the torsional equation of motion for the bridge's deck section, perturbed by a dynamic periodic flexural vibration.

Mathieu-Hill's equations are encountered in various areas of physics and engineering, from the problem of the propagation of electromagnetic waves in a medium with a periodic structure to the problem of the motion of electrons in a crystal lattice, from the investigations of the stability of the oscillatory process in nonlinear systems to certain problems of celestial mechanics, such as the theory of the motion of the moon.

One of the most interesting characteristics of this equation is that, for certain relations between its coefficients, it has unbounded solutions. The values of the coefficients cover certain regions in the plane of the two parameter δ and ε, i.e. the regions of dynamic instability. Figure 4.8 shows the distribution of the regions of instability in the $\delta - \varepsilon$ plane for the Mathieu's equation (4.47). Figure 4.8 represents the so-called Ince-Strutt diagram, where the regions in which the solutions are bounded in time are crosshatched.

Figure 4.8: Ince-Strutt Diagram

It should be remarked that, although this diagram usually refers to truly parametric system where the excitation is provided by an external source, it also applies to the internal resonance case, which provides an auto-parametric phenomenon. According to the Ince-

Strutt diagram and with regards to what already found in §4.3.1, the system shows critical conditions in correspondence of particular frequency ratios, i.e. $\delta = n^2/4$.

The widest region of instability is characterized by $n = 1$ and it represent the 2:1 internal resonance condition, that is the frequency of the flexural perturbation is twice the torsional one. The effect of an increase of damping in the structure affects in a large amount the Ince-Strutt diagram, reducing the extension of the regions of dynamic instability. In fact for a given value of damping c there is a minimum value of the flexural perturbation ε which is required for instability to occur.

4.5.3 *Derivation of the Boundary Frequency Excitation*

Different methods are available to solve the Mathieu's equation (4.47), or fully analytical or approximate. Bolotin [13] argued that the determination of the boundaries of the regions of instability consists in the resolution of the conditions under which the given differential equation has periodic solutions with periods T and 2T. Indeed it can be demonstrated that the regions of unboundedly increasing solutions are separated from the regions of stability by the periodic solutions with periods T and 2T. This method is clearly the same as the one adopted by Herrmann and Hauger [31] to solve the equations for the inverted elastic pendulum in §4.3.1. It leads to two converging systems of infinite equations which can be solved numerically, e.g. with the method of successive approximations.

The solution for the Mathieu's equation can also be obtained through any approximate perturbation method [43], e.g. the multiple scales technique. This method consists in exploiting the solution as a straightforward asymptotic expansion for small values of ϵ.

$$\gamma_m^P = \gamma_{m,0}^P + \epsilon \cdot \gamma_{m,1}^P + \epsilon^2 \cdot \gamma_{m,2}^P + \cdots \tag{4.48}$$

The substitution of the solution (4.48) into the equation (4.47) leads to a system of equations as large as the number of terms retained in the asymptotic expansion. The solution of this system of equations requires the zeroing of the secular terms which provides additional conditions to find the constants of integration.

In order to facilitate the perturbation method let us assume that the value of damping is very small and can be scaled as $c = \epsilon \cdot \mu$. This assumption is not restrictive in the problem considered, because the values of damping characterizing the bridge's behaviour are generally very small. Adopting this method the transition curves correspondent to the 2:1 subharmonic internal resonance can be expressed as:

$$\delta = \frac{1}{4} \pm \frac{\sqrt{\varepsilon^2 - c^2}}{2} + O(\epsilon^2) \tag{4.49}$$

The solution for the boundary frequency excitation (4.49) approximates in a good way the solution of the Mathieu's equation around the value of $\delta = \frac{1}{4}$. Moreover, for a given value of the damping coefficient there is a minimum value of ε required for instability to occur. This value can be easily found starting from equation (4.49):

$$\varepsilon > \sqrt{c^2 + 4 \cdot \left(\delta - \frac{1}{4}\right)^2} \tag{4.50}$$

Figure 4.9 represents the Ince-Strutt diagram in which the regions of instability for the 2:1 resonance phenomenon are plotted considering both the cases of null damping and of damping coefficient $\Delta_{\theta,m} = 0.5\%$. Notice how the effect of damping is relevant only in the zone around the value of $\delta = \frac{1}{4}$, whereas for the other values of δ the two lines depicted are practically coincident.
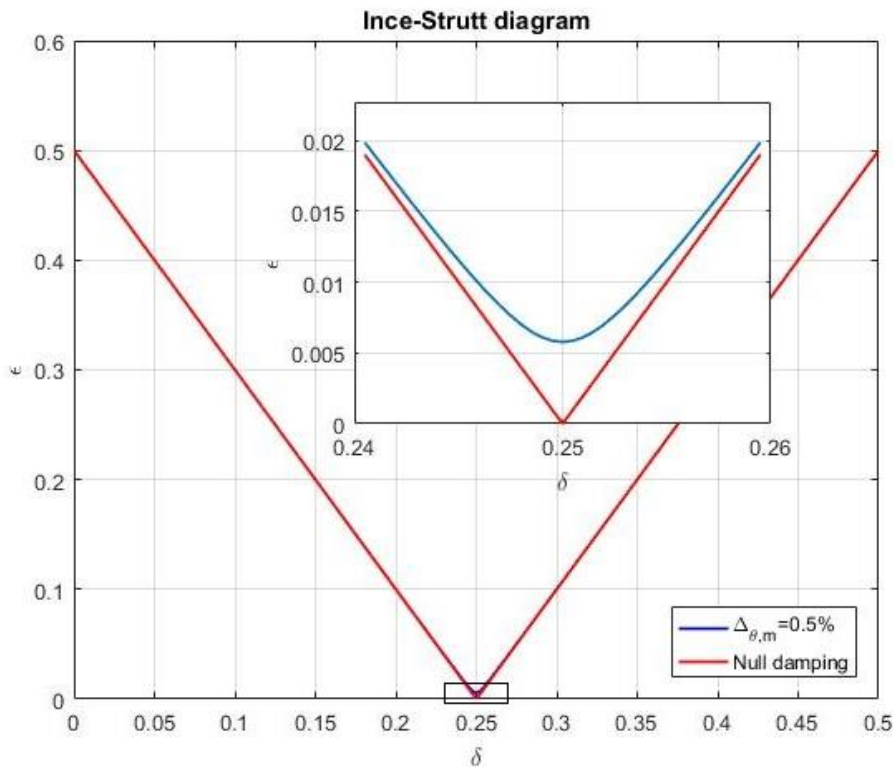
Figure 4.9: Boundaries of the regions of instability in the Ince-Strutt diagram for the subharmonic 2:1 Internal resonance

4.5.4 *Interaction Between Flutter 1-D and Subharmonic 2:1 Resonance*

The advantage to represent the boundaries of instability lines in the Ince-Strutt diagram trough an approximate solution is that it makes possible to find a closed form equation able to explain the interaction between flutter and internal parametric resonance. It is important to remark the fact that, with the hypothesis assumed, we are studying the interaction between 1 DoF torsional flutter and parametric resonance. In fact, the problem is governed by the torsional equation only, which can be excited parametrically by the flexural perturbation due to the vortex shedding phenomenon.

In order to show the possibility of internal parametric resonance to deteriorate the flutter performance of a bridge, let us write the equation (4.50) as:

$$c^2 < \varepsilon^2 - 4 \cdot \left(\delta - \frac{1}{4}\right)^2 \tag{4.51}$$

The substitution into this equation of the definition of the total damping c given by both the structural and Aeroelastic component (4.46), leads to:

$$(1 - \alpha)^2 < \frac{\varepsilon^2}{c'^2} - \frac{4}{c'^2} \cdot \left(\delta - \frac{1}{4}\right)^2 \tag{4.52}$$

This is a second order equation with the α parameter to be determined:

$$\alpha^2 - 2 \cdot \alpha + \left(1 - \frac{\varepsilon^2}{c'^2} + \frac{4}{c'^2} \cdot \left(\delta - \frac{1}{4}\right)^2\right) < 0 \tag{4.53}$$

characterized by the two solutions:

$$\alpha_{1,2} = 1 \pm \frac{\varepsilon}{c'} \sqrt{1 - \frac{4}{\varepsilon^2} \cdot \left(\delta - \frac{1}{4}\right)^2} \tag{4.54}$$

Hence the equation (4.53) is valid for values of α:

$$\alpha > 1 - \frac{\varepsilon}{c'} \sqrt{1 - \frac{4}{\varepsilon^2} \cdot \left(\delta - \frac{1}{4}\right)^2} \tag{4.55}$$

Considering the effect of A_3^* negligible in the determination of the natural frequencies of vibrations, the reduced frequency can be expressed as:

$$K_\theta = \frac{2\sqrt{\tilde{m}_a}}{\sqrt{\tilde{J}_t}\tilde{\Omega}_{\theta,m}\tilde{u}}\tilde{\Omega}_{\theta,m} = \frac{2\sqrt{\tilde{m}_a}}{\sqrt{\tilde{J}_t}\cdot\tilde{u}} \tag{4.56}$$

Thus, the definition of α introduced in the equation (4.42) can be re-written:

$$\alpha = \frac{D_{\theta,m}^{Aero}}{D_{\theta,m}} = \frac{2\tilde{u}\sqrt{\tilde{m}_a}K_\theta A_2^*}{\pi\Delta_{\theta,m}\sqrt{\tilde{J}_t}} = \frac{4}{\pi}\cdot\frac{\tilde{m}_a}{\tilde{J}_t}\cdot\frac{A_2^*}{\Delta_{\theta,m}} = \frac{A_2^*}{\frac{\pi}{4}\cdot\frac{\tilde{J}_t}{\tilde{m}_a}\cdot\Delta_{\theta,m}} = \frac{A_2^*}{A_{2,F}^*} \tag{4.57}$$

being $A_{2,F}^* = \frac{\pi}{4}\frac{\tilde{J}_t}{\tilde{m}_a}\Delta_{\theta,m}$ the value of the A_2^* flutter derivative correspondent to the condition of the onset of flutter, as already found in §3.3.5 by equation (3.51).

Thanks to this definition equation (4.55) can be rewritten as:

$$A_2^* > A_{2,F}^* \cdot \left(1 - \frac{\varepsilon}{c'}\sqrt{1 - \frac{4}{\varepsilon^2}\cdot\left(\delta - \frac{1}{4}\right)^2}\right) \tag{4.58}$$

This equation extends the calculation for the A_2^* flutter derivative correspondent to the onset of flutter provided in equation (3.51), by taking in consideration also the effects due to a vertical perturbation in the initial configuration of the bridge, which can lead to torsional oscillation. The importance of this equation is that it shows in a direct way that the internal parametric resonance phenomenon is able to deteriorate the torsional flutter performances of the bridge.

However, equation (4.58) is not a closed-form equation, because both the terms at the LHS and at the RHS are dependent on the actual wind velocity. Therefore its applicability is very limited. In the present study equation (4.58) will be used in its inverse form, indeed a wind speed very near to the onset of flutter will be assumed, so as to be able to calculate the parameter α. Starting from this, the modal displacement, necessary to activate the instability phenomenon will be computed and it will be compared to the modal displacement provided by vortex shedding.

As clearly shown in Figure 4.9, the most critical situation for the occurrence of the subharmonic 2:1 parametric resonance is when $\delta = \frac{1}{4}$. In fact in this situation the modal amplitudes of oscillation needed to activate the instability phenomenon are as lower as lower is the damping coefficient. Hence the substitution of the most critical condition $\delta = \frac{1}{4}$ into equation (4.58) leads to:

$$A_2^* > A_{2,F}^* \cdot \left(1 - \frac{\varepsilon}{c'}\right) = A_{2,F}^* \cdot \left(1 - \frac{\delta'}{c'} \cdot \frac{K_{\theta w,mn}^{(Q)}}{K_{\theta,m}^{(L)}} \cdot z_{n,0}\right) \tag{4.59}$$

From this last equation, it is even clearer that 1 DoF flutter velocity is deteriorated proportionally to:

1. The magnitude of the non-linear coupling stiffness term $K_{\theta w,mn}^{(Q)}$;

2. The amplitude of the vertical modal amplitude due to vortex shedding $z_{n,0}$.

5 THE ORIGINAL TACOMA NARROWS BRIDGE

The dramatic collapse of the Original Tacoma Narrows Bridge, occurred on November 7, 1940, is certainly the most celebrated structural failure of all times, both because of the impressive video recorded [57] and because of the huge number of studies that it has generated. It has inspired a large amount of thought both among engineers interested in structures and among those interested in aerodynamics and vibrations.

Clark Eldridge, a bridge engineer for the Washington State Toll Bridge Authority, proposed a design in 1938. The central span was 853.4 m (2800 ft) long and 11.9 m (39 ft) wide, with two lanes. A truss below the roadway was 7.6 m (25 ft) deep to stiffen the deck against vertical, lateral, and torsional displacements. The estimated cost was $11 million. The Public Works Authority (PWA) wanted to lower the cost, and a well-known consultant, Leon Moisseiff of New York, was hired. He replaced the truss in Eldridge's design with two vertical stiffening silicon-steel plate girders along the sides, extending 1.22 m (4 ft) above and below the roadway. The new estimated cost was $6.4 million.

Oscillations of considerable amplitudes , caused by wind were apparent during the erection of the Tacoma Narrows Bridge. In spite of certain remedial devices that were installed, these undulations continued after the completion of the structure and its opening to vehicular traffic on July 1, 1940, indeed amplitudes of 0.42 m (1.4 ft) were often recorded. The vertical undulations were regarded as an attraction by the local public and earned the bridge the nickname "Galloping Gertie". However, the same motions were of great concern to the structural engineers, who monitored the vibration pattern of the bridge closely.

On November 7, 1940, a wind speed of 19 m/s (42 mph) was measured at the eastern end of the bridge. The wind was southerly and hit the bridge obliquely. The motion of the deck before 10 a.m. was vertical with an amplitude not more than 0.5 m (1.6 ft) and it had eight or more nodes in the central span. The frequency of the motion was 36 - 38 cycles per minute (0.60 - 0.63 Hz), which was significantly higher than previously reported frequencies. Around 10 a.m., the motion violently switched into a torsional mode with a node at midspan. The initial frequency was 14 cycles per minute (0.23 Hz), but after a short time it decreased to 12 cycles per minute (0.2 Hz), perhaps due to some damage within the deck. After examining the films, Farquharson concluded that the maximum twist angle was about 35°, corresponding to a maximum vertical amplitude of approximately

4.3m (14 ft) along the edge of the deck. The central span collapsed around 11 a.m. and fell into the Tacoma Narrows. Torsional oscillations had not been observed on the bridge prior to its last hour.

5.1   TENTATIVE EXPLANATIONS OF THE FAULT

There have been many attempts to explain the amazing Tacoma Narrows Bridge failure, but none is universally accepted. It is however well established that the main culprit was the unexpected appearance of torsional oscillations.

First attempts for the explanations of the bridge collapse, made by the investigators, concerned with the classical resonance phenomenon between the vortex shedding frequency and one of the bridge's natural frequencies.

Some years later, Scanlan et al. [11] denied this theory and they attributed the failure to the aerodynamic forces generated by the wind-structure interaction. These forces may generate self-excitation and negative damping effects, which for the particular Aerodynamic properties of the bridge led torsional flutter instability. Nowadays, the dominant explanation of the Tacoma collapse relies with this theory.

Further explanations involve vortices, due both to the particular shape of the bridge and to the angle of attack of the wind. Matsumoto et al. [40] studied the aerodynamic interferences between vortex induced heaving vibrations and torsional vibrations which can provoke stabilizing effects, suppressing the torsional flutter. Larsen et al. [36] developed a model for the numerical simulations of two-dimensional viscous incompressible flow past bridge girder cross sections using finite difference and discrete vortex methods. The results of their studies highlighted aerodynamic interferences for bluff cross sections due to the vortex shedding phenomenon.

Arioli and Gazzola [7] suggested that the spark for torsional oscillations was an internal resonance which creates a bifurcation of the Poincaré map and occurs when a certain amount of energy is present into the structure. They emphasized a structural instability considering an ideal isolated bridge in vacuum, in which a certain amount of energy is inserted in the structure. The wind and vortex shedding are usually responsible for introducing energy within the structure.

These theories differ as to what caused the torsional oscillation of the bridge, but they all agree that the extreme flexibility, slenderness, and lightness of the Tacoma Narrows Bridge allowed these oscillations to grow until they destroyed it.

5.2 DATA FOR THE TACOMA NARROWS BRIDGE

The report to the honorable John M. Carmody Administrator for the Federal works Agency Washington, written by Amman et al. [2] contains all the information about the Tacoma Narrows Bridge. Other data necessary for the analysis, such as the elastic modulus, are provided by Malik [39]. All the bridge's data are listed in Table 5.1.

b	=	$5.94\ m\ (19.5\ ft)$	Half-width of the deck cross section
l	=	$853.44\ m\ (2800\ ft)$	Central span length
L_c	=	$868.7\ m$	Cable's length under deck's self weight only
D	=	$2.44\ m\ (8\ ft)$	Depth of the deck cross section
f	=	$70.7\ m\ (232\ ft)$	Cable's sag
A_c	=	$0.123\ m^2\ (190\ sq.\,ins)$	Cable's area
m_d	=	$6354\ kg/m\ (4270\ lb\ p.\,ft)$	deck mass per unit length
m_c	=	$1064\ kg/m\ (715\ lb\ p.\,ft)$	cable mass per unit length
m_{tot}	=	$8482\ kg/m\ (5700\ lb\ p.\,ft)$	Total mass per unit length
I_d	=	$0.1544\ m^4\ (2567\ sq.\,ins\ sq.\,ft)$	Deck moment of inertia
J_d	=	$6.07 \cdot 10^{-6}\ m^4$	Torsional constant of the deck
Γ_d	=	$5.44\ m^6$	Warping constant of the deck
J_t	=	$58097\ kg \cdot m^2/m$	Linear density of the deck's moment of inertia
ρ_d	=	$3.96\ m\ (13\ ft)$	Inertial gyration radius of the deck
E_d	=	$2 \cdot 10^{11}\ N/m^2$	Effective elastic modulus of the deck
G_d	=	$8 \cdot 10^{10}\ N/m^2$	Shear modulus of the deck
E_c	=	$1.85 \cdot 10^{11}\ N/m^2$	Effective elastic modulus of the cables

Table 5.1: Tacoma Narrows Bridge Data

From these available information it is possible to define the fundamental dimensionless parameters entering in the governing equation of motion, listed in Table 5.2.

H	=	$5.35 \cdot 10^7 \, N$	Horizontal projection of the cables tension force
μ^2	=	$3.96 \cdot 10^{-4}$	Steinmann's stiffness factor
λ_1^2	=	183.29	1st order Irvine's parameter
λ_2^2	=	22.91	2nd order Irvine's parameter
λ_3^2	=	2.86	3rd order Irvine's parameter
β^2	=	$1.28 \cdot 10^{-4}$	Ratio between the primary torsional stiffness and the cables one
χ^2	=	0.325	Warping coefficient
γ^2	=	$3.95 \cdot 10^{-4}$	Ratio between the warping torsional stiffness and the cables one
$\tilde{J}_t$	=	0.445	Non-dimensional torsional inertia
$\tilde{m}_d$	=	0.749	Non-dimensional mass
$\tilde{m}_a$	=	0.0160	Aerodynamic mass ($\rho_a = 1.223 \, kg/m^3$)
$\tilde{b}$	=	0.084	Non-dimensional width of the section
$\tilde{\alpha}$	=	4.869	Aspect ratio

Table 5.2: Non-dimensional parameters for the Tacoma Bridge

Thanks to the values listed in Table 5.1 and Table 5.2 it is possible to completely define the Eigen-properties of the bridge by means of the modal superposition analysis (§2.4).

5.3 MODAL ANALYSIS

The analytical formulas already exploited in §2.4 are used for the calculation of the Eigen-properties of the Tacoma Narrows Bridge. The obtained results are compared with the modes of oscillations observed by Professor Farquharson [2].

The first five skew-symmetric Eigen-modes and Eigen-frequencies are computed according to equations (2.48) and (2.51), respectively. The modes of vibrations, characterized by a sinusoidal trend are depicted in Figure 5.1, whilst the Eigen-frequencies are listed in Table 5.3.
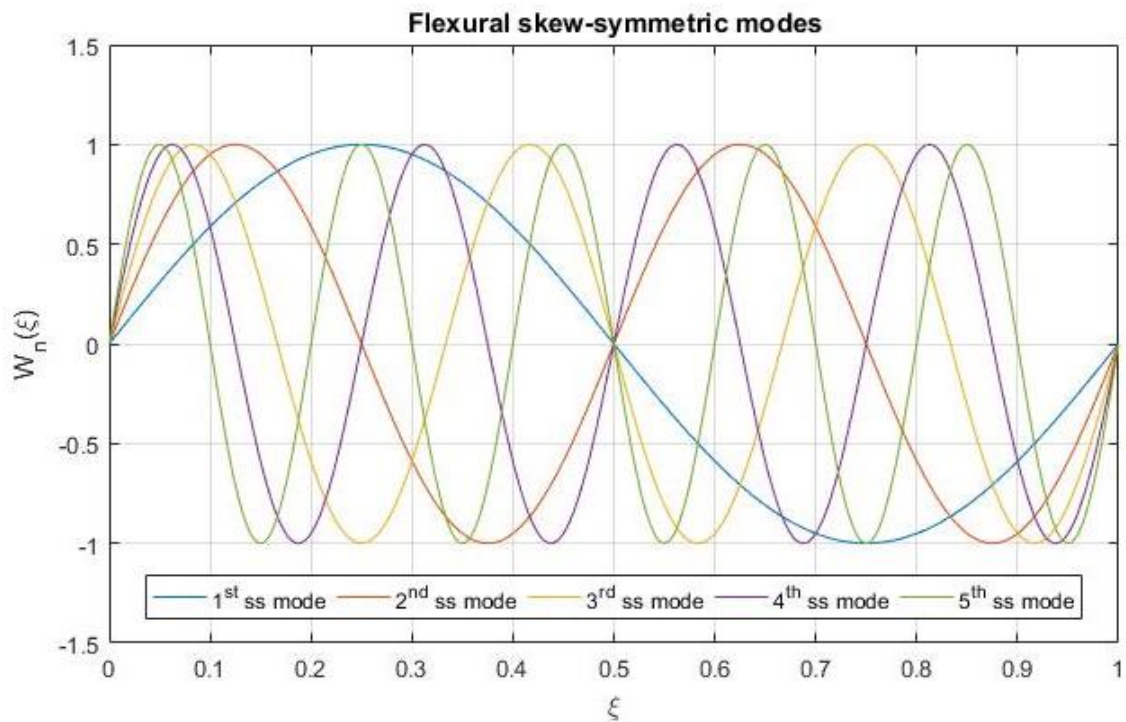
Figure 5.1: First 5 flexural Skew-Symmetric modes of vibration

| Mode No. | Flexural Skew-Symmetric Eigen-frequencies | | | Farquharson | |
	$\tilde{\Omega}_w$	Ω_w $[rad/s]$	f_w $[Hz]$	f_w $[Hz]$	Error [%]
1	6.3321	0.8339	0.1327	0.1450	8.48
2	12.9530	1.7059	0.2715	0.2750	1.27
3	20.1309	2.6512	0.4220	0.4000	5.50
4	28.0982	3.7005	0.5890	0.5667	3.94
5	37.0453	4.8788	0.7765	-	-

Table 5.3: First 5 Flexural Skew-Symmetric Eigen-frequencies

The calculation for the first five symmetric Eigen-modes and Eigen-frequencies is more cumbersome. The modes of vibrations can be computed trough equation (2.59), only once that the Eigen-frequencies are known. The latter are calculated by means of the well known bisection method enforcing the zeroing of the Eigen-function (2.61). Figure 5.2 and Table 5.4 show the flexural symmetric Eigen-modes and Eigen-frequencies, respectively.
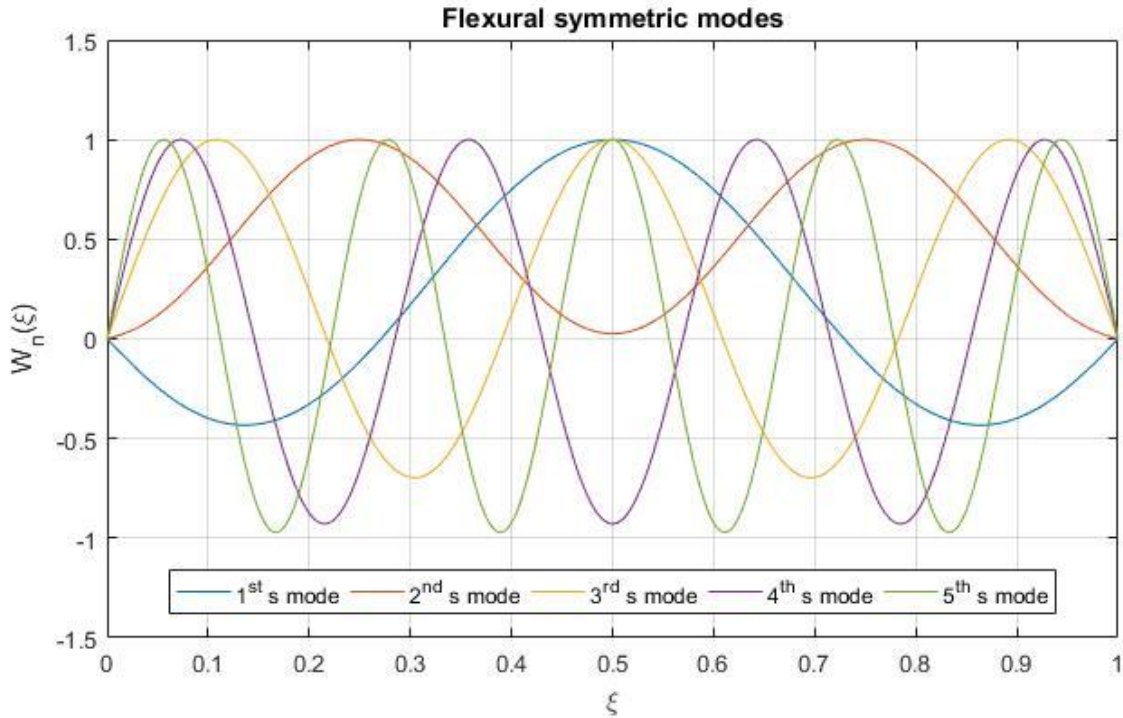
Figure 5.2: First 5 flexural Symmetric modes of vibration

Mode No.	Flexural Symmetric Eigen-frequencies			Farquharson	
	$\tilde{\Omega}_w$	Ω_w $[rad/s]$	f_w $[Hz]$	f_w $[Hz]$	Error $[\%]$
1	8.8112	1.1604	0.1847	0.2000	7.65
2	13.3439	1.7574	0.2797	-	-
3	16.9120	2.2273	0.3545	0.3500	1.29
4	24.0940	3.1731	0.5050	0.4500	12.22
5	32.4705	4.2763	0.6806	0.6333	7.47

Table 5.4: First 5 Flexural Symmetric Eigen-frequencies

In long-span suspension bridges usually the torsional modes of vibration are characterized by higher frequencies with respect to the corresponding flexural modes. It is for this reason that only the first three skew-symmetric Eigen-modes and Eigen-frequencies are calculated. Equations (2.66) and (2.67) are used to obtain the sinusoidal trend of the modes of vibrations (Figure 5.3) and the correspondent Eigen-frequencies (Table 5.5). Notice that the comparison is done for the first skew-symmetric mode of vibration only, which was the observed torsional mode before the collapse.
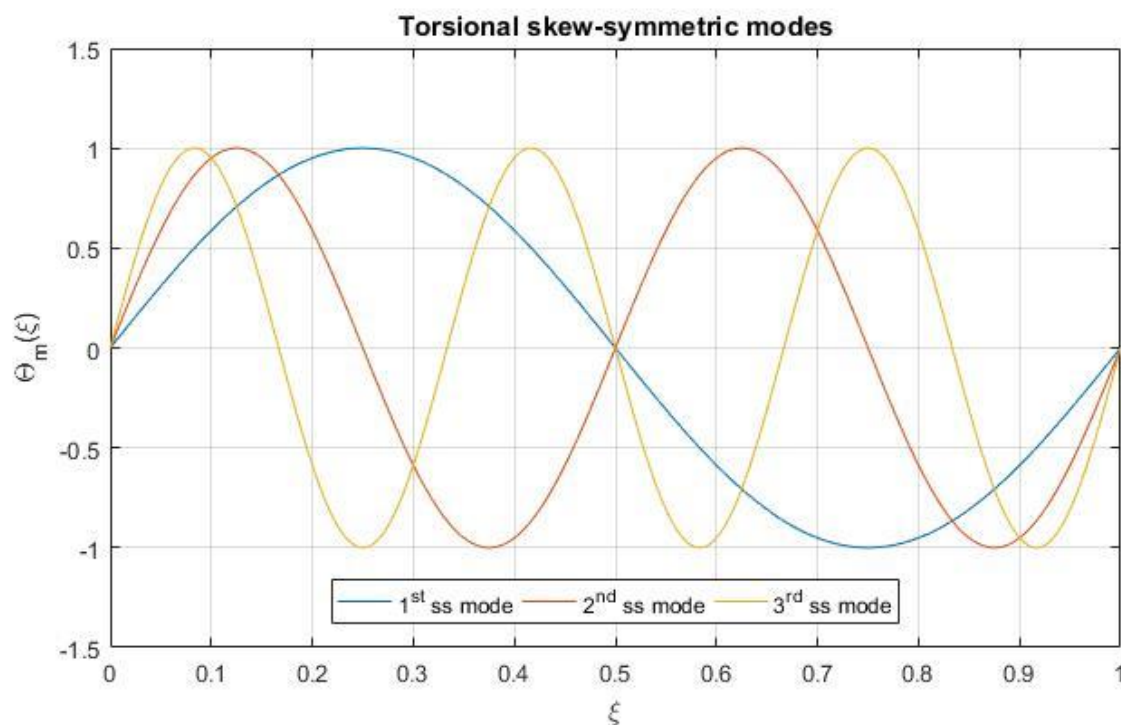
Figure 5.3: First 3 torsional Skew-Symmetric modes of vibration

	Torsional Skew-Symmetric Eigen-frequencies			Farquharson	
Mode No.	$\tilde{\Omega}_\theta$	$\Omega_\theta \ [rad/s]$	$f_\theta \ [Hz]$	$f_\theta \ [Hz]$	Error [%]
1	9.4928	1.2502	0.1990	0.2000	0.50
2	19.4181	2.5573	0.4070	-	-
3	30.1771	3.9743	0.6325	-	-

Table 5.5: First 3 torsional Skew-Symmetric Eigen-frequencies

As in the case of the flexural symmetric Eigen-properties, the torsional symmetric modes of vibrations can be computed trough equation (2.74), once that the correspondent Eigen-frequencies are known. Enforcing the zeroing of the Eigen-function (2.72), the circular frequencies can be calculated and Figure 5.4 and Table 5.6, representing the torsional symmetric Eigen-modes and Eigen-frequencies, are obtained.
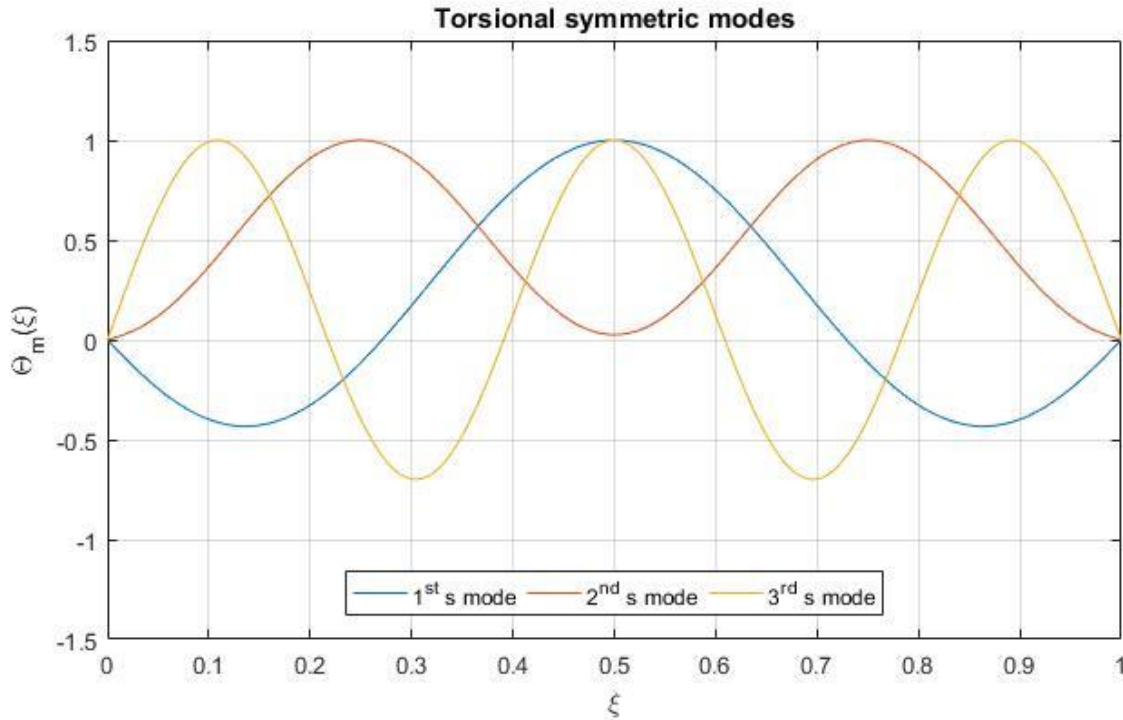
Figure 5.4: First 3 torsional Symmetric modes of vibration

	Torsional Symmetric Eigen-frequencies			Farquharson	
Mode No.	$\tilde{\Omega}_\theta$	$\Omega_\theta \ [rad/s]$	$f_\theta \ [Hz]$	$f_\theta \ [Hz]$	Error [%]
1	13.2092	1.7396	0.2769	-	-
2	20.0038	2.6345	0.4193	-	-
3	25.3543	3.3391	0.5314	-	-

Table 5.6: First 3 torsional Symmetric Eigen-frequencies

The agreement of the theoretical results with the observations of frequencies and modes on both prototype and model is quite good.

The lower order flexural frequencies just computed underestimates the observed values, whilst the higher order frequencies overestimates the prototype values. The reason is hidden behind some assumptions made for the model. On one hand, the model neglects the deformability coming from the motion of pylons and the one coming from the hangers, for which a tenso-rigid constitutive model applies, making the response of the higher flexural modes stiffer. On the other hand, the assumption of perfectly hinged ends gets rid of the flexural stiffening contribution coming from cable's section and from side span, making the response of the lower flexural modes softer.

It seems that the torsional frequency just computed gives an accurate result with respect to the observed value by Farquharson. However on the day of collapse the bridge initially experienced torsional oscillations according to the 1st skew-symmetrical torsional mode with a frequency of 0.23 Hz. Then, perhaps due to some damage within the deck, the torsional frequency of oscillations decreased to 0.2 Hz. It is clear that the theoretical result provided by the model slightly underestimates the initial torsional frequency observed, i.e. 0.23 Hz. The reason of this is that the stiffening effect due to the presence of the pylons and the side spans (not considered in the model) affects in a larger amount the torsional frequencies with respect to the flexural ones (Rannie W.D. [2]), leading to softer results.

According to the report written by Amman et al. [2], before the sudden appearance of torsional oscillations the bridge was oscillating with the 5th symmetric flexural mode. Thus, the modes of interest for our purpose are the 5th symmetric flexural mode, having frequency equal to $f_{w,5} = 0.6806\ Hz$, and the 1st skew-symmetrical torsional mode, having frequency equal to $f_{\theta,1} = 0.199\ Hz$.

Once the Eigen-properties of the structure are obtained, equation (2.75) allows to compute the modal structural mass, damping and stiffness properties related to the modes of interest. As usual in long-span suspension bridges, a damping coefficient equal to 0.5% for both the flexural and the torsional modes of vibration is assumed, i.e. $\Delta_{w,5} = 0.5\%$ and $\Delta_{\theta,1} = 0.5\%$.

$$M_{w,5} = \int_0^1 W_5^2(\xi)d\xi = 0.4882$$

$$J_{\theta,1} = \tilde{J}_t M_{\theta,1} = \tilde{J}_t \int_0^1 \Theta_1^2(\xi)d\xi = 0.2225 \tag{5.1}$$

$$D_{w,5} = 2\Delta_{w,5}\tilde{\Omega}_{w,5}M_{w,5} = 0.1585$$

$$D_{\theta,1} = 2\Delta_{\theta,1}\tilde{\Omega}_{\theta,1}J_{\theta,1} = 0.0211$$

$$K_{w,5}^{(L)} = \tilde{\Omega}_{w,5}^2 M_{w,5} = 514.72$$

$$K_{\theta,1}^{(L)} = \tilde{\Omega}_{\theta,1}^2 J_{\theta,1} = 20.0496$$

$$K_{\theta w,15}^{(Q)} = \lambda_2^2 \left[2\tilde{h}_{\theta_1}\tilde{h}_{W_5'\theta_1'} + \tilde{h}_{W_5}\tilde{h}_{\theta_1'^2} \right] = 37.6016$$

Thanks to the modal Eigen-properties, by means of equation (2.93) it is also possible to find the critical flexural amplitude able to induce the slackening of hangers. For the 5th symmetric flexural mode the onset for slackening is reached for:

$$Z_{n,slack} = 0.83 \, m \tag{5.2}$$

This value is in agreement with the measurements done just before the collapse [57]. In fact, before the sudden occurrence of torsional oscillations, the Tacoma Bridge was oscillating with an amplitude of vibration of 0.46 m, without experiencing slackening of hangers.

Moreover it is worth remembering that a critical torsional amplitude for torsional oscillations cannot be defined, because of the hypothesis that the deck, with its weight, does not introduce any asymmetry in the initial configuration of the hangers.

5.4 DIVERGENCE AND FLUTTER WIND SPEED

5.4.1 *Divergence Velocity*

The wind velocity for the occurrence of static torsional divergence is dependent only on the structural properties of the bridge and it can be calculated trough equation (3.43). For the Tacoma Narrows Bridge, with the parameters listed in Table 5.1 and Table 5.2, and considering the 1st skew-symmetrical torsional non-dimensional circular Eigen-frequency, the divergence wind speed is:

$$U_D = \sqrt{\tilde{J}_t}\,\tilde{\Omega}_{\theta,1}\sqrt{\frac{2H}{\rho\pi l^2}} = 39.2 \, \frac{m}{s} \tag{5.3}$$

As expected, this wind speed is much higher with respect to the velocity measured on the day of collapse. In fact, the dynamic limit for the occurrence of instability is always lower with respect to the static one. Therefore, for this deck's section geometry, it is not admissible to reach the torsional divergence limit within feasible wind speed.

5.4.2 *Flutter Velocity*

In order to compute the flutter wind speed it would be necessary to consider the complete Aeroelastic system of equations. The flutter analysis consists in solving the Eigenvalue problem (3.33) for the determination of the Aeroelastic Eigen-frequencies and Eigen-modes with varying of the wind speed. The instability condition is reached when the determinant of the impedance matrix is null (3.35).

Thus, to accomplish a flutter analysis, wind tunnel tests on a sectional model of the bridge are necessary to find all the Aeroelastic properties of the deck, namely the flutter derivatives. From literature, it is possible to find the trend of some of the most important flutter derivatives for the Tacoma Narrows Bridge. Billah and Scanlan [11], provided the trend of A_2^* for varying reduced wind speed. This information is very useful, because it allows to obtain the approximate wind velocity for the onset of torsional flutter, by means of equation (3.51).

The curve given by Billah and Scanlan [11] can be parameterized by means of two coefficients only, because it has approximately a parabolic shape. This is an useful tool to obtain a numerical expression for the variation point by point of the curve, to be applied on the mathematical model. The differences between the original curve of A_2^* and the parameterized one are shown in Figure 5.5.
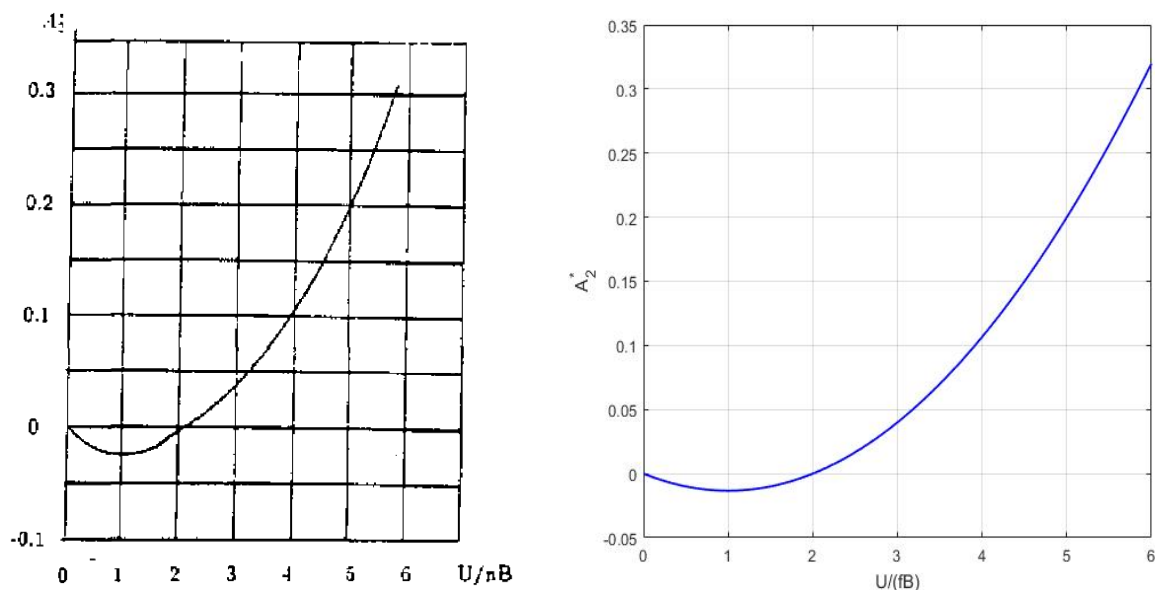
Figure 5.5: Trend of A2* for the Tacoma Narrows Bridge

The parameterized curve for A_2^* can be found by seeking for a parabolic trend passing through the origin:

$$A_2^* = a \cdot \frac{U}{2f_\theta b} + b \cdot \frac{U^2}{(2f_\theta b)^2} \tag{5.4}$$

The two constants can be obtained by enforcing two geometrical conditions, which choice is very important to obtain a good approximation. Since the objective is to find the conditions for the flutter onset, which are guaranteed when $A_2^* > 0$, the proper choice for the boundary conditions are $\left(\frac{U}{2f_\theta b} \cong 2, A_2^* = 0\right)$ and $\left(\frac{U}{2f_\theta b} \cong 5, A_2^* = 0.2\right)$. In this way the constants introduced for the parameterization of the curve are $a = -2.67 \cdot 10^{-2}$ and $b = 1.33 \cdot 10^{-2}$. The curve obtained fits very well with the curve proposed by Billah and Scanlan [11] for positive values of A_2^*, whereas it does not approximate it in a good way for negative values of A_2^*.

The critical value for the onset of flutter can be found from equation (3.51). However, since Billah and Scanlan [11] provided the curve of A_2^* with a different notation for the introduction of the flutter derivatives in the Aeroelastic system of equations, equation (3.51) slightly changes. Hence, the condition for flutter reads as:

$$A_2^* \geq \frac{\pi}{8} \cdot \frac{\tilde{J}_t}{\tilde{m}_a} \cdot \Delta_{\theta,1} = 10.934 \cdot \Delta_{\theta,1} \tag{5.5}$$

This result is slightly lower than the value for the critical aerodynamic derivative in correspondence of flutter found by Billah and Scanlan [11], i.e. $A_{2,F}^* = 14.48 \cdot \Delta_{\theta,1}$. Considering a value for the damping coefficient equal to $\Delta_{\theta,1} = 0.5\%$, in accordance with the value estimated by Farquarhson for the logarithmic decrement for that mode of vibration, the critical value for A_2^* is:

$$A_{2,F}^* = 0.0547 \tag{5.6}$$

Figure 5.6 represents the trend of A_2^* in function of the dimensional velocity (not in function of the reduced velocity). From this curve it is possible to extract the value for the wind speed correspondent to the flutter onset, which is:

$$U_F = 7.70 \frac{m}{s} = 17.36 \, mph \tag{5.7}$$

This value compares reasonably to the critical speed predicted by Billah and Scanlan [11], who found $U_F = 8.36 \frac{m}{s} = 18.6 \, mph$.
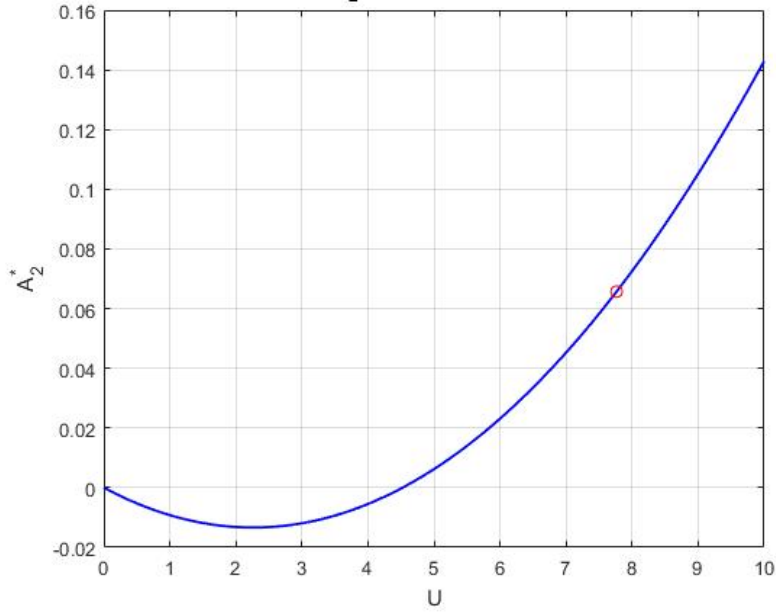
Figure 5.6: Value of the flutter velocity from the A2* curve

Moreover it is possible to compare the flutter speed obtained in equation (5.7) with the results of wind tunnel tests made by Farquharson [28]. These tests provide measurements of the response of the Tacoma Narrows Bridge under smooth flow of an highly accurate 3D dynamic full-bridge model in 1:50 scale. Figure 5.7 was reproduced from that study.
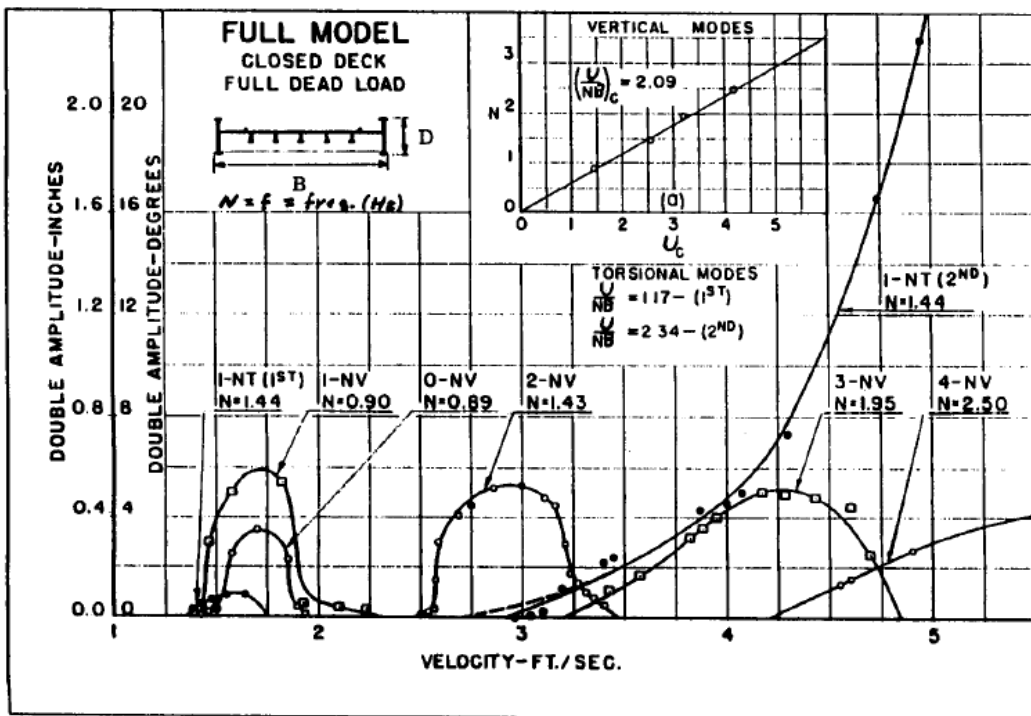
Figure 5.7: Wind-induced amplitude response of various modes of Original Tacoma Narrows full-bridge dynamic model [28]

Flutter, in the mode designated as 1-NT in Figure 5.7, was incipient for a model wind speed of $U_{F,model} = 3.3\ ft/s$. This value corresponds to a prototype flutter speed of:

$$U_F = U_{F,model} \cdot \sqrt{50} = 7.1\frac{m}{s} = 15.9\ mph \qquad (5.8)$$

Again, this result is in agreement to what found trough the simplified equation (5.7).

The flutter wind speed (5.7) can also be compared with some experiments made by Von Kàrmàn and Dunn [2] on an oscillating model simulating the sections of the bridge. The results of the test are shown in Figure 5.8.
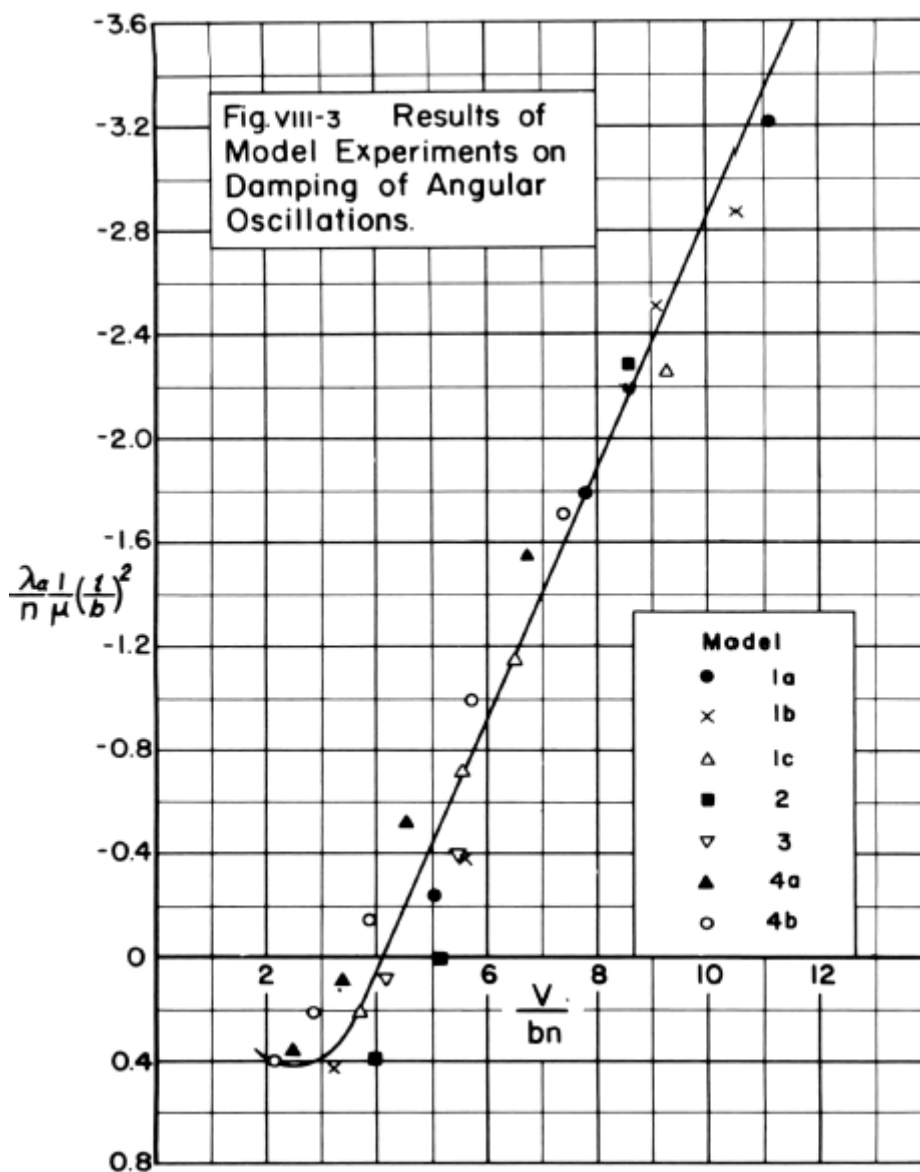
Figure 5.8: Damping of angular oscillations on the Original Tacoma Narrows Bridge model

Figure 5.8 indicates that the total damping is null somewhere in the range $3.4 < \frac{U}{f_\theta B} < 5.1$, i.e. for a velocity of the prototype bridge in between $8\ m/s < U < 12\ m/s$ ($18\ mph < U < 27\ mph$). Also these experimental tests validate the result obtained (5.7).

The increase of the response with the wind speed, beyond the incipient stage, toward higher amplitude flutter, which is influenced by structure-induced turbulence and hence progressively changing values of A_2^*, was witnessed in the full model in Figure 5.7. Therein the response curve designated as 1-NT (2nd) is the divergent flutter response, in fact the model frequency 1.44 Hz corresponds to the destructive prototype frequency observed $f_{\theta,1} = 0.2\ Hz$. The ever-increasing response of mode 1-NT approaches "divergent" amplitudes of vibration at a model velocity of around $U_{model} = 5\ ft/s$, which corresponds to a full-scale speed of about $U = 15.6\ \frac{m}{s} = 35\ mph$.

The wind speed for the onset of flutter predicted by wind tunnel tests by Farquharson (Figure 5.7) is never actually ascertained, because the bridge withstood winds well above the value of 7.1 m/s for a long time before collapsing.

5.4.3 *Possible Explanations for the low value of the Wind Flutter Speed*

Still nowadays the mystery of the low velocity for the onset of torsional flutter on the Tacoma Narrows Bridge has not been solved.

Farquharson [28] tried to explain this fact by centre diagonal stays, which might be possible to stabilize the torsional flutter of the bridge. However, this explanation has not been proven yet.

The hypothesis assumed by Matsumoto et al. [40] was that the vortex-induced heaving vibration might stabilize the torsional flutter phenomenon. In other words the effect of some aerodynamic interferences between heaving and torsional vibrations might be present on the original Tacoma Narrows bridge. The same Farquharson [28] mentioned a possible effect of interferences between vortex-induced vibrations and torsional flutter.

Matsumoto et al. [40] made some free vibration tests in the wind tunnel under smooth flow conditions, analysing an H-shaped section of bluffness ratio $B/D = 5$ (similar to the Tacoma Narrows Bridge), in order to give an explanation to this phenomenon. They discovered that there are two kinds of torsional flutter in the reduced wind velocity region analysed, one is a low-speed torsional flutter and the other is an high speed torsional flutter. The former is generated by vortex convections on the side surface of the body whilst the latter is due to local separation bubbles around the leading edge. Analysing the results of 2 DoF$_s$ responses of their experiments one can deduce that the vortex-induced heaving vibrations can suppress the low-speed torsional flutter, whereas the high-speed torsional flutter can suppress the vortex-induced heaving vibration. Hence, Matsumoto et al. tried to explain the mystery of low torsional flutter wind speed stating that the 5th

symmetric mode of vibration due to vortex shedding suppressed the low-speed torsional flutter. Due to this fact they measured the critical onset velocity as $U_F \cong 17 \frac{m}{s} = 38 \, mph$. This velocity does not agree with the one measured by Farquharson the day of the collapse, i.e. 19 m/s, but due to some uncertainties on this measurement and due to uncertainties on the wind direction at the moment of the accident, the result found by Matsumoto et al. [40] seems very reasonable.

Kubo et al. [32] observed a particular structure of the wake around a bridge's H-shaped cross section and around a rectangular cross section. In both cases a regular pattern of vortices appeared on both the upper and the lower sides of the bridge deck. They speculated that the spacing between consecutive vortices was the likely cause of different vertical and torsional modes of vibration observed during the brief lifetime of the original Tacoma Narrows bridge.

It was Larsen [36] the first to produce a physical model of the bridge collapse based on the hypothesis made by Kubo et al. [32]. In particular, he developed a code able to reproduce the effect of the discrete vortices on the bridge aerodynamic problems, including steady state load coefficients, flutter stability and vortex shedding excitation. By means of this code, he postulated that the key to the torsion instability mechanism was the formation and drift of large-scale vortices from the upwind edge of the bridge girder cross section.

The model proposed by Larsen [34] was based on the calculation of the work generated by vortices as they drift over the bridge. He considered three different cases based on the vortex dimensions, see Figure 5.9. Since a vortex is a low pressure region, a force in the direction of the vortex itself is produced on the bridge. Thus, if the spacing between two consecutive vortices drifting on opposite sides of the section is exactly half of the deck width, they do not produce work over one cycle of oscillation (1st case Figure 5.9). This is the condition to find the critical wind speed, indeed for wind speeds lower than the critical one (3rd case Figure 5.9), the vortices do not cross the entire bridge in one period and produce net torques that dampen the oscillation, whilst for wind speeds higher than the critical one (2nd case Figure 5.9), the vortex crosses the entire bridge in less than one period making work on the bridge.

For a generic H-shaped cross section Larsen found that the critical reduced velocity for the onset of flutter was $\frac{U}{f_\theta B} \cong 4$, which means $U_F \cong 9.5 \frac{m}{s} = 21.3 \, mph$ with the data of the Tacoma bridge. Also this result is in excess with respect to what measured on the day of the collapse.
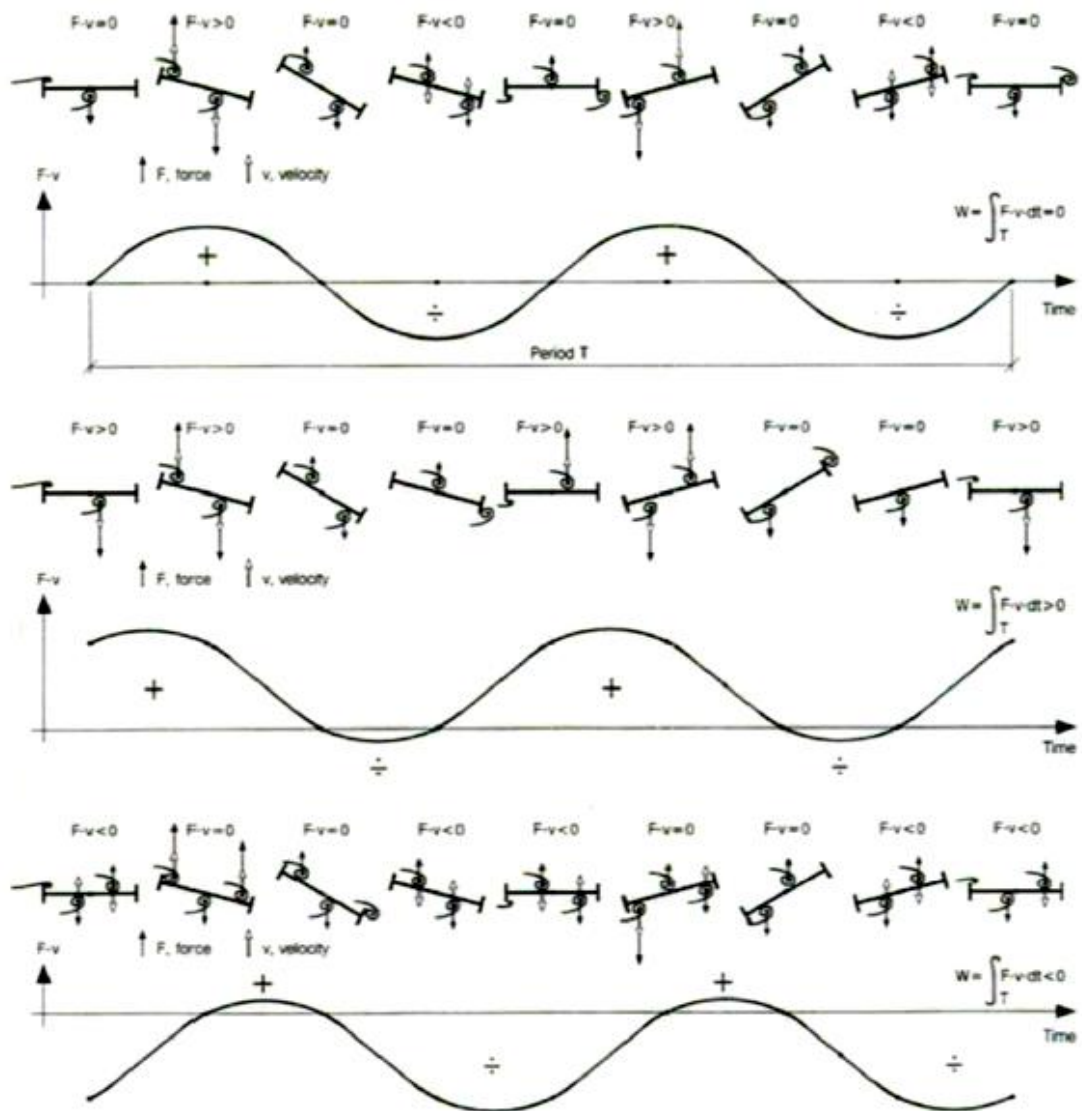
Figure 5.9: Vortex drift pattern and associated fluid work (W) over one circle of torsion oscillation (1st: vortex spacing = b , 2nd: vortex spacing > b , 3rd: vortex spacing < b)

Moreover, Larsen simulated the response of the Tacoma Narrows Bridge at the condition of the destructive wind speed of 19 m/s. Obviously he found divergent torsional oscillations, indicating instability, but accompanied by vertical oscillations of fairly constant amplitude around 1 m, indicating a 2 DoFs classical flutter phenomenon.

5.5 EFFECT OF INTERNAL PARAMETRIC RESONANCE ON THE FLUTTER VELOCITY

In this paragraph the formulas obtained in §4.5.4 are used to demonstrate the erosion of the flutter velocity due to the effect of 2:1 subharmonic resonance. To do this, let us assume to be in the condition of wind speed very near to the flutter onset:

$$U = 0.9 \cdot U_F \cong 7 \, \frac{m}{s} \qquad (5.9)$$

In this particular condition the total net torsional damping is lowered by the effect of the aerodynamic forces. For the value of A_2^* correspondent to the velocity considered in expression (5.9), it is possible to calculate the parameter α (eq. (4.57)), which is a measure of the erosion of the net torsional damping due to Aeroelastic effects.

$$\alpha = \frac{D_{\theta,m}^{Aero}}{D_{\theta,m}} = \frac{A_2^*}{A_{2,F}^*} = 0.667 \qquad (5.10)$$

It is obvious from (5.10) that the Aeroelastic effects produces a reduction of nearly the 70% on the structural torsional damping. Hence the system becomes susceptible to internal 2:1 parametric resonance because the "tongue" of instability in the Ince-Strutt diagram goes down, as shown in the subplot of Figure 5.10.
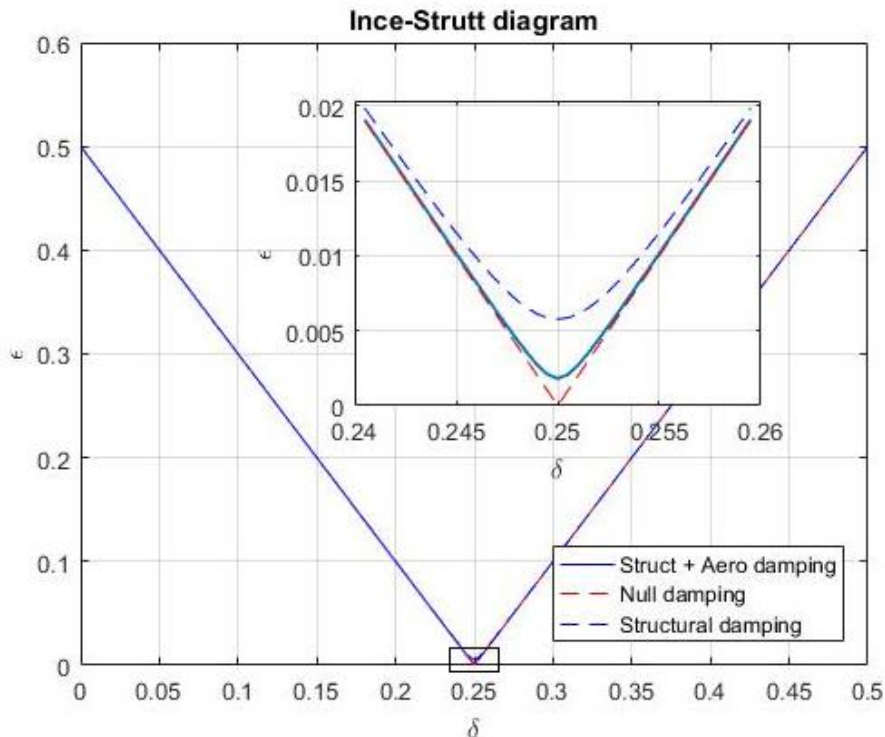
Figure 5.10: Influence of Aeroelastic effects in the stability region of the Ince-Strutt diagram

The erosion of the damping of the system is proportional to the velocity chosen for the assessment of the stability (5.9). In fact the more the velocity is near to the flutter one, the more the net torsional damping is eroded by the effect of the flutter derivative A_2^*. This happens until the condition for the onset of flutter is reached, which correspond to an exponentially increasing response of the structure due to null torsional damping. Thus, the assessment for the stability analysis is strictly dependent on the value of the wind speed assumed, but our objective is to demonstrate that a parametric resonance phenomenon is possible with the values observed.

Having fixed a value for the velocity, the problem does not depend anymore on it. In this scenario it is interesting to compute the flexural modal amplitude of displacement necessary to reach instability caused by parametric resonance. To this purpose, let us assume to be in the condition where the vortex shedding lock-in with the 2:1 subharmonic resonance ($\delta = 1/4$). Then, the amplitude of the perturbation $z_{5,0}$, defined as the modal amplitude of the 5th symmetric flexural mode normalized with respect to the initial cable sag, can be found from the Ince-Strutt diagram, because it corresponds to a specific value of ε. The subplot of Figure 5.11 has two different scales on the y axis, one indicates the values of ε and one the values of the correspondent dimensional flexural modal amplitude $Z_{5,0}$.
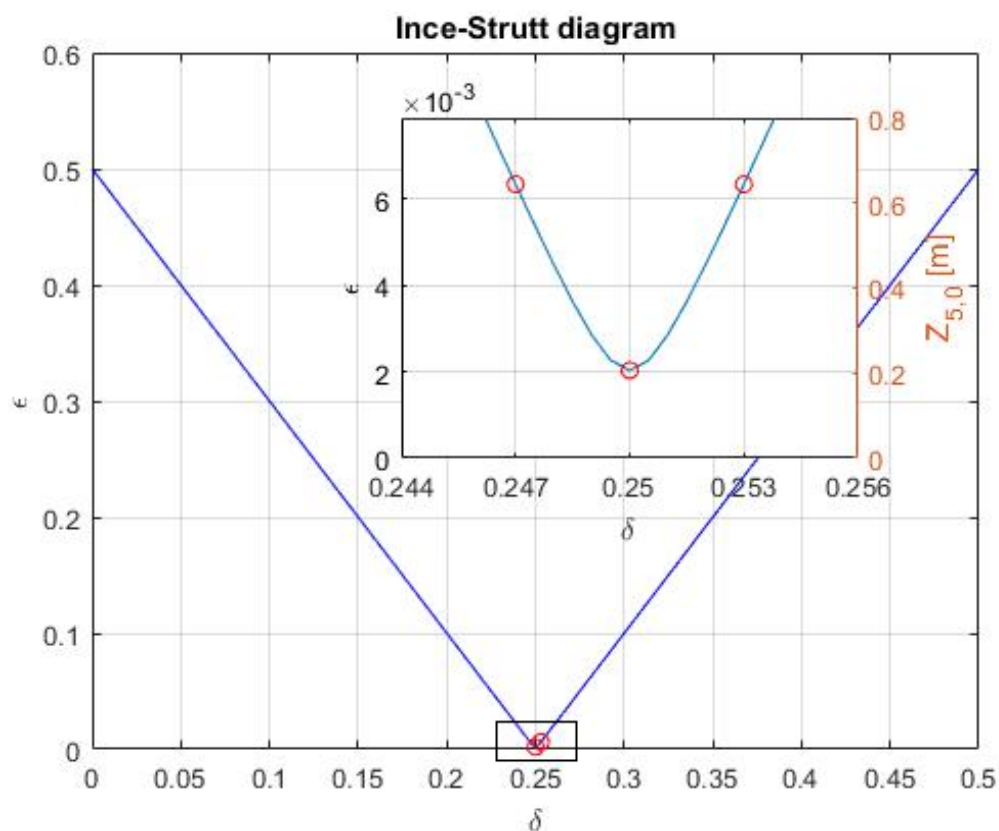
Figure 5.11: Critical values for the 5th symmetric modal amplitudes of vibration

Fixed the value of velocity, i.e. the 90% of the flutter one, the value of flexural modal displacement necessary to activate the resonance phenomenon in correspondence of perfect 2:1 condition is:

$$Z_{5,0} = 0.206 \, m \tag{5.11}$$

Being impossible to reach a perfect 2:1 lock-in condition between the vortex shedding frequency and the torsional structural frequency, it can be useful to take into account for a tolerance around the value of $\delta = \frac{1}{4}$, namely $0.247 < \delta < 0.253$. In this range of frequency ratios, the flexural modal amplitude of vibration can assume values in between:

$$0.20 \, m < Z_{5,0} < 0.64 \, m \tag{5.12}$$

The choice of the range around the 2:1 frequency ratios condition is completely arbitrarily, but it is justifiable from the values of $Z_{5,0}$ found, which are of the same order of magnitude of the flexural oscillations due to vortex shedding measured by Farquharson the day of the Tacoma Narrows bridge disaster.

It is necessary now to find what is the amplitude of oscillation produced by the vortex shedding phenomenon and to compare them with the critical modal amplitude found in (5.12).

5.6 VORTEX SHEDDING RESPONSE

The first step to compute the vortex induced response is to find the lock-in wind velocity. Considering a Strouhal number equal to $St = 0.115$, as obtained by wind tunnel tests by Larsen [36], the vortex shedding frequency locks-in with the 5th symmetrical flexural mode of vibration when:

$$U_{lock-in} = U_D \cdot \left(\frac{\tilde{\Omega}_{w,5}}{\tilde{\Omega}_{\theta,1}} \cdot \sqrt{\frac{\widetilde{m}_a}{\tilde{J}_t}} \cdot \frac{1}{\pi \cdot St \cdot \tilde{\alpha}} \right) = 14.44 \, \frac{m}{s} \tag{5.13}$$

Thus, the lock-in range of wind velocities, for small Scruton number (small values of damping) can be assumed in between $0.8 \cdot U_{lock-in} < U < 1.5 \cdot U_{lock-in}$, which means:

$$11.55 \, \frac{m}{s} < U < 21.66 \, \frac{m}{s} \tag{5.14}$$

This range of wind velocities is in accordance with the measured velocities on the day of the Tacoma Narrows bridge's failure. However, it does not agree with the wind speed for the onset of flutter (5.6). This wind speed, as justified by different authors §5.4.3, is not to be considered as the "real" speed for the onset of flutter. In fact, for this particular cross section, the flutter phenomenon is driven by the shedding of the vortices from the upwind edge. Thus, it seems reasonable to assume that the "real" flutter speed is of the same order of magnitude of the lock-in velocity, may be slightly higher, because it is what emerges from various studies ([32], [34] and [39]).

Without any loss of generality, it is possible to assume a wind speed for the onset of flutter higher with respect to the lock-in velocity. The effect of parametric resonance instability §5.5 still makes sense, because regardless of what the "real" flutter speed is, we considered a velocity slightly lower this limit (e.g. $U = 0.9 \cdot U_F$). In this context, it is reasonable to think that the effect of the aerodynamic damping produces always a reduction of nearly the 70% on the structural torsional damping, leading to the same result for $Z_{5,0}$ found (5.11).

The second step for the calculation of the steady state flexural amplitude is the calculation of the dynamic amplification factor and the phase lag of the response of a 1 DoF oscillator (4.33). It is important to notice that the total flexural damping of the 5$^{\text{th}}$ symmetrical flexural mode is provided by both a structural and an Aeroelastic component, dependent on the flutter derivative H_1^*. In fact:

$$D_{w,n}^{TOT} = D_{w,n} - D_{w,n}^{Aero} = \left(2\Delta_{w,n}\tilde{\Omega}_{w,n} - \frac{1}{\pi}\tilde{u}\sqrt{\tilde{J}_t}\sqrt{\tilde{m}_a}K_w H_1^*\tilde{\Omega}_{\theta,m} \right) M_{w,n} \tag{5.15}$$

Let us assume the contribution of H_1^* to the flexural stiffness as negligible: Thus, the reduced frequency can be simplified as follows.

$$K_w = \frac{2}{\tilde{u}} \cdot \frac{\sqrt{\tilde{m}_a}}{\sqrt{\tilde{J}_t}} \cdot \frac{\tilde{\Omega}_{w,n}}{\tilde{\Omega}_{\theta,m}} \tag{5.16}$$

The substitution of the equation (5.16) into the equation (5.15) leads to:

$$D_{w,n}^{TOT} = 2 \cdot \left(\Delta_{w,n} - \frac{1}{\pi} \cdot \tilde{m}_a H_1^* \right) \cdot \tilde{\Omega}_{w,n} \cdot M_{w,n} = 2 \cdot \xi_{w,n} \cdot \tilde{\Omega}_{w,n} \cdot M_{w,n} \tag{5.17}$$

where the equivalent Aeroelastic damping coefficient is given by:

$$\xi_{w,n} = \Delta_{w,n} - \frac{1}{\pi} \cdot \tilde{m}_a H_1^* \tag{5.18}$$

For the case of the Tacoma Narrows bridge, Scanlan [49] provides a value for the flutter derivative $H_1^* = -1.844$. The latter has been found by the author by means of wind tunnel tests and by averaging the value of H_1^* for different reduced frequencies, i.e. averaging it for different wind velocities. Thus, it is possible to assume this value invariant with the wind speed and to substitute it in the calculation of the equivalent Aeroelastic damping coefficient (5.18).

$$\xi_{w,n} = 0.0144 = 1.44\ \% \tag{5.19}$$

It is obvious that the aerodynamic effect increases the net flexural damping of the bridge and subsequently it decreases the modal displacement produced by vortex induced vibration. The value found for the damping coefficient is in complete agreement with the value estimated by Scanlan [49], which calculated that $0.0147 < \xi_{w,n} < 0.0182$.

Considering the increment of damping due to H_1^* and neglecting the decrement/increment of the flexural stiffness due to H_4^* (depending on its sign), it is possible to compute the dynamic amplification factor and the phase lag for the wind induced response. Figure 5.12 represents the variation of the dynamic amplification factor and the phase lag with the frequency ratio $\beta = \dfrac{\widetilde{\omega}_{VS}}{\widetilde{\Omega}_{w,n}}$, both in the case of considering only the structural damping (red lines), and considering the total Aeroelastic damping (blue lines).
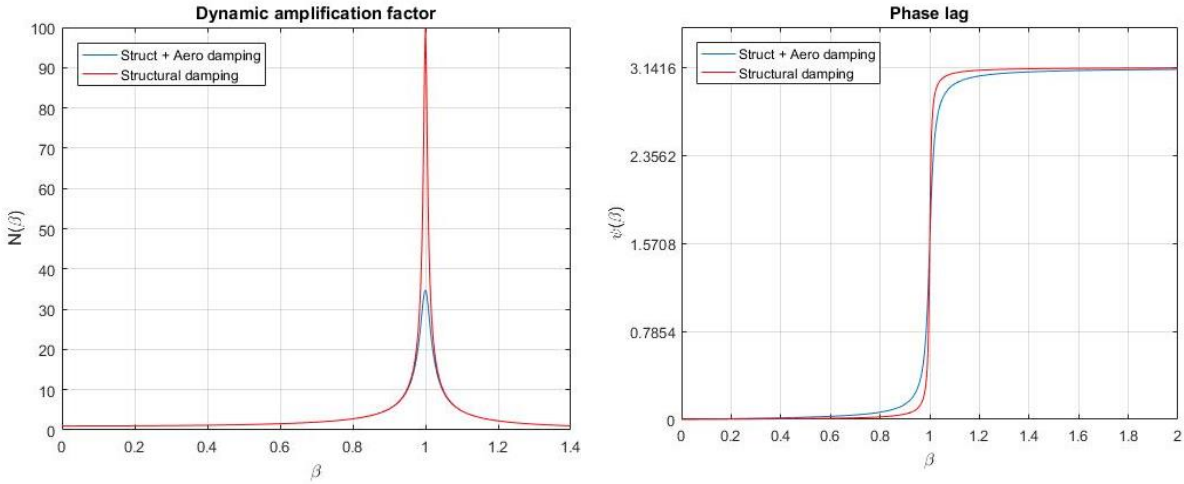
Figure 5.12: Dynamic amplification factor and phase lag both considering the effect due to H₁* and not

Aerodynamic effects are capable to reduce the dynamic amplification factor from the pick value of $N(1) = \dfrac{1}{2\Delta_{w,n}} = 100$ to the pick value $N(1) = \dfrac{1}{2\xi_{w,n}} \cong 35$.

Hence, the value of the 5th symmetric modal amplitude of vibration, considering the value calculated by Scanlan [49] for the lift coefficient of the Tacoma Narrows Bridge, i.e. $\tilde{c}_L = 0.566$, is equal to:

$$Z_{5,0}^{VS} = f \cdot \left(\frac{\Gamma_0 \cdot \tilde{h}_{W_n}}{K_{w,n}^{(L)}} \cdot N(1) \right) = 0.462 \, m \qquad (5.20)$$

The agreement of the theoretical result with the measurements of modal amplitudes made by Farquharson on the day of collapse (i.e. 0.5 m) is remarkably good.

Equation (5.20) justifies the fact that 2:1 subharmonic resonance can erode the wind velocity for the flutter onset (whatever the "real" one it is), because $Z_{5,0}^{VS}$ is of the same order of magnitude of the modal amplitude of vibration needed to activate the internal parametric instability phenomenon $Z_{5,0}$, calculated for a wind velocity equal to the 90 % with respect to the flutter one.

5.7   POSSIBLE REASON OF THE COLLAPSE

In the foregoing the internal parametric resonance has been proven to be the instability phenomenon driving the Tacoma Narrows bridge to the collapse in a condition incipient to flutter. However, the main hypothesis for the occurrence of subharmonic resonance is to have a torsional-to-vertical frequency ratio around the value of 0.5. This condition is not satisfied if one consider the 5th symmetrical flexural and the 1st skew-symmetrical torsional modes of vibration.

In reality, during the day of collapse, before the sudden switch to torsional oscillations (at 10 a.m.) it was noted a slippage of some hangers along the main cable. The diagonal ties attached to the midspan cable band were alternatively becoming slack and taut [46].

It is reasonable to think that this damage introduced some imperfections in the system which led to a sudden reduction of the flexural stiffness. Being the structure slightly damped, an abrupt change in the vertical stiffness led the energy to be transferred from the 5th symmetrical mode of vibration to a configuration characterized by a softer response, e.g. the 4th symmetrical mode. However it is very difficult to quantify the effect of the slippage of some hangers in the contribution to the reduction of stiffness of the system.

The possible modal contribution of the 4th symmetric mode led the system to be susceptible to internal parametric resonance instability, in fact the flexural-to-torsional frequency ratio is around 0.51 (considering the values observed by Farquharson, i.e. $f_{w,4} = 0.45 \, Hz$ and $f_{\theta,1} = 0.23 \, Hz$).

It looks like as a flux of energy, initially from the 5th to the 4th symmetric flexural modes of oscillation, perhaps due to a damage in the cables system which reduced the flexural stiffness, and then from the 4th symmetric flexural mode to the 1st skew-symmetric torsional one because of the effect of parametric 2:1 resonance.

The possible cause of the failure can be therefore summarized as follows:

1. The wind was blowing at a wind speed never observed before (i.e. 19 m/s) producing wind induced oscillations according to the 5th symmetric mode with frequency around 0.6 Hz – 0.63 Hz and modal amplitude of 0.5 m;

2. The vortex-induced phenomenon suppressed the low torsional flutter, leading to higher critical wind speed than the one computed by Farquharson. Thus, the critical flutter condition moved trough velocities slightly higher than the velocities in the lock-in range;

3. A slippage of some hangers with respect to the main cable caused a sudden reduction of the system flexural stiffness leading to a flow of energy from the 5th to the 4th symmetric mode of vibration;

4. The energy is then transferred to the 1st skew-symmetrical torsional mode (0.23 Hz) because of internal parametric resonance instability. Indeed the self-excited forces due to wind effects lowered the structural torsional damping of the system whilst the torsional-to-flexural frequency ratio was around 0.5;

5. The driving mechanism for the occurrence of subharmonic resonance was the flexural modal amplitude of oscillations, measured around 0.5 m;

6. Before the collapse the torsional frequency of oscillation lowered to 0.2 Hz perhaps due to some damage within the deck.

6 NON-FLUTTER DESIGN FOR BRIDGES

The new challenge in bridge's design is to reduce the costs of very long-span suspension bridges by adopting the so called non-flutter design principle that is, to design an aerodynamically stable cross section with the torsional frequency lower than the correspondent flexural one. In fact, it is well known in flat plate aerodynamics that classical flutter cannot occur for torsional-to-flexural frequency ratio below one.

An increase in the length of the span of the bridge leads to an increase in the cables contribution to stiffness compared to the bridge deck, which implies a lowering of the torsional-to-vertical frequency ratio. Moreover, the aerodynamic stiffness tends to decrease the torsional frequency as the wind velocity increases and the aerodynamic coupling between vertical and torsional modes is unavoidable. However, if the torsional still air frequency is below the vertical one, the modes will be decoupled with increasing frequency separation at higher wind speeds.

The first to introduce the concept of non-flutter design principle for long span suspension bridges was Richardson [47]. He indicated that twin-box deck configurations are the most favourable for long-span suspension bridges and he proposed a twin bridge with four main cables and with torsional-to-vertical frequency ratio lower than one as an economical and aerodynamically stable alternative to the single box girder suspension bridges.

Bartoli et al. [9] tested a twin-box suspension bridges, having the same elevation properties of the Messina Strait bridge, but different cross section, in the CRIACIV wind tunnel in Prato, Italy. Classical flutter was not observed in the reported section model tests and torsional divergence did not occur in the range of design wind velocities.

Further Studies have been done by Andersen et al., [3] and [4], which used a multimodal approach to investigate the possibility of flutter of a suspension bridge spanning 3.7 km with a torsional-to-vertical frequency ratio equal to 0.89. It has been proved that classical flutter between similar modes is always prevented with this kind of design.

Despite the fact that the non-flutter design principle is able to prevent the occurrence of any aerodynamic self-induced phenomenon (indeed also torsional flutter cannot occur for an airfoil type cross section) these kind of bridges can be susceptible to internal parametric resonance instability when the frequency ratio becomes equal to 0.5 due to aerodynamic effects. This possibility is investigated in this chapter with the aid of an example.

6.1 TWIN-BOX SECTIONAL MODEL

The analysis for the investigation of internal parametric resonance instability phenomenon is performed on the model analysed by Andersen et al. [3]. It is a twin-box suspension bridge (Figure 6.1) with central span of 3.7 km and sag-to-span ratio equal to 1/10. The two boxes are divided by a length of 20 m and, to obtain a lower torsional stiffness, the cables are placed at the internal side of the deck. The total mass of the twin bridge cross section is $m_{tot} = 14570 \, kg/m$ whit an important contribution of the main cables, i.e. $m_c = 6582 \, kg/m$. All the properties of the sectional model are listed in Table 6.1.
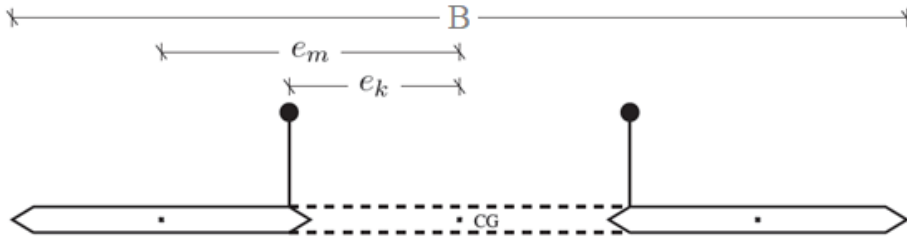
Figure 6.1: Twin-box deck sectional model

B	=	$60 \, m$	Width of the deck cross section
l	=	$3700 \, m$	Central span length
e_k	=	$10 \, m$	Cable's eccentricity
e_m	=	$20 \, m$	Mass eccentricity
L_c	=	$3798 \, m$	Cable's length under deck's self weight only
D	=	$3 \, m$	Depth of the deck cross section
f	=	$370 \, m$	Cable's sag
A_c	=	$1.54 \, m^2$	Cable's area
m_d	=	$930 \, kg/m$	deck mass per unit length
m_c	=	$6582 \, kg/m$	cable mass per unit length
J_t	=	$7002000 \, kg \cdot m^2/m$	Linear density of the deck's moment of inertia
E_d	=	$2.1 \cdot 10^{11} \, N/m^2$	Effective elastic modulus of the deck
G_d	=	$8.1 \cdot 10^{10} \, N/m^2$	Shear modulus of the deck
E_c	=	$2.05 \cdot 10^{11} \, N/m^2$	Effective elastic modulus of the cables

Table 6.1: Properties of the twin-box sectional model

Andersen et al. [3] made a modal analysis of the model, providing the first five flexural and torsional modes of vibration. They are listed in Table 6.2 in ascending order with the terminology: S:symmetryc, A:Anti-symmetric, F:Flexural, T:Torsional.

Vertical mode shapes			Torsional mode shapes		
Type	z_n	$\Omega_{w,n}$	Type	γ_m	$\Omega_{\theta,m}$
1AF	z_2	0.369	1AT	γ_2	0.328
1SF	z_1	0.484	1ST	γ_1	0.412
2SF	z_3	0.647	2ST	γ_3	0.542
2AF	z_4	0.724	2AT	γ_4	0.651
3SF	z_5	0.919	3ST	γ_5	0.819

Table 6.2: First five flexural and torsional modes of vibration for the twin-box deck sectional model

The torsional-to-vertical frequency ratios are listed in Table 6.3.

Torsional-to-vertical frequency ratios $\gamma_w = \frac{\Omega_{\theta,m}}{\Omega_{w,n}}$				
$\Omega_{w,2}$	$\Omega_{w,1}$	$\Omega_{w,3}$	$\Omega_{w,4}$	$\Omega_{w,5}$
$\Omega_{\theta,2}$ 0.88	0.68	0.51	0.45	0.36
$\Omega_{\theta,1}$ 1.11	0.9	0.64	0.57	0.45
$\Omega_{\theta,3}$ 1.47	1.12	0.89	0.75	0.59
$\Omega_{\theta,4}$ 1.76	1.34	1.01	0.85	0.71
$\Omega_{\theta,5}$ 2.22	1.69	1.27	1.13	0.84

Table 6.3: Torsional-to-vertical frequency ratios

Classical flutter can occur only between torsional and vertical modes of similar shape, hence it is not likely to happen in this model because all the frequency ratios in the "main diagonal" of Table 6.3 are lower than one. However, the ratio between the first skew-symmetric torsional mode, namely $\Omega_{\theta,2}$, and the second symmetric flexural mode, namely $\Omega_{w,3}$, is near to 1/2, thus being susceptible to subharmonic parametric resonance also for low wind velocities. In fact a small reduction of the torsional Eigen-frequency, due to the self-induced forces acting on the deck, is enough to lock-in the phenomenon to the perfect 2:1 condition for the subharmonic resonance.

In order to be able to consider the Aeroelastic effects acting on the bridge, the theory of the self-excited forces acting on a thin flat plate provided by Theodorsen [53] is adapted to the flutter derivatives theory introduced by Scanlan [52]. Dyrbie and Hansen [25] provide the expressions for the flat plate flutter derivatives.

6.2 FLAT PLATE AERODYNAMIC DERIVATIVES

For Theodeorsen's airfoil the following expressions for the flutter derivative are valid:

$$H_1^*(k) = -\pi \cdot \frac{F(k)}{k} \qquad\qquad A_1^*(k) = -\pi \cdot \frac{F(k)}{4k}$$

$$H_2^*(k) = -\frac{\pi}{4k} \cdot \left(1 + F(k) + 2\frac{G(k)}{k}\right) \qquad A_2^*(k) = -\frac{\pi}{16k} \cdot \left(1 - F(k) - 2\frac{G(k)}{k}\right)$$

$$H_3^*(k) = \frac{\pi}{2k^2} \cdot \left(F(k) - \frac{kG(k)}{2}\right) \qquad A_3^*(k) = \frac{\pi}{8k^2} \cdot \left(F(k) - \frac{kG(k)}{2}\right)$$

$$H_4^*(k) = \frac{\pi}{2} \cdot \left(1 + \frac{2G(k)}{k}\right) \qquad\qquad A_4^*(k) = \frac{\pi}{4} \cdot \frac{G(k)}{k}$$

(6.1)

where F and G are the real and imaginary parts of the Theodorsen circulatory function (Figure 6.2) and k is the reduced frequency based on the half-width of the deck section, i.e. $k = \frac{K}{2}$. F and G are given by:

$$F(k) = \frac{J_1(J_1 + Y_0) + Y_1(Y_1 - J_0)}{(J_1 + Y_0)^2 + (Y_1 - J_0)^2}$$

$$G(k) = -\frac{J_1 J_0 + Y_1 Y_0}{(J_1 + Y_0)^2 + (Y_1 - J_0)^2}$$

(6.2)

being J_i and Y_i the Bessels functions of the first and second kind, respectively, of order i.
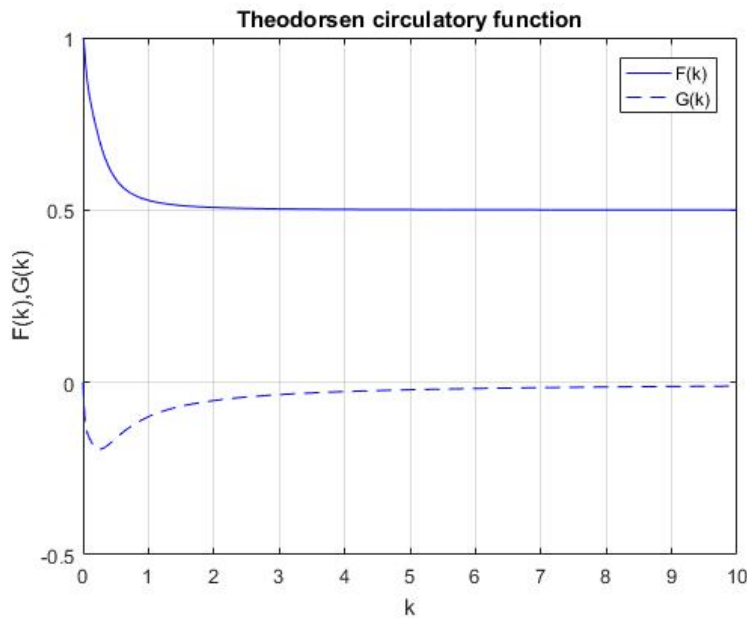
Figure 6.2: Real F(k) and imaginary G(k) parts of the Theodorsen circulatory function

Remembering that the reduced frequency is the inverse of the reduced velocity, it is possible to plot all the flutter derivatives in function of the reduced velocity $U^* = \frac{U}{fB}$.
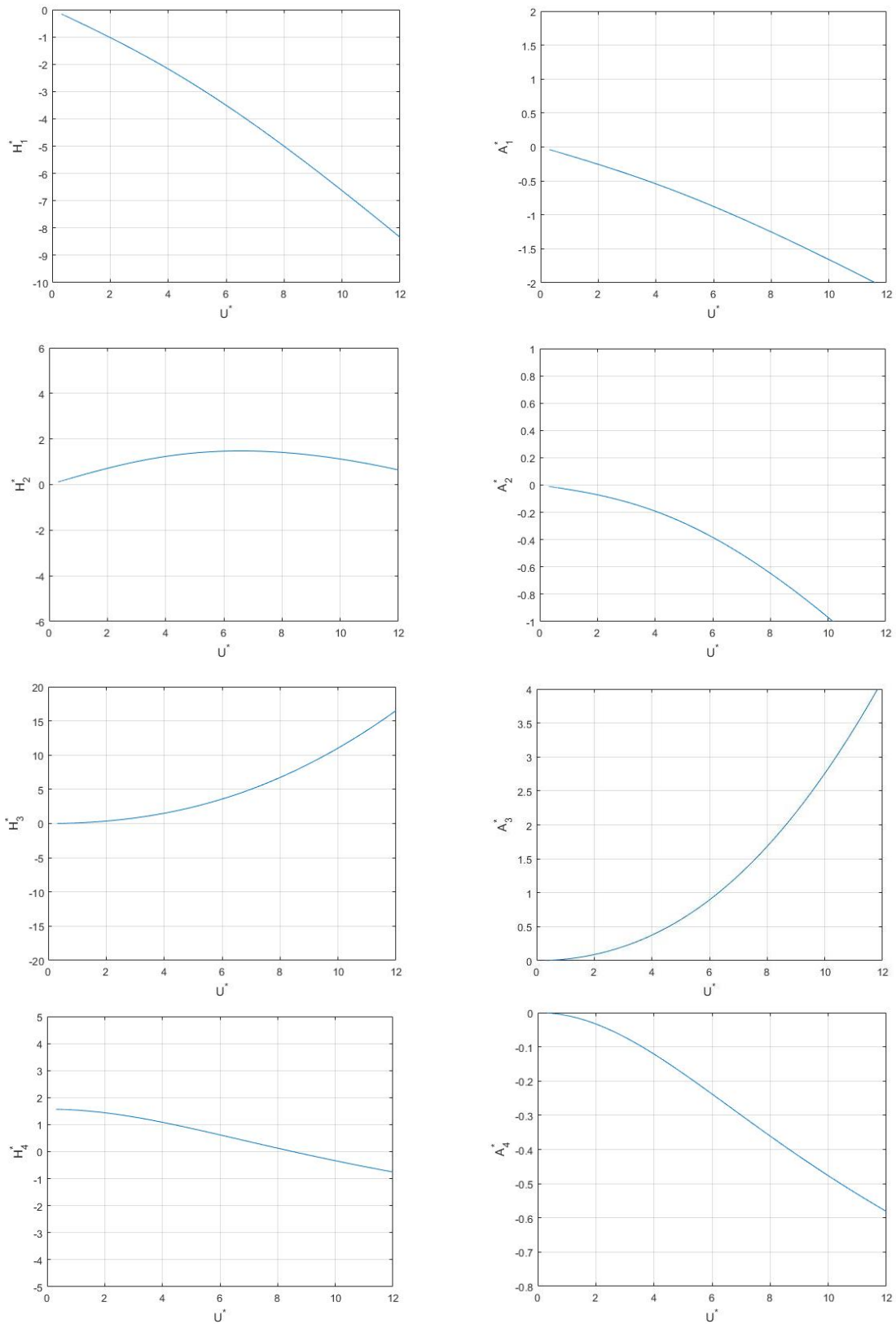
Figure 6.3: Flutter derivatives for a flat plate

6.3 EFFECT OF INTERNAL PARAMETRIC RESONANCE

Thanks to the flat plate flutter derivatives just introduced, for each torsional-to-vertical frequency ratio (Table 6.3) it is possible to compute the wind velocity which leads the frequencies to be in the exact 2:1 parametric resonance condition, i.e. the vertical frequency is exactly the double of the torsional frequency.

The A_3^* flutter derivative is positive for each wind velocity, which means that the self-excited forces produce a reduction of the net torsional stiffness and, as a consequence, a reduction of the torsional Eigen-frequency. Hence, the most critical situation is related to the ratio between the first skew-symmetric torsional mode $\Omega_{\theta,2}$ and the second symmetric flexural mode $\Omega_{w,3}$.

Considering that the vertical oscillations are due to vortex shedding and making the hypothesis to be in the lock-in range of velocity $\left(\Omega_{w,3} = \omega_{VS}\right)$, the value of A_3^* needed for the 2:1 subharmonic condition can be calculated from the expression (4.46) of the frequency ratio δ in the Mathieu's equation:

$$\delta = 0.25 = \delta'(1 - \beta) = \frac{\tilde{\Omega}_{\theta,2}^2}{\tilde{\omega}_{VS}^2}\left(1 - \frac{8}{\pi} \cdot \frac{\tilde{m}_a}{\tilde{J}_t} A_3^*\right) \tag{6.3}$$

So:

$$A_3^* = 1 - \frac{\pi}{8} \cdot \frac{\tilde{J}_t}{\tilde{m}_a} \cdot \frac{\delta}{\delta'} = 0.0286 \tag{6.4}$$

The wind speed correspondent to the value of A_3^* expressed in equation (6.4) can be easily found from the plot of this flutter derivative with respect to the velocity (Figure 6.3):

$$U \cong 3.55 \frac{m}{s} \tag{6.5}$$

Given this wind velocity, it is possible to compute the contribution given by the flutter derivative A_2^* to damping.

$$A_2^* = -0.0372 \tag{6.6}$$

Self-excited forces introduce additional net torsional damping to the system because of the negative sign of A_2^*. Due to this beneficial effect, the "tongue" in the Ince-Strutt diagram goes up, reducing the instability regions. Figure 6.4 shows the effect of an increase in the torsional net damping due to Aeroelastic effects when the wind speed is equal to 3.55 m/s.
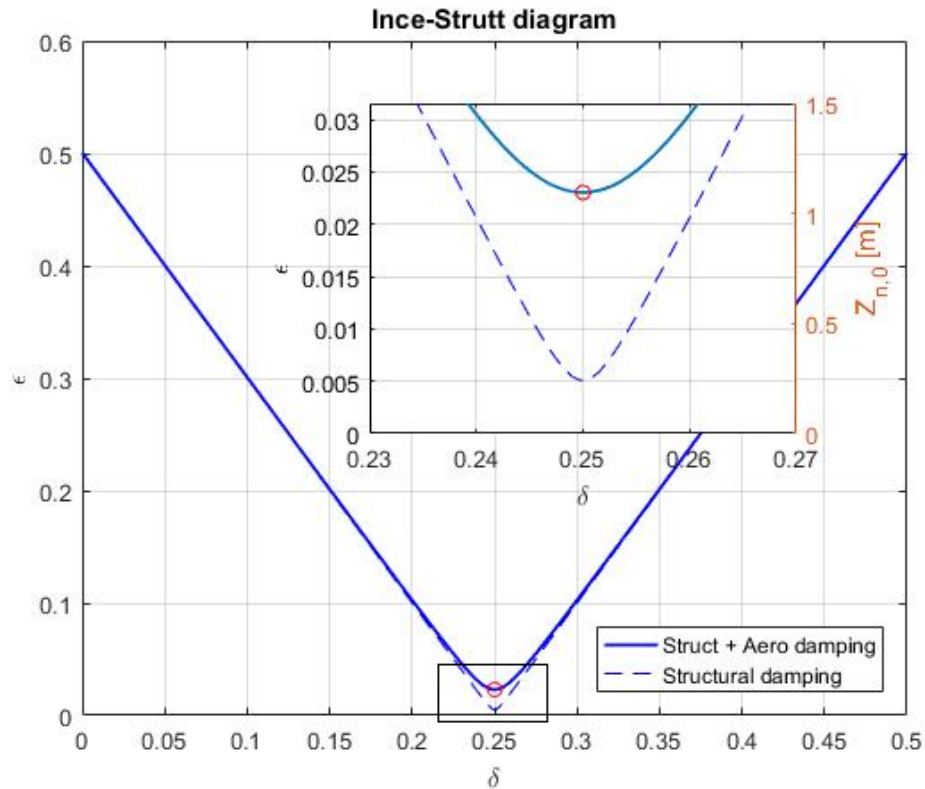
Figure 6.4: Ince-Strutt diagram for the twin-box section model (U=3.55 m/s)

Because of the assumed flat plate flutter derivatives, Aeroelastic forces produce an increment of the net torsional damping which leads the modal amplitude of vibration necessary to activate the 2:1 internal parametric resonance instability to pass from a value of $Z_{3,0} \cong 0.25\ m$ to a value of $Z_{3,0} \cong 1.1\ m$.

In general, for streamlined cross-sections the value of A_2^* is negative for any reduced velocity, with increasing absolute values as the wind speed increases (Same trend as the flat plate flutter derivative). Hence, the flexural modal amplitude of vibrations values leading to parametric instability conditions becomes higher and higher with the increase of the wind velocity. The torsional-to-vertical frequency ratio chosen for the instability analysis is the one leading to 2:1 subharmonic conditions for the lowest value of wind speed, thus being the most critical case among all the frequency ratios in Table 6.3.

Moreover, experimental investigations [3] evidenced the fact that the values of A_2^* and A_3^* are lower for a twin-box cross section with respect to the flat plate condition, meaning that the aerodynamic contribution to the torsional stiffness is smaller, whilst the one to the torsional damping is larger. For this reason, the assumption of the flat plate flutter derivatives leads to smaller values of critical flexural displacements with respect to the adoption of the flutter derivatives characterizing the twin-box section model. Thus, the analysis implies a lower value of $Z_{3,0}$ with respect to the real situation, leading to results on the safe side.

Now it is necessary to compute the modal flexural displacement due to vortex shedding and to compare this value with the displacement necessary for the onset of instability, namely $Z_{3,0} = 1.1\ m$.

Some assumptions have to be made to compute the vortex shedding of the twin-box model:

1. The Strouhal number considered is the one correspondent to a flat plate with fairings at the outermost windward and leeward edges, i.e. $St = 0.17$ from Figure 3.7;

2. The lift coefficient for a twin box section is strongly different with respect to a bluff deck section such as the one of Tacoma Narrows Bridge. $\tilde{c}_L = 0.1$ can be a reasonable value for the considered section;

3. Both H_1^* and H_4^* flutter derivatives are considered for the calculation of the dynamic amplification factor and for the phase lag. H_1^* is negative for all the wind velocities, so it produces an increase of the net flexural damping, whilst H_4^* changes sign (from positive to negative) when $U^* \cong 8.1$, decreasing the net flexural stiffness for values of reduced velocities below this limit.

The wind velocity which locks-in with the second symmetric flexural mode $\Omega_{w,3}$ is:

$$U_{lock-in} = U_D \cdot \left(\frac{\tilde{\Omega}_{w,3}}{\tilde{\Omega}_{\theta,2}} \cdot \sqrt{\frac{\widetilde{m}_a}{\tilde{J}_t}} \cdot \frac{1}{\pi \cdot St \cdot \tilde{\alpha}} \right) = 2.35\ \frac{m}{s} \tag{6.7}$$

The dynamic amplification factor and the phase lag of the wind induced response are depicted in Figure 6.5, where there is a comparison between the structural and the Aeroelastic response.
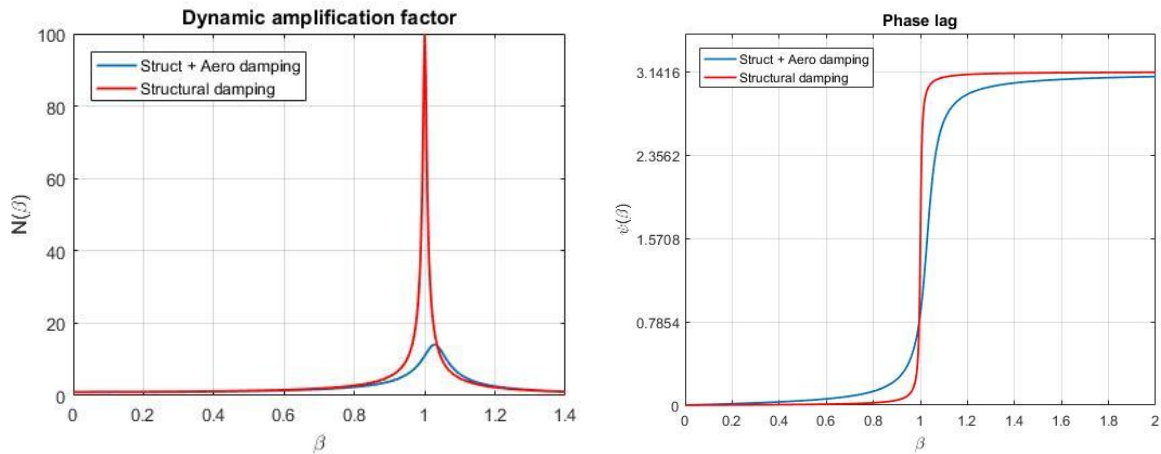
Figure 6.5: Dynamic amplification factor and phase lag for the twin-box cross section

It is noticeable that the change in the net flexural stiffness due to Aeroelastic effects is such that the pick of the dynamic amplification factor is not in correspondence of the value $\beta = 1$, but slightly shifted because of the change of the flexural frequency of vibration.

Thence, the value of the flexural modal amplitude induced by vortex shedding is:

$$Z_{3,0}^{VS} = f \cdot \left(\frac{\Gamma_0 \cdot \tilde{h}_{W_n}}{K_{w,n}^{(L)}} \cdot N \right) \cong 0.14 \, m \tag{6.8}$$

This value is strongly lower with respect to the value of modal displacement needed to activate the internal parametric resonance instability phenomenon, i.e. $Z_{3,0} \cong 1.1 \, m$. It seems that the twin-box girder section cannot manifest instability phenomena due to subharmonic 2:1 resonance.

However, the range of wind velocities in which the vortex shedding frequency locks-in with the flexural frequency of vibration, i.e. $1.89 \, m/s < U < 3.06 \, m/s$ does not correspond to the velocity used for the calculation of the "tongue" of instability in the Ince-Strutt diagram, i.e. $U = 3.55 \, m/s$. Since the torsional-to vertical frequency ratio considered for the analysis is very near to the condition for the occurrence of 2:1 resonance condition, it seems reasonable to find the critical amplitude of vibration correspondent to the lower value of the lock-in range velocity. i.e. $U = 1.89 \, m/s$.

For this wind speed the values of A_2^* and A_3^* are:

$$A_2^* = -0.0191$$
$$A_3^* = 0.0080 \tag{6.9}$$

The region of instability in the Ince-Strutt diagram is depicted in Figure 6.6.
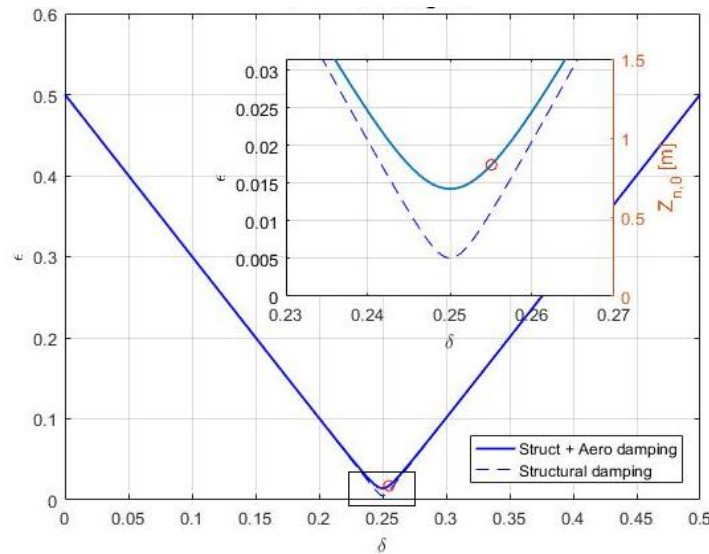
Figure 6.6: Ince-Strutt diagram for the twin-box section model (U=1.89 m/s)

It is noticeable that in this situation the value of A_3^* is not so high to bring the frequency ratio δ to perfect 2:1 resonant conditions however, being the value A_2^* smaller in absolute value than the one in equation (6.6), the region of instability is wider. Hence, the modal amplitude of vibration for the occurrence of instability is:

$$Z_{3,0} = 0.83 \, m \tag{6.10}$$

This value is in any case around eight time larger than the flexural amplitude of vibrations produced by the vortex induced response. Hence, it is obvious that internal parametric resonance instability cannot occur for twin-box cross sections designed with the non-flutter principle.

The reason of this is mainly due to two important aerodynamic properties:

1. A_2^* does not change sign for any value of the reduced wind speed, remaining always negative and contributing to increase the net torsional damping with the increase of the wind speed.

2. The vortex shedding phenomenon is not able to generate high flexural oscillations of the girder, also if the span of the bridge is considerably long.

Both properties are valid for streamlined airfoil type deck cross sections, properly designed to reduce self-excited forces due to the wind action.

7 CONCLUSIONS

Due to their high flexibility long-span suspension bridges are susceptible to wind-induced effects. Aerodynamic studies on girder cross sections started after the dramatic failure of the Tacoma Narrows bridge, occurred on November 7, 1940. Nowadays, it is well known that Aeroelastic effects introduce in the structural system a coupling between the modes of vibration and an asymmetry in the damping and stiffness matrices. For this reason, different kinds of dynamic instabilities can occur, namely 1 DoF flexural instability, torsional flutter and classical 2 DoF$_s$ flutter.

Recent studies assert that internal parametric resonance phenomena are a possible contributing cause for the occurrence of critical instability conditions in long-span suspension bridges. Such structures are strongly characterized by an intrinsic geometric non-linear behaviour which causes a soft coupling between the flexural and the torsional responses. Arioli and Gazzola [7] found out that, also in isolated systems, vertical oscillations may switch to torsional ones when a critical value of energy threshold is reached.

Inspired by the pioneering work of Herrmann and Hauger [31] the perturbed equations of motion of the bridge sectional model have been obtained with the aim of demonstrating a possible interaction between parametric resonance and flutter. The problem has been strongly simplified by assuming negligible coupling flutter derivatives. Thus, the two equations of motion are coupled only by the quadratic stiffness term, which survives also in a linearized formulation because of the linear dependence on both the flexural and torsional DoF$_s$. As a result we obtain the torsional equation of motion governing the problem dependent on some paramethers only, namely the two flutter derivatives A_2^* and A_3^*, the modal amplitude of oscillations $z_{n,0}$ and the quadratic coupling stiffness term $K_{\theta w,mn}^{(Q)}$.

The torsional equation of motion can be rewritten in the well-known Mathieu's format and the stability of the system can be detected by Ince-Strutt diagrams. The solution for the boundaries of instability of first kind, i.e. the 2:1 subharmonic resonance, is found by means of the multiple scales technique. The analytical approach allows for the determination of an interaction formula between the flutter performances of the bridge and the non-linear coupling term responsible for parametric resonance instability.

$$A_2^* > A_{2,F}^* \cdot \left(1 - \frac{\delta'}{c'} \cdot \frac{K_{\theta w,mn}^{(Q)}}{K_{\theta,m}^{(L)}} \cdot z_{n,0} \right)$$

The aforementioned formula clearly highlights the fact that the A_2^* flutter derivative is eroded proportionally to the magnitude of the non-linear structural stiffness term and to the modal amplitude of flexural oscillations. Hence in the case of positive values of A_2^* (necessary condition for reaching the onset of torsional flutter), the critical instability threshold can be reached for lower values of wind velocities with respect to the flutter ones.

In the assumed scenario, in which classical flutter is not likely to happen because of the absence of the coupling flutter derivatives, theoretical results showed that the interaction between internal parametric resonance and torsional flutter is possible and it is governed mainly by these parameters:

1. The trend of A_2^*, responsible for the decrement or increment of net torsional damping;

2. The value of flexural modal amplitude of oscillation due to vortex shedding $z_{n,0}$;

3. The magnitude of the quadratic stiffness coupling term $K_{\theta w,mn}^{(Q)}$;

4. The torsional-to-vertical frequency ratio δ'.

Numerical results confirmed what found with the theoretical approach. Two different deck sectional model have been analyzed, the Tacoma narrows bridge and a twin-box section designed with the non-flutter principle.

The Tacoma Narrows bridge had a bluff section susceptible to vortex induced vibrations and to torsional flutter. The latter phenomenon was considered by many authors as the one causing the collapse. However, the flutter velocity calculated by Farquharson trough wind tunnel tests was never ascertained because too low with respect to the observed one on the day of collapse. Regardless of the "real" value of the flutter velocity, we considered for the analysis a velocity of 90% with respect to the flutter one. In this scenario the system is highly susceptible to parametric resonance because the "tongue" of instability in the Ince-Strutt diagram lowers down due to the negative effect of A_2^*. In perfect 2:1 subharmonic conditions the critical amplitude of oscillations calculated are $Z_{5,0} = 0.20\,m$ whilst the amplitude of oscillations' provided by vortex shedding in the lock-in range are $Z_{5,0}^{VS} = 0.46\,m$. Thus parametric instability is likely to happen in a range of torsional-to-vertical frequency ratios, e.g. $0.247 < \delta < 0.253$.

On the contrary the twin-box bridge is characterized by a streamlined section not susceptible neither to torsional nor to classical 2 DoFs flutter. However the low torsional-to-frequency ratio are near to the perfect 2:1 subharmonic condition, making us think to the possible occurrence of parametric instability. Instead, numerical results showed that in the

lock-in range of velocity the amplitude of oscillations provided by vortex shedding are $Z_{3,0}^{VS} = 0.14 \, m$, whilst the amplitude needed for instability to occur are $Z_{3,0} = 0.83 \, m$. Thus, critical conditions due to internal parametric resonance are unlikely to be reached because of the shape of modern cross sections. First and foremost a streamlined girder is less susceptible to vortex induced vibrations which is the driver for the occurrence of subharmonic resonance. Besides the airfoil type cross section is characterized by negative values of A_2^* which provide an increase of the net torsional damping and a consequent reduction of the region of instability with increasing wind speed.

APPENDIX A

This appendix deals with the determination of the analytical formulas for the modal superposition analysis in the case of symmetric modes of vibrations (§2.4).

The solution for the flexural mode of vibration can be expressed by the superposition of an homogeneous and a particular solution.

$$
W_n(\xi) = W_{n,0}(\xi) + W_{n,p}(\xi) = \left(\frac{\lambda_1^2 \tilde{h}_{W,n}}{\tilde{\Omega}_{w,n}^2} + C_{n,1} \cdot \exp(\Psi_{w,n}\xi) + C_{n,2} \cdot \right.
$$
$$
\left. \exp(-\Psi_{w,n}\xi) + C_{n,3} \cdot \exp(i \cdot \eta_{w,n}\xi) + C_{n,4} \cdot \exp(-i \cdot \eta_{w,n}\xi) \right)
$$

(A.1)

where:

$$
\eta_{w,n}^2 = \frac{1}{2\mu^2} \left(\sqrt{1 + 4\mu^2 \tilde{\Omega}_{w,n}^2} - 1 \right)
$$

$$
\Psi_{w,n}^2 = \frac{1}{2\mu^2} \left(\sqrt{1 + 4\mu^2 \tilde{\Omega}_{w,n}^2} + 1 \right) = \eta_{w,n}^2 + \frac{1}{\mu^2}
$$

(A.2)

To find the constants of integrations present in the solution (A.1) the boundary conditions of a simply supported beam must be enforced:

$$
W_n(0) = W_n(1) = 0
$$
$$
W_n''(0) = W_n''(1) = 0
$$

(A.3)

Thus:

$$
W_n(0) = 0 \quad \Rightarrow \quad \left(\frac{\lambda_1^2 \tilde{h}_{W,n}}{\tilde{\Omega}_{w,n}^2} + C_{n,1} + C_{n,2} + C_{n,3} + C_{n,4} \right) = 0
$$

$$
W_n''(0) = 0 \quad \Rightarrow \quad (C_{n,1} + C_{n,2}) \cdot \Psi_{w,n}^2 - (C_{n,3} + C_{n,4}) \cdot \eta_{w,n}^2 = 0
$$

$$
W_n(1) = 0 \quad \Rightarrow \quad \left(\frac{\lambda_1^2 \tilde{h}_{W,n}}{\tilde{\Omega}_{w,n}^2} + C_{n,1} \exp(\Psi_{w,n}) + C_{n,2} \exp(-\Psi_{w,n}) + C_{n,3} \exp(i \cdot \eta_{w,n}) + \right.
$$
$$
\left. + C_{n,4} \exp(-i \cdot \eta_{w,n}) \right) = 0
$$

(A.4)

$$
W_n''(1) = 0 \quad \Rightarrow \quad (C_{n,1} \exp(\Psi_{w,n}) + C_{n,2} \exp(-\Psi_{w,n})) \cdot \Psi_{w,n}^2 - (C_{n,3} \exp(i \cdot \eta_{w,n}) +
$$
$$
C_{n,4} \exp(-i \cdot \eta_{w,n})) \cdot \eta_{w,n}^2 = 0
$$

The constants of integration assume the following expression:

$$C_{n,1} = -\frac{\lambda_1^2 \tilde{h}_{W,n}}{\tilde{\Omega}_{w,n}^2} \cdot \frac{\eta_{w,n}^2}{\Psi_{w,n}^2 + \eta_{w,n}^2} \cdot \frac{1 - \exp(-\Psi_{w,n})}{\exp(\Psi_{w,n}) - \exp(-\Psi_{w,n})}$$

$$C_{n,2} = \frac{\lambda_1^2 \tilde{h}_{W,n}}{\tilde{\Omega}_{w,n}^2} \cdot \frac{\eta_{w,n}^2}{\Psi_{w,n}^2 + \eta_{w,n}^2} \cdot \frac{1 - \exp(\Psi_{w,n})}{\exp(\Psi_{w,n}) - \exp(-\Psi_{w,n})}$$

$$C_{n,3} = -\frac{\lambda_1^2 \tilde{h}_{W,n}}{\tilde{\Omega}_{w,n}^2} \cdot \frac{\Psi_{w,n}^2}{\Psi_{w,n}^2 + \eta_{w,n}^2} \cdot \frac{1 - \exp(-i \cdot \eta_{w,n})}{\exp(i \cdot \eta_{w,n}) - \exp(-i \cdot \eta_{w,n})}$$

$$C_{n,4} = \frac{\lambda_1^2 \tilde{h}_{W,n}}{\tilde{\Omega}_{w,n}^2} \cdot \frac{\Psi_{w,n}^2}{\Psi_{w,n}^2 + \eta_{w,n}^2} \cdot \frac{1 - \exp(i \cdot \eta_{w,n})}{\exp(i \cdot \eta_{w,n}) - \exp(-i \cdot \eta_{w,n})}$$

(A.5)

The substitution of the four constants (A.5) into the general solution (A.1) leads to:

$$W_n(\xi) = W_{n,0}(\xi) + W_{n,p}(\xi) = \frac{\lambda_1^2 \tilde{h}_{W,n}}{\tilde{\Omega}_{w,n}^2}\left[1 - \frac{1}{\Psi_{w,n}^2 + \eta_{w,n}^2} \cdot \left(\eta_{w,n}^2 \cdot \right.\right.$$
$$\frac{\exp(\Psi_{w,n}\cdot\xi) - \exp(\Psi_{w,n}\cdot(\xi-1)) + \exp(-\Psi_{w,n}\cdot\xi) - \exp(-\Psi_{w,n}\cdot(\xi-1))}{\exp(\Psi_{w,n}) - \exp(-\Psi_{w,n})} + +\Psi_{w,n}^2 \cdot$$
$$\left.\left.\frac{\exp(i\cdot\eta_{w,n}\cdot\xi) - \exp(i\cdot\eta_{w,n}\cdot(\xi-1)) + \exp(-i\cdot\eta_{w,n}\cdot\xi) - \exp(-i\cdot\eta_{w,n}\cdot(\xi-1))}{\exp(i\cdot\eta_{w,n}) - \exp(-i\cdot\eta_{w,n})}\right)\right]$$

(A.6)

Exploiting the well-known Euler formulas the solution can b e expressed as:

$$W_n(\xi) = \frac{\lambda_1^2 \tilde{h}_{W,n}}{\tilde{\Omega}_{w,n}^2}\left[1 - \frac{1}{\Psi_{w,n}^2 + \eta_{w,n}^2} \cdot \left(\eta_{w,n}^2 \cdot \frac{\sinh(\Psi_{w,n}\cdot\xi) - \sinh(\Psi_{w,n}\cdot(\xi-1))}{\sinh(\Psi_{w,n})} + \Psi_{w,n}^2 \cdot \right.\right.$$
$$\left.\left.\frac{\sin(\eta_{w,n}\cdot\xi) - \sin(\eta_{w,n}\cdot(\xi-1))}{\sin(\eta_{w,n})}\right)\right]$$

(A.7)

Now remembering that:

$$\sinh(\alpha) \pm \sinh(\beta) = 2 \cdot \sinh\left(\frac{\alpha\pm\beta}{2}\right) \cdot \cosh\left(\frac{\alpha\mp\beta}{2}\right)$$

$$\sin(\alpha) \pm \sin(\beta) = 2 \cdot \sin\left(\frac{\alpha\pm\beta}{2}\right) \cdot \cos\left(\frac{\alpha\mp\beta}{2}\right)$$

(A.8)

then:

$$\sinh(\Psi_{w,n} \cdot \xi) - \sinh\left(\Psi_{w,n} \cdot (\xi - 1)\right) = 2 \cdot \sinh\left(\frac{\Psi_{w,n}}{2}\right) \cdot \cosh\left(\Psi_{w,n} \cdot \left(\xi - \frac{1}{2}\right)\right)$$

$$\sin(\eta_{w,n} \cdot \xi) - \sin\left(\eta_{w,n} \cdot (\xi - 1)\right) = 2 \cdot \sin\left(\frac{\eta_{w,n}}{2}\right) \cdot \cos\left(\eta_{w,n} \cdot \left(\xi - \frac{1}{2}\right)\right)$$

(A.9)

Moreover by exploiting also the multiple angle formulae:

$$\sinh(2\alpha) = 2 \cdot \sinh(\alpha) \cdot \cosh(\alpha)$$

$$\sin(2\alpha) = 2 \cdot \sin(\alpha) \cdot \cos(\alpha)$$

(A.10)

it is possible to write the ratios between trigonometric functions as:

$$\frac{\sinh(\Psi_{w,n})}{\sinh\left(\frac{\Psi_{w,n}}{2}\right)} = 2 \cdot \cosh\left(\frac{\Psi_{w,n}}{2}\right)$$

$$\frac{\sin(\eta_{w,n} \cdot \xi)}{\sin\left(\frac{\eta_{w,n}}{2}\right)} = 2 \cdot \cos\left(\frac{\eta_{w,n}}{2}\right)$$

(A.11)

After all this trigonometric relations has been exploited the solution for the flexural mode shape can be expressed as in equation (2.59).

$$W_n(\xi) = \frac{\lambda_1^2 \widetilde{h}_{W,n}}{\widetilde{\Omega}_{W,n}^2}\left[1 - \frac{1}{\Psi_{w,n}^2 + \eta_{w,n}^2}\left(\eta_{w,n}^2 \cdot \frac{\cosh\left(\Psi_{w,n}\left(\xi - \frac{1}{2}\right)\right)}{\cosh\left(\frac{\Psi_{w,n}}{2}\right)} + \Psi_{w,n}^2 \cdot \frac{\cos\left(\eta_{w,n}\left(\xi - \frac{1}{2}\right)\right)}{\cos\left(\frac{\eta_{w,n}}{2}\right)}\right)\right]$$

(A.12)

For the torsional modes of vibration the passages to be done are exactly the same, leading to the expression (2.70).

$$\Theta_m(\xi) = \frac{\lambda_1^2 \widetilde{h}_{\theta,m}}{\widetilde{J}_t \widetilde{\Omega}_{\theta,m}^2}\left[1 - \frac{1}{\Psi_{\theta,m}^2 + \eta_{\theta,m}^2}\left(\eta_{\theta,m}^2 \cdot \frac{\cosh\left(\Psi_{\theta,m}\left(\xi - \frac{1}{2}\right)\right)}{\cosh\left(\frac{\Psi_{\theta,m}}{2}\right)} + \Psi_{\theta,m}^2 \cdot \frac{\cos\left(\eta_{\theta,m}\left(\xi - \frac{1}{2}\right)\right)}{\cos\left(\frac{\eta_{\theta,m}}{2}\right)}\right)\right]$$

(A.13)

APPENDIX B

This appendix deals with the determination of the boundaries of instability of the first kind, i.e. the subharmonic resonance, for the 3 DoFs inverted pendulum proposed by Herrmann and Hauger [31] (§4.3.1).

The assumed solution $q_j(\tau)$ having period $T_1 = 4\pi$,

$$q_j(\tau) = \sum_{k=1,3,5,\ldots}^{+\infty} \left(a_{jk} \sin\left(\frac{k\tau}{2}\right) + b_{jk} \cos\left(\frac{k\tau}{2}\right) \right), \quad (j = 1,2) \tag{B.1}$$

must be substituted into the dimensionless system of variational equations:

$$(p_1 + p_2)(\lambda^2 + 2\lambda\xi \cos(\tau)) \cdot \ddot{q}_1 + p_2(\lambda + \xi \cos(\tau)) \cdot \ddot{q}_2 - 2(p_1 + p_2)(\lambda\xi \sin(\tau)) \cdot \dot{q}_1 +$$
$$+(2r - \lambda s - s\xi \cos(\tau)) \cdot q_1 - (r - \lambda\alpha s - \alpha s\xi \cos(\tau)) \cdot q_2 = 0$$

$$p_2(\lambda + \xi \cos(\tau)) \cdot \ddot{q}_1 + p_2 \cdot \ddot{q}_2 - 2p_2\xi \sin(\tau) \cdot \dot{q}_1 - (r + p_2\xi \cos(\tau)) \cdot q_1 +$$
$$+[r - (1 - \alpha)s + p_2\xi \cos(\tau)] \cdot q_2 = 0 \tag{B.2}$$

This leads to:

$$\sum_{k=1,3,5,\ldots}^{+\infty} \left\{ (p_1 + p_2)(\lambda^2 + 2\lambda\xi \cos(\tau))\frac{k^2}{4}\left(-a_{1k} \sin\left(\frac{k\tau}{2}\right) - b_{1k} \cos\left(\frac{k\tau}{2}\right)\right) + \right.$$
$$+p_2(\lambda + \xi \cos(\tau))\frac{k^2}{4}\left(-a_{2k} \sin\left(\frac{k\tau}{2}\right) - b_{2k} \cos\left(\frac{k\tau}{2}\right)\right) + -2(p_1 +$$
$$p_2)(\lambda\xi \sin(\tau))\frac{k}{2}\left(a_{1k} \cos\left(\frac{k\tau}{2}\right) - b_{1k} \sin\left(\frac{k\tau}{2}\right)\right) + +(2r - \lambda s -$$
$$s\xi \cos(\tau))\left(a_{1k} \sin\left(\frac{k\tau}{2}\right) + b_{1k} \cos\left(\frac{k\tau}{2}\right)\right) + -(r - \lambda\alpha s - \alpha s\xi \cos(\tau))\left(a_{2k} \sin\left(\frac{k\tau}{2}\right) + \right.$$
$$\left. b_{2k} \cos\left(\frac{k\tau}{2}\right)\right)\right\} = 0 \tag{B.3}$$

$$\sum_{k=1,3,5,\ldots}^{+\infty} \left\{ p_2(\lambda + \xi \cos(\tau))\frac{k^2}{4}\left(-a_{1k} \sin\left(\frac{k\tau}{2}\right) - b_{1k} \cos\left(\frac{k\tau}{2}\right)\right) + \right.$$
$$+p_2\frac{k^2}{4}\left(-a_{2k} \sin\left(\frac{k\tau}{2}\right) - b_{2k} \cos\left(\frac{k\tau}{2}\right)\right) - 2p_2\xi \sin(\tau)\frac{k}{2}\left(a_{1k} \cos\left(\frac{k\tau}{2}\right) - b_{1k} \sin\left(\frac{k\tau}{2}\right)\right) +$$
$$-(r + p_2\xi \cos(\tau))\left(a_{1k} \sin\left(\frac{k\tau}{2}\right) + b_{1k} \cos\left(\frac{k\tau}{2}\right)\right) + +[r - (1 - \alpha)s +$$
$$p_2\xi \cos(\tau)]\left(a_{2k} \sin\left(\frac{k\tau}{2}\right) + b_{2k} \cos\left(\frac{k\tau}{2}\right)\right)\right\} = 0$$

Developing all the multiplications inside the system of equation (B.3) and exploiting the well-known Werner formulas:

$$\sum_{k=1,3,5,\dots}^{+\infty}\left\{(p_1+p_2)\frac{\lambda^2 k^2}{4}a_{1k}\sin\left(\frac{k\tau}{2}\right)-(p_1+p_2)\frac{\lambda k^2}{4}\xi a_{1k}\left[\sin\left(\frac{k\tau}{2}-\tau\right)+\right.\right.$$
$$\sin\left(\frac{k\tau}{2}+\tau\right)\bigg]-p_2\frac{\lambda k^2}{4}a_{2k}\sin\left(\frac{k\tau}{2}\right)-p_2\xi\frac{k^2}{8}a_{2k}\left[\sin\left(\frac{k\tau}{2}-\tau\right)+\sin\left(\frac{k\tau}{2}+\tau\right)\right]+$$
$$-(p_1+p_2)\lambda\xi\frac{k}{2}a_{1k}\left[-\sin\left(\frac{k\tau}{2}-\tau\right)+\sin\left(\frac{k\tau}{2}+\tau\right)\right]+(2r-\lambda s)a_{1k}\sin\left(\frac{k\tau}{2}\right)+$$
$$-\frac{s\xi}{2}a_{1k}\left[\sin\left(\frac{k\tau}{2}-\tau\right)+\sin\left(\frac{k\tau}{2}+\tau\right)\right]-(r-\lambda\alpha s)a_{2k}\sin\left(\frac{k\tau}{2}\right)+\frac{\alpha s\xi}{2}a_{2k}\left[\sin\left(\frac{k\tau}{2}-\tau\right)+\right.$$
$$+\sin\left(\frac{k\tau}{2}+\tau\right)\bigg]-(p_1+p_2)\frac{\lambda^2 k^2}{4}b_{1k}\cos\left(\frac{k\tau}{2}\right)-(p_1+p_2)\frac{\lambda k^2}{4}\xi b_{1k}\left[\cos\left(\frac{k\tau}{2}-\tau\right)+\right.$$
$$\cos\left(\frac{k\tau}{2}+\tau\right)\bigg]-p_2\frac{\lambda k^2}{4}b_{2k}\cos\left(\frac{k\tau}{2}\right)-p_2\xi\frac{k^2}{8}b_{2k}\left[\cos\left(\frac{k\tau}{2}-\tau\right)+\cos\left(\frac{k\tau}{2}+\tau\right)\right]+$$
$$-(p_1+p_2)\lambda\xi\frac{k}{2}b_{1k}\left[\cos\left(\frac{k\tau}{2}-\tau\right)+\cos\left(\frac{k\tau}{2}+\tau\right)\right]+(2r-\lambda s)b_{1k}\cos\left(\frac{k\tau}{2}\right)+$$
$$-\frac{s\xi}{2}b_{1k}\left[\cos\left(\frac{k\tau}{2}-\tau\right)+\cos\left(\frac{k\tau}{2}+\tau\right)\right]-(r-\lambda\alpha s)b_{2k}\cos\left(\frac{k\tau}{2}\right)+\frac{\alpha s\xi}{2}b_{2k}\left[\cos\left(\frac{k\tau}{2}-\right.\right.$$
$$\left.\left.\left.\tau\right)+\cos\left(\frac{k\tau}{2}+\tau\right)\right]\right\}=0$$

(B.4)

$$\sum_{k=1,3,5,\dots}^{+\infty}\left\{-p_2\frac{\lambda k^2}{4}a_{1k}\sin\left(\frac{k\tau}{2}\right)-p_2\xi\frac{k^2}{8}a_{1k}\left[\sin\left(\frac{k\tau}{2}-\tau\right)+\sin\left(\frac{k\tau}{2}+\tau\right)\right]+\right.$$
$$-p_2\frac{k^2}{4}a_{2k}\sin\left(\frac{k\tau}{2}\right)-p_2\xi\frac{k}{2}a_{1k}\left[-\sin\left(\frac{k\tau}{2}-\tau\right)+\sin\left(\frac{k\tau}{2}+\tau\right)\right]-ra_{1k}\sin\left(\frac{k\tau}{2}\right)+$$
$$-p_2\frac{\xi}{2}a_{1k}\left[\sin\left(\frac{k\tau}{2}-\tau\right)+\sin\left(\frac{k\tau}{2}+\tau\right)\right]+[r-(1-\alpha)s]a_{2k}\sin\left(\frac{k\tau}{2}\right)+$$
$$p_2\frac{\xi}{2}a_{2k}\left[\sin\left(\frac{k\tau}{2}-\tau\right)+\sin\left(\frac{k\tau}{2}+\tau\right)\right]-p_2\frac{\lambda k^2}{4}b_{1k}\cos\left(\frac{k\tau}{2}\right)-p_2\xi\frac{k^2}{8}a_{1k}\left[\cos\left(\frac{k\tau}{2}-\tau\right)+\right.$$
$$\cos\left(\frac{k\tau}{2}+\tau\right)\bigg]-p_2\frac{\lambda k^2}{4}b_{2k}\cos\left(\frac{k\tau}{2}\right)-p_2\xi\frac{k}{2}b_{1k}\left[\cos\left(\frac{k\tau}{2}-\tau\right)-\cos\left(\frac{k\tau}{2}+\tau\right)\right]-$$
$$rb_{1k}\cos\left(\frac{k\tau}{2}\right)-p_2\frac{\xi}{2}b_{1k}\left[\cos\left(\frac{k\tau}{2}-\tau\right)+\cos\left(\frac{k\tau}{2}+\tau\right)\right]+[r-(1-\alpha)s]b_{2k}\cos\left(\frac{k\tau}{2}\right)+$$
$$\left.p_2\frac{\xi}{2}b_{2k}\left[\cos\left(\frac{k\tau}{2}-\tau\right)+\cos\left(\frac{k\tau}{2}+\tau\right)\right]\right\}=0$$

Equation (B.4) is characterized by some sinusoidal terms shifted of a phase lag equal to τ. These terms correspond to take coefficients a_{jk} and b_{jk} with $(k-2)$ or $(k+2)$, depending on the sign of the phase lag. Dividing the terms multiplied by the sine and the cosine functions and equating them to zero, two system of equations for the coefficient a_{jk} and b_{jk} are found:

$$\left[-(p_1+p_2)\frac{\lambda^2 k^2}{4}+2r-\lambda s\right]\cdot a_{1k}+\left[-(p_1+p_2)\xi\frac{\lambda(k-2)^2}{4}+(p_1+p_2)\xi\frac{\lambda(k-2)}{2}-\frac{s\xi}{2}\right]\cdot$$
$$a_{1(k-2)}-\left[(p_1+p_2)\xi\frac{\lambda(k+2)^2}{4}+(p_1+p_2)\xi\frac{\lambda(k+2)}{2}+\frac{s\xi}{2}\right]\cdot a_{1(k+2)}-\left[p_2\frac{\lambda k^2}{4}+r+\right.$$
$$\left.-\lambda\alpha s\right]\cdot a_{2k}+\left[-p_2\xi\frac{(k-2)^2}{8}+\frac{\alpha s\xi}{2}\right]\cdot a_{2(k-2)}+\left[-p_2\xi\frac{(k+2)^2}{8}+\frac{\alpha s\xi}{2}\right]\cdot a_{2(k+2)}=0$$

(B.5)

$$\left[-p_2\frac{\lambda k^2}{4} - r\right] \cdot a_{1k} + \left[-p_2\xi\frac{(k-2)^2}{8} + p_2\xi\frac{(k-2)}{2} - \frac{p_2\xi}{2}\right] \cdot a_{1(k-2)} - \left[-p_2\xi\frac{(k+2)^2}{8} + \right.$$
$$\left. +p_2\xi\frac{(k+2)}{2} + \frac{p_2\xi}{2}\right] \cdot a_{1(k+2)} + \left[-p_2\frac{k^2}{4} + r - (1-\alpha)s\right] \cdot a_{2k} + \left[\frac{p_2\xi}{2}\right] \cdot a_{2(k-2)} + \left[\frac{p_2\xi}{2}\right] \cdot$$
$$a_{2(k+2)} = 0$$

$$\left[-(p_1+p_2)\frac{\lambda^2 k^2}{4} + 2r - \lambda s\right] \cdot b_{1k} - \left[(p_1+p_2)\xi\frac{\lambda(k-2)^2}{4} + (p_1+p_2)\xi\frac{\lambda(k-2)}{2} + \frac{s\xi}{2}\right] \cdot$$
$$b_{1(k-2)} - \left[(p_1+p_2)\xi\frac{\lambda(k+2)^2}{4} - (p_1+p_2)\xi\frac{\lambda(k+2)}{2} + \frac{s\xi}{2}\right] \cdot b_{1(k+2)} - \left[p_2\frac{\lambda k^2}{4} + r + \right.$$
$$\left. -\lambda\alpha s\right] \cdot b_{2k} + \left[-p_2\xi\frac{(k-2)^2}{8} + \frac{\alpha s\xi}{2}\right] \cdot b_{2(k-2)} + \left[-p_2\xi\frac{(k+2)^2}{8} + \frac{\alpha s\xi}{2}\right] \cdot b_{2(k+2)} = 0$$

(B.6)

$$\left[-p_2\frac{\lambda k^2}{4} - r\right] \cdot b_{1k} - \left[p_2\xi\frac{(k-2)^2}{8} + p_2\xi\frac{(k-2)}{2} + \frac{p_2\xi}{2}\right] \cdot b_{1(k-2)} - \left[p_2\xi\frac{(k+2)^2}{8} + \right.$$
$$\left. -p_2\xi\frac{(k+2)}{2} + \frac{p_2\xi}{2}\right] \cdot b_{1(k+2)} + \left[-p_2\frac{k^2}{4} + r - (1-\alpha)s\right] \cdot b_{2k} + \left[\frac{p_2\xi}{2}\right] \cdot b_{2(k-2)} + \left[\frac{p_2\xi}{2}\right] \cdot$$
$$b_{2(k+2)} = 0$$

The two system of equations (B.5) and (B.6) are analogous to (4.17) and (4.18). By seeking a solution with period $T_2 = 2\pi$ and by substituting it into the system of variational equations (B.2), with the same passages proposed in this appendix, it is possible to obtain the same systems (B.5) and (B.6).

LIST OF FIGURES

LIST OF TABLES

REFERENCES

[1] Abdel-Ghaffar A.M., *Suspension bridge vibration: continuum formulation*, 1982

[2] Amman O.H. , Von Kàrmàn T., Woodruff G.B, *The Failure of the Tacoma Narrows Bridge, a report to the honorable John M. Carmody Administrator, Federal works Agency Washington, D.C.*, 1941

[3] Andersen M.S., Læsø J.R., Lenius M., Johansson J., *Non-flutter design principle for twin boxes*, 14th International Conference on Wind Engineering, Porto Alegre, Brazil, June 21-26, 2015

[4] Andersen M.S., Sahin E., Laustsen B., Lenius M., Læsø J.R., *Implementation of the Non-flutter design principle*, XIII Conference of the Italian Association for Wind engineering, 22-25 June 2014, Genova, Italy

[5] Anicin B.A., Davidovic D.M., Babovic V.M., *On the linear theory of the elastic pendulum*, 1992

[6] Arinstein A., Gitterman M., *Inverted spring pendulum driven by a periodic force: linear versus nonlinear analysis*, 2008

[7] Arioli G., Gazzola F., *A new Mathematical Explenation of what triggered the Catastrophic Torsional Mode of the Tacoma Narrows Bridge*, 2014

[8] Baccarin D., *Is internal Parametric resonance a potential failure mode for suspension bridges?*, Master Thesis, 2013

[9] Bartoli G., D'Asdia P., Febo S., Mannini C., Noè S., Procino L., *Innovative configurations for long-span suspension bridges*, EACWE 5, Florence, Italy, 19th – 23rd July 2009

[10] Bergot P., Civati L., *Dynamic Structural instability in Suspension Bridges with particular attention to Tacoma Narrows Bridge*, Master Thesis, 2014

[11] Billah K.Y., Scanlan R.H., *Resonance, Tacoma Narrows bridge failure, and undergraduate physics textbooks*, 1990

[12] Bisplinghoff R.L., Ashley H., Halfman R.L., *Aeroelasticity*, 1955

[13] Bolotin V.V., *The Dynamic Stability of Elastic Systems*, 1964

[14] Buonopane S.G., Billington D.P., *Theory and history of suspension bridge design from 1823 to 1940*, 1993

[15] Butikov E.I., *Analytical expressions for stability regions in the Ince-Strutt diagram of Mathieu equation*, 2018

[16] Capsoni A., Ardito R., Guerrieri A., *Stability of Dynamic Response of Suspension Bridges*, 2017

[17] Cevik M., Pakdemirli M., *Non-linear vibrations of suspension bridges with external excitation*, 2002

[18] Chen X., *Improved Understanding of Bimodal Coupled Bridge Flutter based on Closed-form solutions*, 2007

[19] Chen X., Kareem A., *Revisiting Multimode Coupled Bridge Flutter, Some New Insights*, 2006

[20] Chen X., Kareem A., *Understandying the underlaying phisics of multimode coupled bridge flutter based on closed-form solutions*, 2006

[21] Cobo D., *An Analysis of Wind Stability. Improvements to the Response of Suspension Bridges*, PhD Thesis, 1998

[22] Cobo D., Aparicio A.C., *Preliminary Static Analysis of Suspension Bridges*, 2001

[23] Cross R., *Experimental investigations of an elastic pendulum*, 2017

[24] Dowell E.H., Clark R., Cox D., Curtiss JR. H.C., Edwards J.W., Hall K.C., Peters D.A., Scanlan R., Simiu E., Sisto F., Strganac T.W., *A modern course in Aeroelasticity 4th revised and enlarged edition*, 2005

[25] Dyrbye C., Hansen S.O., *Wind loads on structures*, John Wiley & Sons, New York, 1997

[26] Green D., Unruh W.G., *The failure of the Tacoma Bridge: a physical model*, 2006

[27] Diana G., *Lecture notes in Wind Engineering*, 2016

[28] Farquharson F.B., *Aerodynamic Stability of Suspension Bridges*. Univ. of Washington Experimental Station, Bulletin No. 116. Parts I-V, 1949-1954.

[29]   Guerrieri A., *Internal Parametric Resonance and Aeroelastic Effects in Long-Span Suspension Bridges*, Master Thesis, 2013

[30]   Herrmann G., Bungay R.W., *On the stability of elastic systems subjected to nonconservative forces*, 1964

[31]   Herrmann G., Hauger W., *On the interrelation of divergence flutter and internal parametric resonance*, 1973

[32]   Kubo Y., Hirata K., Mikawa., *Mechanism of aerodynamic vibration of shallow bridge girder section*, 1992

[33]   Larsen A., *Advances in Aeroelastic analyses on suspension and cable-stayed bridges*, 1998

[34]   Larsen A., *Aerodynamics of the Tacoma Narrows Bridge, 60 years later*, 2000

[35]   Larsen A., Larose G.L., *Dynamic wind effects on suspension and cable-stayed bridges*, 2014

[36]   Larsen A., Walther J.H., *Aeroelastic analysis of bridge girder sections based on discrete vortex simulations*, 1997

[37]   Luco J.E.,Turmo J., *Linear vertical vibrations of suspension bridges: A review of continuum model sand some new results*, 2010

[38]   Luco J.E.,Turmo J., *Effect of Hanger Flexibility on Dynamic Response of Suspension Bridges*, 2010

[39]   Malìk J., *Sudden lateral asymmetry and torsional oscillations in the original Tacoma suspension bridge*, 2013

[40]   Matsumoto M., Shirato H., Yagi T., Shijo R., Eguchi A., Tamaki H., *Effects of aerodynamic interferences between heaving and torsional vibration of bridge decks: the case of Tacoma Narrows Bridge*, 2003

[41]   Matsuzaki Y., Furuta S., *Bifurcation Analysis of the Motion of an Asymmetric Double Pendulum Subjected to a Follower Force*, 1991

[42]   McLachlan N.W., *Theory and application of Mathieu functions*, 1947

[43]   Nayfeh A.H., *Introduction to perturbation techniques*, 1981

[44]   Nayfeh A.H., *Nonlinear Oscillations*, 1979

[45]   Nayfeh A.H., *Perturbation Methods*, 1973

[46]   Plaut R.H., *Snap loads and torsional oscillations of the Original Tacoma Narrows Bridge*, 2007

[47]   Richardson J.R., *The development of the concept of the twin suspension bridge*, 1981

[48]   Sado D., *Energy transfer in 2 dofs vibrating system*, 1993

[49]   Scanlan R.H., *Bridge flutter derivatives at vortex lock-in*, 1998

[50]   Scanlan R.H., *The action of flexible bridges under wind. 1:flutter theory*, 1978

[51]   Selberg A., *Oscillation and aerodynamic stability of suspension bridge*, 1961

[52]   Simiu E., Scanlan R.H., *Wind Effects on Structures*, 1996

[53]   Theodorsen T., *General theory of aerodynamic instability and the mechanism of flutter*, 1979

[54]   Wang H., Tao T., *Parameter sensitivity study on flutter stability of long-span triple tower suspension bridge*, 2014

[55]   Welte J., Kniffa T., Ecker H., *Parametric excitation in a two degree of freedom MEMS system*, 2013

[56]   Zhang M., Xu F., Ying X., *Experimental Investigations on the Nonlinear Torsional Flutter of a Bridge Deck*, 2017

[57]   Original video recording of the Tacoma Narrows Bridge collapse, https://www.youtube.com/watch?v=3mclp9QmCGs, 1940